WYLE LABORATORIES - RESEARCH STAFF

REPORT WR 71-2

EXPERIMENTAL STUDY OF VIBRO-ACOUSTIC RESPONSE OF STIFFENED CYLINDRICAL SHELLS

WYLE LABORATORIES
TESTING DIVISION, HUNTSVILLE FACILITY

WYLE LABORATORIES - RESEARCH STAFF

REPORT WR 71-2

EXPERIMENTAL STUDY OF VIBRO-ACOUSTIC RESPONSE OF STIFFENED CYLINDRICAL SHELLS

By

V.M. Conticelli
R.W. White

Work Performed Under Contract No. NAS9-10423

January 1971

WYLE LABORATORIES
RESEARCH DIVISION, HUNTSVILLE FACILITY

SUMMARY

This report presents the results of an experimental vibro-acoustic research program in which an aluminum cylindrical shell was subjected to a reverberant acoustic field. Dimensions of the shell are 8 ft. (length) x 4 ft. (diameter) x 0.08 in. (wall thickness). The shell was tested with various stiffener configurations, namely: without stiffeners, with two ring frames, with two ring frames and four stringers, and with two ring frames and eight stringers. All stiffeners were uniformly spaced; and all configurations were tested with both ends of the shell closed by thick plywood bulkheads.

Measurements made included one-third octave band levels of the external acoustic field, internal acoustic field, axial and circumferential strains of the shell wall, and accelerations of the shell wall and stiffeners. These data are presented in tabulated form and are presented in graphs of normalized acceleration power spectral density. Theoretical response predictions are made for each configuration tested and for several assumed values of damping; and, these results are compared with measured response data. The comparison shows reasonably close agreement between theory and test when relatively low structural damping values are used in the computations. Measured transient decay rates obtained from impact tests of the speciman partially validate the low damping values used theoretically.

The experimental program presented herein was conducted for NASA-MSC and is a companion to an experimental program conducted for NASA-MSFC in which extensive impedance measurements were made on various stiffened configurations of the test specimen and another geometrically similar shell.

ACKNOWLEDGMENTS

The authors wish to express their appreciation to Mr. D. J. Bozich who planned and supervised the experimental program; to Mr. E.N. Esslinger who conducted the experiments; to Mr. D. L. Lister who performed the computerized vibration analyses; to Mr. J. A. Cockburn for his helpful review of the experimental results; and, to Messrs. L. Sutherland and K. Eldred for valuable discussions, review and guidance of this research project.

TABLE OF CONTENTS

TABLE OF CONTENTS (Continued)

LIST OF TABLES

LIST OF FIGURES

LIST OF FIGURES (Continued)

LIST OF SYMBOLS

A (dB)	One-third octave acceleration level; dB/third-octave Re: 1.0 g
c_0	Speed of sound in air; 1.34×10^4 in./sec
D	Plate bending stiffness of shell wall; lb-in.
D_x	Plate bending stiffness of shell wall along cylinder axis; lb-in.
D_y	Plate bending stiffness of shell wall around circumference; lb-in.
f	Frequency; Hz
f_0	Ring frequency; Hz
f_c	Acoustic coincidence frequency and band center frequency; Hz
f_{cx}	Acoustic coincidence frequency along cylinder axis; Hz
f_{cy}	Acoustic coincidence frequency around circumference; Hz
f_{mn}	Resonance frequency of (m,n)-mode of cylindrical shell; Hz
g	Gravity acceleration; 386.4 in./sec^2
$H(f_{mn}/f)$	Single degree of freedom dynamic magnification factor for the (m,n)-mode
$j_m^2(\omega)$	Coupling factor (joint-acceptance) between the axial bending modes of the shell and the reverberant acoustic field
$j_n^2(\omega)$	Coupling factor (joint-acceptance) between the circumferential modes and the reverberant acoustic field
K_e	In-plane extensional stiffness of shell wall
L	Length of cylinder
m	Number of elastic half-waves along shell axis
n	Number of elastic full-waves around shell circumference

P (dB)	One-third octave sound pressure level; dB/third-octave, Re: 2×10^{-5} N/m^2
Q	Dynamic magnification factor (quality factor) at resonance for a mode of vibration of the shell
R	Radius of shell; 24.0 in.
S (dB)	One-third octave strain level; dB/third-octave, Re: 1.0 μ in./in.
S_p	Acoustic pressure spectrum; (psi)^2/Hz
$S_{\ddot{u}}$	Acceleration spectrum; g^2/Hz
S_σ	Strain spectrum; (μ in./in.)^2/Hz
T_r	Reverberation time; sec

Greek Symbols

β_n	Factor which accounts for space average of modal mass with the circumferential mode number n
β_x	Axial stiffness parameter
β_y	Circumferential stiffness parameter
μ	Mass per unit area; lb-sec^2/in.^{3}
μg	Weight per unit area; lb/in.^{2}
ω	Angular frequency; rad/sec

1.0 INTRODUCTION

During recent years, the search for advanced methods to predict structural response of space vehicles subjected to random acoustic excitations has been attempted by many researchers. Although several methods (modal, statistical energy and empirical) are now used for vibro-acoustic response predictions, all of them are affected by various limitations and their degrees of applicability are not completely defined. It is then evident that, at the present time, experimental data can provide the most useful information for a better understanding of vibro-acoustic response of space vehicle structures. Toward this goal a thin cylindrical shell with various degrees of stiffening provided by ring frames and stringers was selected for a series of vibro-acoustic experiments. The experiments consisted of subjecting the cylindrical shell, in its various stiffened configurations, to a reverberant acoustic field which represents the standard qualification acoustic test environment and of recording, in one-third octave levels, the acceleration responses of various points of the specimens. These measurement points were chosen in such a manner that the most useful information could be obtained; and for this purpose, the accelerometers were located on the shell wall, on the rings, on the stringers, and at the intersection between the rings and the stringers. Also, strain measurements on the unstiffened shell were taken. Finally, measurements of the acoustic pressure field inside the cylinder were made to determine internal noise reduction.

The experimental program presented herein was conducted for NASA-MSC and is a companion to an experimental program conducted for NASA-MSFC (Reference 4) in which extensive measurements were made on various stiffened configurations of the test specimen and another geometrically similar shell. Additional experiments on these two shells are currently in progress under a NASA-MSFC contract; and, the results should be available in the near future.

Structural configurations and design characteristics of the test specimens are described in Section 2.0. Analytical estimates of response are presented in Section 3.0. In Section 4.0, the experimental data are evaluated. Finally, Section 5.0 is dedicated to the conclusions.

2.0 DESCRIPTION OF TEST SPECIMEN

The test specimen used in the experiments consists of a cylindrical shell whose overall dimensions are:

- Diameter = 48.0 in.
- Length = 96.0 in.
- Wall thickness = 0.080 in.

Vibro-acoustic tests were conducted for four different configurations in the following sequence:

- Configuration No. 1 — Unstiffened shell
- Configuration No. 2 — Configuration No. 1 plus two ring frames located 32.0 in. from the two ends.
- Configuration No. 3 — Configuration No. 2 plus four stringers uniformly spaced around the circumference at 90° angular separation.
- Configuration No. 4 — Configuration No. 3 plus four additional stringers so that all eight stringers are uniformly spaced around the circumference at 45° angular separation.

The basic cylindrical shell, ring frames and stringers were constructed of aluminum. The ring frames are built-up channel sections which are attached to the inside surface of the shell wall by means of rivets; and, the stringers are angle sections which are similarly attached to the outside surface of the shell wall. Two heavy end rings consisting of angle sections were welded to the inside surface at the two ends of the shell wall; and, thick circular plywood bulkheads were bolted to the end rings. These bulkheads are common to all configurations, and are used to provide radial constraint at the ends of the shell wall and to provide acoustic seals. A diagram of the final stiffened Configuration No. 4 is shown in Figure 1. Details regarding design and fabrication of the various structural components of the test specimen are presented in Sections 2.1 - 2.4 below.

2.1 Basic Shell Design

The basic unstiffened cylindrical shell has overall dimensions of 96.0 in. (length) x 48.0 in. (diameter) x 0.08 in. (wall thickness). This shell was constructed from four sheets of aluminum each having dimensions of 48.0 in. (length) x 75.4 in. (width) x 0.08 in. (thickness) and rolled to a radius of 24.0 in., so that each sheet formed one-quarter of the shell wall. Two of these sheets were butt-welded along their straight edges to form the upper half of the shell, and similarly for the other two sheets to form the lower half of the shell; and, the two half-shells were butt-welded around the circumference to form the complete shell. The axial weld lines for the

upper half-shell are circumferentially displaced by about 90^{o} relative to those of the lower half-shell. These weld lines are shown by Items 7, 8 and 9 in Figure 1.

Inspection showed that the welds were reasonably clean welds with a relatively small overall thickness; and as a result, the welds were not polished to a flush finish with the surfaces of the shell wall. These weld lines create some degree of discontinuity in the mass and stiffness distributions of the shell wall; however, these discontinuities are expected to be relatively small and to have only second order effects on the vibration response characteristics of the shell. The method of construction described above was used in order to minimize fabrication costs. As indicated in Table 2, the overall weight of the bare shell is 116 lbs.

2.2 Ring Frame Design

The test specimen has two ring frames which are attached to the inside surface of the shell wall and which are positioned so that they divide the shell into three cylindrical shell segments having equal axial lengths. The ring frames are denoted as Item 4 in Figure 1.

The ring frames have C-channel cross-sections whose geometry and dimensions are shown in Figure 2. The ring frames have a 2.0 in. web, 1.0 in. flange and a gage thickness of 0.05 in.. Each ring frame is built-up from three sheets of aluminum which form the inner flange, web and outer flange. Each flange is joined to the web by means of a continuous bead of high strength epoxy glue and by 24 rivets which are uniformly spaced around the circumference of the ring. Thus a total of 48 rivets were used to attach the two flanges to the web. The rivet sizes were selected so that the diameter of the shank of the rivet was about one-half of the dimension (d-b) shown in Figure 2.

The outer flange of each ring frame was attached to the inside surface of the shell wall by means of rivets (Item 6 in Figure 2) through the flange and shell wall. These rivets are the same size as those denoted as Item 5 in Figure 2. Twenty-four rivets used for this attachment, and an additional rivet was included for each stringer attached to the outside of the shell wall as shown in Figure 4. Thus, in the final stiffened configuration which included 8 stringers, the ring frame flange was attached to the shell wall by means of 32 rivets which were uniformly spaced around the circumference.

Each ring frame was constructed with a single cut through the cross-section. This cut provided an expandable joint that allowed the ring diameter to be adjusted so that the outer flange of the ring could be brought into continuous contact with the inner surface of the shell wall. During installation, the ring was riveted to the shell wall beginning at one end of the cut and progressing around the circumference to the other end of the cut. The two ends of the cut were then joined to form a continuous ring by the addition of small aluminum plates riveted to the web and flange on both sides of the cut.

The type of construction described above for manufacturing the ring frames was employed in order to minimize fabrication costs. Ideally, the ring frames should have an integral one-piece cross-section; however, it is difficult to roll deep channel sections, and the cost of forming the rings would have been excessive. Initially, it was considered satisfactory to use only high strength epoxy glue to join the flanges to the web; however, the development of local failures in the glue made it necessary to add the rivets (Item 5 in Figure 2). After manufacture of the basic shell, it was discovered that the shell exhibited some degree of out-of-roundness which could not be corrected by riveting the frames to the shell wall. As a result, a small gap about 12 in. long existed between the shell wall and each ring frame.

Properties of the ring frames are listed in Table 1. The mass of each ring frame is small relative to the mass of the shell wall. The radius of gyration of the ring frame is much greater than that of the shell wall; and hence, the ring frames should add significant bending stiffness to the shell wall.

2.3 Stringer Design

Formed aluminum angles available in standard sizes were used for the stringers. As shown in Figure 1 (Item 3), the stringers have the same length as the shell, and they are attached to the outside surface of the shell wall at 45° on center. Cross-section dimensions and the method of attachment to the shell are shown in Figures 3, 4 and 5. Each stringer is attached to the shell wall by means of 16 rivets which include a single rivet through each end ring and each ring frame.

Properties of the stringers are listed in Table 1. Stringer mass is seen to be much less than the mass of the shell; while the radius of gyration is much greater than the radius of gyration for the shell wall. Hence, the stringers primarily add bending stiffness to the shell wall.

2.4 End Rings and Bulkheads

The end rings were formed by rolling straight segments of aluminum angles to the desired radius, butt-welding the ends to form a continuous ring, and spot welding the ring to the inside surface at the end of the shell wall. Cross-sections of the end rings and the attachment to the shell wall are shown in Figure 5. The end rings consist of 2.0 in. x 2.0 in. x 0.25 in. angles. These rings were used for support of the flat, circular plywood bulkheads at the ends of the test speciman. These bulkheads were bolted to the end rings and are also shown in Figure 5. The purposes of the bulkheads are to constrain the ends of the shell in the radial direction and to provide the acoustic seal necessary for the acoustic response tests.

The masses of the end rings and end bulkheads are compared to the masses of the basic shells in Table 2. There it is seen that the end rings and bulkheads add considerable mass at the ends of the test specimen. Note that the stringers and ring frames add very little additional mass.

3.0 PREDICTED RESPONSES OF TEST SPECIMEN

Analytical methods exist for estimating vibration response levels of a thin cylindrical shell immersed in an ideal diffuse acoustic field. Either a modal analysis method or a statistical energy method may be employed to provide such estimates over a broad frequency range. Such estimates are often helpful in the interpretation and evaluation of experimentally measured response data. For this purpose, a computerized modal analysis technique was used to determine space average acceleration spectra for the four test specimen configurations exposed to a reverberant field. Several experiments were conducted to obtain estimates of the damping capacity of the specimen, and these indicated that damping values could vary over a broad range. Hence, response estimates were made for several values of damping. The results of the analyses are presented in Tables 5 and 6 and in graphical form in Appendix A. The analysis procedure, assumptions and results are briefly discussed below.

3.1 Response Quantities

Responses are computed in the form of a normalized acceleration spectrum which is defined as:

$S_{\ddot{U}}/S_p$ = normalized acceleration spectrum ~ $g^2/(psi)^2$

$S_{\ddot{U}}$ = space average acceleration spectrum ~ g^2/Hz

S_p = acoustic pressure spectrum ~ $(psi)^2/Hz$

These qualities are also expressed in the convenient form:

A (dB) - P (dB) = normalized acceleration spectrum averaged over one-third octave bands ~ dB/Hz

A (dB) = one-third octave acceleration level ~ dB/third-octave relative to 1.0 g

P (dB) = one-third octave sound pressure level relative to 2×10^{-5} N/m^2 (= 2.93×10^{-9} psi)

The experimental data in Section 4.0 include strain data and here it is necessary to define symbols for strain spectra. These symbols are:

S_σ/S_p = normalized strain spectrum ~ $(\mu$ in./in.$)^2/(psi)^2$

S_σ = strain spectrum ~ $(\mu$ in./in.$)^2/Hz$

S (dB) - P (dB) = normalized strain spectra averaged over one-third octave bands ~ dB/Hz

S (dB) = strain spectrum ~ dB/third octave bands relative to 1.0 μ in./in.

3.2 Response Equations

The equations used to compute $S_{\ddot{u}}/S_p$ by the modal analysis technique for a cylindrical shell immersed in a reverberant acoustic field are presented in References 1 and 2. The complete equations are too lengthy to present here; and hence only the primary equation which shows the summation of the modal spectra is shown here. This equation is:

$$\frac{S_{\ddot{u}}}{S_p} = \frac{1}{(\mu g)^2} \sum_{m=1}^{\infty} \sum_{n=0}^{\infty} \beta_n \cdot H^2 (f_{mn}/f) \cdot j_m^2(\omega) \cdot j_n^2(\omega)$$

f = frequency (Hz)

f_{mn} = resonance frequency of (m,n) - mode of shell

μg = weight per unit area of shell ($lb/in.^2$)

β_n = factor which accounts for space average of modal mass with the circumferential mode number n

$H(f_{mn}/f)$ = single degree of freedom dynamic magnification factor for the (m,n)-mode

$j_m^2(\omega)$ = coupling factor (joint-acceptance) between the axial bending modes of the shell and the reverberant acoustic field

$j_n^2(\omega)$ = coupling factor (joint-acceptance) between the circumferential modes and the reverberant acoustic field

Equations for the latter four quantities can be found in References 1 and 2. The above response equation for $S_{\ddot{u}}/S_p$ assumes that all modes respond independently so that the acceleration spectra for all modes can be added to give the total acceleration spectrum.

Modes included in the analysis consist of all modes having resonance frequencies within the overall frequency range of interest, which for the present analysis is 10-4000 Hz. Highly efficient digital computer programs are available at Wyle Laboratories to perform these numerical analyses. For the analyses of the subject test specimen, ourputs from the computer program consist of:

- Graphs of $S_{\ddot{u}}/S_p$ which are based on spectrum values computed for 100 frequencies (uniformly spaced on a log scale) per decade. These graphs are presented in Appendix A for four values of Q for the four test configurations.

- Graphs of $S_{\ddot{u}}/S_p$ which have been averaged over one-third octave bands. These are also presented in Appendix A.

- Tables of values of A (dB) - P (dB) which are presented in Tables 5 and 6.

3.3 Influence of Internal Acoustic Field

The computerized version of the modal analysis technique, employed for the response analyses presented in this report, does not account for the influence of the internal acoustic field on the response of the shell. A simplified statistical energy analysis showed that this effect is relatively small. Hence significant errors in the modal analyses should not be incurred as a result of neglecting the internal acoustic field.

3.4 Damping

A key input parameter to the vibration analyses is the damping of the shell. In the response equations, the damping is represented by the "quality factor" Q (Resonant dynamic magnification factor) which is assigned to each mode. This quantity is important since mean square response levels over third-octave frequency bands are approximately proportional to Q. Generally values of Q are not known and must be assumed. Often, values of Q = 10-30 are used for complex built-up structures. Preliminary analyses of the test specimen showed that a value of Q = 15 for each mode produced response levels considerably below those measured during testing in the reverberation room. Analyses with damping values of Q = 50 - 200 produced response levels comparable to those measured during testing. As a result, analytical response predictions were made for Q = 15, 50, 100 and 200 for each of the four configurations tested, where Q is assumed to be the curve for all modes.

Several experiments were conducted on the test specimen to verify independently that such high values of Q are realistic. These experiments were conducted on Configuration No. 4. The procedure used consisted of:

- Inducing a small amplitude, short duration, mechanical impact at a point on the shell wall (on skin between stiffeners).

- Using an accelerometer mounted on the shell wall to sense the ensuing transient response.

- Passing the accelerometer signal through a third-octave filter centered at frequency ω_c (rad/sec).

- Displaying the filtered output on an oscilloscope or graphic level recorder.

- Measuring the reverberation time T_r (time for the signal to decay exponentially by 60 dB), and computing the Q from the equation $Q = \omega_c T_r/2.2$.

The results of these tests showed that Q = 10 - 50 were realistic for the lowest resonance frequencies of the shell while Q = 50 - 200 were possible at higher frequencies. Relatively large values of Q (of the order to 100) have been measured previously for thin cylindrical shells as discussed in Reference 3.

3.5 Masses and Stiffnesses of Test Specimen Configurations

Parameters which must be specified for the response analyses are:

- Surface weight density: μg (lb/in^2.)

- Bending stiffness along the axis of the shell wall: D_x (lb-in.)

- Bending stiffness around the circumference of the shell wall: D_y (lb-in.)

- In plane extensional stiffness: K_e (lb/in.)

It is assumed in the analyses that the mass and stiffness distributions are uniform over the surface of the shell. Hence, masses and stiffnesses for the ring frames and stringers are averaged in with the mass and stiffness of the skin. The resulting values of the above parameters are listed in Table 3 for the four configurations of the test specimen. It should be noted that D_x and D_y have different values for each of the configurations No. 2, 3, and 4, and hence these configurations are represented by uniform orthotropic shells. Note that K_e is unaffected by the addition of ring frames and stringers.

3.6 Resonance Frequencies

A knowledge of the approximate resonance frequencies of the shell are necessary when performing modal response analyses, and are helpful in the interpretation of experimental results. The resonance frequencies are denoted as f_{mn} and are determined by the equation:

$$\frac{f_{mn}}{f_0} = \left[\left\{ \frac{\lambda_m^2}{\lambda_m^2 + n^2} \right\}^2 + \left\{ \beta_x \lambda_m^2 + \beta_y (n^2 - 1) \right\}^2 \right]^{1/2}$$

m = 1, 2, 3, . . . = number of elastic half-waves along shell axis

n = 0, 1, 2, 3, . . . = number of elastic full-waves around shell circumference

λ_m = $m \pi R/L$

= 0.785 m for the test specimen

β_x = $[D_x/K_e]^{1/2}/R$

β_y = $[D_y/K_e]^{1/2}/R$

} Non-dimensional stiffness parameters for orthotropic shell, see Table 3 for numerical values.

f_0 = ring frequency (Hz)

= $[K_e/\mu]^{1/2}/2\pi R$ see Table 3 for numerical values.

Numerical values of the ring frequency f_0 are listed in Table 3. Variations of f_0 with configuration is due to the naviation of the surface weight density μ g. The above equation for f_{mn} was used to compute the first ten resonance frequencies for each of the four configurations; and the frequencies are listed in Table 4.

Special attention should be given to the resonance frequency of the (m, n) = (1,2) - mode since this mode is clearly evident in the measured response data. Values of $f_{1,2}$ are listed in Table 3 for the four configurations. Note that this resonance frequency is relatively insensitive to bending stiffness of the wall. The effective stiffness associated with this mode of vibration is controlled by membrane stiffness; and the values of $f_{1,2}$ are essentially due to the first term under the radical in the above frequency equation.

3.7 Acoustic Coincidence Frequencies

Acoustic coincidence frequency is the frequency at which the bending wave speed is equal to the speed of sound in air. For a thin flat plate, this frequency is given by the equation:

$$f_c = \frac{c_0^2}{2\pi}\sqrt{\frac{\mu}{D}} \quad = \text{acoustic coincidence frequency (Hz)}$$

c_0 = 13,440 in./sec = speed of sound in air

μ = mass per unit area of plate ($lb\text{-}sec^2/in^3$)

D = plate bending stiffness (lb-in.)

For an aluminum plate with 0.08 in. thickness, the coincidence frequency is $f_c = 6200$ Hz. As bending stiffness is added to the plate, such as with the addition of stiffeners, the coincidence frequency decreases. For the subject test specimen, axial and circumferential bending stiffnesses are different; and hence, the stiffened configurations No. 2, 3, and 4 have different coincidence frequencies along the axis and aroung the circumference. These frequencies are listed in Table 3.

The significance of these coincidence frequencies is that acceleration responses tend to be high in the neighborhood of the coincidence frequency (or frequencies). Above the coincidence frequency, acceleration spectrum levels for reverberant field excitation roll-off at 6 dB/octave.

3.8 Predicted Response Spectra

Normalized acceleration response spectra were computed by the above described modal analysis procedure for Q = 15, 50, 100, and 200 for each of the configurations No. 1, 2, 3, and 4. The results are presented graphically in Appendix A in the form of curves of $S_{\ddot{w}}/S_p$ versus frequency. In Appendix A, two graphs are shown for each value of Q and configuration number. The left-hand graph was developed from computations of $S_{\ddot{w}}/S_p$ at 100 discrete frequencies per decade. The right-hand graph was developed from third-octave band averages of the left-hand graph. Third-octave band average values of the normalized acceleration are presented in Tables 5 and 6 in the forms of A (dB) - P (dB).

Key features of the graphs in Appendix A are summarized below:

- At low frequencies these spectra consist of resonant responses of well-separated modes; while at high frequencies, the modes become densely packed to produce a type of non-resonant response.

- For a given configuration, an increase in Q leads to greater average response levels and to greater resolution of the resonant modal response peaks.

- As stiffness is added to the shell, the average response levels decrease; thus Configuration No. 4 has lower spectrum levels than Configuration No. 1.

- For configuration No. 1, the highest acceleration levels occur over a frequency band which extends from about 175 Hz to 130 Hz. Resonance of the (1,2)-mode at $f_{1,2} = 178$ Hz occurs at the lower end of this band, while resonance of the (m,0)-ring modes at 1300 Hz dominate the upper end of this band. The third-octave average spectra show that the responses are greater at 1300 Hz than at 175 Hz for all values of Q considered in the

analysis. Below 175 Hz, the first few dominant peaks in Figure A1 correspond to the (1,5), (1,4), (1,7), and (1,3) modes, respectively. Above 1300 Hz, the spectrum levels decrease rapidly to values somewhat greater than mass law response [1.70×10^4 $g^2/(psi)^2$] ; and then the spectrum levels increase as the coincidence frequency of 6200 Hz is approached.

- The acceleration spectra for configurations No. 2, 3, and 4, are similar in character to those for configuration No. 1, except that above the ring resonance the spectrum levels roll-off less rapidly. The latter is caused by the fact that the circumferential coincidence frequency lies below the ring frequency. Also the fundamental resonance frequency for these cases is the (1,2)-mode.

4.0 EVALUATION OF EXPERIMENTAL DATA

Six vibro-acoustic experiments of the test specimen were conducted within Wyle Laboratories' 100,000 cubic foot reverberation room. In these tests the shell was suspended six inches off the floor in an upright position as shown in Figure 6. Microphones were used to measure sound pressure levels exterior to and within the test specimen. Accelerometers were used to measure radial responses of the shell wall, ring frames and stringers, and axial responses of the end bulkheads. Strain gages were used to measure both axial and circumferential strains of the shell wall. Two additional experiments were conducted in order to survey the sound pressure levels over the surface of the test specimen and to measure variations in noise reduction within the shell. Using analog recording and analysis techniques, these data were obtained in the form of one-third octave rms levels. From these data, normalized acceleration and strain spectra of the shell wall and stiffeners, normalized acceleration spectra of the end bulkheads, and noise reduction spectra are developed. Measured acceleration spectra averaged over octave bands are compared with comparable analytically predicted acceleration spectra for each of the four configurations tested. The results of these tests are compared with measured responses presented in the literature for other types of cylindrical shell structures.

A brief description of each of the eight experiments is presented in Section 4.1 below. The experimental data obtained and the techniques for analyzing these data are discussed in Section 4.2. A detailed evaluation of the experimental results, along with comparisons between theoretical and experimental results, are presented in Sections 4.3 and 4.4. Finally in Section 4.5, the measured acceleration responses of the subject test specimen are compared with responses of other cylindrical structures.

4.1 Test Configurations

Three experiments were conducted for the unstiffened configuration No. 1; and one experiment was conducted for each of the three configurations No. 2, 3, and 4. For each of these six experiments, the approximate position of the test specimens within the reverberation room, and the locations of all transducers relative to the test specimen are shown in Figures 7-12. Brief descriptions of experiments No. 1-6 are presented below

- Experiment No. 1 – This experiment was conducted for Configuration No. 1. As shown in Figure 7, the external microphones (M1, M2) were located 18 inches from the surface of the shell; and microphone (M2) was located on the centerline at 16.0 inches above the lower end-bulkhead. Five radially oriented accelerometers (A1, A2, A3, A4, and A5) were located at various positions on the external surface at the unstiffened shell wall. The axial strain gage (SG1) and the circumferential strain gage (SG2) are mounted on the exterior wall of the shell at the same location.

- Experiment No. 2 – This test is a repeat of Experiment No. 1 and was conducted for the purpose of obtaining vibration response levels of the two end bulkheads. As seen in Figure 8, the two accelerometers (A2 and A5) were moved from the shell wall to the centers of the upper and lower end-bulkheads. Vertical acceleration responses of these two bulkheads provide a measure of the transmission losses that can be expected to occur across these bulkheads.

- Experiment No. 3 – This experiment is also a test of Configuration No. 1. The purpose of this test is to show the possible influence of variations of the sound pressure levels within the reverberation room on localized response levels of the structure. As seen in Figure 9, the test specimen was rotated 180° about its vertical centerline. With this exception, all transducer locations are the same as in Experiment 2.

- Experiment No. 4 – This experiment is a test of Configuration No. 2 which has two ring frames attached to the inside surface of the shell wall. Location of the test specimen within the reverberation room and locations of all transducers relative to the test specimen are shown in Figure 10. Accelerometers A3 and A5 are mounted on the unstiffened skin while accelerometers A1 and A4 are mounted on the upper ring frame. Note that for this test, microphones M1 and M3 have been moved to new locations relative to the test specimen.

- Experiment No. 5 – This experiment is a test of Configuration No. 3 which includes two interior ring frames and four exterior stringers having 90° angular separations around the circumference. Transducer locations for this experiment are shown in Figure 11. Here, accelerometers A2 and A4 are mounted on the upper ring frame; accelerometer A3 is mounted on the stringer between ring frames; and accelerometer A1 is mounted at the intersection of the upper ring frame and stringer.

- Experiment No. 6 – This is a test of Configuration No. 4 which includes two interior ring frames and eight exterior stringers located at 45° increments around the circumference. Instrumentation for this test is shown in Figure 12. Accelerometer A1 is located at the intersection of the upper ring and stringer; accelerometer A2 is located on the upper ring between stringers; and accelerometer A3 is located on a stringer between the two ring frames; and accelerometer A4 is located on the skin between stiffeners.

Two additional experiments were conducted for the purpose of measuring noise reductions within the test specimen and the variations of sound pressure levels over the exterior surface of the test specimen. These experiments are discussed below:

- Experiment No. 7 – This test was conducted for the purpose of measuring noise reduction for Configuration No. 4. Two microphones (M1 and M2), located 4.0 ft above the floor, were used to measure sound pressure levels exterior to the test specimen. Microphone M1 was located approximately 15 ft (far-field) from the test specimen; while microphone M2 was located less than 1.0 in. (near-field) from the surface of the shell. Three microphones (M3, M4, and M5) were used to measure sound pressure levels within the shell. Microphone M3 was located at the mid-height of the shell and within 1.0 in. of the interior wall of the shell. Microphone M4 was located at the mid-height and on the centerline of the shell. Microphone M5 was located along the upper interior edge of the shell.

- Experiment No. 8 – The purpose of this test was to measure variations in the sound pressure levels over the exterior surface of the test specimen for Configuration No. 4. Two external microphones were used in this test. One of the microphones was located at a fixed position about 15 ft (far-field) from the test specimen. A second microphone was positioned within 1.0 in. (near-field) of the exterior wall of the shell and was moved to various heights above the floor and various positions around the circumference.

4.2 Presentation of Measured Data

In order to provide a permanent record of the basic data measured during Experiments No. 1-7, one-third octave band analog plots for all microphones, accelerometers, and strain gages are presented in Appendix B. The one-third octave band levels from these plots are listed in Tables 7-13. For convenience, all of these data are presented in units of dB/third octave and appropriate reference values (0 dB levels) of sound pressure levels, acceleration and strain are indicated. One-third octave analog plats of sound pressure levels obtained during Experiment No. 8 were not available for reproduction in this report. However, the measured sound pressure levels are listed in Tables 14-15 in units of dB/third-octave.

It is necessary to define a common reference for all experiments so that response levels obtained for different experiments can be compared. Ideally this reference would be the sound pressure level of the reverberant acoustic field at a relatively large distance (several shell diameters) from the test specimen. For Experiments No. 1-3, it is necessary to approximate this reference sound pressure level by the average of the sound pressure levels measured by microphone M1 and M3 which are located 18.0 in. from the exterior surface of the test specimen. For Experiments No. 4-6, it is assumed that the reference sound pressure level is provided by microphone M1 which is 105.3 in. from the exterior surface of the test specimen.

A normalized acceleration spectrum, A (dB) - P (dB) in units of dB/Hz, can be obtained for any acceleration, A (dB), in Tables 7-12 by subtracting from A (dB) the corresponding reference sound pressure level, (P (dB). Such a normalized acceleration spectrum can be expressed as $S_{\ddot{u}}/S_p$, having units of $g^2/(psi)^2$, by use of the following relationship:

$$A\ (dB) - P\ (dB) = 10 \log_{10} \left[S_{\ddot{u}}/S_p \right] - 170.7$$

Numerical values of $S_{\ddot{u}}/S_p$ were determined for each measured acceleration in the six experiments and for each of the third-octave band center frequencies. The results are presented graphically in Figures 13-18. These graphs have the same format as those represented in Appendix A for analytically predicted results. For convenience, locations of the accelerometers are also indicated in Figures 13-18.

These noise reduction curves are presented in Figure 19. These were developed from the data in Table 13. For example noise reduction at M3 is obtained by subtracting P (dB) for microphone M3 from P (dB) for microphone M1. Similar for the noise reduction curves associated with microphones M4 and M5.

Normalized strain spectra, S_σ/S_p, are developed from data listed in Tables 7-9 and are presented in Figures 20-22. The computation of S_σ/S_p from values of S (dB) and the reference P (dB) can be accomplished by use of the equation:

$$S\ (dB) - P\ (dB) = 10 \log_{10} \left[S_\sigma/S_p \right] - 170.7$$

The measured acceleration spectra shown in Figures 13-18 and the predicted spectra in Appendix A exhibit many "Peaks" and "Valleys" which make comparisons between measured and theoretical results difficult. It is expected that theory will not provide reasonable predictions for the "fine structure" of a response spectrum; however, theory may provide a reasonably good estimate of the average response spectrum. For this reason the measured sound pressure levels and accelerations in Tables 7-12 were averaged over octave bands, and the results were used to construct average normalized acceleration spectra.

All of the octave band average spectra for a given experiment were then grouped and enveloped to give a band of average acceleration spectra. These bands are shown in Figures 23-26 for Experiments No. 1, 4, 5, 6. Similar octave band averages of the predicted normalized acceleration spectra were developed from Tables 5 and 6; and the resulting average theoretical spectra are also shown in Figures 23-26.

4.3 Discussion of Measured Data and Comparisons with Analytical Predictions

The purpose of this section is to review the final experimental data; to discuss and interpret the key features of these data, and to make comparisons with analytical predictions. For convenience, these discussions are divided into sub-sections which evaluate low frequency response characteristics, high frequency response characteristics, noise reduction, strain response, sound pressure level survey over the shell, and the final comparisons between average response spectra obtained experimentally and analytically.

4.3.1 Low Frequency (45-100 Hz) Response of the Unstiffened Shell

The fundamental resonance frequency for configuration No. 1 is about 46 Hz according to Table 4. Acceleration levels at this frequency were too small to be measureable during experiments No. 1, 2, and 3 as indicated in Figures 13-15; however, the strain spectra in Figures 20-22 show that low level resonant response does exist between 40-60 Hz. These measured results are partially in agreement with theoretical predictions since the acceleration spectra in Figure A1 show low-level resonant response between 45-100 Hz. Also, in Figure 23, the measured spectrum level at 63 Hz (which is an average over the 50, 63, and 80 Hz third-octave bands) is equal to the comparable spectrum level predicted for Q = 15.

It should be possible to compare measured and predicted response levels in the 45-100 Hz frequency band. This could be done by determining the theoretical strain spectrum associated with responses of the first four dominant modes of vibration shown in the left-hand graph in Figure A1. The first four resonant peaks in this graph correspond to the (1,5), (1,4), (1,7), and (1,3)-mode, respectively. It can be shown analytically that the (1,6)-mode, which is the second mode of vibration listed in Table 4, has a negligibly small response level. The theoretical strain spectrum could then be compared with those in Figures 20-22 for the 45-100 Hz band. Differences between theoretical and measured strain spectrum levels would be due to differences between theoretical and actual damping values, acoustic-structure coupling factors (joint acceptances), or structural mode shapes. Since it would not be possible to separate the effects of these three parameters on the basis of measured data available, this calculation is not presented here.

4.3.2 Low Frequency (100-200 Hz) Responses of Unstiffened and Stiffened Shell Configurations

The unstiffened shell and all of the stiffened configurations of the test specimen exhibit an overall resonant response in the 100-200 Hz band. This resonance is observed in the acceleration spectra presented in Figures 13-18 and in the strain spectra presented in Figures 20-22. Special attention is given to this resonance because of the very large measured strain level shown in Figure 20.

There is strong evidence to support the conclusion that this resonance is associated with the (1,2)-mode of the shell. First, Table 3 indicates that, for all four configurations, the theoretical resonance frequency of this mode lies in the range $f_{1,2}$ = 177.8 to 183.1 Hz. Tables 7-12 indicate that the resonance of interest lies in either the 125 Hz or the 160 Hz third-octave bands. It is certainly possible then that the actual resonance frequency of the (1,2)-mode of the test specimen lies within the 125 Hz or the 160 Hz band. Secondly, Figures A1-A4 show that the first dominant resonant response predicted for the unstiffened shell occurs at about 180 Hz; and it can be shown that this resonance is associated with the (1,2)-mode. Figures A5-A16 indicate that the first dominant resonance predicted for the stiffened configurations No.2, 3, and 4 also occurs at about 180 Hz, and from Table 4 it is evident that this resonance corresponds to the (1,2)-mode. These theoretical predictions are in agreement with Figures 13-18 which show that the first dominant resonance of the test specimen occurs at about the frequency associated with resonance of the (1,2)-mode. Finally, although other modes of the shell may have theoretical resonance frequencies close to 180 Hz, theoretical response predictions indicate that only the (1,2)-mode has a large response in this frequency range. On the basis of these arguments, it is concluded that the 100-200 Hz resonance appearing in Figures 13-18 and Figures 20-22 is caused by the (1,2)-mode.

The spectral amplitude of the 100-200 Hz resonance shown in Figure 13 lies between 6×10^5 $g^2/(psi)^2$ and 7×10^5 $g^2/(psi)^2$. The right-hand graph in Figure A3 shows that the predicted spectral amplitude for this same resonance is 7×10^5 $g^2/(psi)^2$ when Q = 100. Other values of Q lead to different spectral amplitudes for this mode. Thus, if the assumed joint-acceptances are correct, a reasonable value for damping associated with the (1,2)-mode is Q = 100.

4.3.3 High Frequency Response Characteristics

Inspection of Figures 13-18 shows several significant features concerning the high frequency response characteristics of the test specimen. These features are briefly outlined below:

- The ring frequency of the test specimen is estimated to be about 1300 Hz. The modal density of the shell is maximum at this frequency; and hence, the acceleration response should be maximum at 1300 Hz. Figures 13, 14, and 15 show that maximum responses of the unstiffened cylinder occur between 600-1000 Hz, or at an average frequency of 800 Hz. Thus the maximum responses occur at a frequency (800 Hz) which is somewhat less than the theoretical ring frequency (1300 Hz). This deviation from theory could be associated with the mass loading effect of the accelerometers (1.0 ounce) used in these experiments. If a lighter transducer such as 0.1 ounce accelerometers, were used the frequency at which the peak occurs would tend to move toward the theoretical limit (zero mass loading) of

1300 Hz. For frequencies of 1000 Hz - 2000 Hz, it is estimated that the acceleration spectra might increase by 3-6 dB.

- The measured response data of the unstiffened cylinder presented in Figures 13, 14, and 15 show a sharp decrease above the ring frequency. This trend is also encountered in the theoretical predictions, as shown in Figures A1-A4 of Appendix A and is due to the low coupling of the (acoustically slow) modes whose resonance frequencies fall between the ring frequency and the flat plate coincidence frequency (6200 Hz).

- The responses for configuration No. 1 measured during experiments 2 and 3, Figures 14 and 15, are essentially equal, indicating that the locations of the accelerometers with respect to the acoustic field in the room are not significant.

- Figures 16-18 indicate that, when stiffeners are added, the response peak at the ring frequency broadens while the average response level is somewhat reduced. This change in response is more evident between the unstiffened and fully stiffened shells as shown in Figures 13 (or 14, 15) and 18. This effect is also evident in the theoretical predictions as can be seen in Figures, for example, A1 and A13 in Appendix A. This change in response is also discussed in Section 3.0.

- Figure 21 shows that response on rings and shell sigments between rings are approximately equal. This implies that the shell and ring frames are well coupled dynamically.

- According to Figure 17, considerable deviation in response occurs for different locations on the shell at high frequencies. This includes accelerometers A2 and A4 which are mounted 135° apart on the same ring. This may be caused by a small gap between the shell wall and the ring frame at the point where the accelerometer A4 is mounted.

4.3.4 Noise Reduction

Figure 19 shows representative noise reductions obtained for configuration No. 4. Noise rediction varies with frequency and position inside the volume of the test specimen. The three noise reduction curves in Figure 19 were obtained from three microphones located at different positions. Microphone M4 was located on the outer-line at the mid-height of the shell. Microphone M3 was located within 1.0 in. of the interior wall at the mid-height of the shell. Microphone M5 was located in the upper corner of the shell. Key features observed from these data are:

- The greatest noise reduction occurs at the center of the test specimen because radial acoustic modes within the cylindrical volume have pressure modes on the centerline.

- Variations in noise reduction on the centerline are probably associated with axial acoustic modes within the shell. The first two axial acoustic modes which have pressure modes at the center of the shell have resonance frequencies of 70 Hz and 210 Hz; and at these frequencies, the noise reductions should be relatively high. The first axial acoustic mode having a pressure maximum at the center of the shell has a resonance frequency of 140 Hz; and it is seen that this corresponds closely to the small noise reduction measured in the 125 Hz third-octave band.

- Noise reductions at the wall should be lower than at the outer-line because the interior wall is a location of pressure maxima for all radial acoustic modes of the shell volume. This is seen to be the case for microphone M3. Note that the noise reduction is nearly zero in the 160 Hz band; and this may be caused by the high response level of the (1,2)-mode of the shell which was discussed in Section 4.3.2.

- Noise reduction in the upper corner (M5) is minimum because the interior acoustic modes have pressure maxima at this corner. Note, from Figure 19 that the noise reduction here is essentially flat above 200 Hz. It is estimated that the space average noise reduction is approximately 6 dB greater than that obtained by M5; that is about 9 dB above 200 Hz.

- Figures 14 and 15 show that the response levels of the end bulkheads are much less than those of the shell wall, as a result, the transmission loss across these bulkheads should be much greater than across the shell wall. It is concluded than that noise reduction within the volume of the shell is controlled by vibrations of the shell wall.

- At high frequencies, the three noise reduction curves converge indicating that noise reduction becomes essentially independent of position within the shell. This is expected since the internal acoustic field approaches a diffuse field as frequency increases.

4.3.5 Strain Response

Strain spectra were obtained only for configuration No. 1 and are shown in Figures 20-23. Three key features of these spectra are:

- The circumferential strain is much greater than the axial strain. Strain is inversely proportional to the square of the elastic wave length of any mode of vibration. Elastic wave lengths around the circumference are generally much smaller than elastic wave lengths along the axis because the circumferential mode number (n) is generally greater than the axial mode number (m) for the modes showing the highest response levels. As an example, the resonance which appears between 40-60 Hz in Figures 20-22 is associated with m = 1 and n = 4-7 as described in Section 4.3.1. Also, the sharp resonance between 100-200 Hz shown in Figure 20 is associated with m = 1 and n = 2 as discussed in Section 4.3.2.

- Both axial and circumferential strains exhibit similar resonance effects below 500 Hz; while above 500 Hz, the circumferential strain appears to be non-resonant. In the neighborhood of the theoretical ring resonance at 1300 Hz, the dominant response modes are the (m,n) = (1,0), (2,0), (3,0), . . .,- modes. Thus it is expected that the circumferential strain should be nearly uniform within the higher frequency range while the axial strain would show some evidence of resonance; and this can be seen in Figure 21.

- Above 1300 Hz, the circumferential strains decrease rapidly with increasing frequency. For the unstiffened shell, theoretical predictions show that the responses of the (m,0) modes chop off sharply with increasing frequency. The effect of this can be seen in the rapid roll-off of the circumferential strain above 1300 Hz.

4.3.6 Survey of Sound Pressure Levels Over Test Specimen

The sound pressure level survey presented in Table 14 and 15 indicate that the sound pressure level near the shell wall is higher than the sound pressure level in the far-field. Although the difference is neither constant nor following a well defined trend with frequency, for practical purposes a pressure increment near the shell wall of 2-3 dB can be considered a reasonable estimate. This survey also shows that no significant variations in sound pressure level occurs over the surface of the test specimen.

4.3.7 Comparison of Experimental and Analytical Responses

The octave-band average spectra presented in Figures 23-26 provide a meaningful comparison between theoretical and measured responses of the test specimen. Key features to be observed in this comparison are:

- The general shapes of of the theoretical and corresponding measured response spectra are similar, except at low frequencies for the stiffened configurations.

- For the unstiffened configuration No. 1 (see Figure 23), it is apparent from the spectral amplitudes that the shell probably has low damping values and that Q-values between 100 and 200 are reasonable. This is expected since the shell has no joints except at the end bulkheads.

- For the stiffened configurations no. 2, 3, and 4, (see Figures 24-26), the spectral amplitudes indicate that Q-values between 50 and 100 might be reasonable. These lower Q-values are consistent with the added damping that is expected from sliding friction that occurs at the joints between the shell wall and stiffeners.

4.4 Comparison of Measured Responses for Six Cylindrical Shell Structures

A brief literature survey was conducted to obtain other experimental data for cylindrical shell structures, and they are presented in Figure 27. In this figure, the ordinate represents the non-dimensional quantity $(\mu g)^2 \; S_{\ddot{U}}/S_p$ where μg is the surface weight density, $S_{\ddot{U}}$ is the acceleration PSD and S_p is the pressure level PSD. Mass law response corresponds to the value $(\mu g)^2 \; S_{\ddot{U}}/S_p = 1.0$. The absicissa is the product of frequency (in Hz) and diameter (feet). This type of graph was used by Franken in Reference 5 to present Titan vibration data. Curves presented in Figure 27 are:

- Curve 1 — Average of response data observed on Jupiter and Titan I vehicles (Reference 5).

- Curve 2 — Data obtained by NASA-MSC on Apollo Spacecraft SLA for progressive wave-duct excitation (References 1 and 2).

- Curve 3 — Response data of Republic Steel Cylinder No. 7 obtained by Wyle Laboratories dueing air-helium experiments for NASA-MSFC (Reference 6). This cylinder dimensions are: Diameter = 36 in., Height = 36 in., and Thickness = 0.018 in.

- Curve 4 — Response data of cylindrical, aluminum-honeycomb shroud obtained during static firing tests of Saturn V at NASA-Mississippi Testing Facility. The shroud dimensions are: Diameter = 260.0 in., Height = 300.0 in., and Thickness = 1.0 in.

- Curve 5 – Data reduced from Experiment No. 1 for the unstiffened test specimen. The acceleration spectrum is obtained from Figure 13 for response of the skin.

- Curve 6 – Response data from Experiment No. 6 for the fully stiffened version of the subject test specimen. The curve is obtained from Figure 18 and corresponds to response of the skin.

From the analysis of these curves, the following conclusions may be made:

- The scattering of measured data related to different cylinders indicates that other structural parameters, (such as bending stiffness and extensional stiffness) influence the response of shells to an acoustic field.

- The choice of $(\mu g)^2 \ S_{\ddot{u}}/S_p$ as ordinate is convenient to show whether or not high frequency vibrations are controlled by mass law. Since most of the measured data shown in Figure 45 consist of relatively low frequency vibration, it might be more convenient to use $K^2 \cdot S_u/S_p$, or its equivalent $(K^2/\omega^4)\ S_{\ddot{u}}/S_p$, as the ordinate, where

  K = typical stiffness parameter

  S_u = PSD of deflection response = $S_{\ddot{u}}/\omega^4$

  By using $k^2\ S_u/S_p$, the spread of the data at low frequencies should be less than that shown in Figure 27. (Realistic values of K were not immediately available for the structures included in Figure 27).

- Further review of Figure 27 shows that peak responses do not necessarily occur at the ring frequency, as might be expected for uniform cylindrical shells. This could be explained in some cases by non-uniformity of the shell structures, and local mass loading of the shell wall.

- It is clear from Figure 27 that responses of most shell structures are well above those predicted by simple mass law.

5.0 CONCLUSIONS

Eight experiments were conducted in which a thin cylindrical shell, having four stiffener configurations, was subjected to a reverberant acoustic field. Measurements were made of external and internal sound pressure levels, acceleration response levels of the shell wall and stiffeners, and strain levels of the external shell wall. Several impact experiments were conducted in order to obtain approximate values of damping of the test specimen. A series of analyses were conducted in order to estimate acoustically-induced vibration responses of the shell wall for each stiffener configuration and for four damping values represented by Q = 15, 50, 100, 200. Comparisons were made between measured and theoretical acceleration spectra. The principle conclusions resulting from this vibro-acoustic research program are:

- Based on measured vibration decay rates, the impact tests showed that the test specimen has relatively high values of Q over most of the frequency range of interest. Average third-octave band values of Q were greater than 50 for almost all third-octave bands analyzed; and Q-values of 100-200 were obtained for many of these bands. Such high values of Q are typical for "one-piece" structures which have few joints, such as the subject test specimen. Actual flight hardware is often built-up from many smaller frame and plate components; and as a result, the numerous joints generally yield lower Q-values in the range of 10-30. In this sense the test specimen is a representation model of flight hardware in terms of mass and stiffness, but not damping. Scaled damping is generally not achieved in dynamic models of actual structures. Hence damping of model and prototype should be measured and then analyses should be used to adjust measured results of model studies for differences between model and prototype damping.

- The unstiffened cylindrical shell exhibits an acceleration response spectrum which, when normalized by the acoustic pressure spectrum, is maximum in the neighborhood of the ring frequency. The shape of the measured response spectrum is similar to that which can be predicted theoretically; and analytical response levels are comparable to measured response levels when a damping of Q = 100-200 is assumed. In particular, the predicted sharp roll-off of response levels above the ring frequency is evident in the measured acceleration spectra.

- Stiffened configurations of the test specimen exhibit acceleration response spectra which tend to be more uniform (flat) at high frequencies and to have lower amplitudes than the acceleration spectra for the unstiffened shell. The increase in high frequency response with the addition of ring frames and stringers is clearly evident when the acceleration spectra for the unstiffened and fully stiffened configurations are compared. The

increased response of the stiffened shells above the ring frequency is partially in agreement with theoretical predictions; however, in addition, this phenomenon is partly due to dynamic decoupling of plate segments and stiffeners.

- When realistic values of effective structural damping are known, the modal analysis technique, coupled with the inclusion of a sufficient number of modes of vibration, provides a reasonably accurate estimate, over a broad frequency range, of vibration response levels of a cylindrical shell with and without stiffeners.

- In a reverberant acoustic field, the sound pressure levels at the surface of a cylindrical test specimen are about 2-3 dB higher, on the average, than sound pressure levels at a large distance from the cylinder. As frequency increases, these surface pressures should approach values which are 3 dB higher than pressures far from the cylinder. Furthermore, the sound pressure levels over the surface of the shell are fairly uniformly distributed.

- For the subject test specimen, vibration levels are approximately the same for the shell wall and stiffeners, indicating that these components are well coupled dynamically. This is explained partly by the fact that the masses of the stiffeners are small relative to the mass of the shell. In some instances, the shell wall between stiffeners exhibits up to 6 dB greater response than the stiffeners.

- Noise reduction at the internal corner microphone is approximately constant, and equal to 3 dB, for frequencies above 200 Hz. Noise reduction on the axis of the shell exhibits several minima and maxima which occur at frequencies that closely correspond to standing interior acoustic waves along the axis of the shell. At high frequencies, the noise reduction, tends to be relatively independent of position within the volume of the test specimen and tends towards the value of noise reduction in the corner. At sufficiently high frequencies, noise reduction in the corner should approach a value of 6 dB higher than the space average noise reduction.

- Measured circumferential strain levels for the unstiffened shell are significantly higher than axial strain levels throughout most of the frequency range because, for those modes having the highest response levels, the elastic wave lengths around the circumference are generally smaller than those along the axis. The axial and circumferential strain spectra appear to be quite similar in shape including three or four well defined resonance peaks below 600 Hz. The use of strain gages in experimental programs of the type reported herein is recommended since strain gage values can distinguish between circumferential and axial components of bending response. Furthermore the use of internal and

external strain gages on opposite sides of the shell wall can be used to separate circumferential bending modes (n = 1, 2, 3, . . .) from the circumferential extensional modes (n = 0).

- The survey of responses of a number of cylindrical shells indicates that response levels are generally maximum and well above mass law response in the neighborhood of the frequency of the ring resonance. The method used in Figure 27 to normalize cylindrical shell responses has only limited value since many other factors (such as bending stiffeners, stiffener spacing, etc.) not accounted for can have significant influences on shell response characteristics.

The results of the experimental/analytical program discussed in this report have provided insight into the many complex phenomena which govern acoustically-induced responses of cylindrical shells and have provided considerable validation of theoretical methods used to predict vibration responses.

REFERENCES

1. White, R. W., "Predicted Vibration Responses of Apollo Structure and Effects of Pressure Correlation Lengths on Response," Wyle Laboratories Research Staff Report WR 67-4, March 1967 and Revised March 1968.

2. Bozich, D. J. and White, R. W., "A Study of the Vibration Responses of Shells and Plates to Fluctuating Pressure Environments," NASA CR-1515, March 1970.

3. Kana, D. D., "Response of a Cylindrical Shell to Random Acoustic Excitation," Interim Report to NASA-MSFC under Contract No. NAS8-21479; Southwest Research Institute, July 1969.

4. Conticelli, V. M., Kao, G. C., and White, R. W., "Experimental Study of Input Impedances of Stiffened Cylindrical Shells," Wyle Laboratories Research Staff Report WR 70-12, August 1970.

5. Franken, P. A., "Sound Induced Vibrations of Cylindrical Vehicles," JASA 34, p. 453-454, 1962.

6. Holmes, J. R., "Air-Helium Noise Reduction Studies," Wyle Laboratories Research Staff Report WR 70-3, January 1970.

TABLE 1. Summary of Dimensions, Stiffness and Mass Properties of Ring Frames and Stringers

Property	Unit	Dimensions	
		Ring	Stringer
Mean radius	in	23.0	----
Overall length	in	144.5	96.0
Cross-section area	in^2	.215	.123
Area moment of inertia	in^4	.135	.0119
Radius of gyration	in	.790	.310
Weight per unit length	lbs/in	.0215	.0123
Weight per stiffener	lbs	3.10	1.18
Weight all stiffeners	lbs	6.20	9.44

TABLE 2. Summary of Component and Overall Weights

Component	Weight
Bare shell	116 lbs
Two end rings	28 lbs
Two end bulkheads*	70 lbs
Total weight (no stiffeners)	214 lbs
Total weight (with all stiffeners)*	243 lbs

* These weights were measured; while all other weights were calculated

TABLE 3. Structural Characteristics and Coincidence Frequencies of the Four Configurations of Test Specimen

Property	Dimension	Configurations			
		1	2	3	4
Weight per Unit Area	μg (lb/in^2.)	7.8×10^{-3}	8.1×10^{-3}	8.4×10^{-3}	8.7×10^{-3}
Extensional Stiffness	K_e (lb/in.)	8×10^5	8×10^5	8×10^5	8×10^5
Axial Bending Stiffness	D_x (lb-in.)	4.9×10^2	4.9×10^2	6.7×10^3	1.3×10^4
Circumferential Bending Stiffness	D_y (lb-in.)	4.9×10^2	1.1×10^5	1.1×10^5	1.1×10^5
Axial Stiffness Parameter	β_x	1.03×10^{-3}	1.03×10^{-3}	3.81×10^{-3}	5.31×10^{-3}
Circumferential Stiffness Parameter	β_y	1.03×10^{-3}	1.55×10^{-2}	1.55×10^{-2}	1.55×10^{-2}
Ring Frequency	f_0 (Hz)	1307	1282	1260	1238
Resonance Frequency of (1,2)-Mode	f_{12} (Hz)	177.8	184.1	181.1	178.2
Axial Coincidence Frequency	f_{cx} (Hz)	6200	6200	1680	1210
Circumfer. Coincidence Frequency	f_{cy} (Hz)	6200	390	390	390

TABLE 4. Summary of Resonance Frequencies, f_{mn}, for First Ten Modes of the Four Configurations of the Test Specimen

Configuration No. 1			Configuration No. 2			Configuration No. 3			Configuration No. 4		
Mode Number		Resonance Frequency	Mode Number		Resonance Frequency	Mode Number		Resonance Frequency	Mode Number		Resonance Frequency
m	n	Hz	m	n	Hz	m	n	Hz	m	n	Hz
1	5	45.57	1	3	183.08	1	2	181.14	1	2	178.17
1	6	52.57	1	2	184.05	1	3	181.39	1	3	179.03
1	4	52.78	1	4	308.78	1	4	304.81	1	4	300.27
1	7	67.17	2	3	324.64	2	3	322.74	2	3	319.14
1	3	84.51	2	4	353.01	2	4	353.64	2	4	351.00
1	8	86.19	3	4	457.03	3	4	461.58	3	4	460.16
2	7	92.16	1	5	488.51	1	5	481.00	1	5	473.20
2	6	97.63	1	1	495.16	1	1	485.35	1	1	476.37
2	8	100.26	2	2	499.30	2	2	490.59	2	2	482.18
1	9	108.53	2	5	503.67	2	5	502.17	2	5	497.21

TABLE 5. Predicted Normalized Acceleration Spectra for Configurations No. 1 and 2

Freq. f_c (Hz)	Normalized Acceleration Spectra A(dB) - P(dB) : dB/Hz							
	Configuration No. 1				Configuration No. 2			
	Q=15	Q=50	Q=100	Q=200	Q=15	Q=50	Q=100	Q=200
10	-186.1	-186.1	-186.1	-186.1	-205.5	-215.9	-215.9	-215.9
12	-180.8	-180.8	-180.8	-180.8	-200.6	-200.8	-200.8	-200.8
16	-174.5	-174.5	-174.5	-174.5	-194.9	-206.5	-206.5	-206.5
20	-168.1	-168.1	-168.1	-168.1	-188.1	-192.3	-192.3	-192.3
25	-161.4	-161.4	-161.4	-161.4	-183.3	-198.1	-198.1	-198.1
31	-153.9	-153.9	-153.9	-153.9	-177.7	-183.7	-183.7	-183.7
40	-142.8	-142.5	-142.5	-142.5	-172.1	-189.3	-189.3	-189.3
50	-129.8	-123.2	-119.4	-116.2	-146.8	-166.8	-166.8	-166.8
63	-133.3	-130.4	-129.5	-129.1	-142.0	-162.0	-162.0	-162.0
80	-130.9	-125.2	-123.0	-122.0	-137.8	-157.8	-157.8	-157.8
100	-132.4	-128.8	-126.8	-125.3	-133.6	-153.6	-153.6	-153.6
125	-134.0	-129.9	-128.6	-128.2	-125.5	-145.5	-147.0	-147.0
160	-125.4	-121.8	-120.8	-119.8	-109.7	-128.9	-128.8	-128.8
200	-122.2	-115.5	-112.0	-110.0	-101.4	-115.7	-113.1	-111.1
250	-127.1	-124.8	-123.5	-122.5	-111.4	-131.3	-131.3	-131.3
315	-122.0	-116.4	-114.9	-114.3	-101.8	-115.8	-111.7	-107.5
400	-125.7	-123.5	-122.4	-121.7	-104.3	-121.2	-120.0	-119.6
500	-119.3	-114.0	-112.2	-111.2	- 98.7	-113.0	-110.1	-107.0
630	-119.6	-114.7	-112.2	-109.4	-110.9	-116.7	-113.8	-110.4
800	-118.1	-112.9	-109.9	-107.6	- 98.9	-113.4	-110.4	-107.6
1000	-117.4	-112.3	-109.3	-106.4	- 97.9	-112.4	-109.2	-105.9
1250	-116.4	-110.9	-107.8	-104.8	- 95.5	-109.7	-106.4	-103.2
1600	-122.6	-121.0	-119.7	-117.8	- 98.7	-113.8	-111.1	-108.2
2000	-125.1	-123.6	-122.2	-120.4	-100.3	-115.2	-112.0	-108.6
2500	-125.0	-123.4	-121.8	-119.8	-101.2	-116.1	-113.2	-110.1
3100	-121.9	-118.1	-115.8	-113.4	-101.6	-116.4	-113.3	-110.1
4000	-119.1	-114.5	-111.9	-109.5	-102.2	-117.1	-114.2	-111.3

TABLE 6. Predicted Normalized Acceleration Spectra for Configurations No. 3 and 4

Freq. f_c (Hz)	Normalized Acceleration Spectra A(dB) - P(dB) : dB/Hz							
	Configuration No. 3				Configuration No. 4			
	Q=15	Q=50	Q=100	Q=200	Q=15	Q=50	Q=100	Q=200
10	-215.8	-215.8	-215.8	-215.8	-215.7	-215.7	-215.7	-215.7
12	-210.7	-210.7	-210.7	-210.7	-220.6	-220.6	-220.6	-220.6
16	-206.4	-206.4	-206.4	-206.4	-206.4	-206.4	-206.4	-206.4
20	-192.2	-192.2	-192.2	-192.2	-192.2	-192.2	-192.2	-192.2
25	-198.0	-198.0	-198.0	-198.0	-197.8	-197.8	-197.8	-197.8
31	-183.6	-183.6	-183.6	-183.6	-183.6	-183.6	-183.6	-183.6
40	-189.2	-189.2	-189.2	-189.2	-189.1	-189.1	-189.1	-189.1
50	-166.9	-166.9	-166.9	-166.9	-167.0	-167.0	-167.0	-167.0
63	-162.1	-162.1	-162.1	-162.1	-162.1	-162.1	-162.1	-162.1
80	-157.9	-157.9	-157.9	-157.9	-157.9	-157.9	-157.9	-157.9
100	-153.6	-153.6	-153.6	-153.6	-153.6	-153.6	-153.6	-153.6
125	-145.4	-145.3	-145.3	-145.3	-145.1	-145.1	-145.1	-145.1
160	-128.4	-127.1	-126.9	-126.9	-126.9	-123.9	-123.4	-123.2
200	-122.1	-116.5	-114.9	-114.3	-123.1	-116.0	-111.4	-108.0
250	-131.9	-131.8	-131.8	-131.8	-132.3	-132.2	-132.2	-132.2
315	-122.2	-116.9	-114.9	-114.0	-122.5	-116.6	-132.5	-111.5
400	-124.7	-121.2	-119.6	-118.9	-125.2	-123.2	-122.7	-122.5
500	-119.1	-113.2	-109.6	-106.2	-119.4	-113.4	-109.9	-106.5
630	-220.2	-116.4	-113.5	-111.1	-121.3	-116.7	-115.1	-114.4
800	-119.7	-114.2	-110.5	-106.3	-120.3	-115.1	-112.4	-109.8
1000	-119.1	-113.6	-110.3	-107.1	-119.7	-114.2	-110.6	-106.9
1250	-117.7	-112.3	-109.5	-107.0	-118.7	-113.2	-110.2	-107.6
1600	-119.2	-113.9	-110.9	-107.9	-120.3	-114.9	-111.9	-109.3
2000	-120.6	-115.4	-112.5	-109.6	-121.6	-116.4	-113.5	-110.8
2500	-121.7	-116.5	-113.2	-110.0	-122.3	-117.4	-114.2	-110.9
3100	-122.7	-117.3	-114.2	-111.2	-123.7	-118.5	-115.7	-112.9
4000	-123.8	-118.7	-115.8	-113.0	-124.7	-119.5	-116.4	-113.2

TABLE 7. Measured One-Third Octave Sound Pressure Levels, Accelerations and Strains for Configuration No. 1, Experiment No. 1

Center Frequency f_c (Hz)	Sound Pressure Levels			Acceleration Response Levels					Strain Levels	
	dB/third-octave									
	Re: 2×10^{-5} N/m^2			Re: 1.0 g					Re: 1.0 μ in./in.	
	External		Internal	Skin					Axial	Circumf.
	M1	M3	M2	A1	A2	A3	A4	A5	SG 1	SG 2
50	125.0	120.0	100.0					-10.0	8.5	17.7
63	128.0	121.0	110.0					-12.0	9.5	15.1
80	125.0	119.0	101.0	- 8.0	- 8.0	- 9.0	-10.0	-10.0	5.9	8.5
100	122.6	125.0	102.0	- 2.6	- 2.0	- 2.0	- 3.0	- 4.0	11.9	19.9
125	126.0	119.2	119.0	10.0	11.0	10.4	10.0	11.0	21.5	30.5
160	124.0	123.5	121.5	6.6	9.0	8.0	6.0	6.0	18.5	27.9
200	120.0	122.0	106.5	4.0	5.0	- 2.0	1.0	3.0	8.9	19.5
250	124.0	121.7	112.0	13.0	14.0	7.6	9.6	9.6	15.9	22.5
315	123.5	120.5	116.5	13.0	12.0	8.4	13.0	11.0	14.5	13.5
400	122.5	123.3	119.6	15.6	13.0	10.0	13.0	14.0	13.5	23.1
500	124.7	125.0	115.2	17.0	17.0	14.0	16.0	15.0	14.5	22.5
630	126.0	123.1	116.0	17.0	18.0	16.0	15.6	15.6	13.5	21.9
800	122.5	122.5	116.5	17.0	17.0	16.0	16.0	16.0	13.5	19.5
1000	120.0	118.5	113.0	11.0	11.0	12.0	11.0	12.0	10.5	15.5
1250	116.8	115.5	112.3	6.6	6.6	8.4	6.0	6.0	6.9	13.5
1600	116.5	114.5	110.0	1.0	2.0	2.0	1.0	0	5.5	9.1
2000	112.0	111.0	105.0	- 7.0	- 7.0	- 6.0	- 8.0	- 7.6	0.5	3.5

TABLE 8. Measured One-Third Octave Sound Pressure Levels, Accelerations and Strains for Configuration No. 1, Experiment No. 2

Center Frequency f_c (Hz)	Sound Pressure Levels			Acceleration Response Levels					Strain Levels	
	dB/third-octave									
	Re: 2×10^{-5} N/m^2			Re: 1.0 g					Re: 1.0 μ in./in.	
	External		Internal	Skin			Bulkheads		Axial	Circumf.
							Upper	Lower		
	M1	M3	M2	A1	A3	A4	A2	A5	SG1	SG2
50	121.7	123.2	104.5	—					6.5	11.5
63	122.0	118.0						-16.0	12.9	3.5
80	123.0	119.5	98.0	-12.0	- 8.0	-10.0	- 4.0	- 5.6	2.1	6.7
100	121.0	125.0	101.5	- 2.4	-10.0	- 4.0	- 9.6	-14.6	3.9	12.5
125	123.0	121.2	121.6	4.4	5.0	6.0	- 2.0	-11.0	13.9	15.1
160	122.2	124.1	120.0	8.0	8.0	6.0	1.0	- 7.0	12.3	21.5
200	123.0	119.0	108.0	5.0	- 1.0	2.6	- 3.0	- 4.0	2.5	13.5
250	122.5	121.1	108.5	13.6	8.4	11.4	- 3.0	- 5.4	7.1	15.9
315	121.8	122.7	116.2	14.0	9.0	12.0	- 8.0	-10.4	9.5	16.7
400	125.0	124.0	119.5	14.0	17.0	14.4	2.4	0	6.3	15.5
500	122.2	124.0	118.2	14.4	13.0	18.0	- 1.6	- 4.6	8.5	14.9
630	123.0	123.0	117.0	18.0	15.0	18.6	1.4	- 2.0	6.7	13.5
800	123.0	123.0	115.7	16.6	17.0	17.6	2.4	- 1.0	6.7	12.5
1000	120.0	118.2	115.0	12.0	14.4	12.0	0.8	- 2.0	3.5	8.5
1250	118.0	117.2	114.0	7.0	9.0	8.4	3.0	- 1.0	0.5	6.5
1600	115.5	116.5	112.0	1.0	3.0	1.4	- 7.0	- 2.0	- 0.5	5.5
2000	113.0	113.2	106.0	- 7.0	- 5.0	- 6.0	- 1.0	- 5.0	- 7.1	- 3.1

TABLE 9. Measured One-Third Octave Sound Pressure Levels, Accelerations and Strains in Configuration No. 1, Experiment No. 3

Center Frequency f_c (Hz)	Sound Pressure Levels			Acceleration Response Levels					Strain Levels	
	dB/third-octave									
	Re: 2×10^{-5} N/m^2			Re: 1.0 g					Re: 1.0 μ in./in.	
	External		Internal	Skin			Bulkheads		Axial	Circumf.
							Upper	Lower		
	M1	M3	M2	A1	A3	A4	A2	A5	SG 1	SG 2
50	123.0	120.0	94.0		- 6.4	-13.0		-26.0	9.5	15.1
63	124.0	116.0	104.0	-10.0	-12.0	-14.0	-10.4	-15.2	11.1	5.5
80	123.5	119.0	98.0	- 4.0	- 5.0	- 6.4	- 4.6	- 5.8	1.5	1.1
100	123.0	122.5	99.5	- 4.0	- 8.0	- 1.0	- 6.0	-15.0	6.1	12.1
125	124.0	121.0	123.0	4.8	6.8	9.2	- 2.0	-14.4	13.1	19.5
160	125.2	124.0	118.0	8.0	10.0	5.2	0	- 4.4	10.1	19.5
200	121.0	120.0	105.0	4.0	1.2	3.6	- 2.0	- 3.4	3.1	12.5
250	122.0	122.0	105.3	12.0	8.0	11.8	- 3.0	- 4.6	10.1	17.5
315	122.8	122.0	115.0	14.0	0.4	13.4	- 7.0	- 9.2	9.5	15.5
400	123.8	123.0	120.0	14.6	13.8	14.6	3.0	3.0	6.5	15.1
500	125.0	124.0	117.8	18.0	15.0	18.6	0	- 2.0	8.5	18.5
630	124.0	123.8	117.0	18.0	16.2	19.0	5.0	- 0.6	6.5	13.5
800	124.0	123.8	116.5	17.0	18.0	18.0	4.0	- 1.2	6.9	13.5
1000	120.0	120.0	116.0	12.6	16.0	13.2	2.0	0.4	2.1	9.1
1250	118.0	118.0	115.0	7.4	12.0	9.0	4.6	1.0	1.5	7.7
1600	117.0	118.0	114.0	2.0	4.8	4.0	4.2	- 1.0	- 0.5	4.9
2000	113.0	114.0	106.0	- 6.0	- 4.0	- 4.0	0.8	- 4.0	- 6.1	- 2.9

TABLE 10. Measured One-Third Octave Sound Pressure Levels and Accelerations for Configuration No. 2, Experiment No. 4

Center Frequency f_c (Hz)	Sound Pressure Levels			Acceleration Response Levels			
	dB/third-octave						
	Re: 2×10^{-5} N/m^2			Re: 1.0 g			
	External		Internal	Skin		Ring	
	M1	M3	M2	A3	A5	A1	A4
50	117.8	119.5	94.0	-20.0	-22.0	-22.0	-22.0
63	118.5	124.0	104.0	-18.0	-17.0	-17.6	-17.0
80	124.0	125.0	108.2	-15.0	-15.0	-18.0	-19.0
100	125.0	125.8	101.0	-10.0	- 7.6	- 6.0	-14.0
125	125.5	126.0	116.0	6.0	0	8.0	0
160	127.0	128.0	120.0	5.0	2.4	2.0	2.0
200	123.0	126.0	101.0	4.0	5.0	0	- 2.0
250	123.8	124.5	104.0	9.0	7.4	10.0	8.0
315	122.8	123.0	114.0	11.0	10.0	6.0	4.0
400	122.3	123.5	112.0	9.0	11.0	7.0	7.4
500	120.0	121.5	108.0	10.0	9.0	10.0	8.4
630	118.0	120.0	108.0	8.0	10.0	10.0	9.6
800	115.0	116.0	104.0	6.0	6.0	6.0	7.0
1000	110.0	113.0	104.0	3.0	4.0	4.0	3.0
1250	106.0	109.0	104.0	- 1.0	- 1.0	- 1.0	- 1.0
1600	104.0	106.0	100.0	- 6.0	- 6.4	- 4.4	- 6.0
2000	110.0	102.5	98.0	- 8.0	- 8.0	- 7.6	- 8.0
2500	97.0	98.0	94.0	-10.0	-12.0	-10.0	-11.0
3150	94.0	95.5	91.0	-14.0	-15.0	-13.0	-14.0
4000	93.0	94.0	90.0	-16.0	-19.0	-15.0	-20.0
5000	94.0	93.0	91.0	-18.0	-22.0	-20.0	-22.0

TABLE 11. Measured One-Third Octave Sound Pressure Levels and Accelerations for Configuration No. 3, Experiment No. 5

Center Frequency f_c (Hz)	Sound Pressure Levels			Acceleration Response Levels			
	dB/Third-Octave						
	Re: 2×10^{-5} N/m^2			Re: 1.0g			
	External		Internal	Ring		Stringer	Ring Stringer
	M1	M3	M2	A2	A4	A3	A1
50	118.0	121.0	96.0	-22.0	-26.0	-19.0	-20.0
63	123.0	124.0	106.0	-20.0	-21.0	-18.0	-15.0
80	124.0	122.0	108.0	-15.0	-18.0	-15.0	-14.0
100	126.0	124.0	101.0	- 8.0	- 8.0	- 5.0	- 2.0
125	128.0	125.0	114.0	4.0	8.0	7.0	12.0
160	126.0	126.0	118.0	6.0	4.0	2.0	0.0
200	124.0	124.0	115.0	- 2.0	2.0	0.0	0.0
250	125.5	125.0	116.0	5.0	10.0	5.0	7.0
315	124.0	123.0	111.0	2.0	7.0	6.0	5.0
400	123.0	122.0	117.0	6.0	10.0	7.0	5.0
500	122.0	121.0	111.0	7.0	2.0	7.0	7.0
630	120.0	120.0	110.0	6.0	10.0	5.0	6.0
800	116.0	117.0	105.0	5.0	8.0	3.0	5.0
1000	114.0	114.0	107.0	- 1.0	6.0	0.6	3.0
1250	110.0	110.0	105.0	- 5.0	2.0	- 1.0	- 2.0
1600	108.0	108.0	103.0	-10.0	- 2.0	- 4.0	- 4.0
2000	104.0	103.0	99.0	-16.0	- 6.0	- 6.0	-11.0
2500	101.0	98.0	96.0	-19.0	-19.0	-11.0	- 9.0
3150	97.0	93.0	90.8	-24.0	-12.0	-12.0	-15.0
4000	93.0	92.0	90.2	0.0	-19.0	-16.0	-15.0
5000	91.0	91.0	90.4	0.0	-25.6	-17.0	-16.0

TABLE 12. Measured One-Third Octave Sound Pressure Levels, Accelerations and Strains for Configuration No. 4, Experiment No. 6

Center Frequency f_c (Hz)	Sound Pressure Levels		Acceleration Response Levels			
	dB/Third-Octave					
	Re: 2×10^{-5} N/m^2		Re: 1.0 g			
	External	Internal	Skin	Ring	Stringer	Ring Stringer
	M1	M2	A4	A2	A3	A1
20	97.0					
25	112.0	82.0		-19.0		-19.0
31	122.0	86.0		-25.0	-23.0	-25.0
40	120.0	88.0		-25.0	-24.0	-24.0
50	123.0	96.0	-18.0	-25.0	-20.0	-19.0
63	124.0	104.0	-14.0	-21.0	-13.0	-18.0
80	124.0	106.0	- 4.0	- 7.0	- 7.0	-10.0
100	126.0	105.0	10.0	- 4.0	2.0	0.0
125	128.0	116.0	17.0	7.0	10.0	8.0
160	126.0	122.0	12.0	6.0	8.0	4.0
200	127.0	106.0	10.0	2.0	2.0	0.0
250	124.0	106.0	12.0	10.0	6.0	10.0
315	126.0	110.0	12.0	6.0	7.0	4.0
400	125.0	120.0	12.0	11.0	8.0	7.0
500	122.0	114.0	10.0	11.0	8.0	7.0
630	122.0	110.0	11.0	10.0	6.0	8.0
800	119.0	106.0	8.0	7.0	3.0	5.0
1000	115.0	107.0	6.0	4.0	0.0	2.0
1250	114.0	106.0	2.0	0.0	0.0	- 1.0
1600	110.0	102.0	- 3.0	- 6.0	- 4.0	- 6.0
2000	106.0	98.0	- 7.0	- 8.0	- 7.0	-11.0
2500	104.0	94.0	-11.0	-10.0	-12.0	-12.0
3150	100.0	89.0	-13.0	-12.0	-11.0	-13.0
4000	97.0	87.0	-17.0	-16.0	-16.0	-10.0

TABLE 13. Measured One-Third Octave Band Pressure Levels Obtained During Noise Reduction Experiment No. 7

Frequency f_c Hz	Third-Octave Sound Pressure Levels - dB Re: 2×10^{-5} N/m^2				
	External Microphones		Internal Microphones		
			Mid-Length		
	*Far-Field M1	**Near-Field M2	Near Wall M3	On Axis M4	Upper Corner M5
50	120.0	121.0	-	-	-
63	122.0	123.0	102.0	-	111.0
80	124.0	127.0	100.0	106.0	116.0
100	128.0	127.0	110.0	108.0	109.0
125	128.0	129.0	124.0	123.0	121.0
160	128.0	128.0	130.0	122.0	125.0
200	128.0	131.0	120.0	104.0	126.0
315	127.0	130.0	117.0	110.0	124.0
400	124.0	126.0	116.0	115.0	121.0
500	126.0	126.0	121.0	108.0	123.0
630	121.0	122.0	115.0	109.0	118.0
800	117.0	118.0	112.0	116.0	114.0
1000	114.0	117.0	110.0	106.0	112.0
1250	111.0	111.0	108.0	105.0	108.0
1600	108.0	106.0	104.0	104.0	103.0
2000	105.0	103.0	102.0	101.0	101.0
2500	101.0	100.0	101.0	100.0	100.0
3150	97.0	97.0	98.0	-	-

* Far-field implies a distance of several shell diameters away from test specimen

** Near-field implies a distance within 1.0 in. of the exterior surface of the test specimen

TABLE 14. Measured One-Third Octave Sound Pressure Levels for Various Positions Along the Exterior Surface of the Test Specimen

Frequency f_c Hz	Third-Octave Sound Pressure Levels - dB Re: 2×10^{-5} N/m^2					
		** Near-Field at Various Heights, h, from Floor				
	*Far-Field	h = 0.5 ft	h = 2.5 ft	h = 4.5 ft	h = 6.5 ft	h = 8.5 ft
50	120.0	123.0	122.5	124.0	122.0	121.0
63	122.0	128.0	126.0	126.0	123.0	122.0
80	122.0	127.0	125.0	128.0	125.0	126.0
100	127.0	130.0	128.0	128.0	128.5	125.0
125	128.0	129.0	128.0	128.0	128.0	127.0
160	128.0	131.0	129.0	129.0	129.5	129.0
200	127.0	132.0	131.0	131.0	130.0	128.0
250	126.0	129.5	130.5	129.0	127.5	126.5
315	125.0	128.0	129.0	127.0	127.0	125.0
400	124.0	127.0	127.5	127.0	128.0	126.0
500	125.5	128.0	128.5	127.5	129.0	127.0
630	121.0	122.0	122.0	123.0	123.5	121.0
800	116.5	118.0	119.0	120.0	121.5	118.0
1000	114.5	116.0	118.0	117.5	117.5	115.0
1250	111.5	111.0	114.0	113.5	113.0	111.0
1600	108.0	107.5	110.0	106.5	109.0	108.5
2000	105.0	103.5	106.0	106.5	106.0	105.0
2500	101.0	101.0	102.0	102.0	101.0	103.0

* Far-field implies a distance of several shell diameters away from test specimen

** Near-field implies a distance within 1.0 in. of the exterior surface of the test specimen

TABLE 15. Far-Field and Near-Field Sound Pressure Levels around the Circumference at Mid-Length of Cylinder

Frequency f_c (Hz)	Third-Octave Sound Pressure Levels				
	dB Re: 2×10^{-5} N/m^2				
	* Far Field	** Near Field at Various Angles, θ. ***			
		θ=0°	θ=90°	θ=180°	θ=270°
50	123.0	121.0		124.0	
63	124.0	128.0	125.0	120.0	126.0
80	124.0	127.0	126.0	126.0	127.0
100	128.0	130.0	128.0	126.0	129.0
125	128.0	130.0	132.0	129.0	129.0
160	129.0	130.0	131.5	130.0	130.5
200	129.0	130.0	131.5	131.0	130.0
250	128.0	129.0	131.0	130.0	130.0
315	125.0	128.0	127.5	127.0	129.0
400	125.0	126.0	127.0	129.0	129.0
500	123.0	126.5	126.0	127.0	127.0
630	118.0	122.0	121.0	122.0	123.0
800	116.0	119.0	119.0	120.5	119.0
1000	113.0	115.5	116.5	117.5	117.0
1250	109.0	112.0	111.0	112.5	113.0
1600	104.0	108.5	108.0	109.5	109.0
2000	101.0	103.0	104.0	105.0	106.0
2500			100.0	101.0	101.0

*** Angles are counted leftwise starting from the point in correspondence with the horn.

** Near-field implies a distance within 1.0 in. of the exterior surface of the test specimen

* Far-field implies a distance of several shell diameters away from test specimen

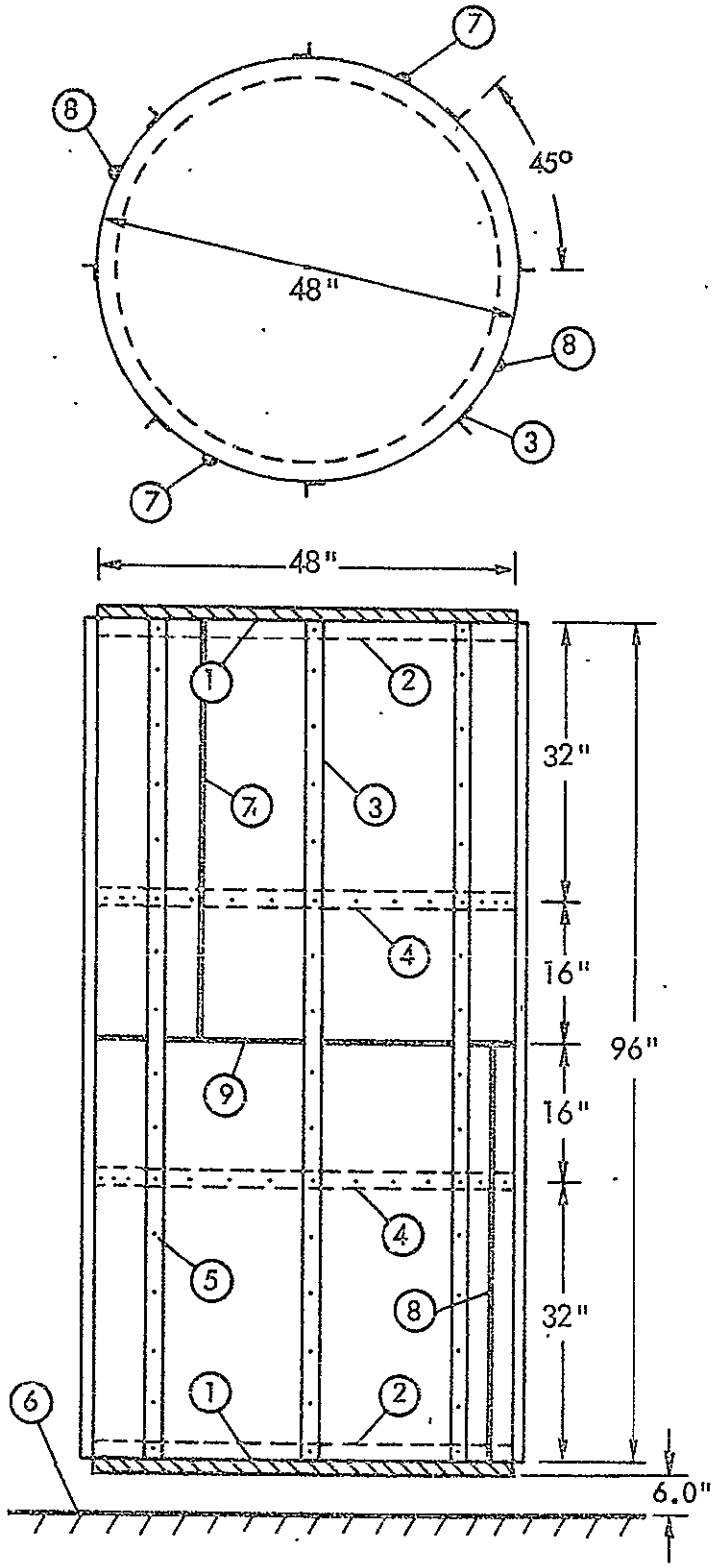

1. Two flat circular plywood bulkheads
2. Two angle section end rings
3. Eight angle section stringers
4. Two channel section ring frames
5. 176 pop rivets
6. Floor of reverberation room
7. Upper axial weld lines
8. Lower axial weld lines
9. Circumferential weld line

FIGURE 1. Geometry and Dimensions of Fully Stiffened Configuration No. 4

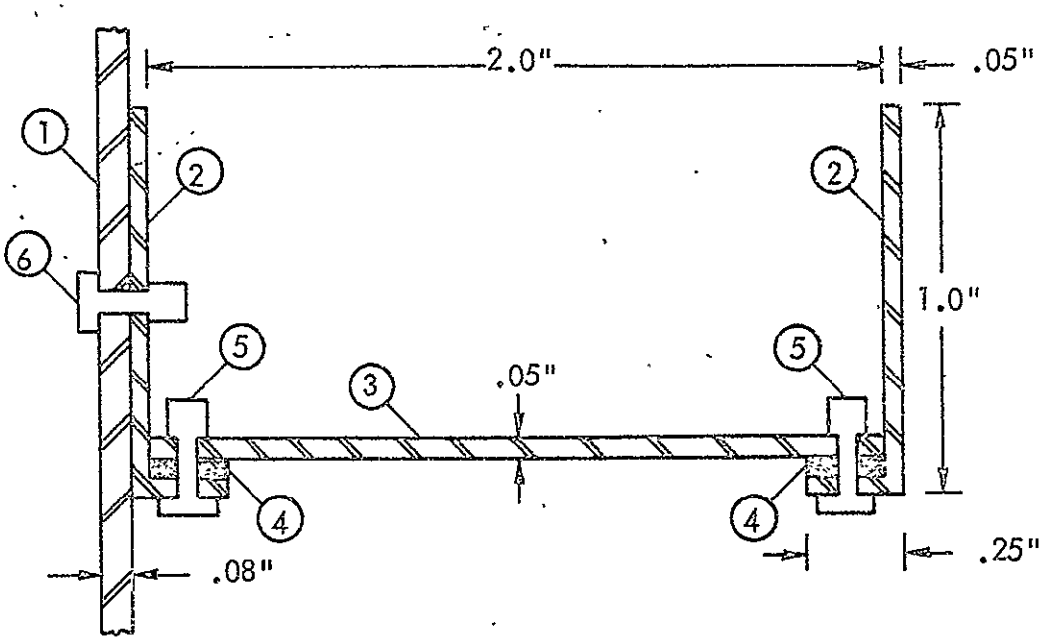

1. Shell wall (outer surface).
2. Flanges of ring frame.
3. Web of ring frame.
4. Continuous bead of high strength epoxy glue.
5. Rivets between flanges and web; total of 48 per ring frame; average circumferential spacing between rivets is 6.0 in.
6. Rivet between flange and shell wall; total of 24 per ring frame between stringers; total of 32 per ring frame including those through stringers.

FIGURE 2. Geometry and Dimensions of Cross-Section of Ring Frames

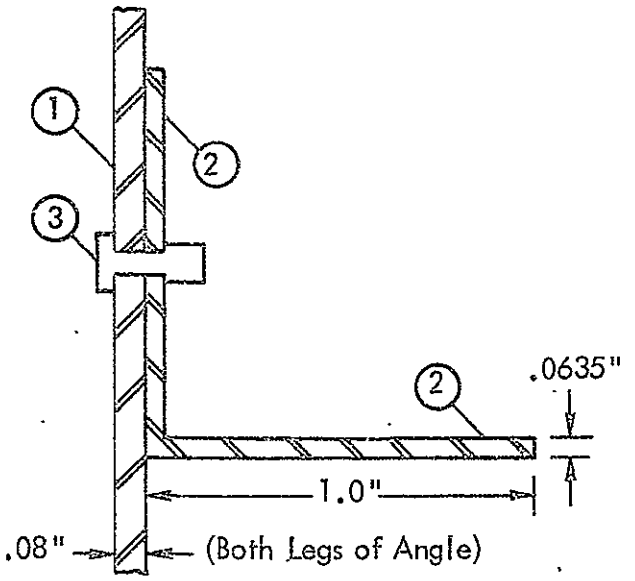

1. Shell wall (inside surface).
2. Legs of angle.
3. Rivet between angle leg and shell wall;
   total of 12 per stringer between rings;
   total of 16 per stringer including those through rings;
   average axial spacing between rivets is 6.0 in.

FIGURE 3. Geometry and Dimensions of Cross-Section of Stringers

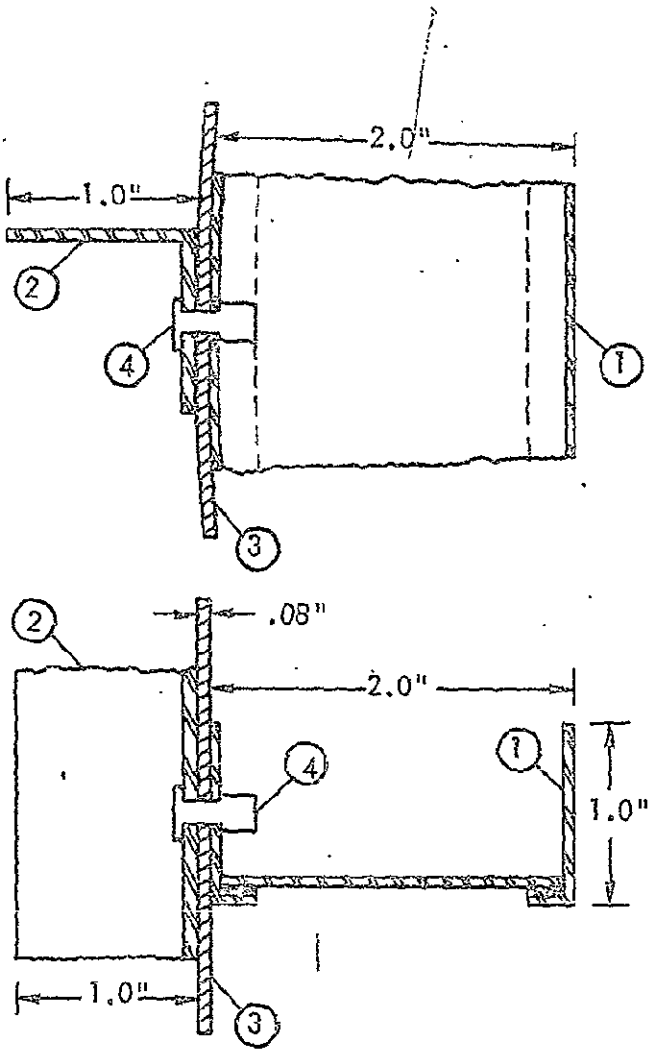

1. Ring frame
2. Stringer
3. Shell wall (inside surface)
4. Rivet through stringer, shell wall and ring frame

FIGURE 4. Geometry and Dimensions of Joint Between Ring Frame, Shell Wall and Stringer

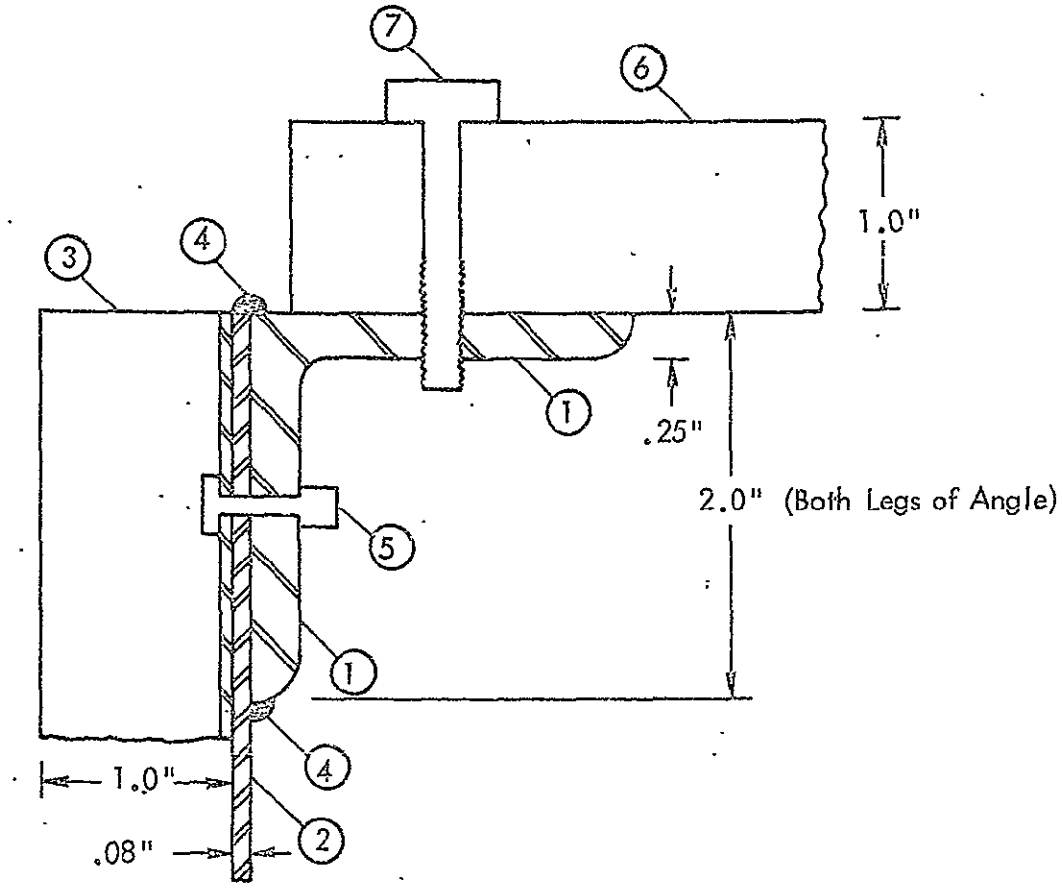

1. Legs of end ring angle.
2. Shell wall (inside surface).
3. Stringer.
4. Spot welds between end ring and shell wall; total of 14-16 per end ring.
5. Rivet through stringer, shell wall and end ring; total of 8 per end ring for 8 stringers; total of two per stringer (at each end).
6. Circular, plywood bulkhead.
7. Machine screw between bulkhead and end ring; total of 8

FIGURE 5. Geometry and Dimensions of Joint Between End Ring, Shell Wall, Stringer and Bulkhead

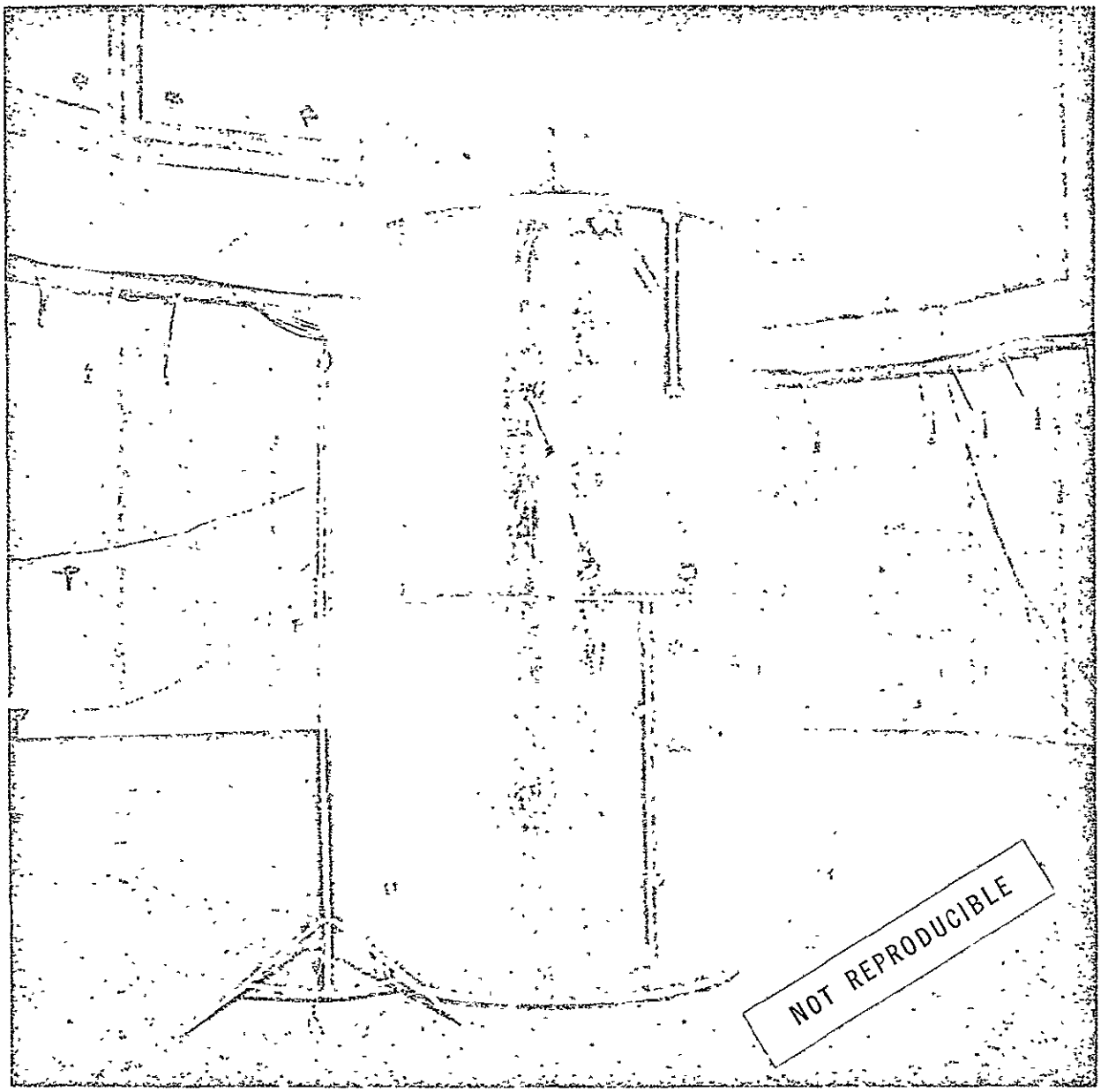

FIGURE 6. Test Specimen Suspended Inside the 100,000 Cubic Foot Wyle Reverberation Room

Instrumentation

M1 = External Microphone located 16.0" above floor

M2 = Internal Microphone

M3 = External Microphone located 16.0" above floor

A1, A2, A3, A4, A5 = External Accelerometers

SG1, SG2 = External Strain Gages

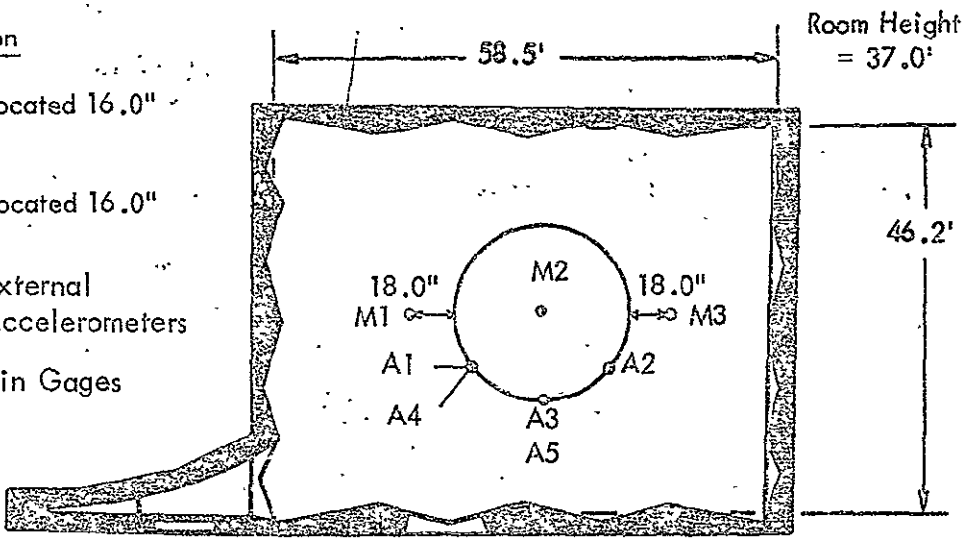

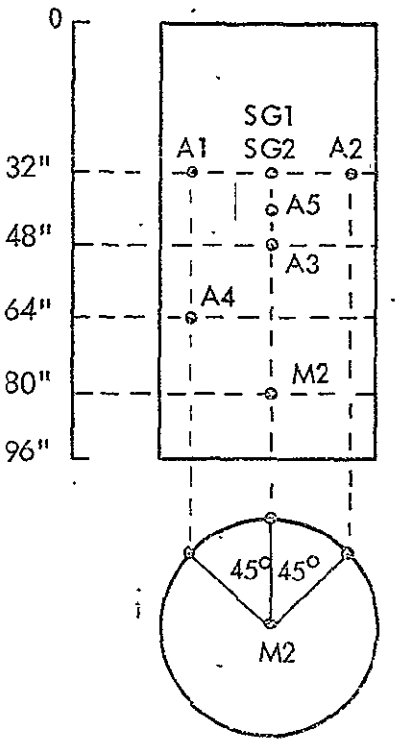

Unstiffened Shell
Configuration No. 1

FIGURE 7. Test Configuration for Experiment No. 1

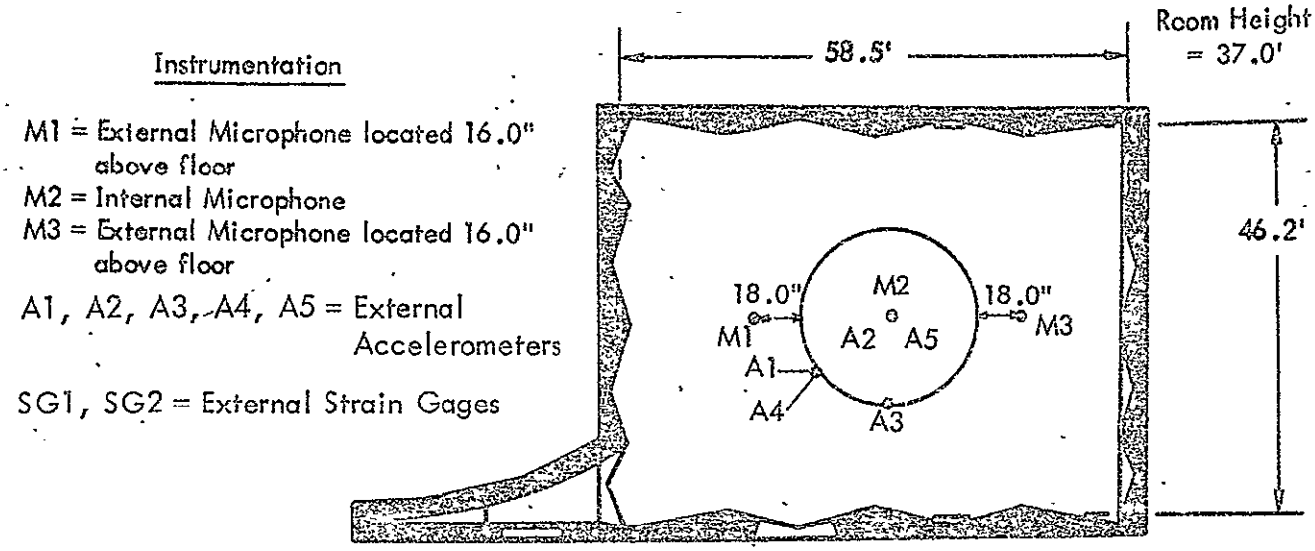

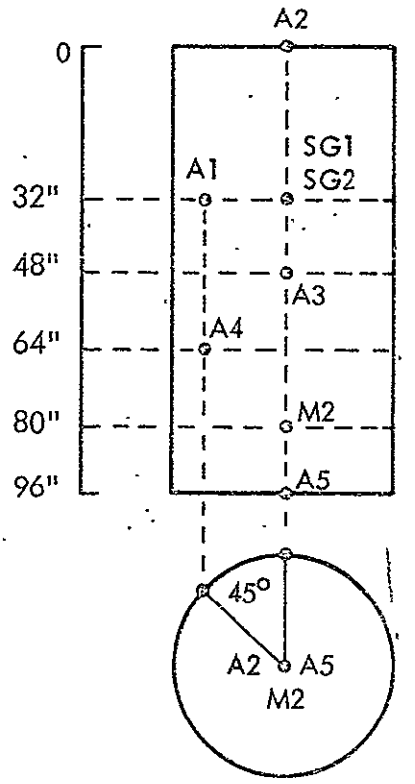

Unstiffened Shell
Configuration No. 1

FIGURE 8. Test Configuration for Experiment No. 2

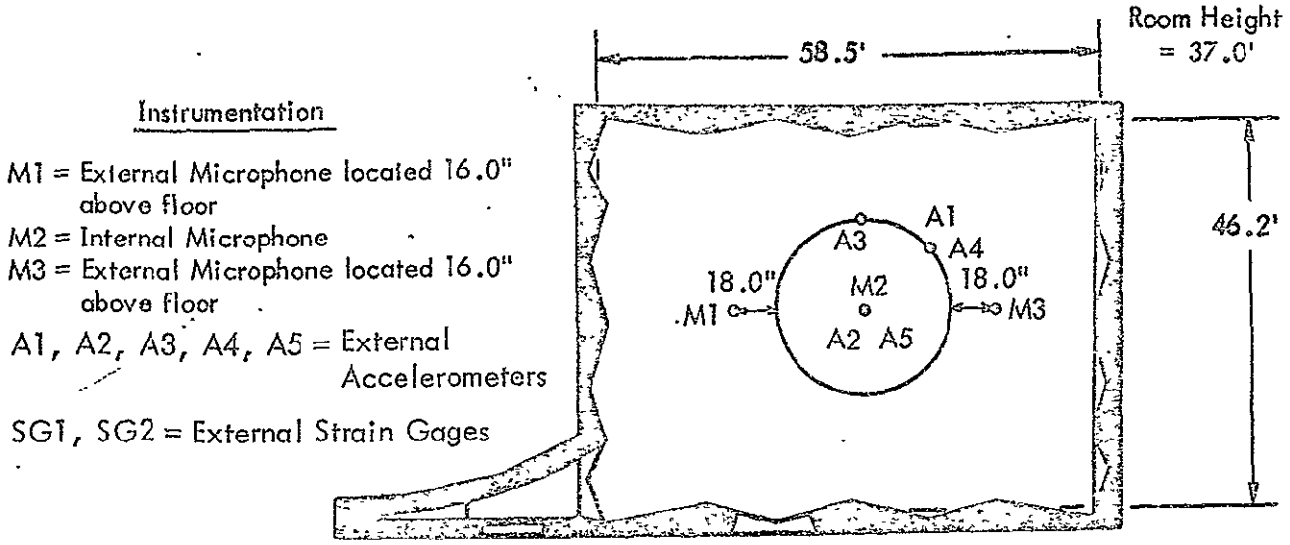

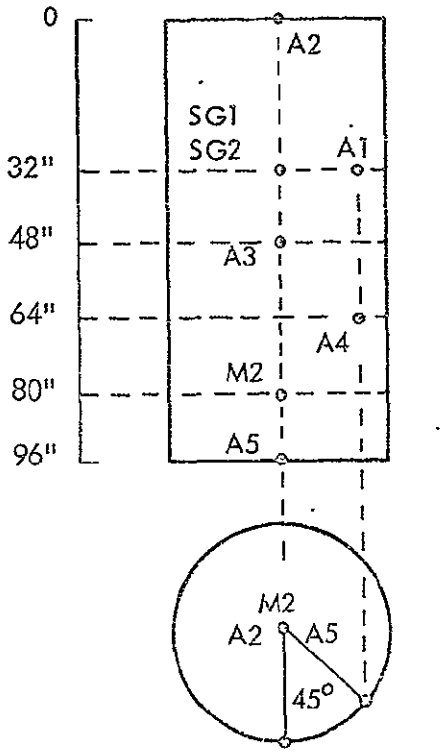

Unstiffened Shell
Configuration No. 1

FIGURE 9. Test Configuration for Experiment No. 3

Instrumentation

M1 = External Microphone located 70.25 in. above floor and 129.3 in. from centerline of test specimen

M2 = Internal Microphone

M3 = External Microphone located 56.75 in. above floor and 74.50 in. from centerline of test specimen

A1, A3, A4, A5 = External Accelerometers

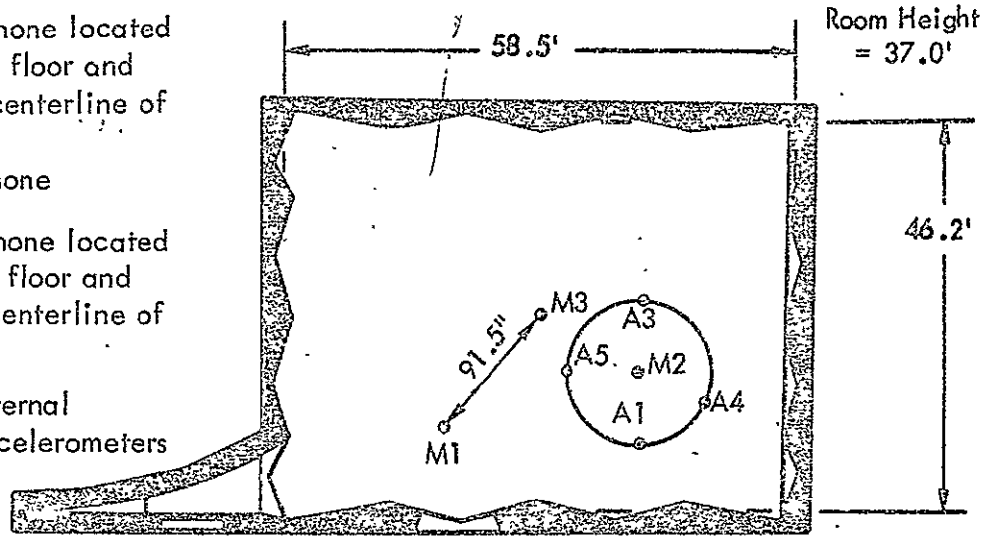

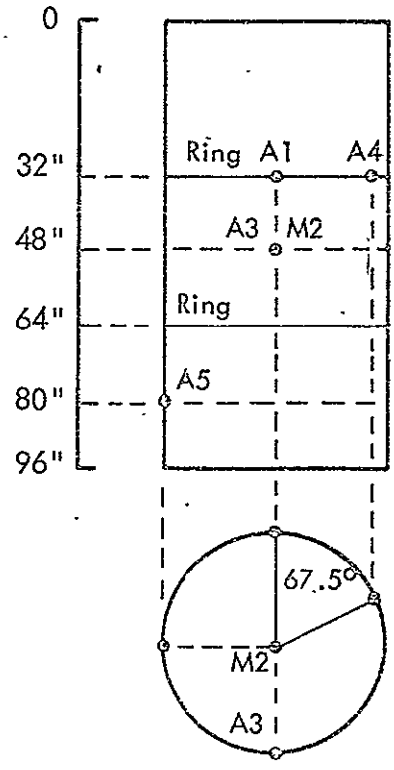

Shell with two rings
Configuration No. 2

FIGURE 10. Test Configuration for Experiment No. 4

Instrumentation

M1 = External Microphone located 70.25 in. above floor and 129.3 in. from centerline of test specimen

M2 = Internal Microphone

M3 = External Microphone located 56.75 in. above floor and 74.50 in. from centerline of test specimen

A1, A2, A3, A4 = External Accelerometers

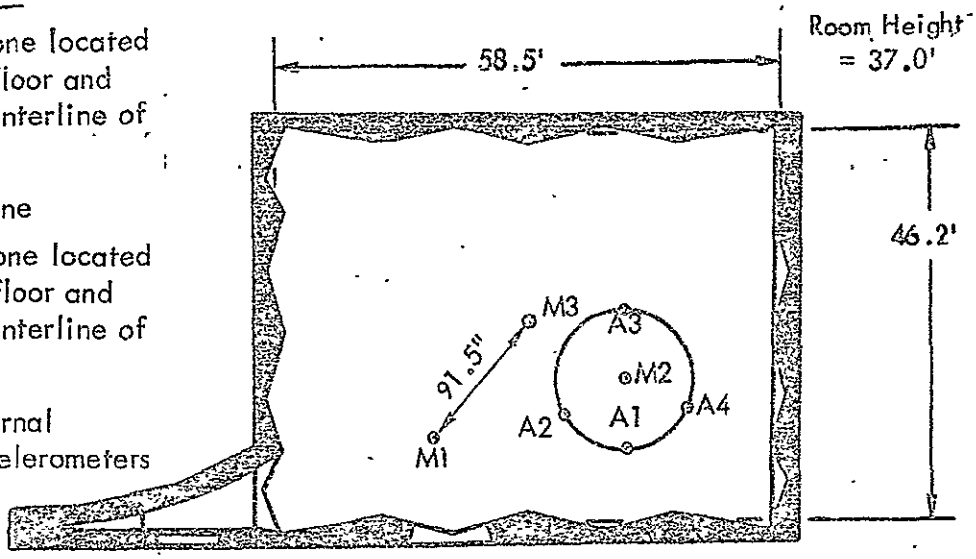

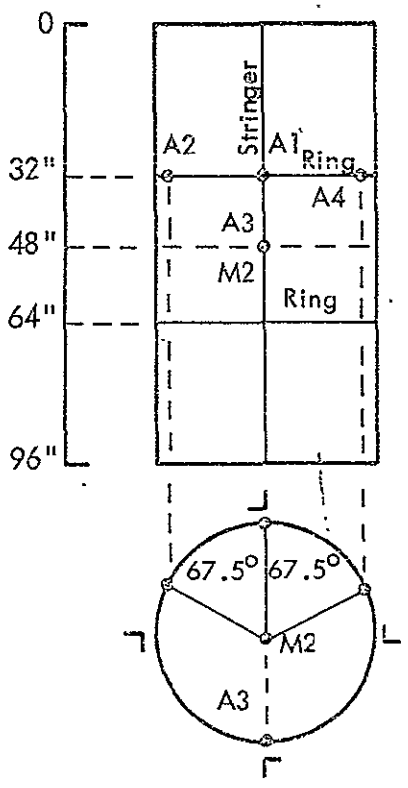

Shell with two Rings and Four Stringers (L)
Configuration No. 3

FIGURE 11. Test Configuration for Experiment No. 5

Instrumentation

M1 = External Microphone located 70.25 in. above floor and 129.3 in. from centerline of test specimen

M2 = Internal Microphone

A1, A2, A3, A4 = External Accelerometers

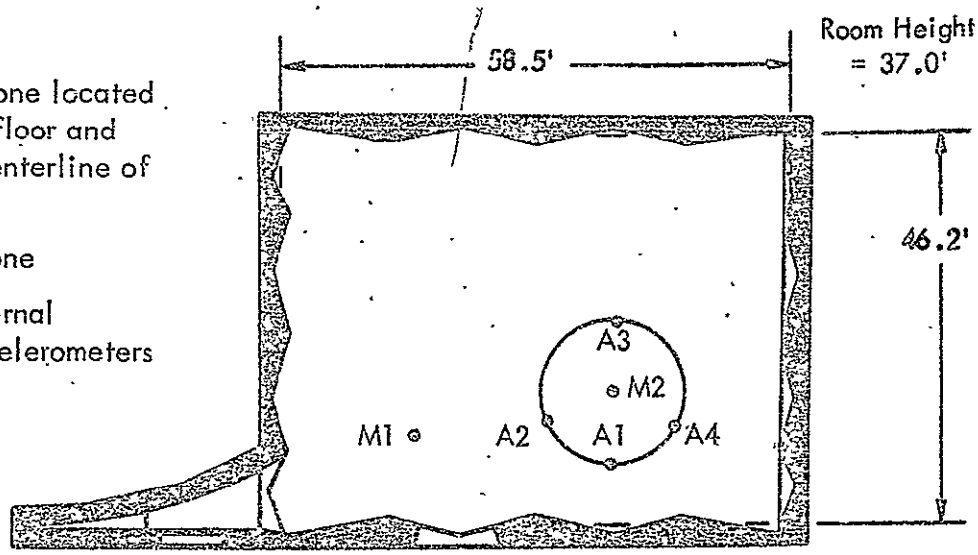

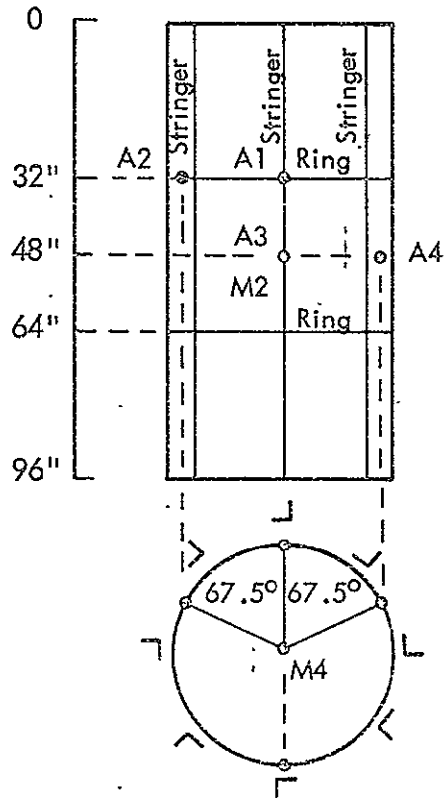

Shell with two Rings and Eight Stringers (L)
Configuration No. 4

FIGURE 12. Test Configuration for Experiment 6

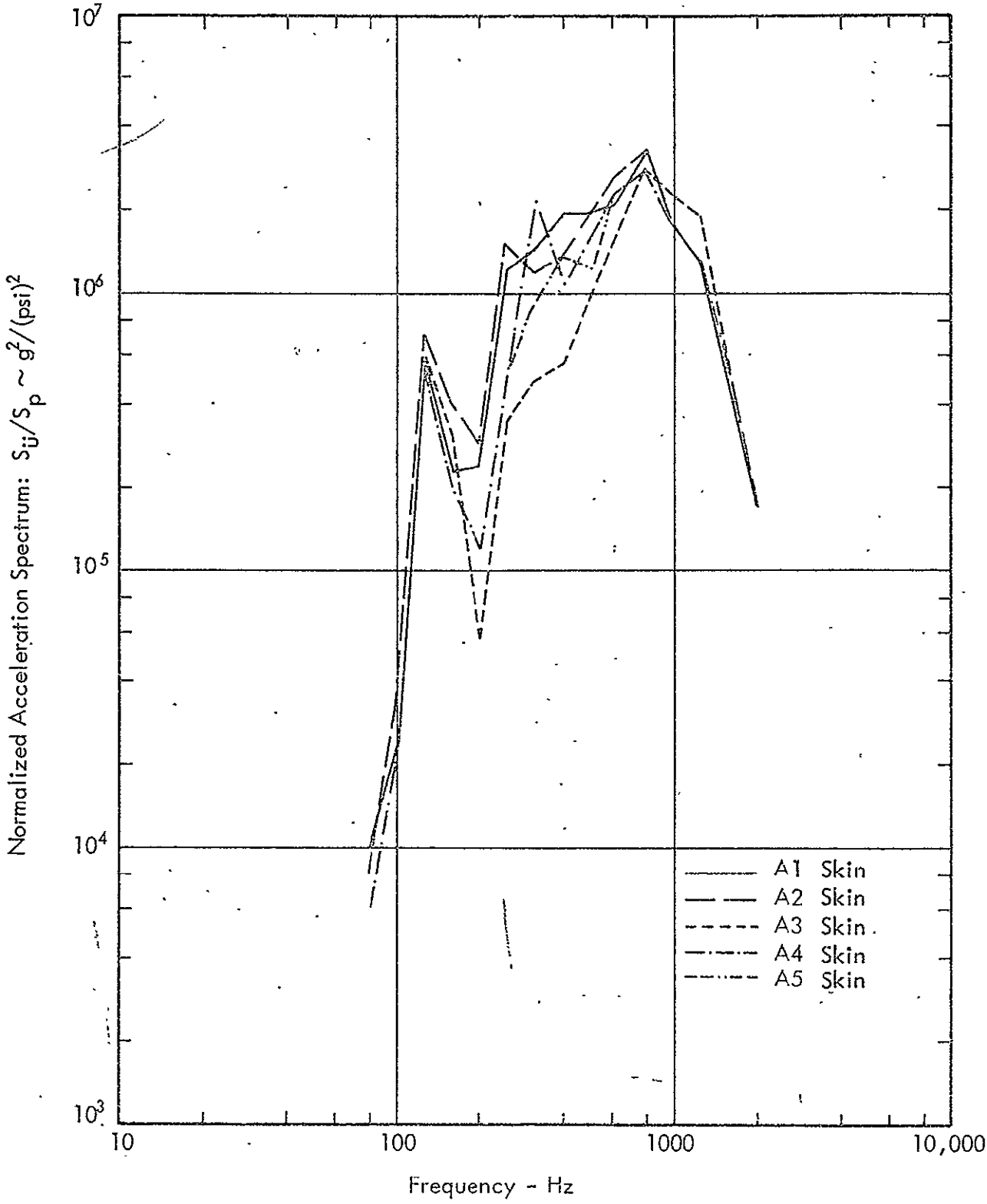

FIGURE 13. Acceleration Responses for Configuration No. 1, Measured During Experiment 1

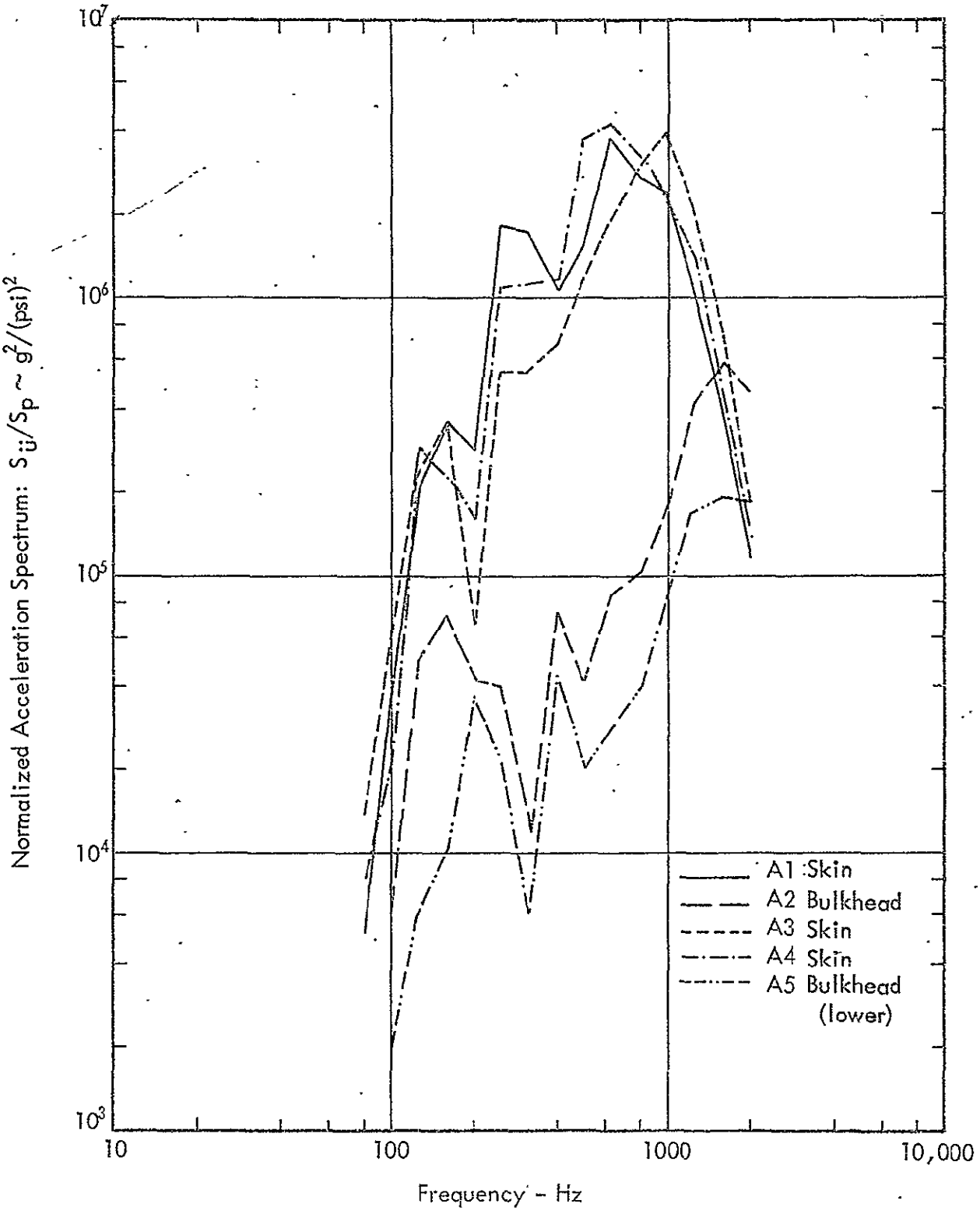

FIGURE 14. Acceleration Responses for Configuration No. 1, and of End Plates Measured During Experiment No. 2

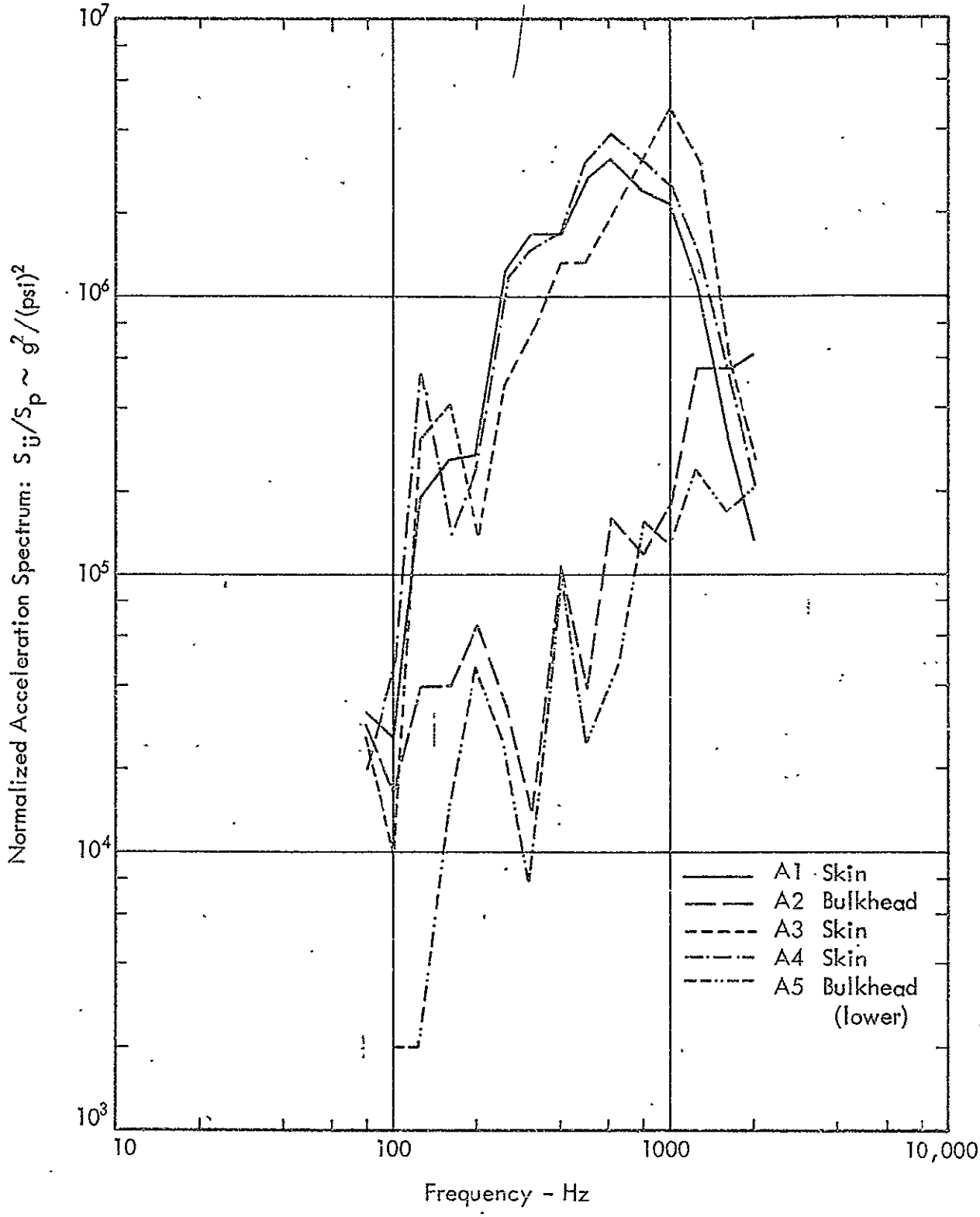

FIGURE 15. Acceleration Responses for Configuration No. 1, and of End Plates Measured During Experiment 3

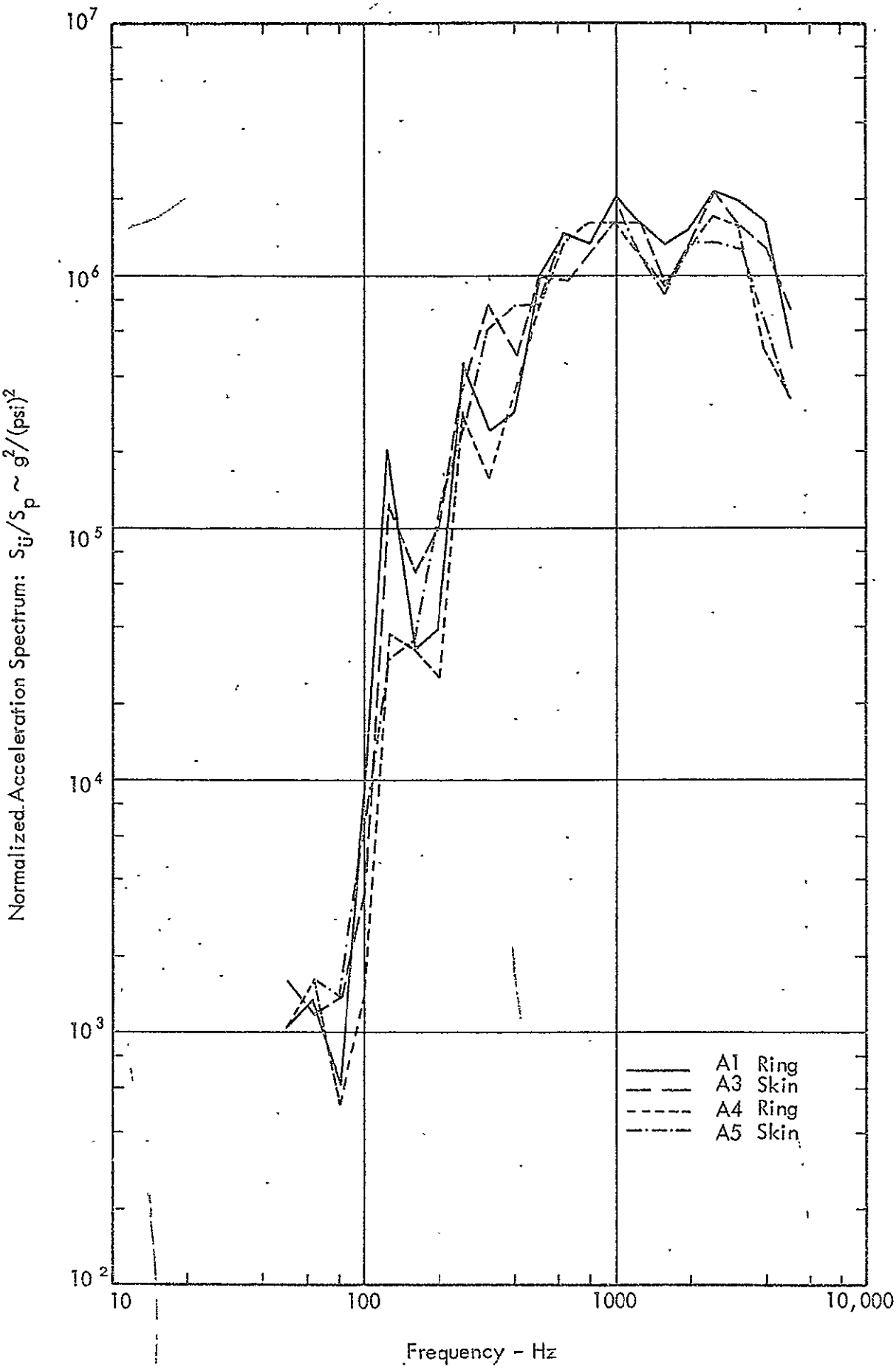

FIGURE 16. Acceleration Responses for Configuration No. 2, Measured During Experiment 4

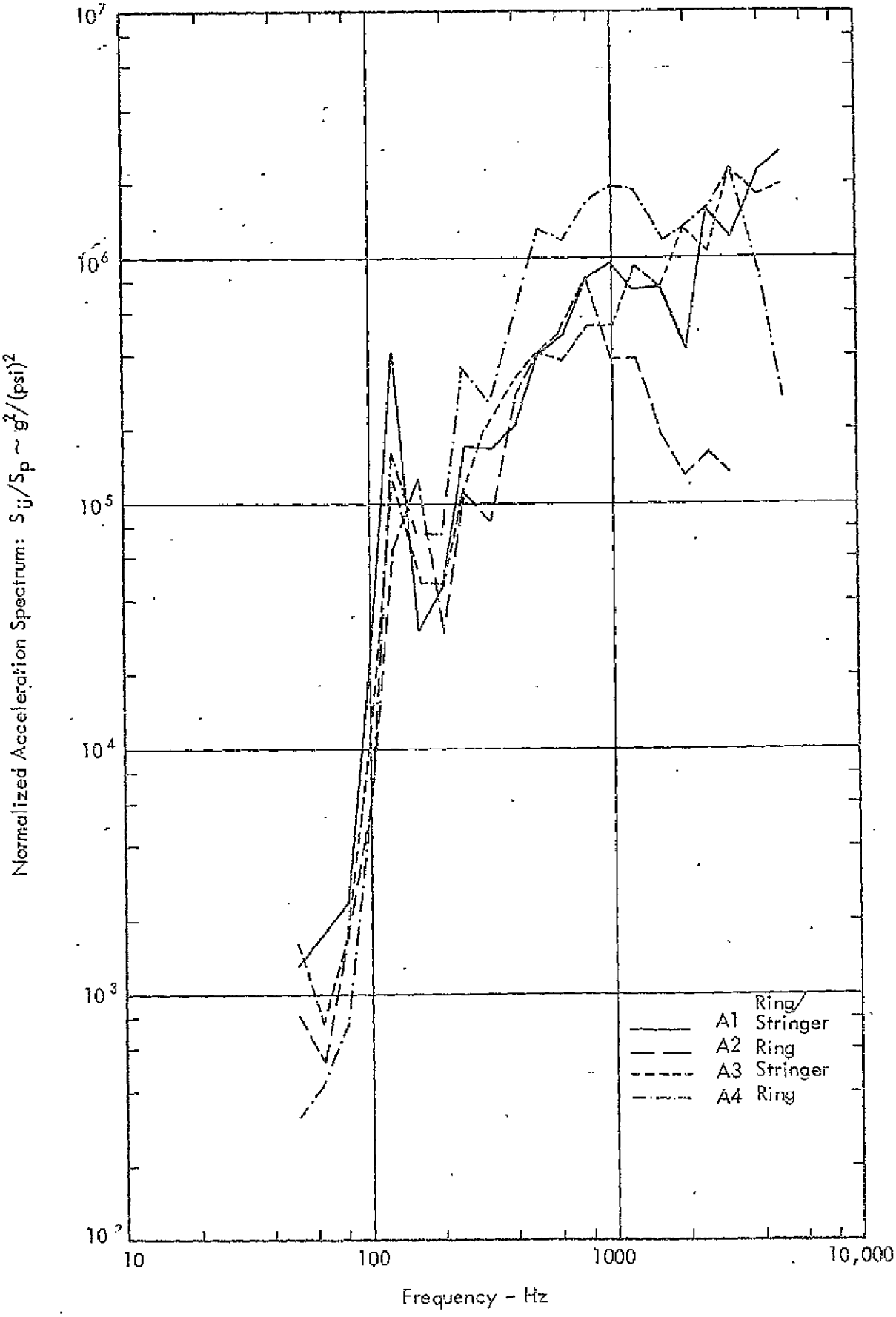

FIGURE 17. Acceleration Responses for Configuration No. 3, Measured During Experiment 5

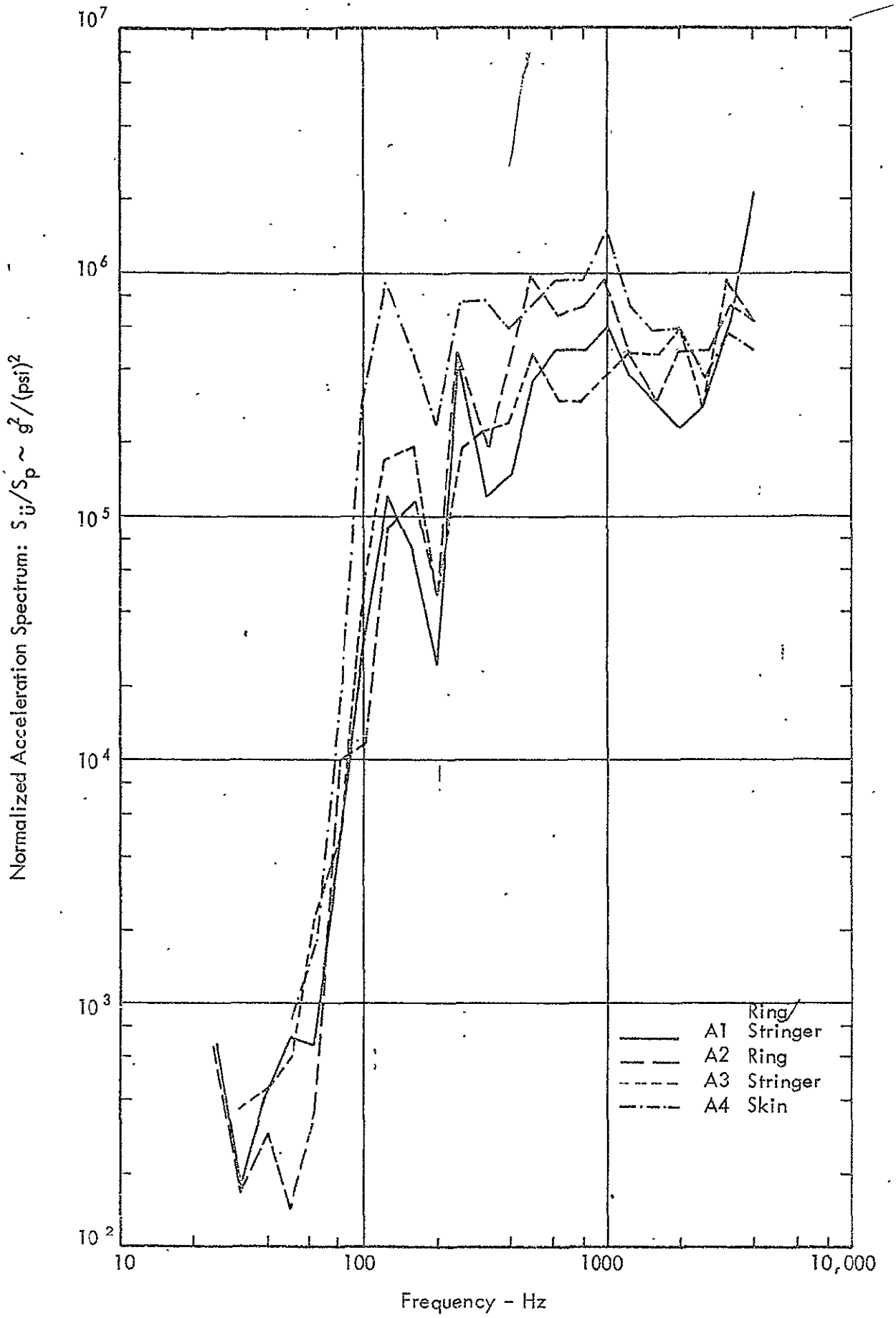

FIGURE 18. Acceleration Responses for Configuration No. 4, Measured During Experiment 6

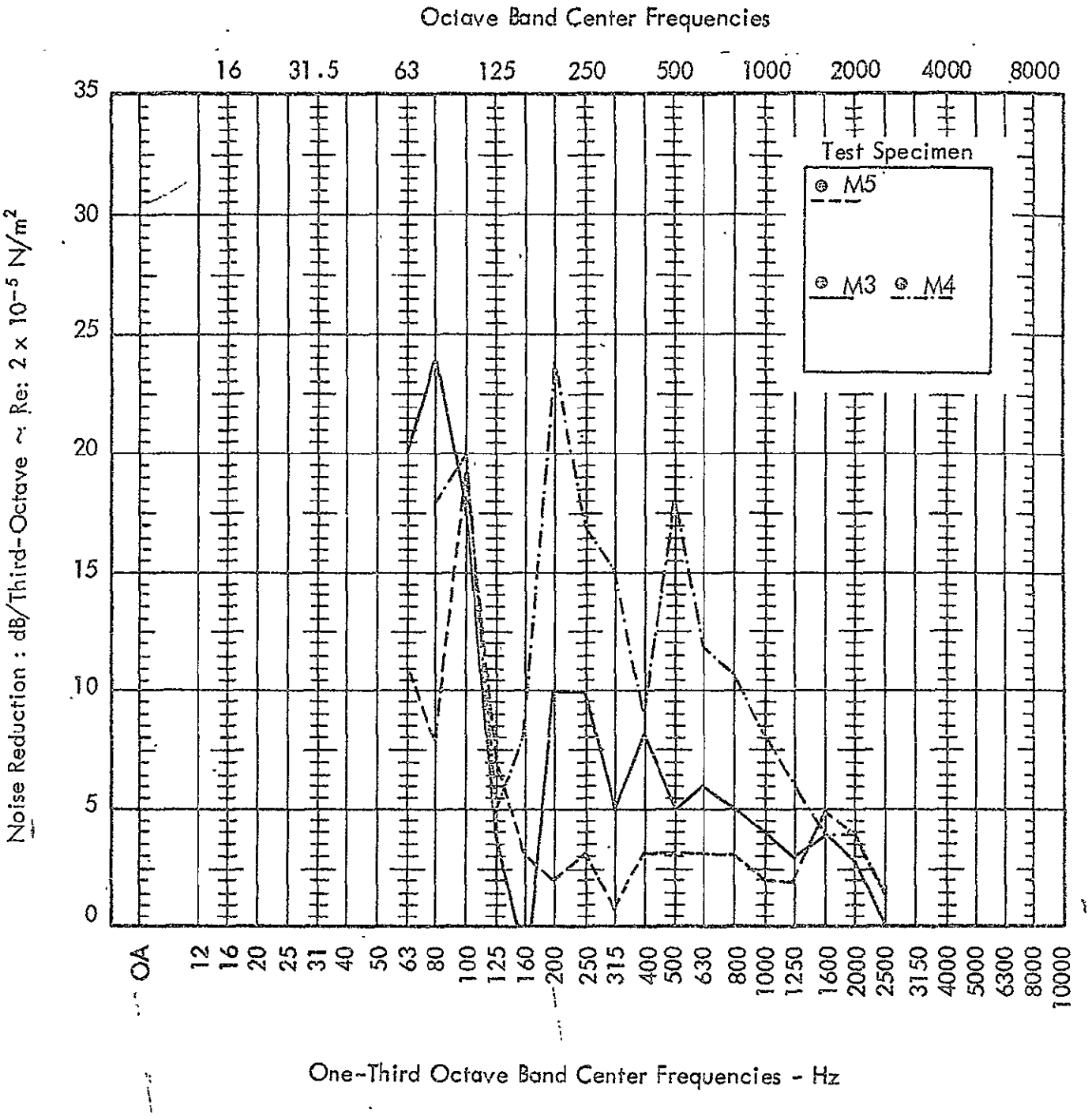

FIGURE 19. Noise Reduction Measured at Different Locations Inside Cylinder, Configuration No. 4, During Experiment No. 7

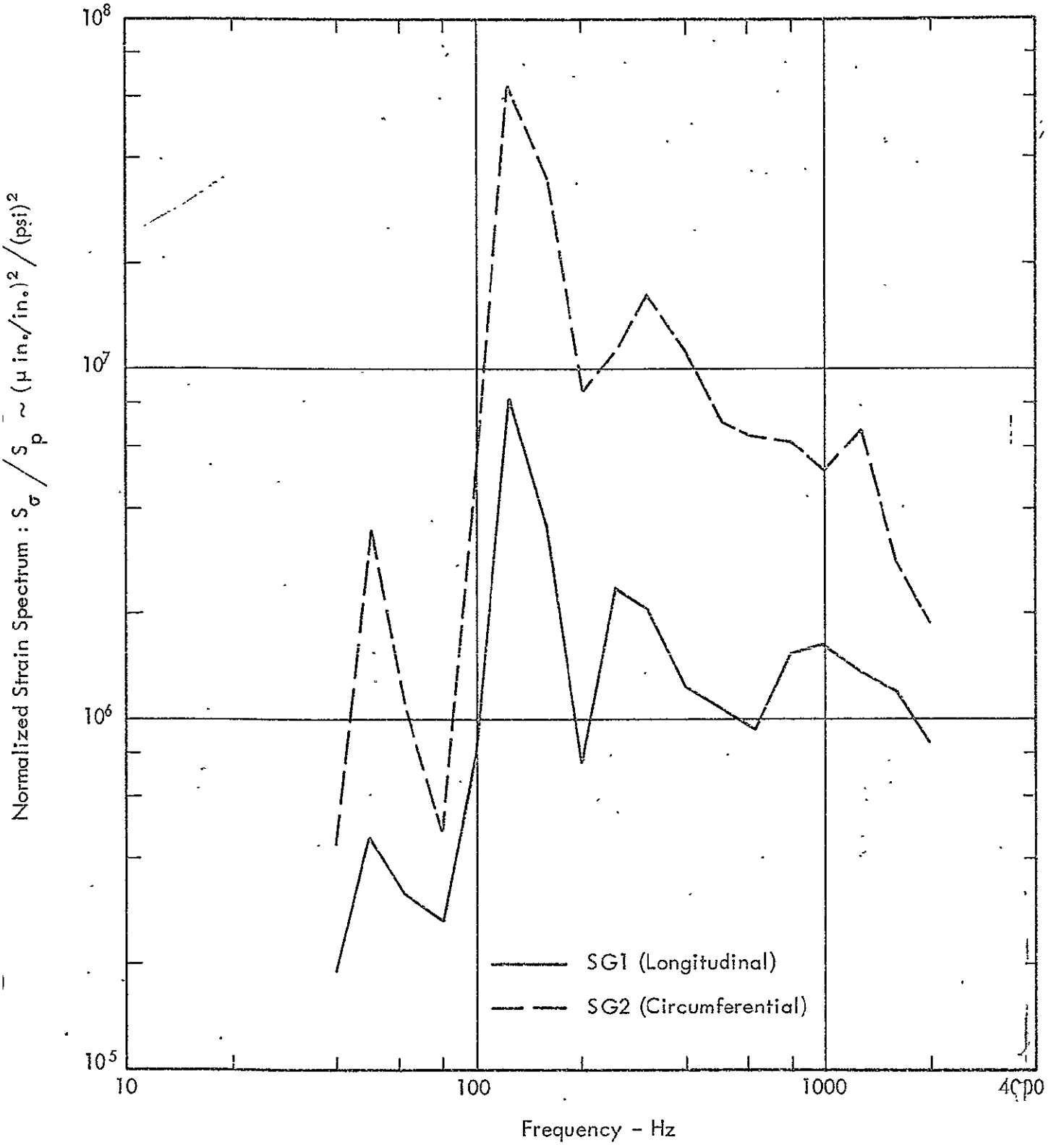

FIGURE 20. Levels of Longitudinal and Circumferential Strain for Configuration No. 1, Measured During Experiment 1

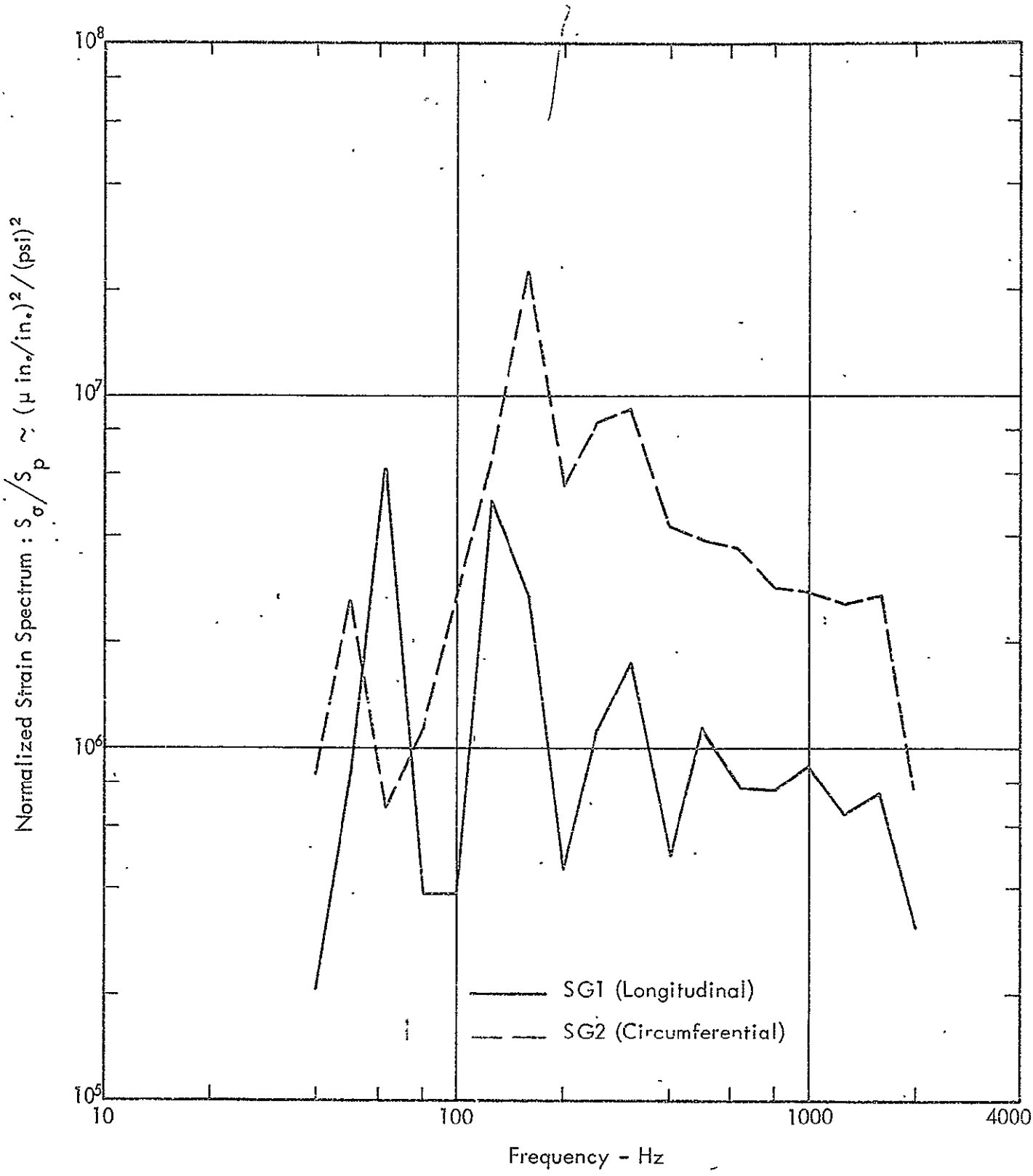

FIGURE 21. Levels of Longitudinal and Circumferential Strain for Configuration No. 1, Measured During Experiment 2

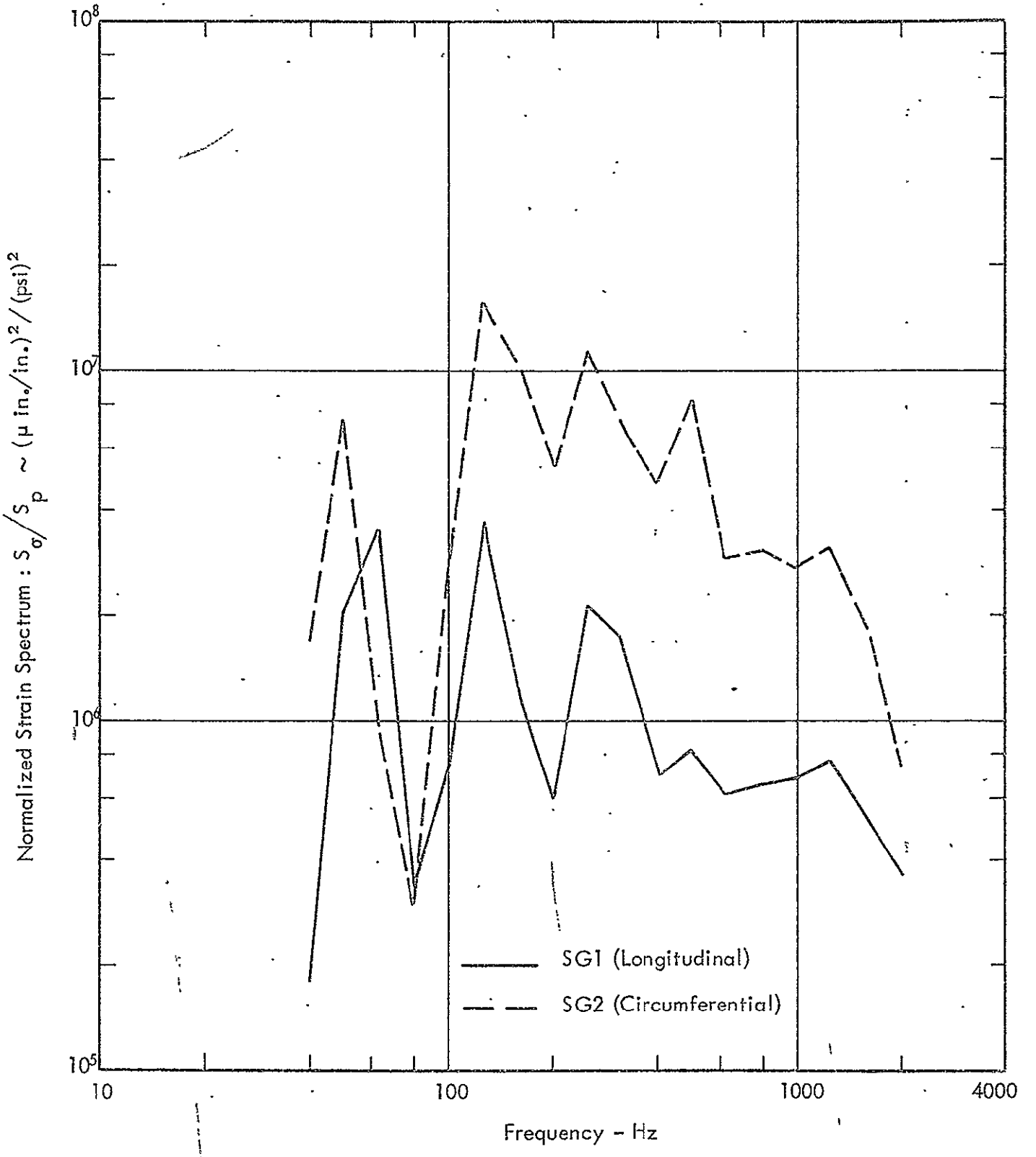

FIGURE 22. Levels of Longitudinal and Circumferential Strain for Configuration No. 1, Measured During Experiment 3

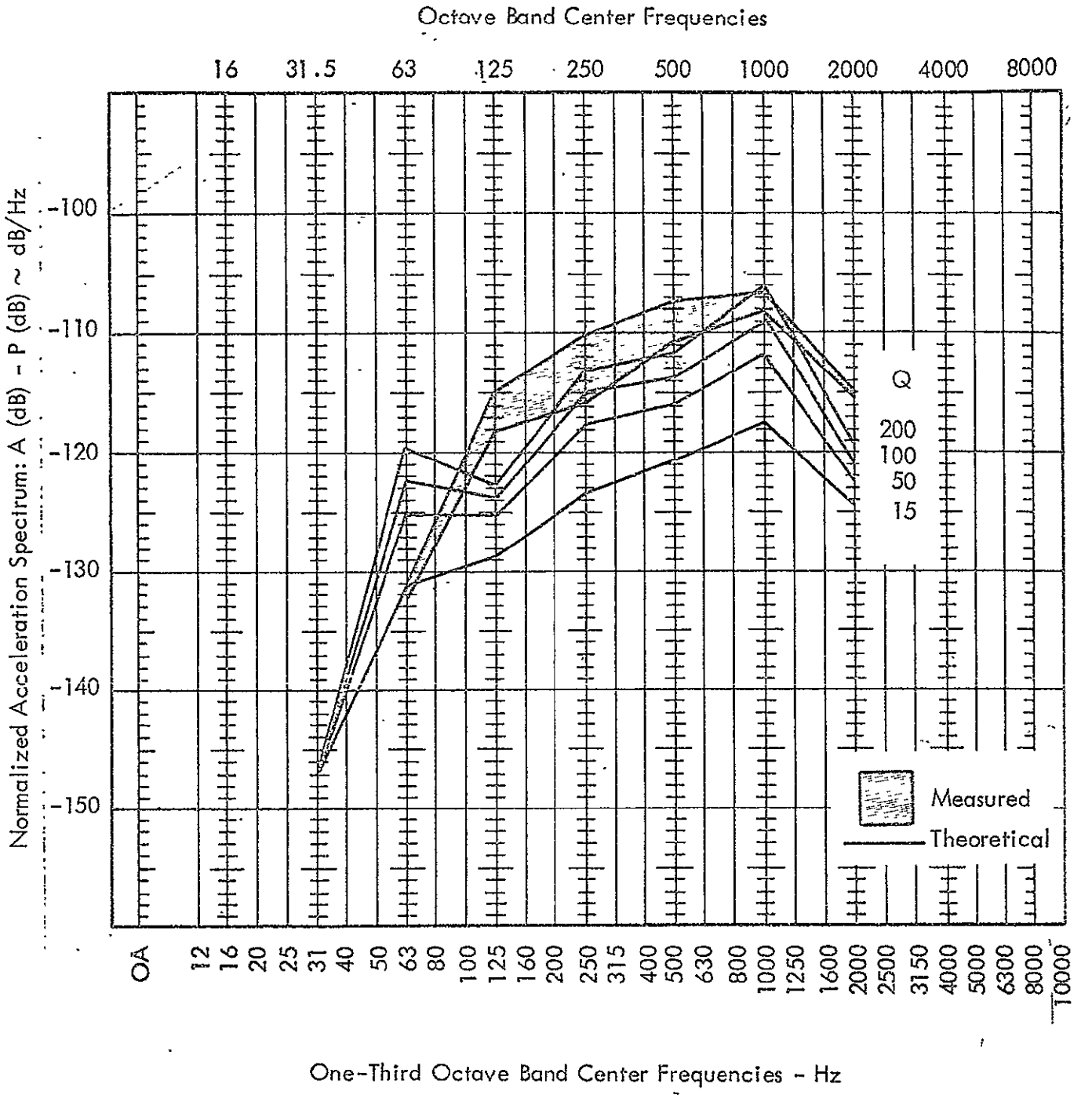

FIGURE 23. Comparison of Measured and Predicted Acceleration Spectra for Configuration No. 1. Based on Octave Band Averages; Experiment No. 1

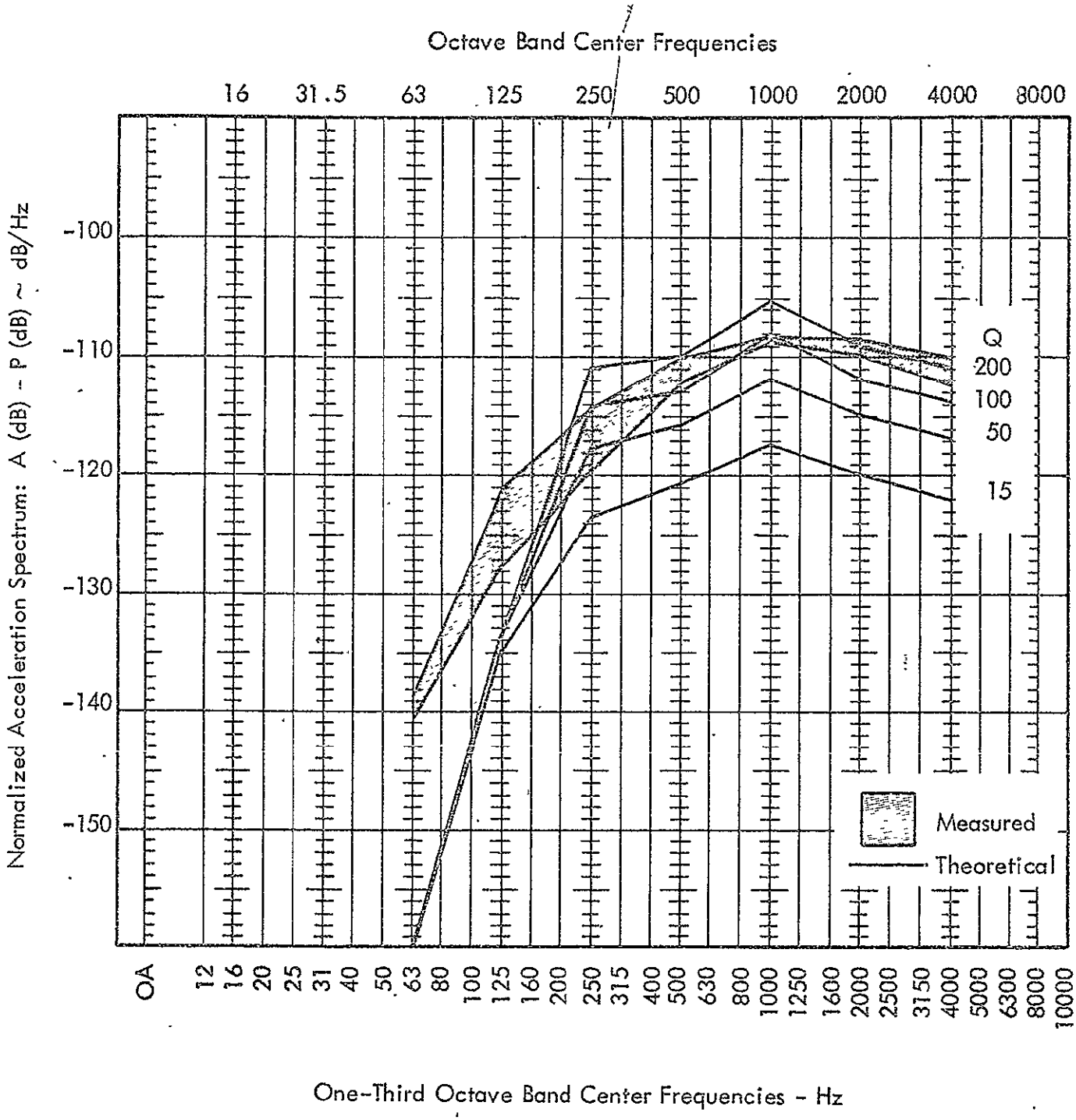

FIGURE 24. Comparison of Measured and Predicted Acceleration Spectra for Configuration No. 2. Based on Octave Band Averages; Experiment No. 4

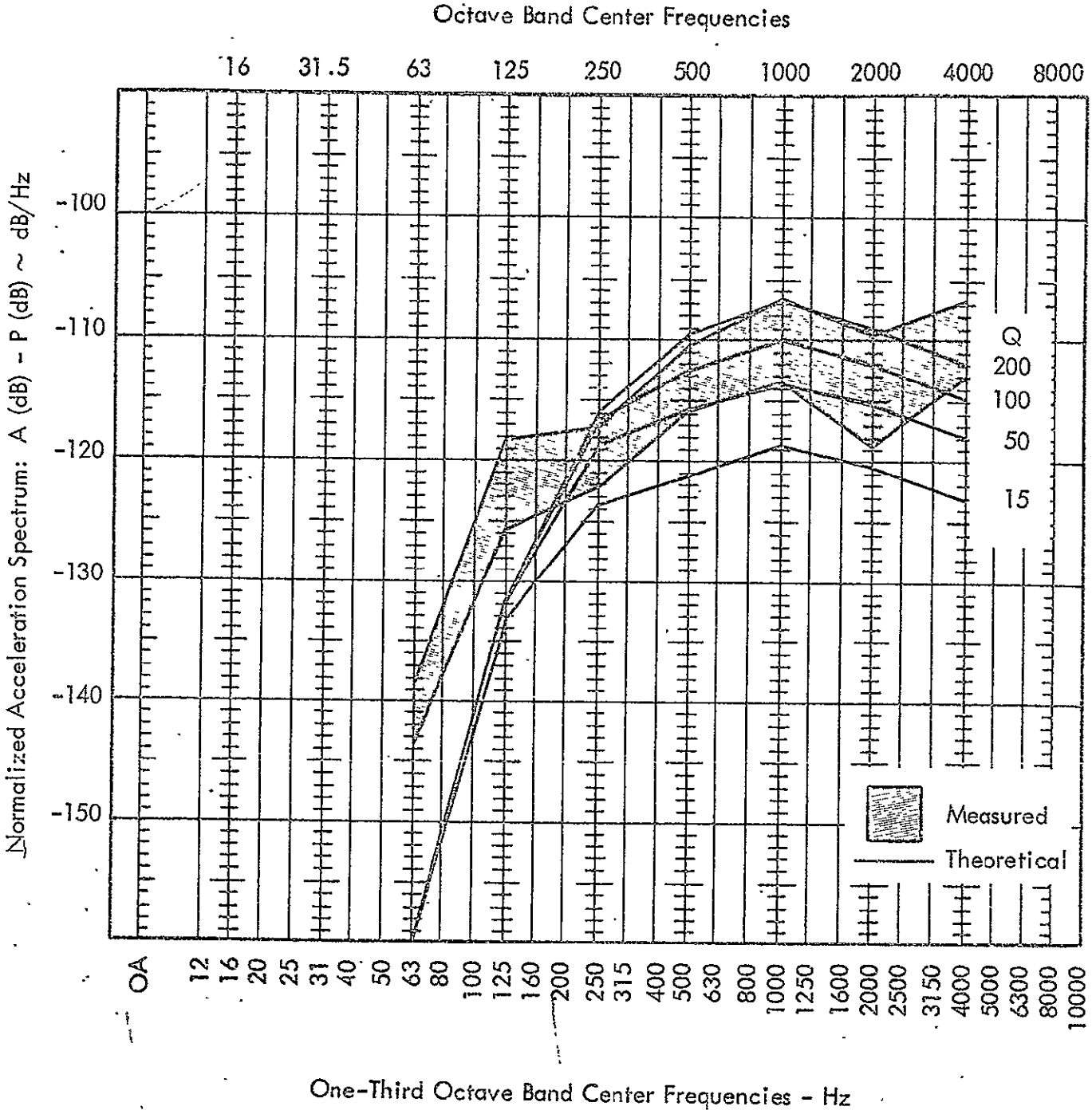

FIGURE 25. Comparison of Measured and Predicted Acceleration Spectra for Configuration No. 3. Based on Octave Band Averages; Experiment No. 5

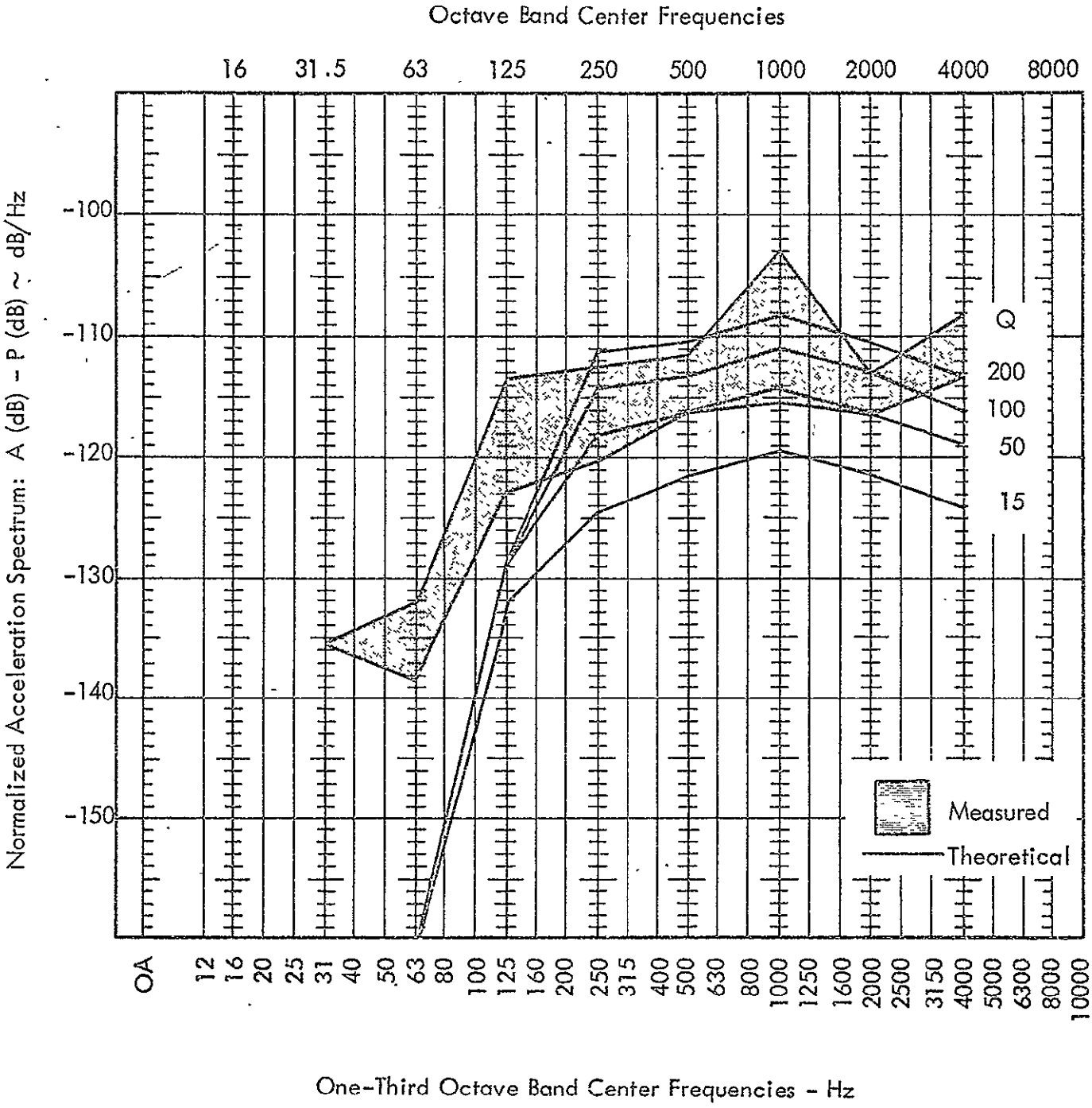

FIGURE 26. Comparison of Measured and Predicted Acceleration Spectra for Configuration No. 4. Based on Octave Band Averages; Experiment No. 6

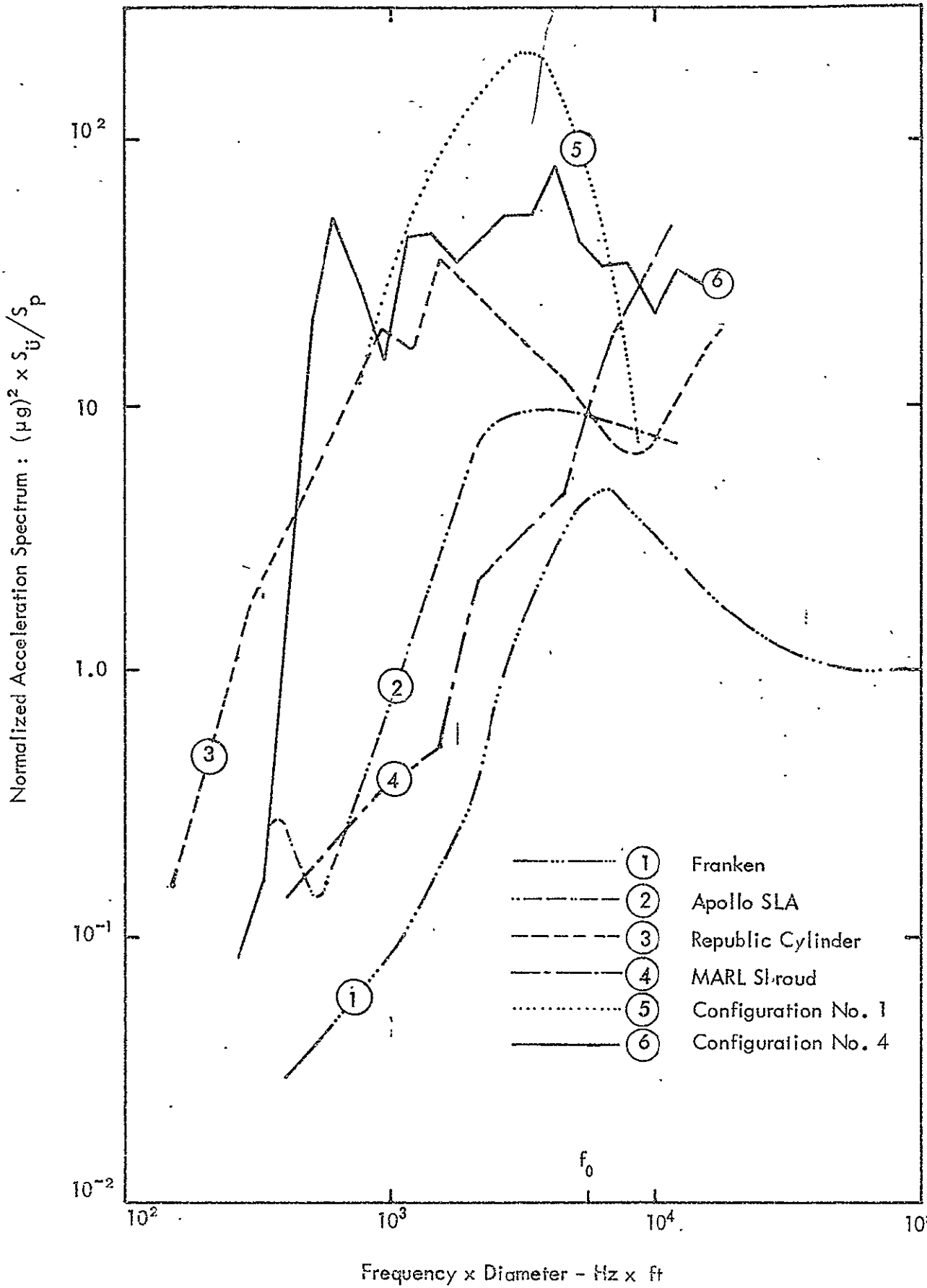

FIGURE 27. Measured Responses of Cylindrical Shells to Acoustic Excitation

APPENDIX A

Predicted Normalized Acceleration Response Spectra

For

Configurations No. 1, 2, 3, 4 for Q = 15, 50, 100, 200

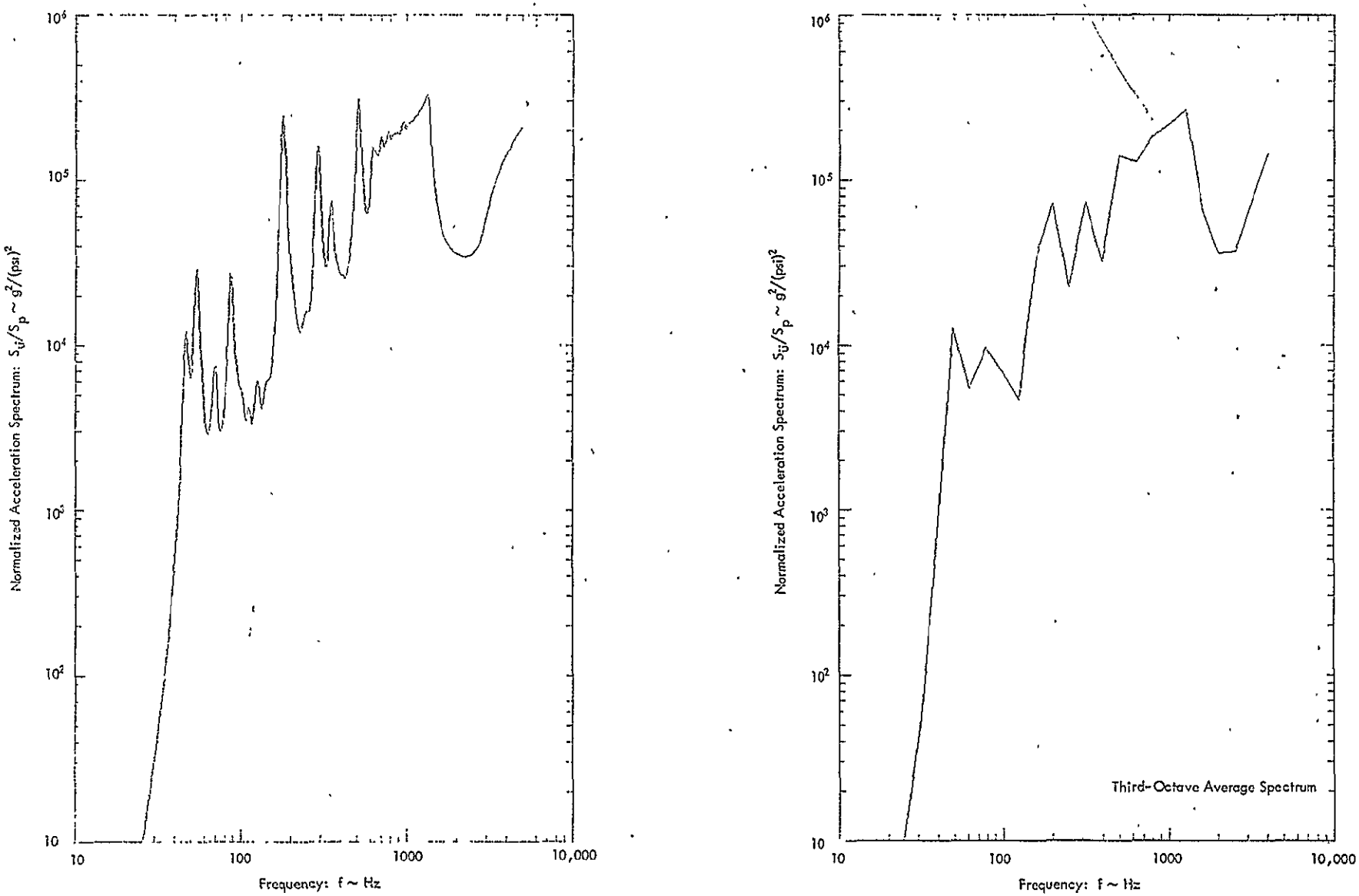

Figure A-1 : Predicted Normalized Acceleration Response of Cylinder for Configuration No. 1; Q = 15

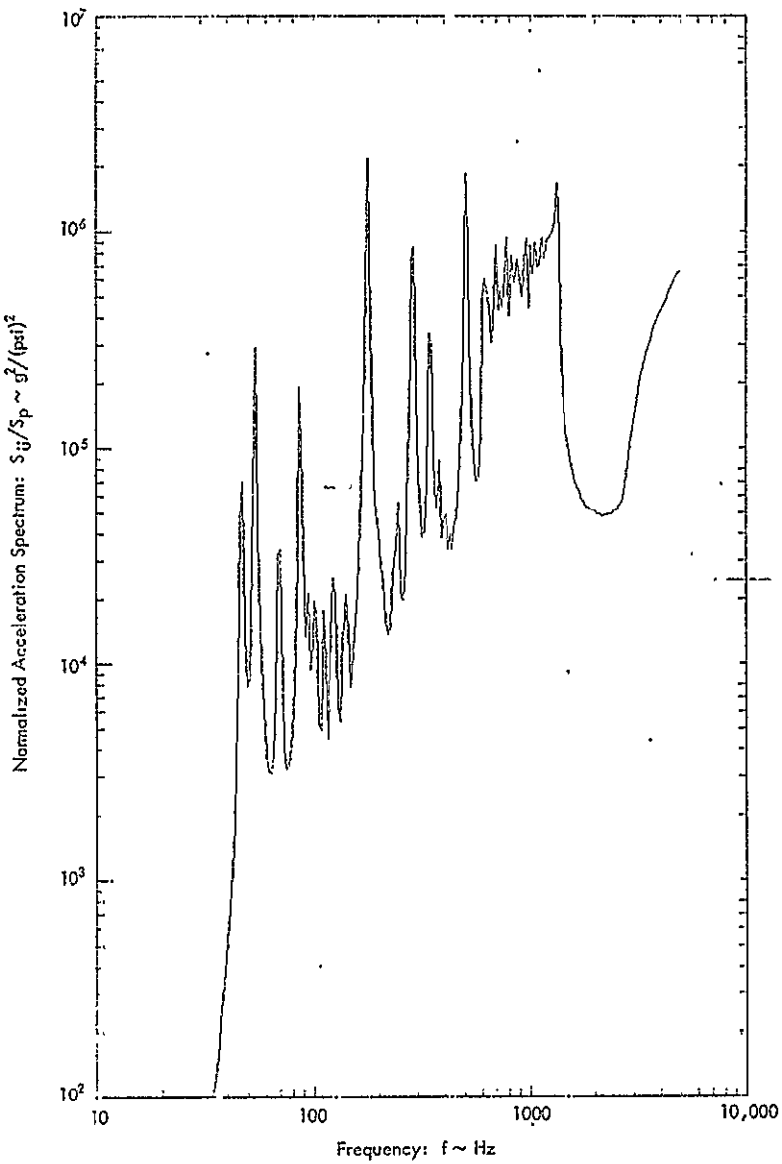

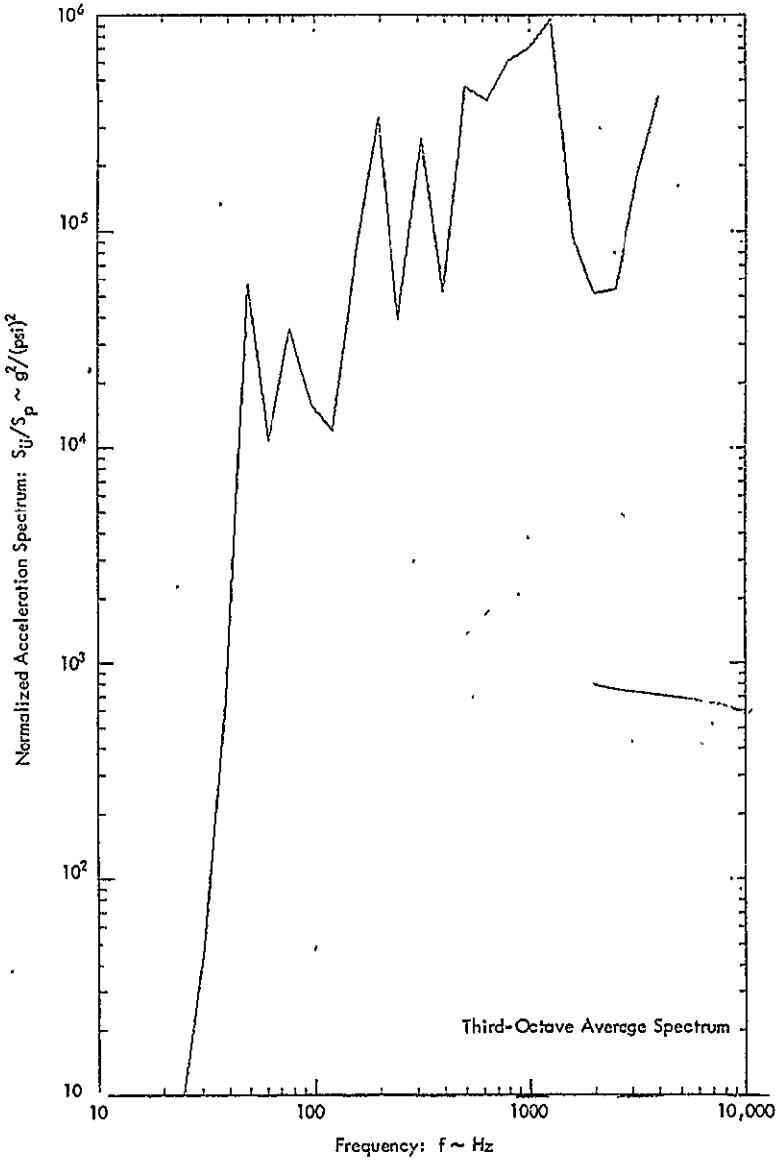

Figure A-2 : Predicted Normalized Acceleration Response of Cylinder for Configuration No. 1; Q = 50

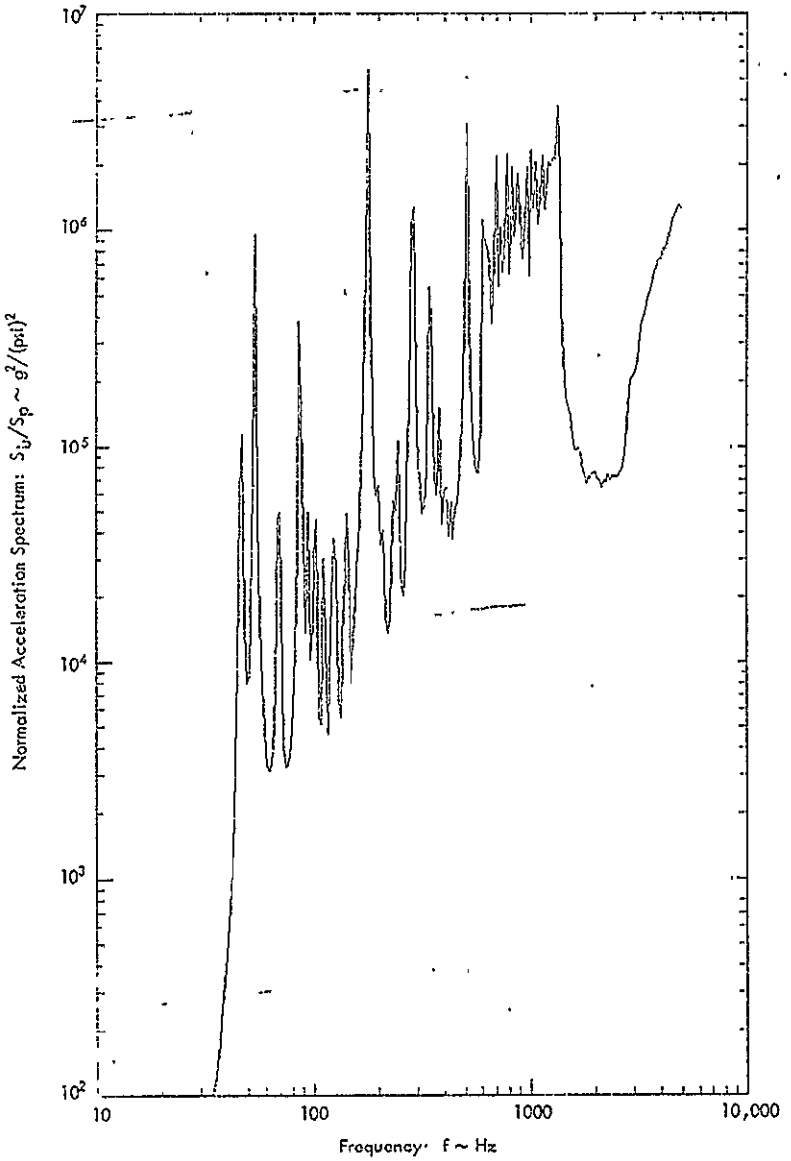

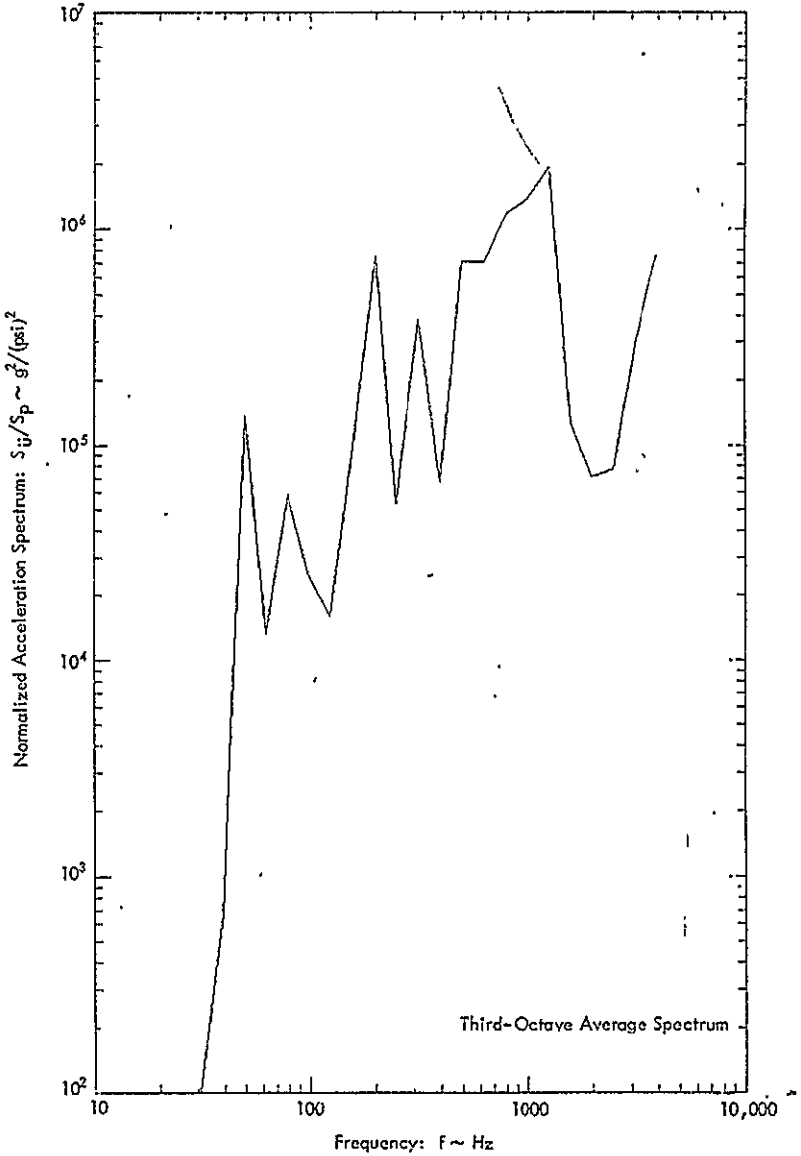

Figure A-3 : Predicted Normalized Acceleration Response of Cylinder for Configuration No. 1; Q = 100

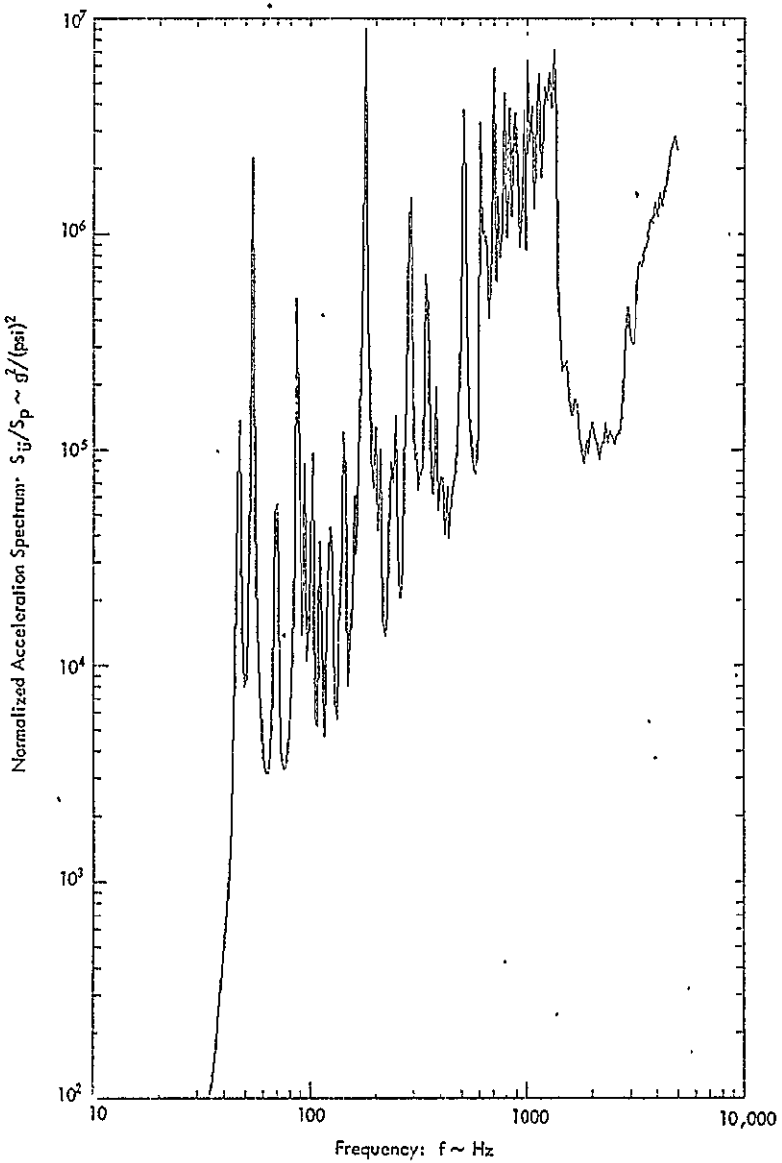

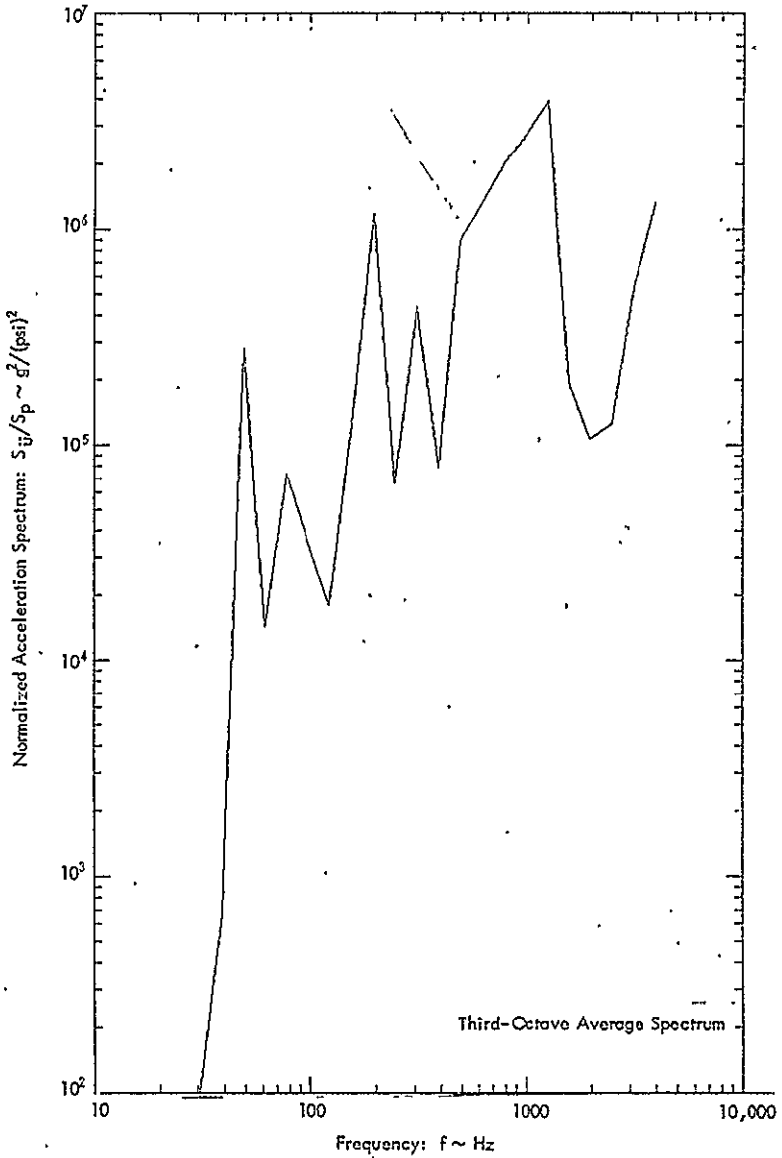

Figure A-4 : Predicted Normalized Acceleration Response of Cylinder for Configuration No. 1; Q = 200

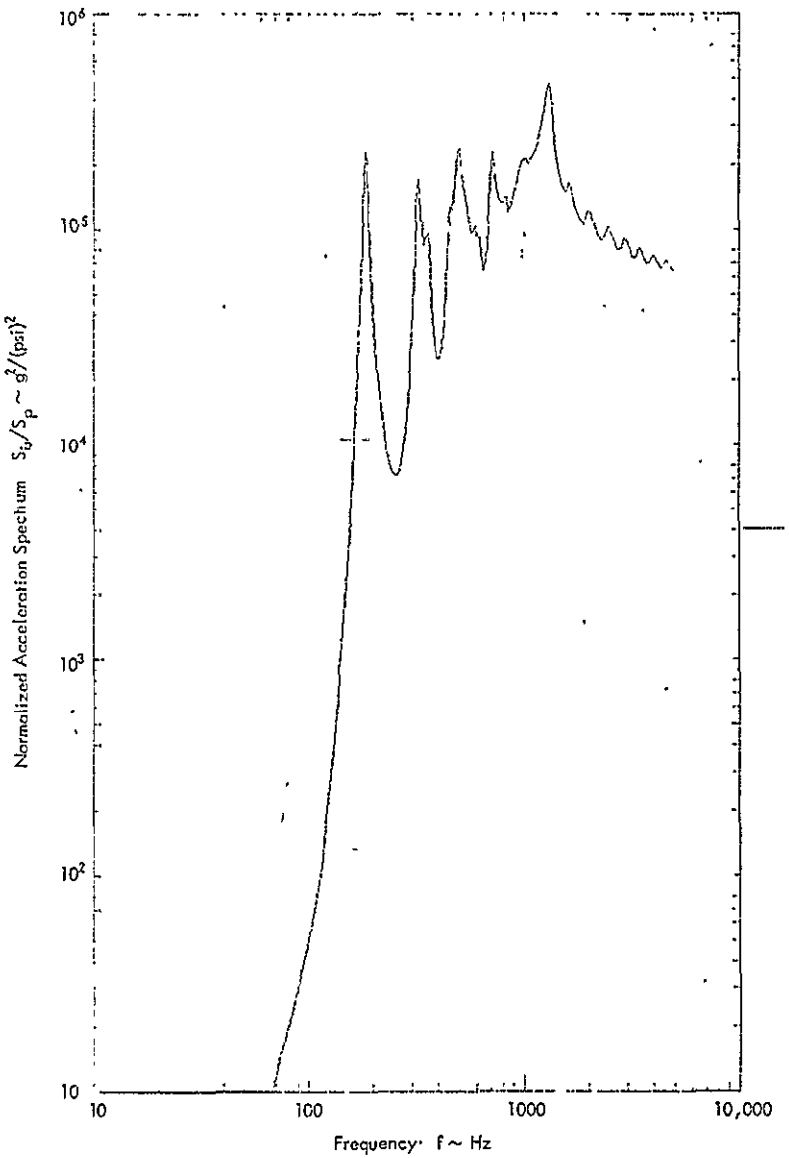

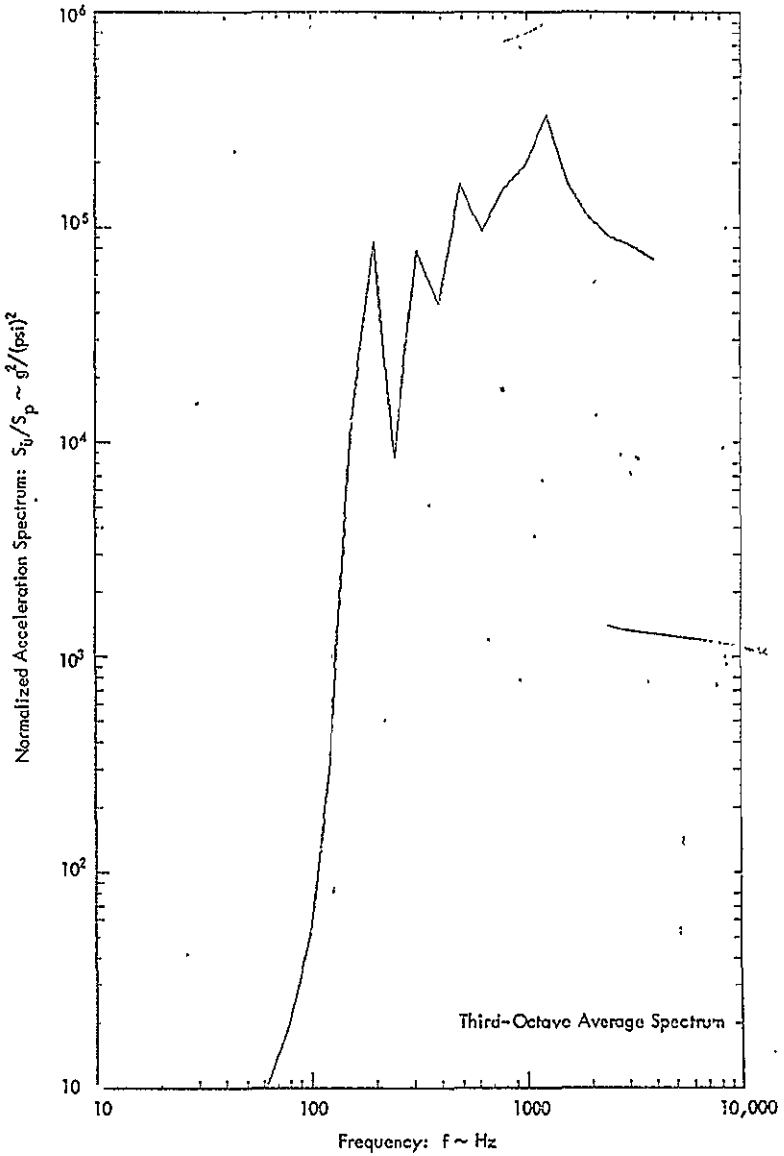

Figure A-5 : Predicted Normalized Acceleration Response of Cylinder for Configuration No. 2; Q = 15

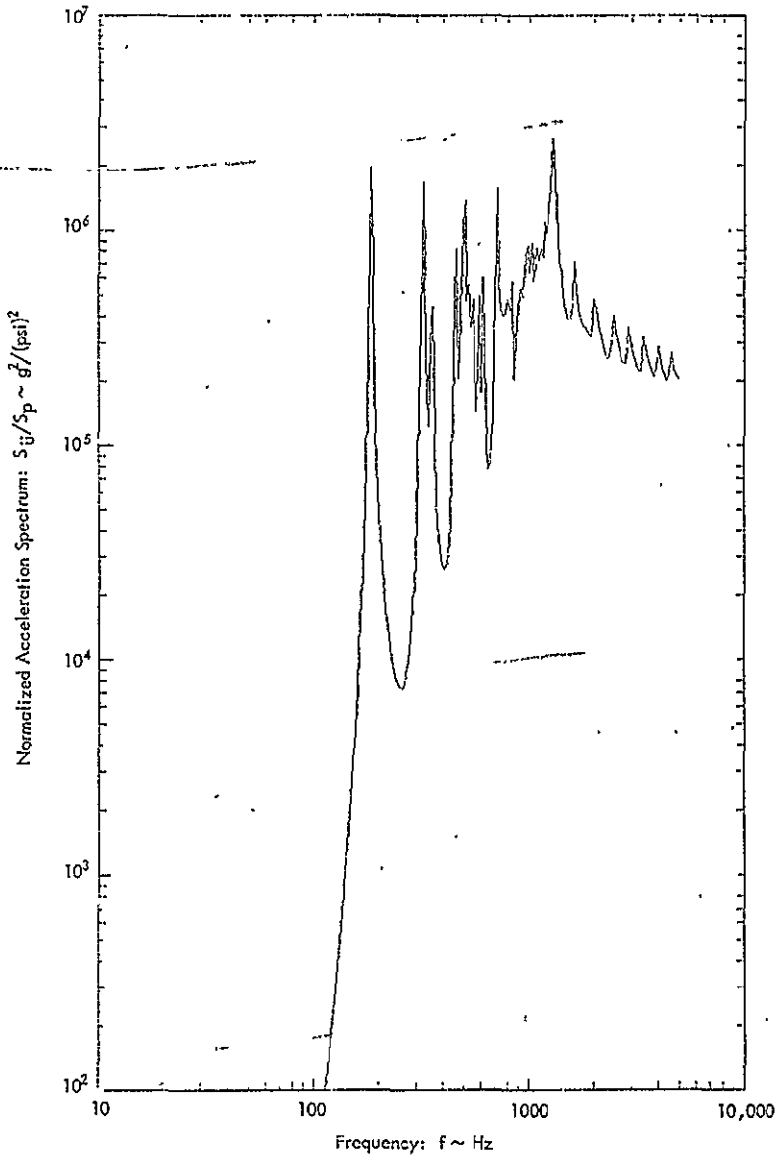

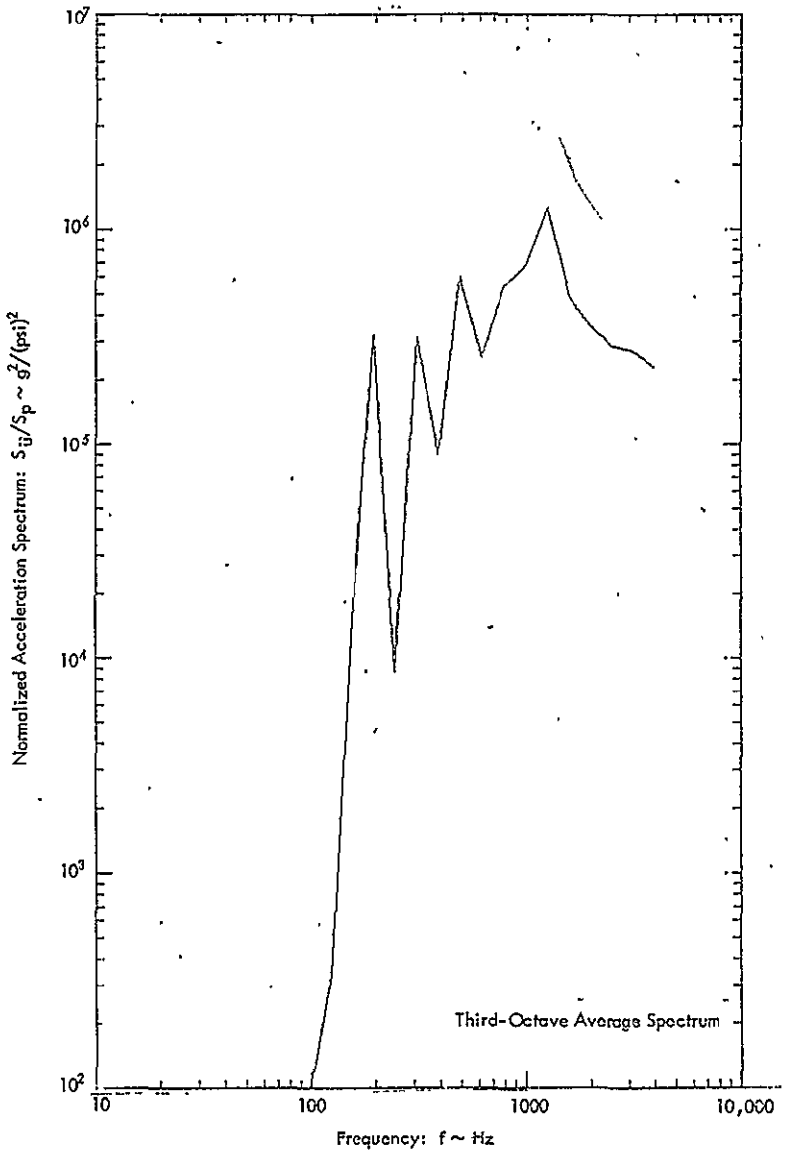

Figure A-6 : Predicted Normalized Acceleration Response of Cylinder for Configuration No. 2; Q = 50

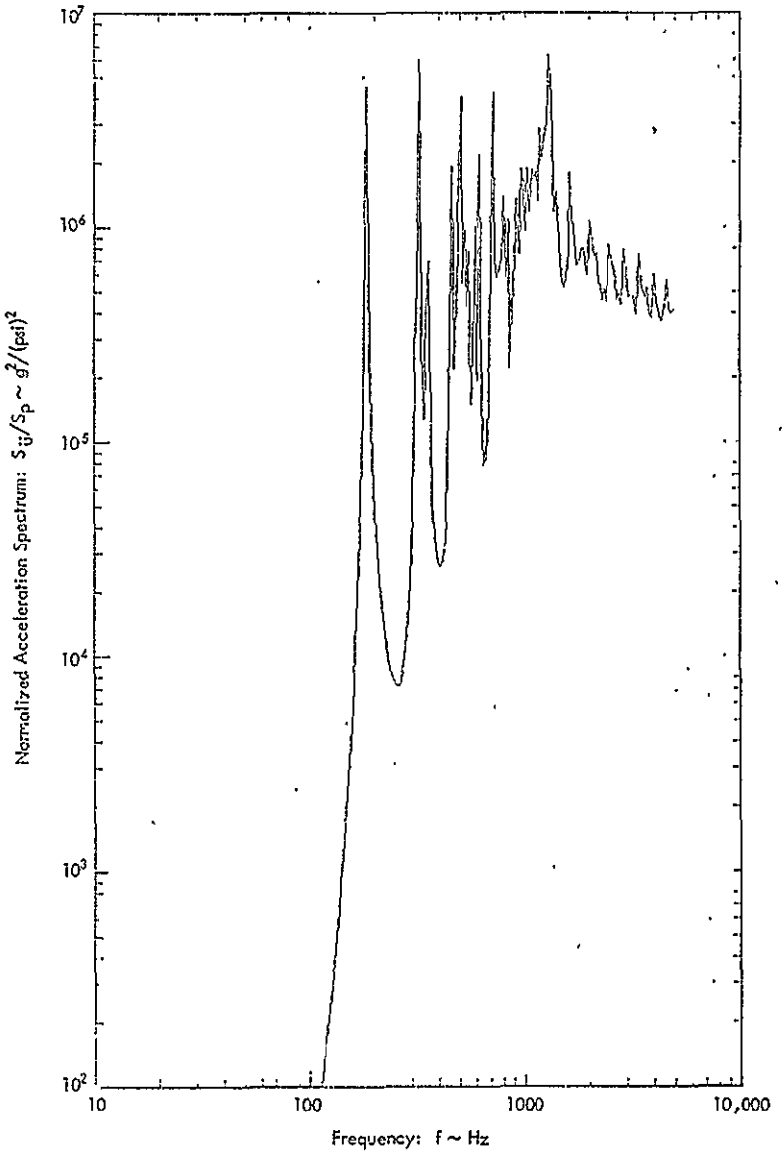

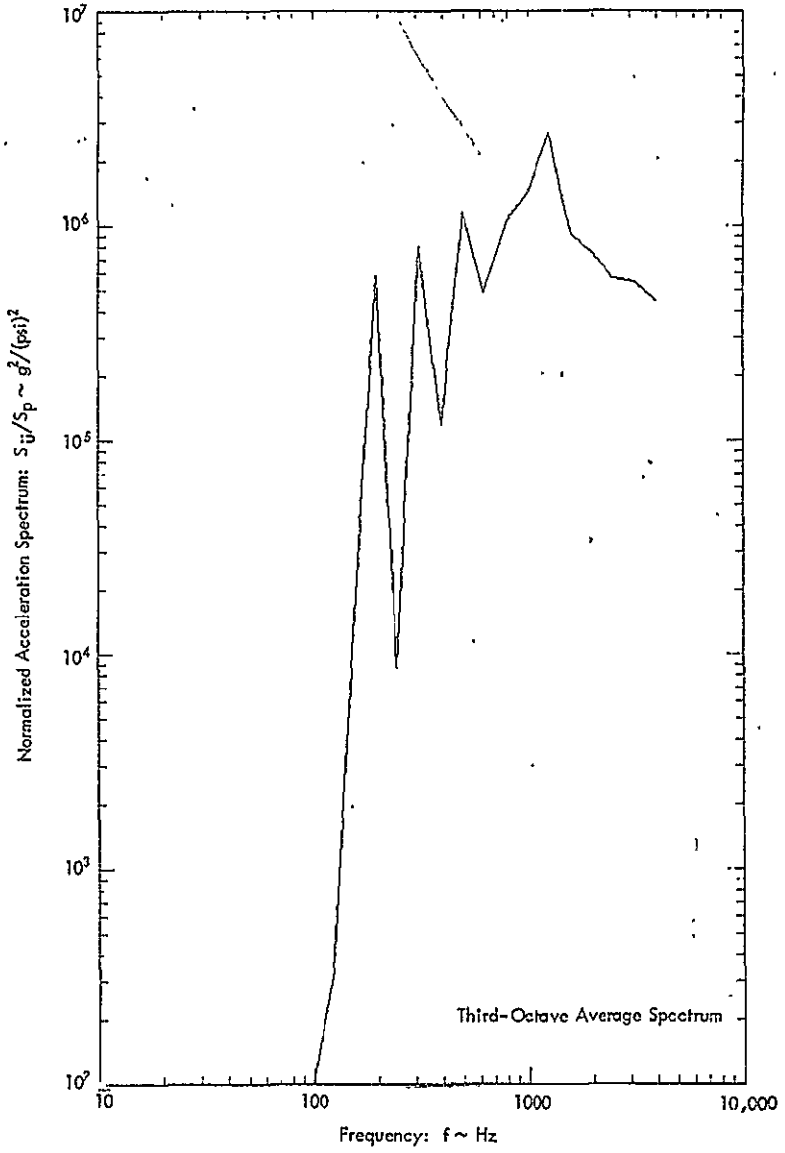

Figure A-7 : Predicted Normalized Acceleration Response of Cylinder for Configuration No. 2; Q = 100

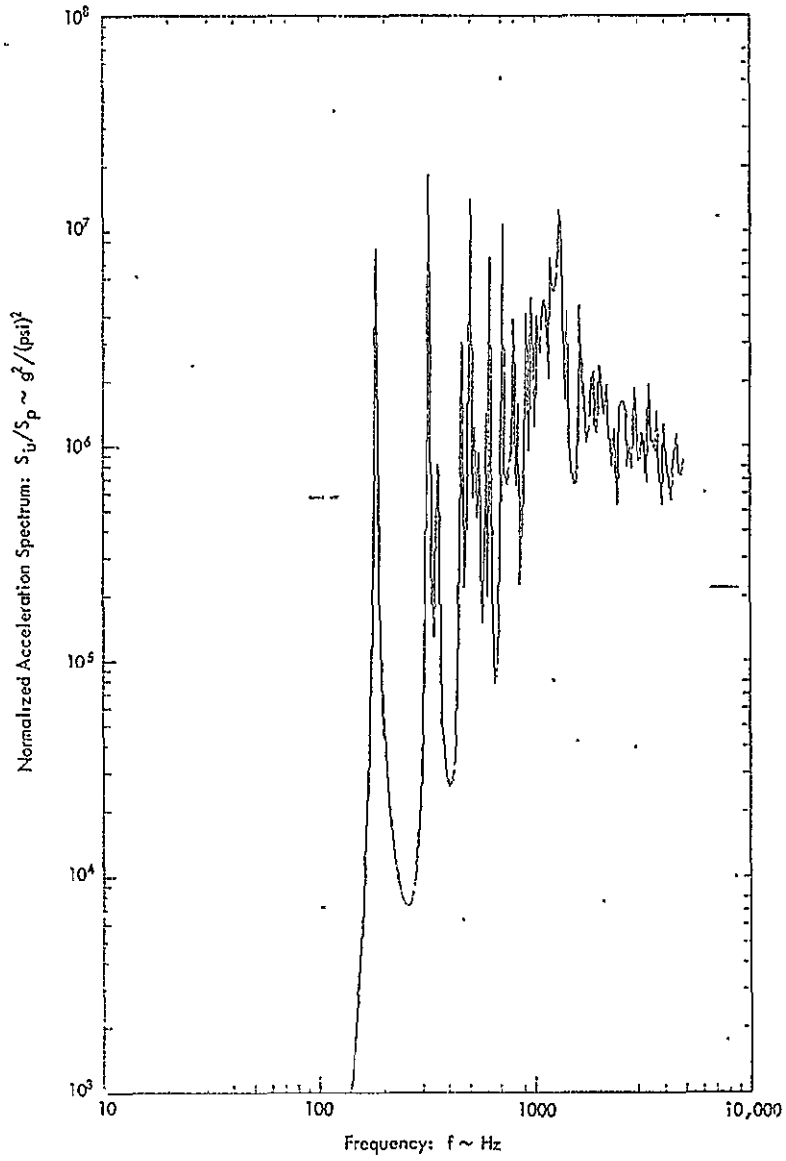

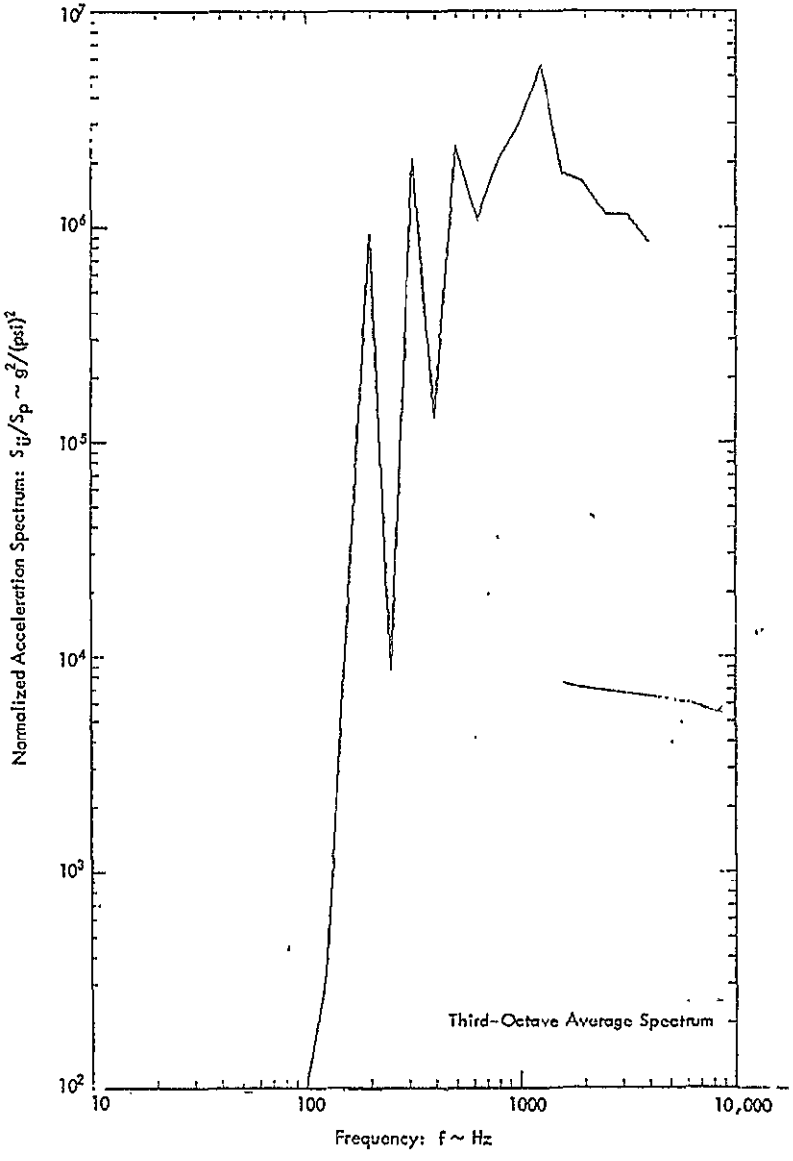

Figure A-8 : Predicted Normalized Acceleration Response of Cylinder for Configuration No. 2; Q = 200

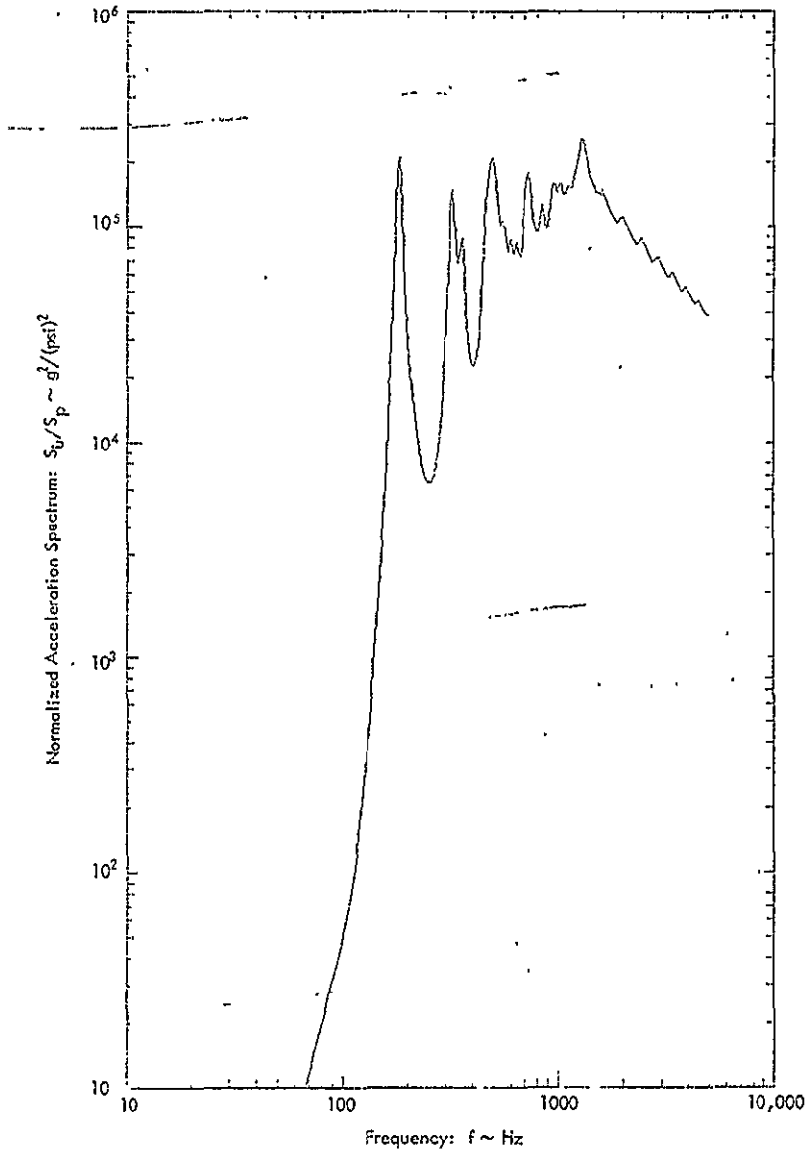

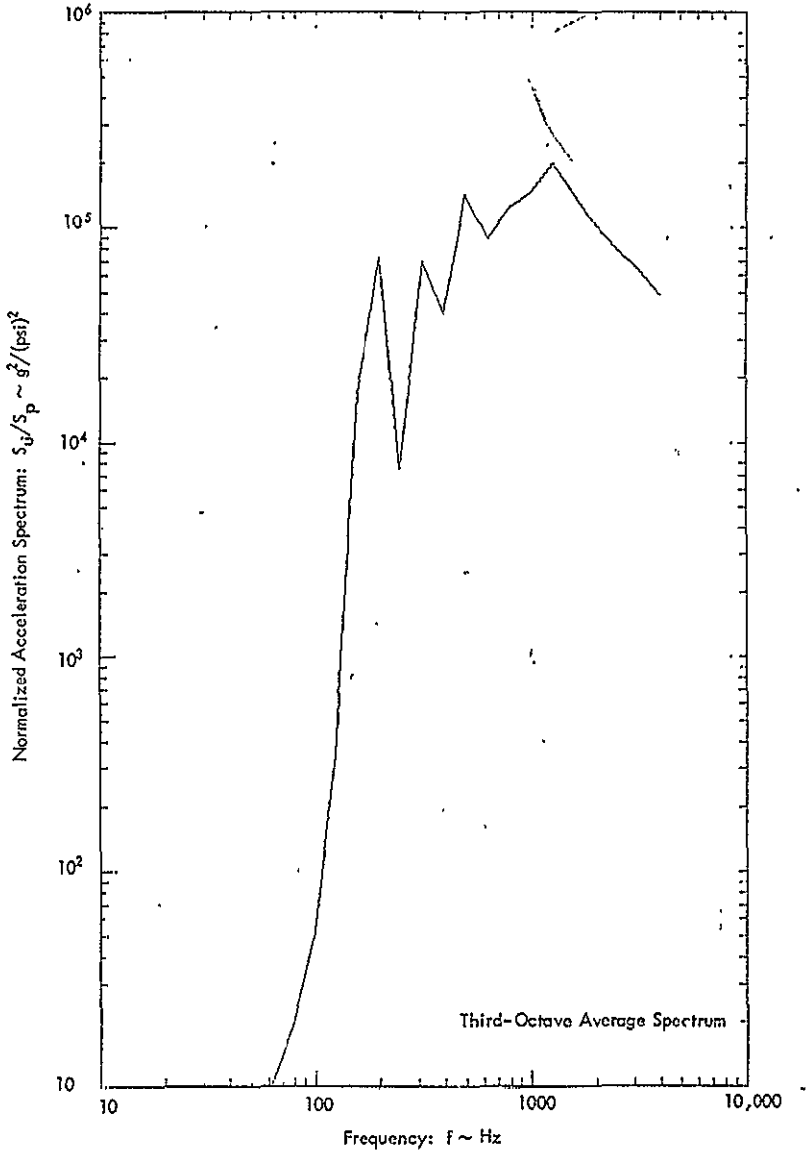

Figure A-9 : Predicted Normalized Acceleration Response of Cylinder for Configuration No. 3 ; Q = 15

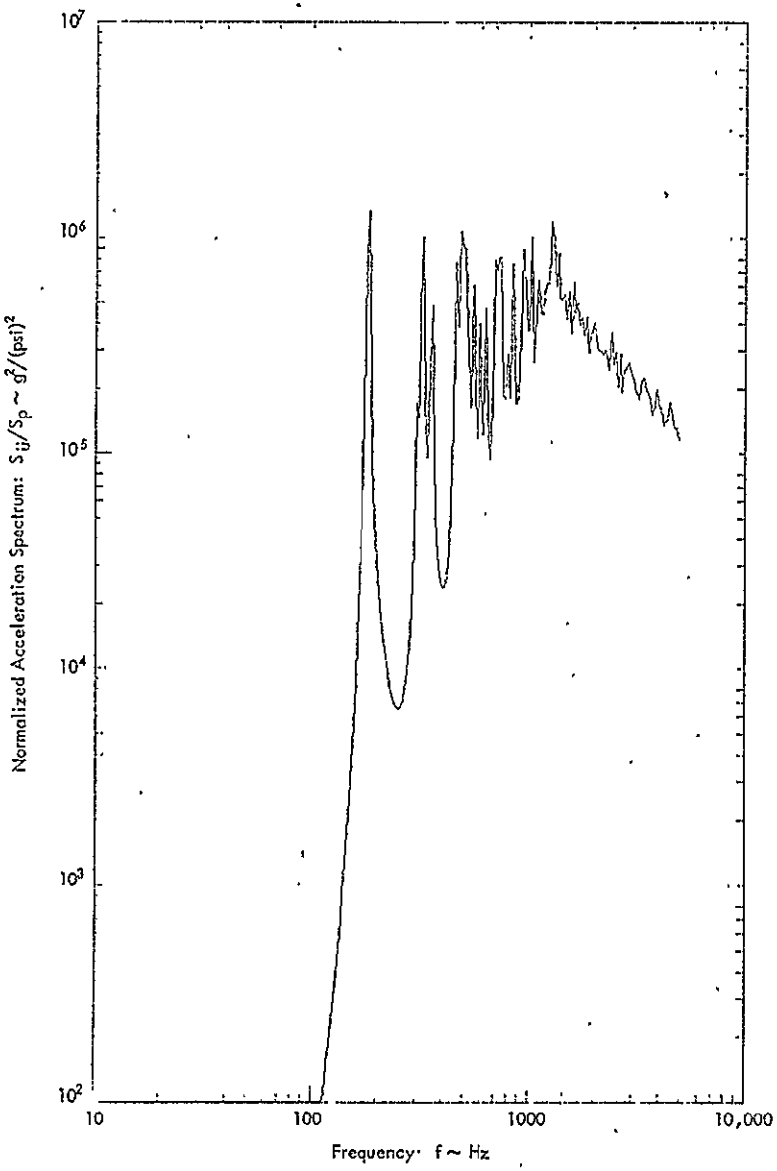

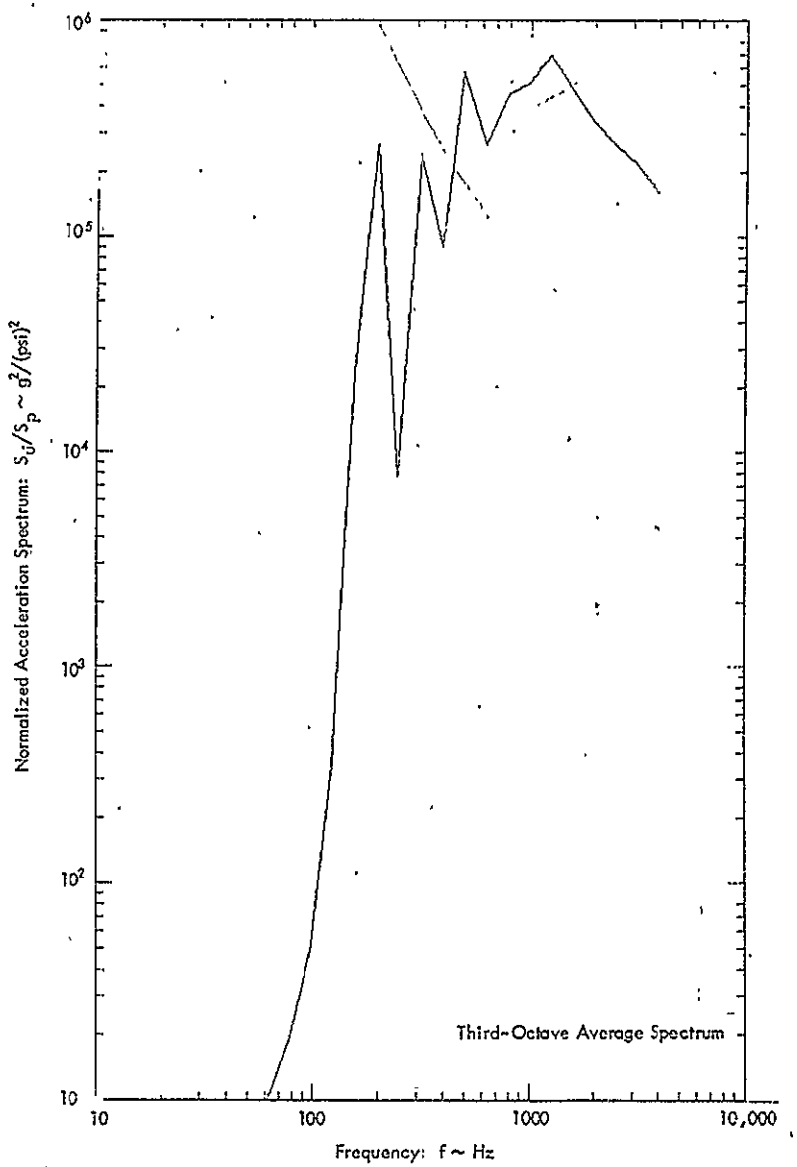

Figure A-10: Predicted Normalized Acceleration Response of Cylinder for Configuration No. 3; Q = 50

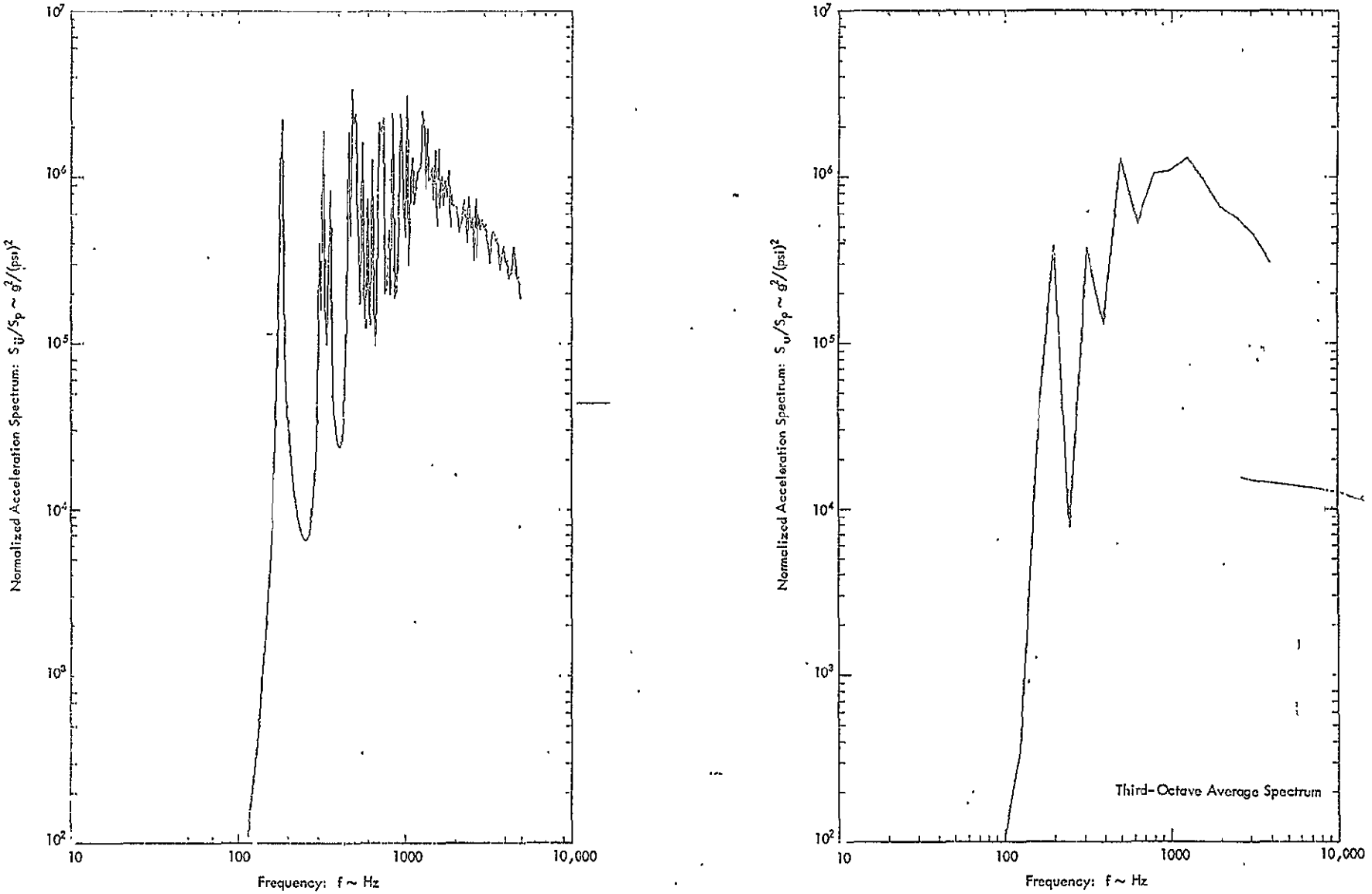

Figure A-11: Predicted Normalized Acceleration Response of Cylinder for Configuration No. 3; Q = 100

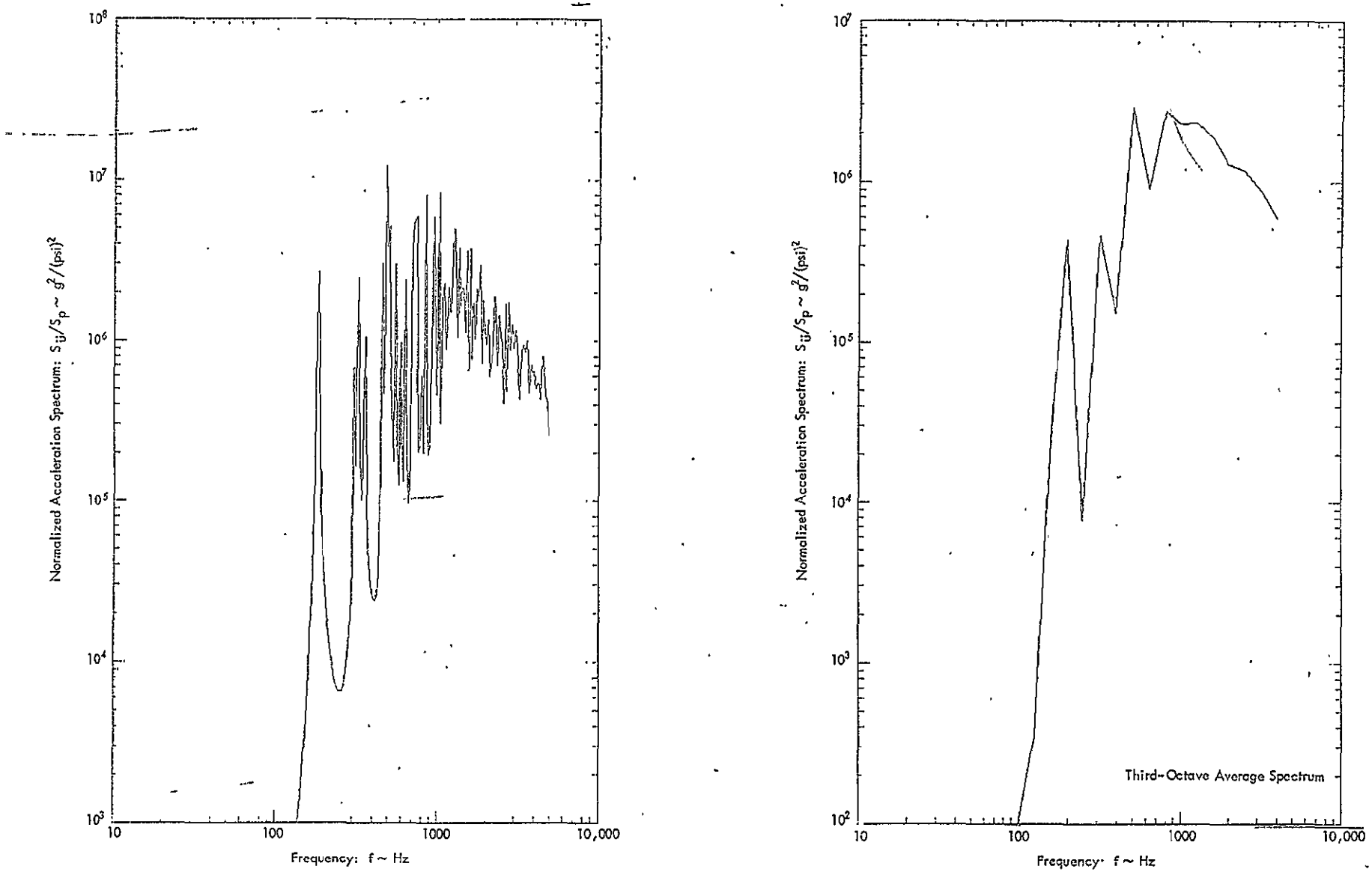

Figure A-12: Predicted Normalized Acceleration Response of Cylinder for Configuration No. 3; Q = 200

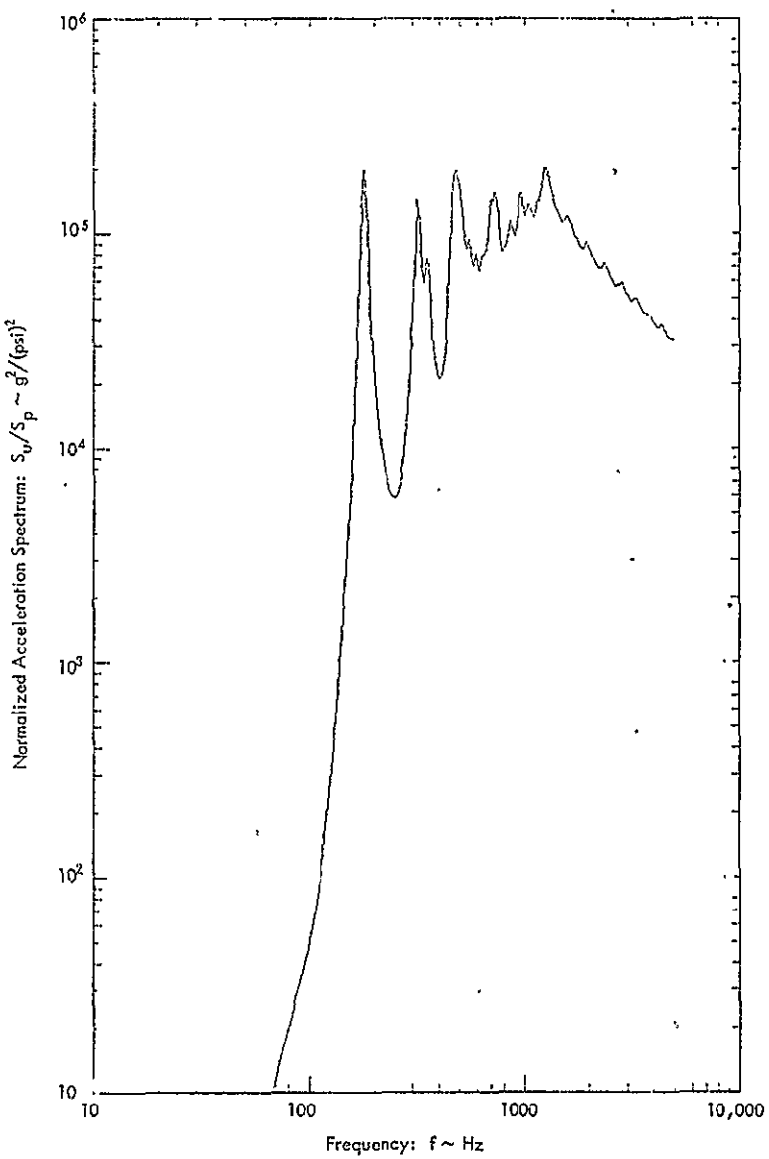

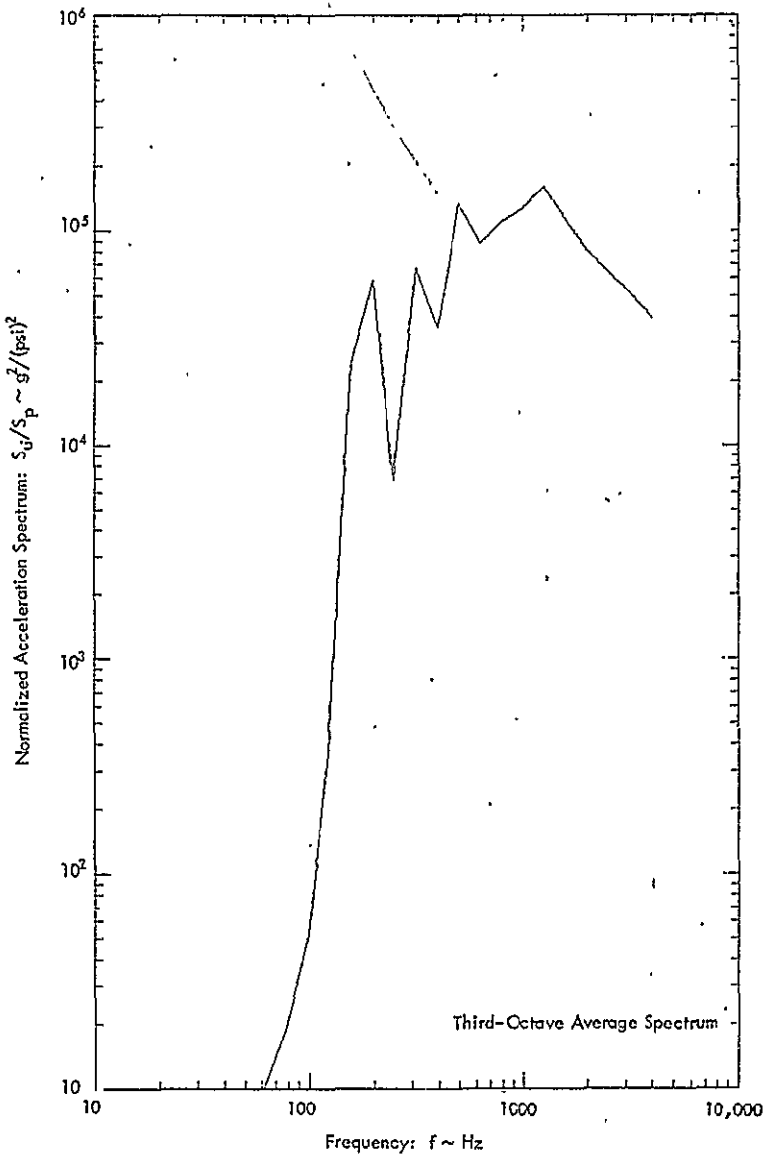

Figure A-13: Predicted Normalized Acceleration Response of Cylinder for Configuration No. 4; Q = 15

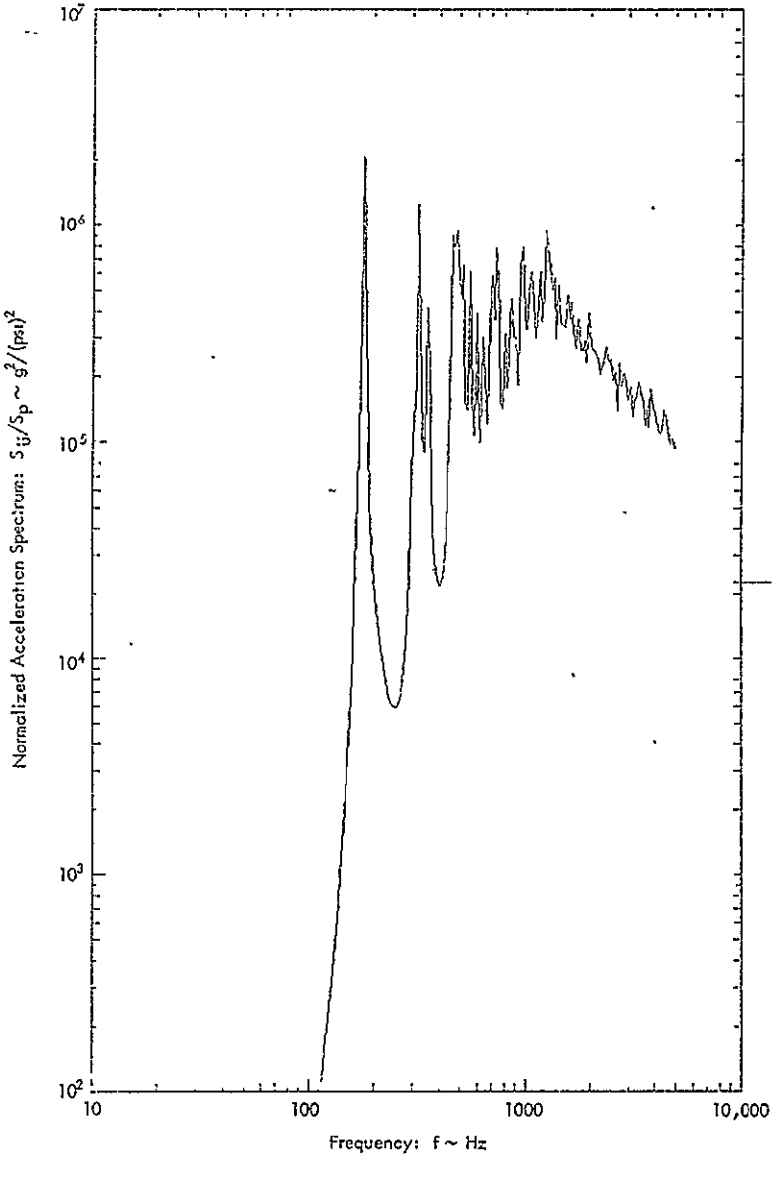

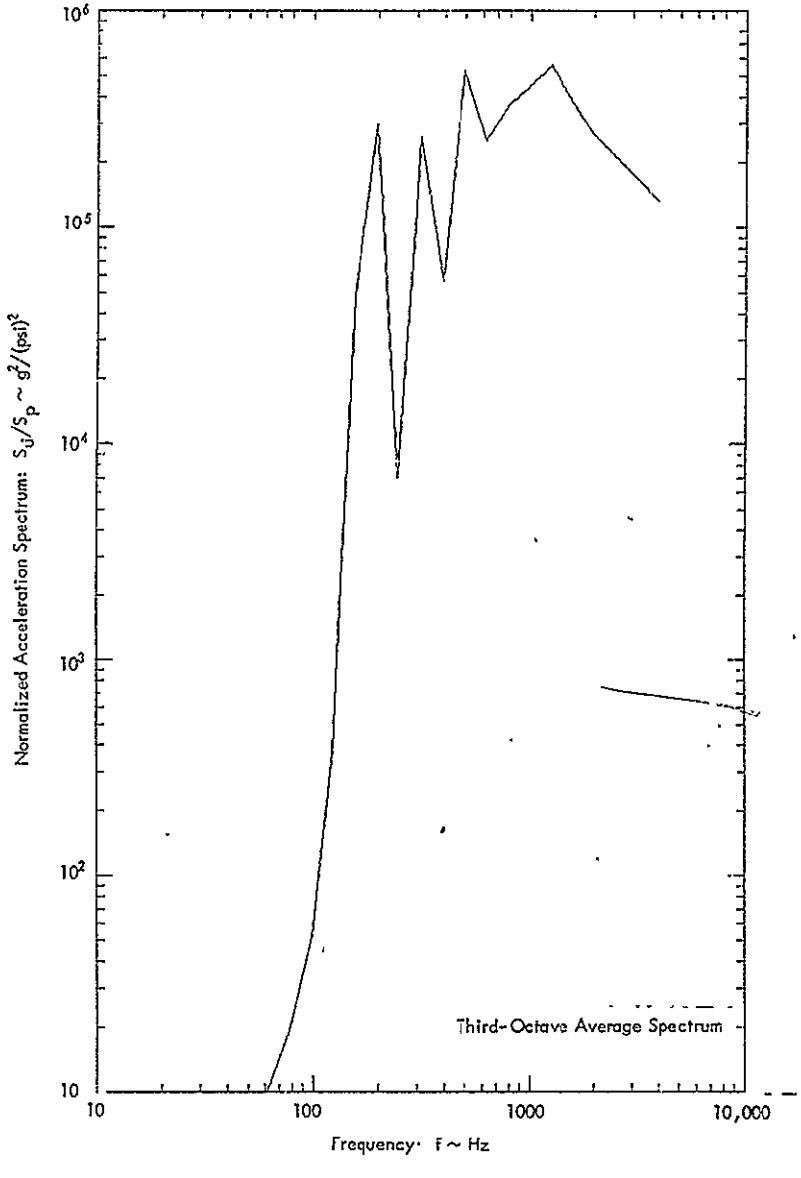

Figure A-14: Predicted Normalized Acceleration Response of Cylinder for Configuration No. 4 ; Q = 50

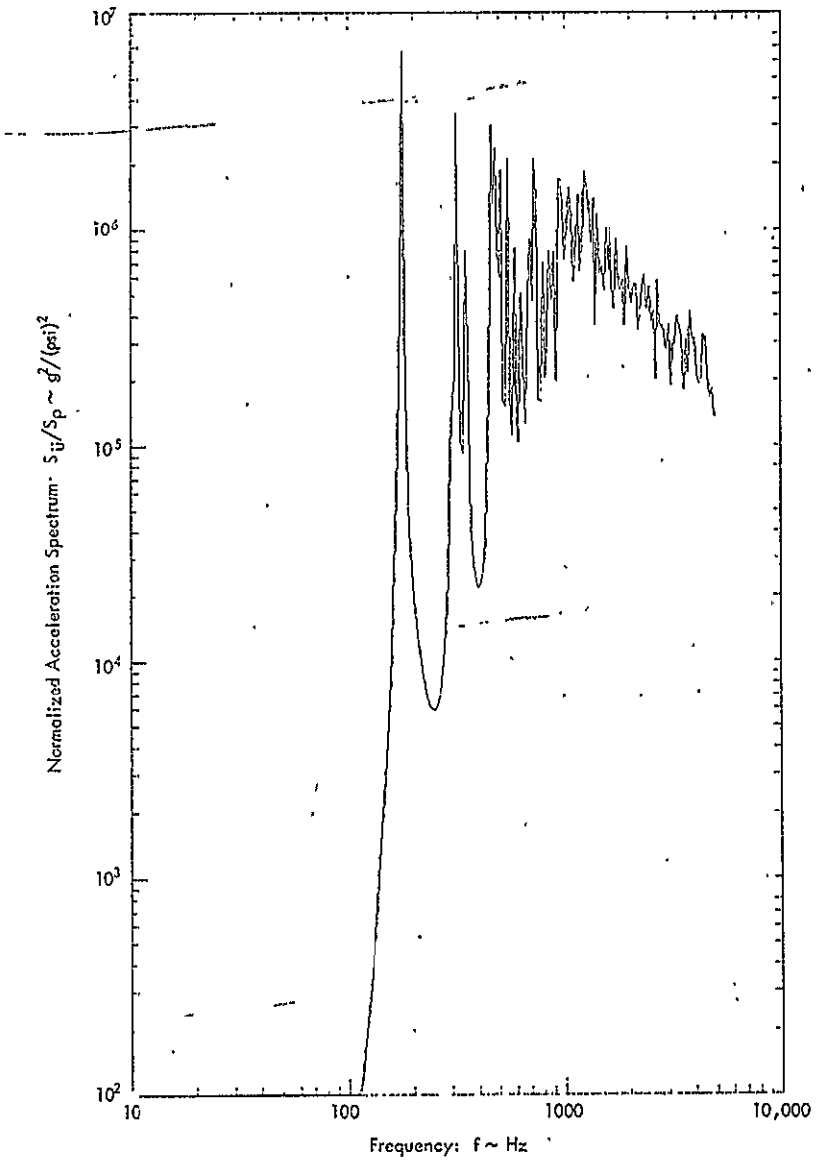

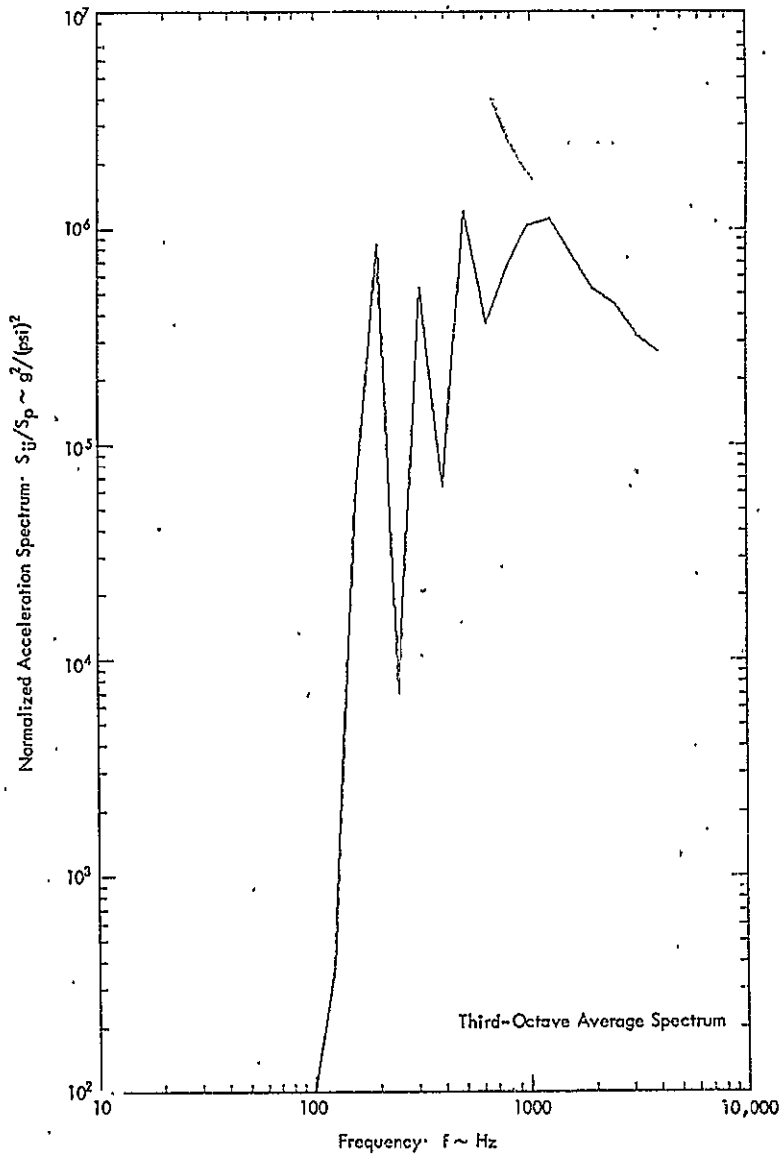

Figure A-15: Predicted Normalized Acceleration Response of Cylinder for Configuration No. 4; Q = 100

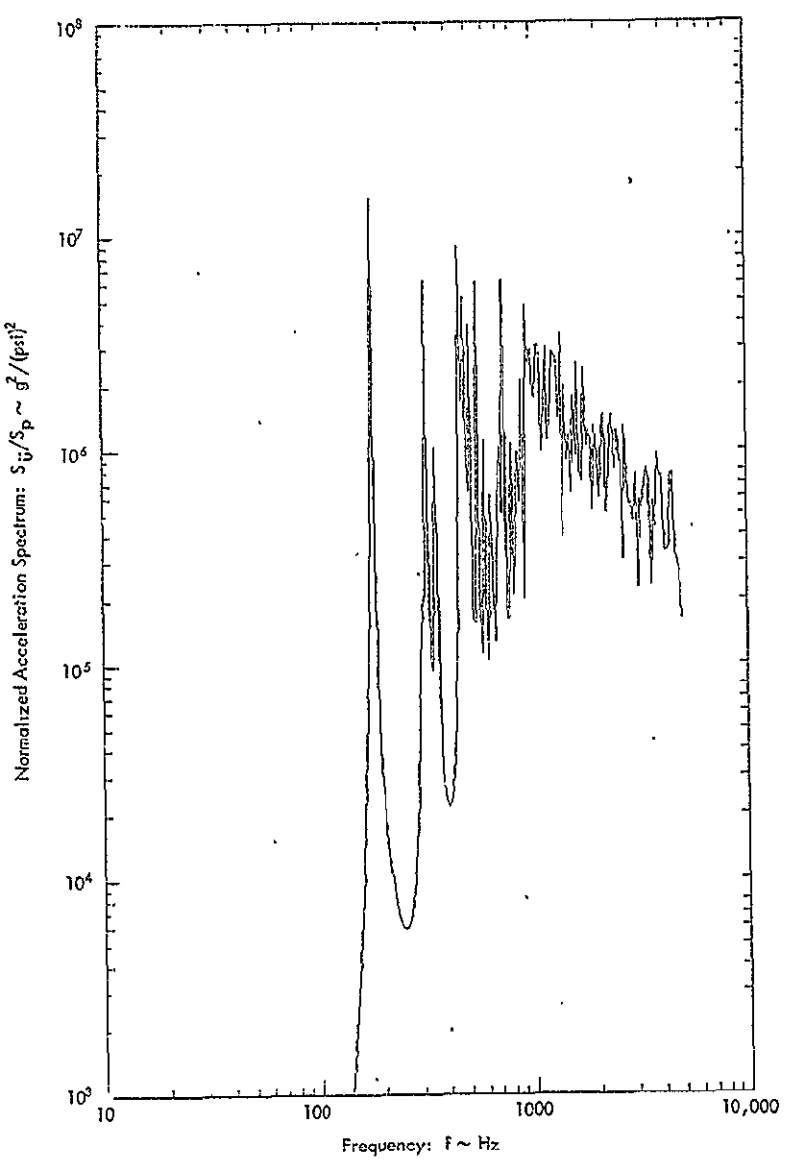

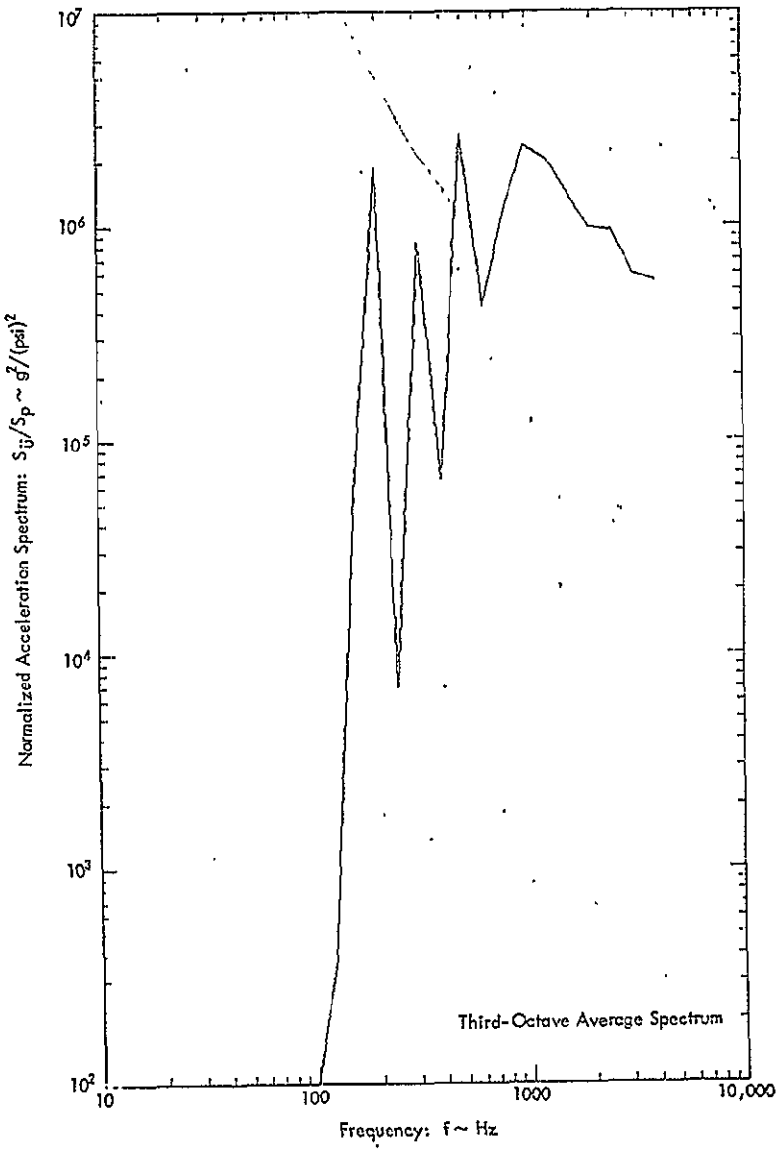

Figure A-16: Predicted Normalized Acceleration Response of Cylinder for Configuration No. 4; Q = 200

APPENDIX B

Measured One-Third Octave Sound Pressure Level, Acceleration and Strain Data

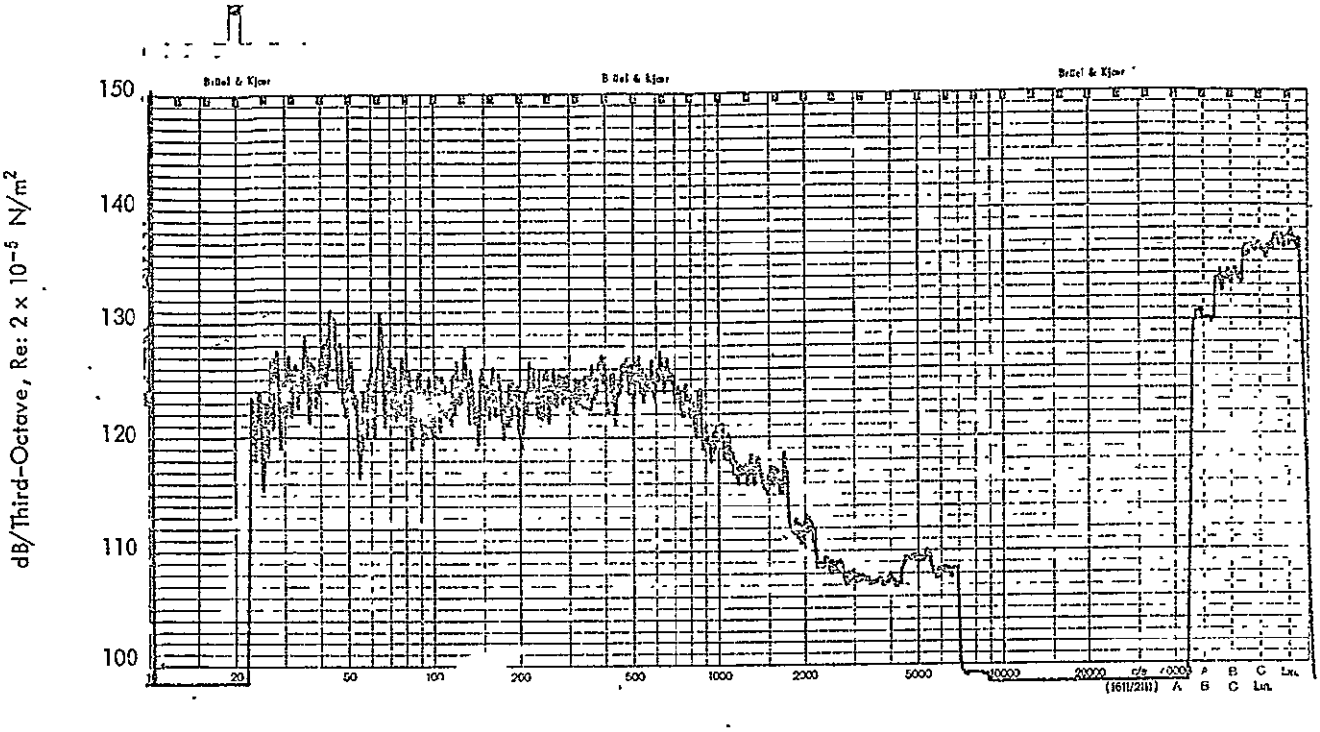

Figure B-1: Measured One-Third Octave Sound Pressure Levels, Experiment No. 1; External Microphone M1

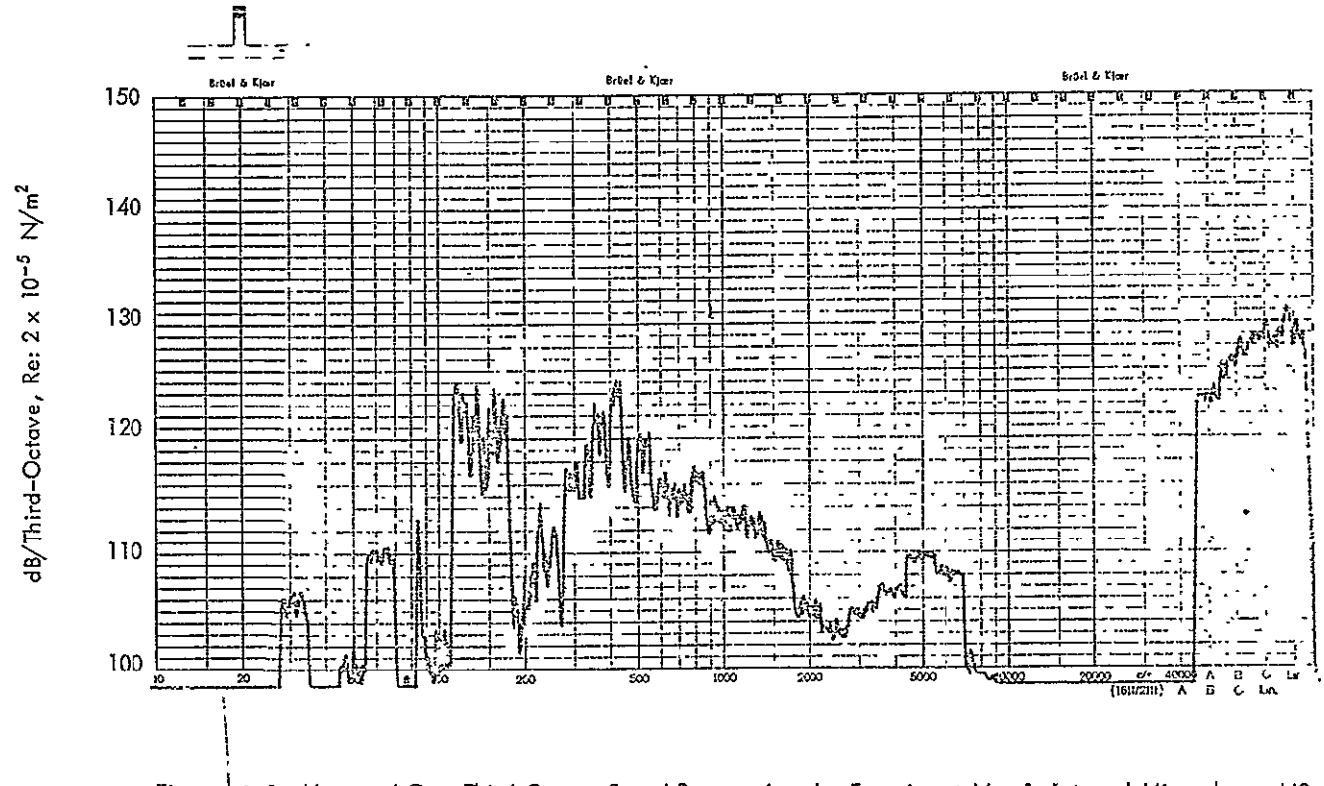

Figure B-2: Measured One-Third Octave Sound Pressure Levels, Experiment No. 1; Internal Microphone M2

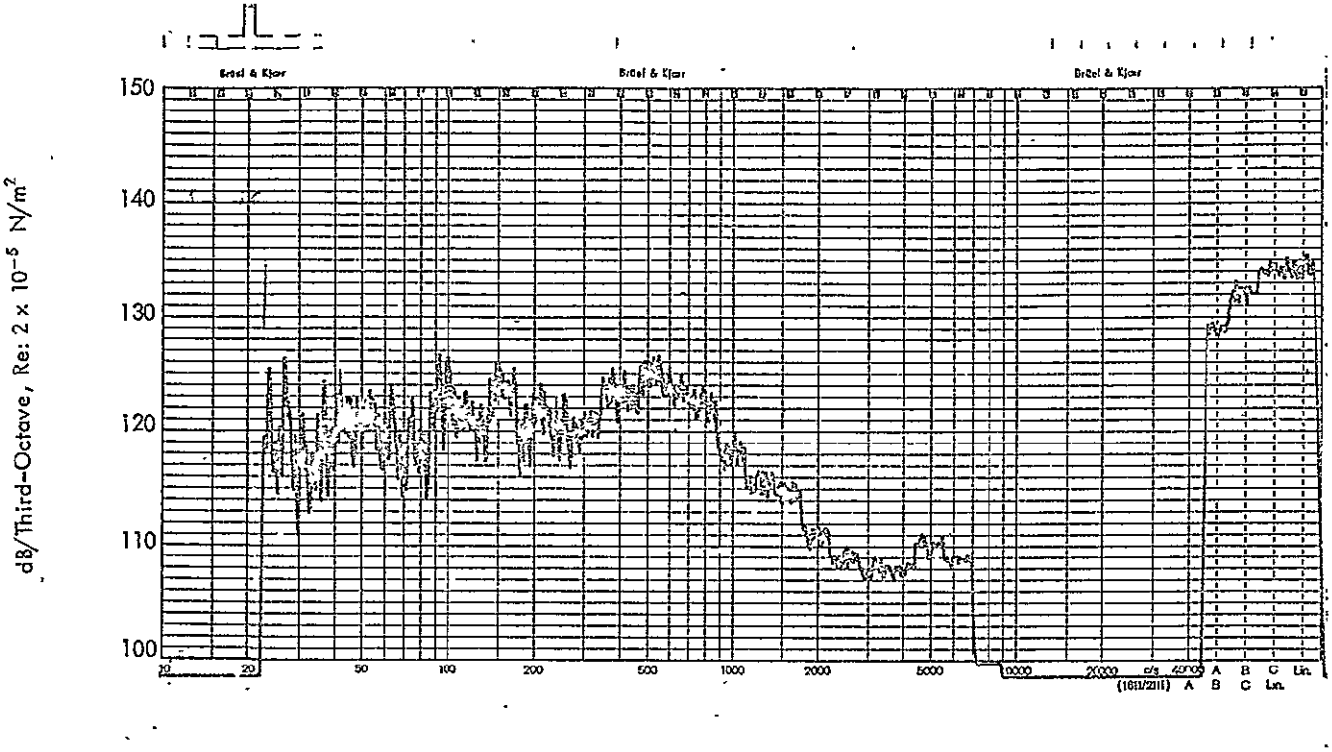

Figure B-3: Measured One-Third Octave Sound Pressure Levels, Experiment No. 1; External Microphone M3

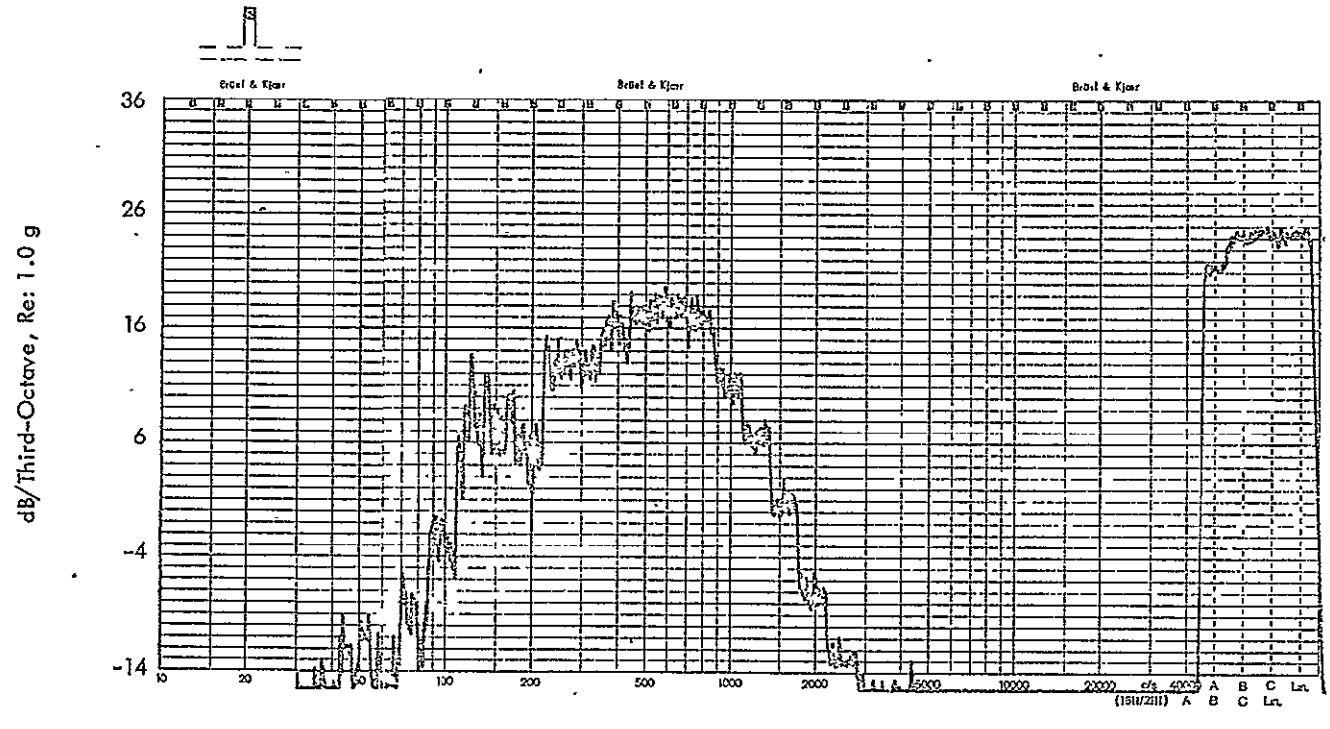

Figure B-4 : Measured One-Third Octave Acceleration Response Levels, Experiment No. 1; Accelerometer A1

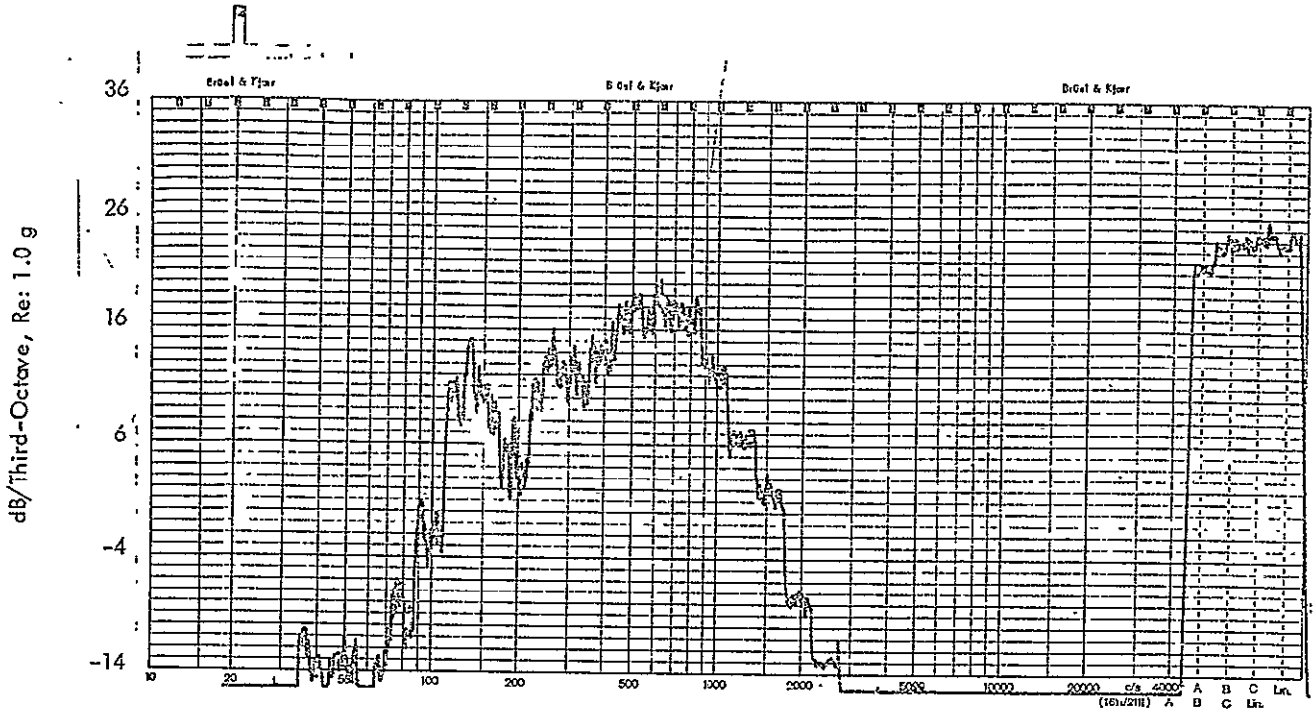

Figure B-5: Measured One-Third Octave Acceleration Response Levels, Experiment No. 1; Accelerometer A2

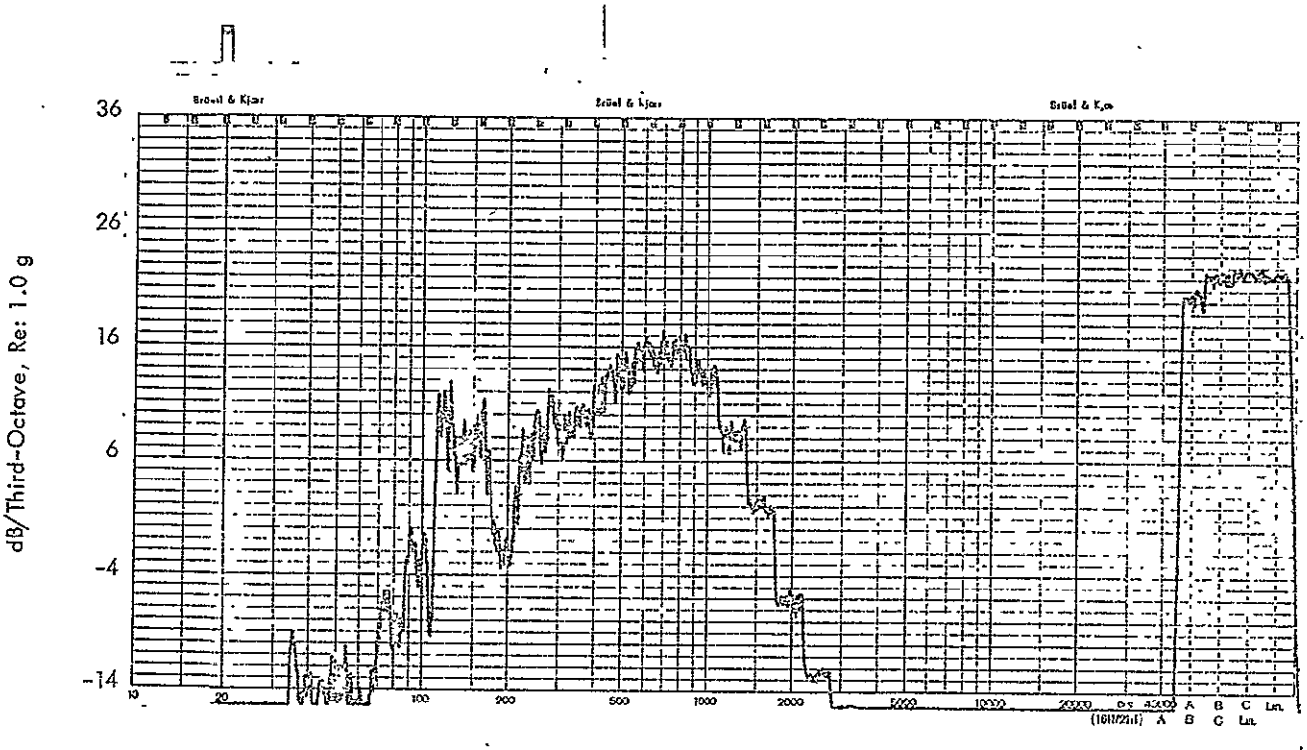

Figure B-6: Measured One-Third Octave Acceleration Response Levels, Experiment No. 1; Accelerometer A3

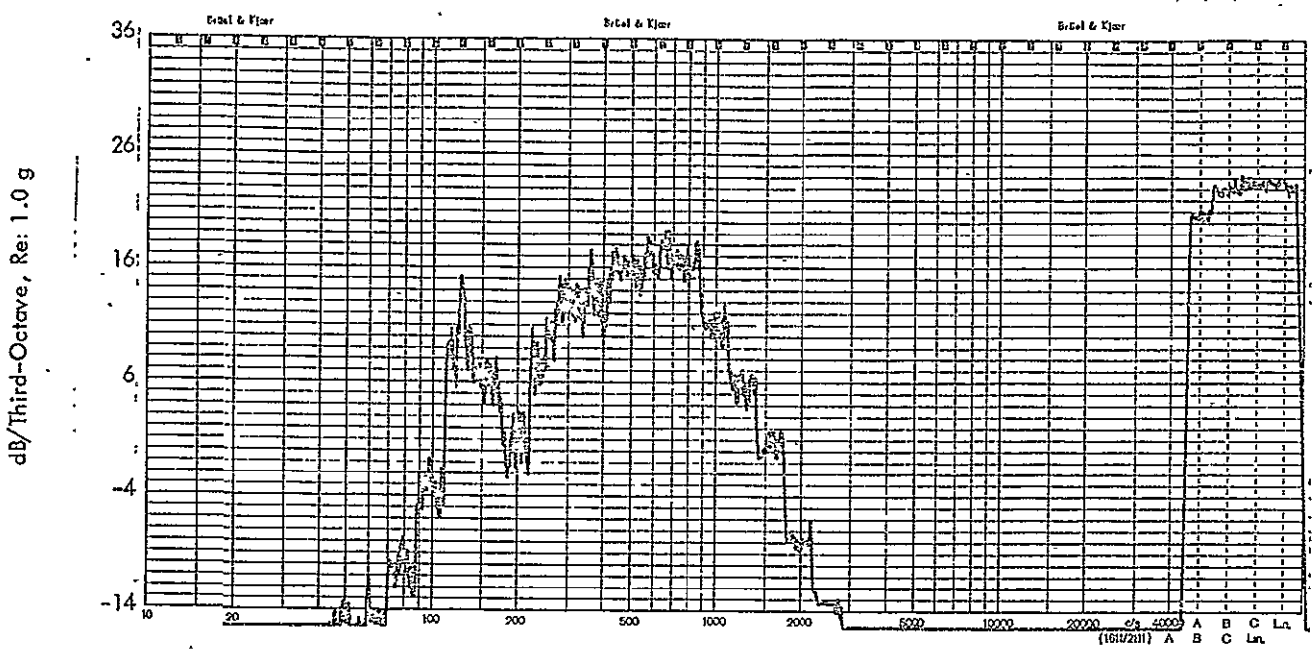

Figure B-7: Measured One-Third Octave Acceleration Response Levels, Experiment No. 1; Accelerometer A4

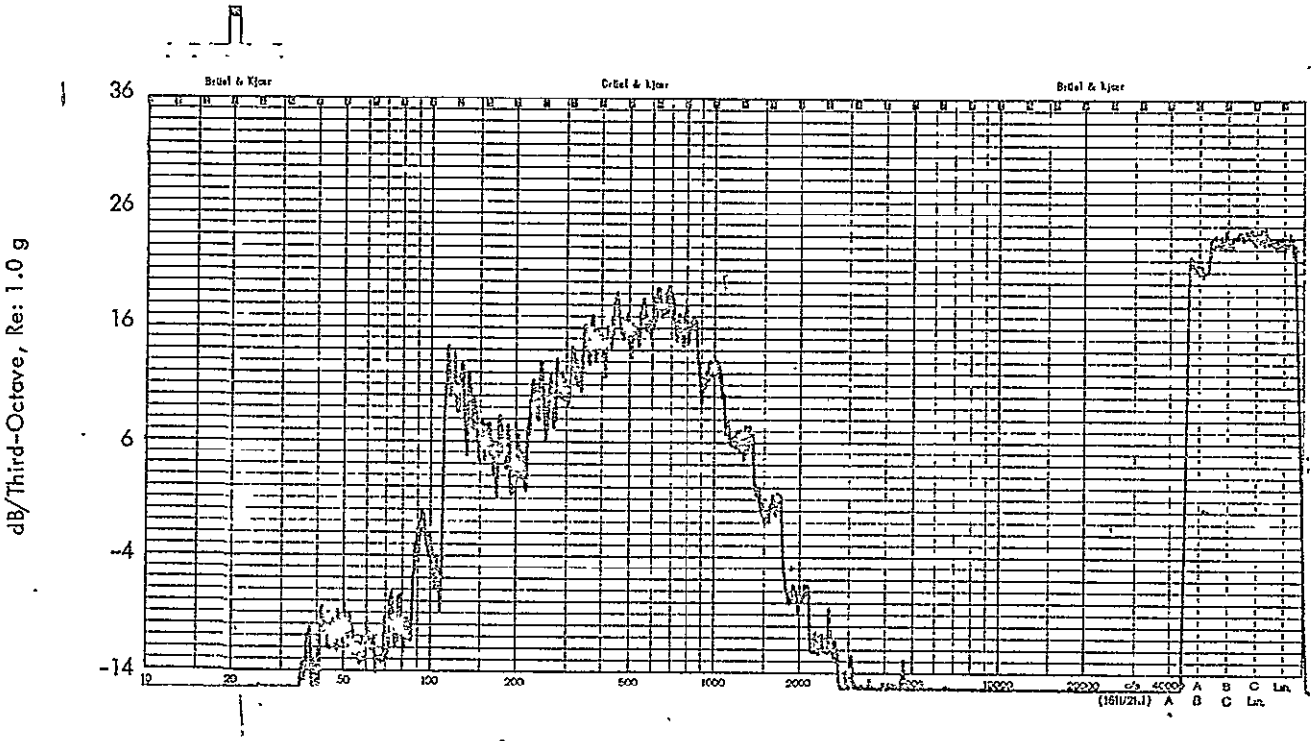

Figure B-8 : Measured One-Third Octave Acceleration Response Levels, Experiment No. 1; Accelerometer A5

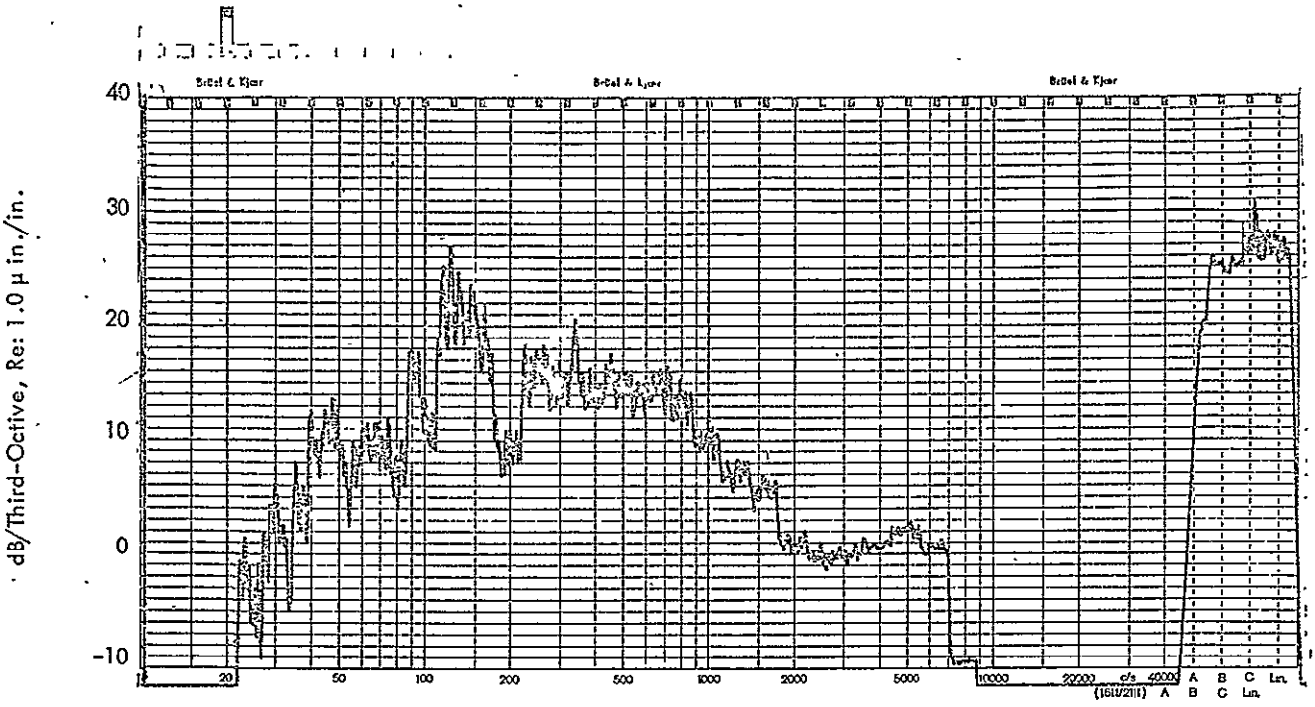

Figure B-9: Measured One-Third Octave Strain Levels, Experiment No. 1; Strain Gauge SG1

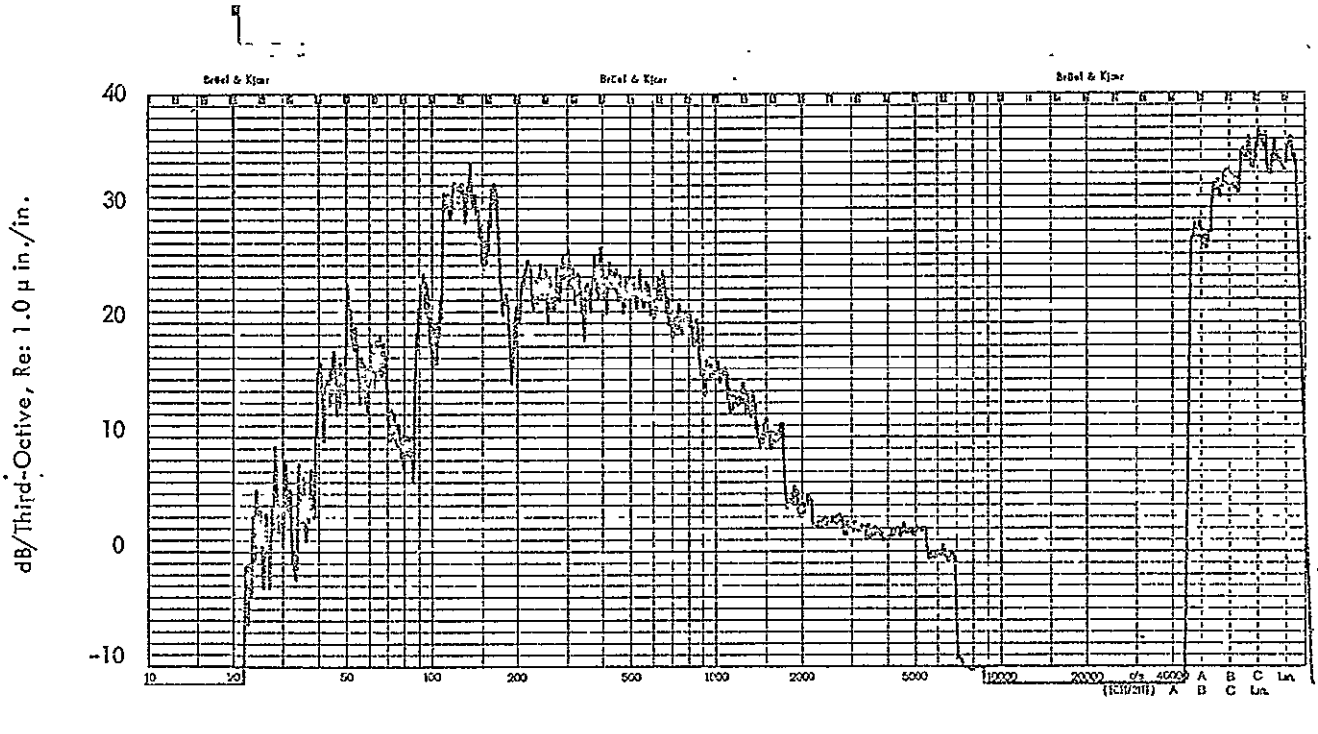

Figure B-10: Measured One-Third Octave Strain Levels, Experiment No. 1; Strain Gauge SG2

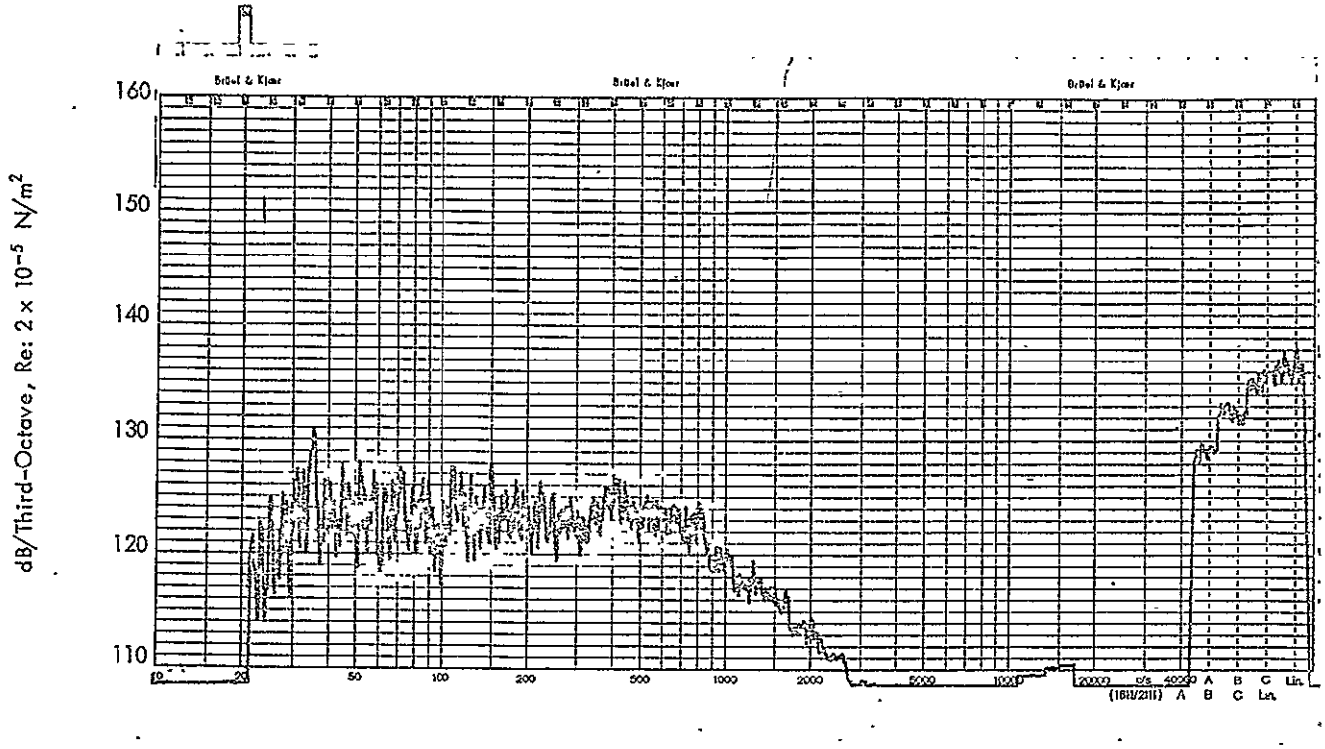

Figure B-11: Measured One-Third Octave Sound Pressure Levels, Experiment No. 2; External Microphone M1

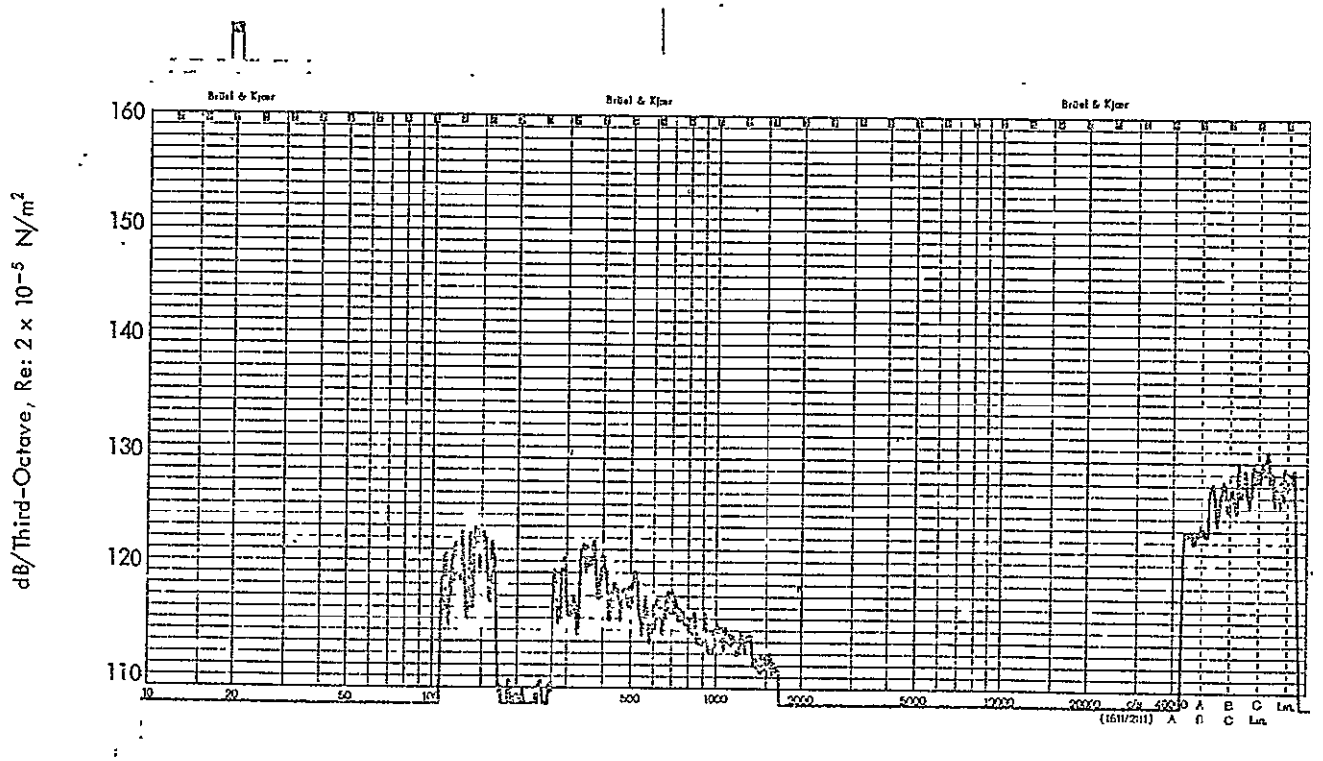

Figure B-12: Measured One-Third Octave Sound Pressure Levels, Experiment No. 2; Internal Microphone M2

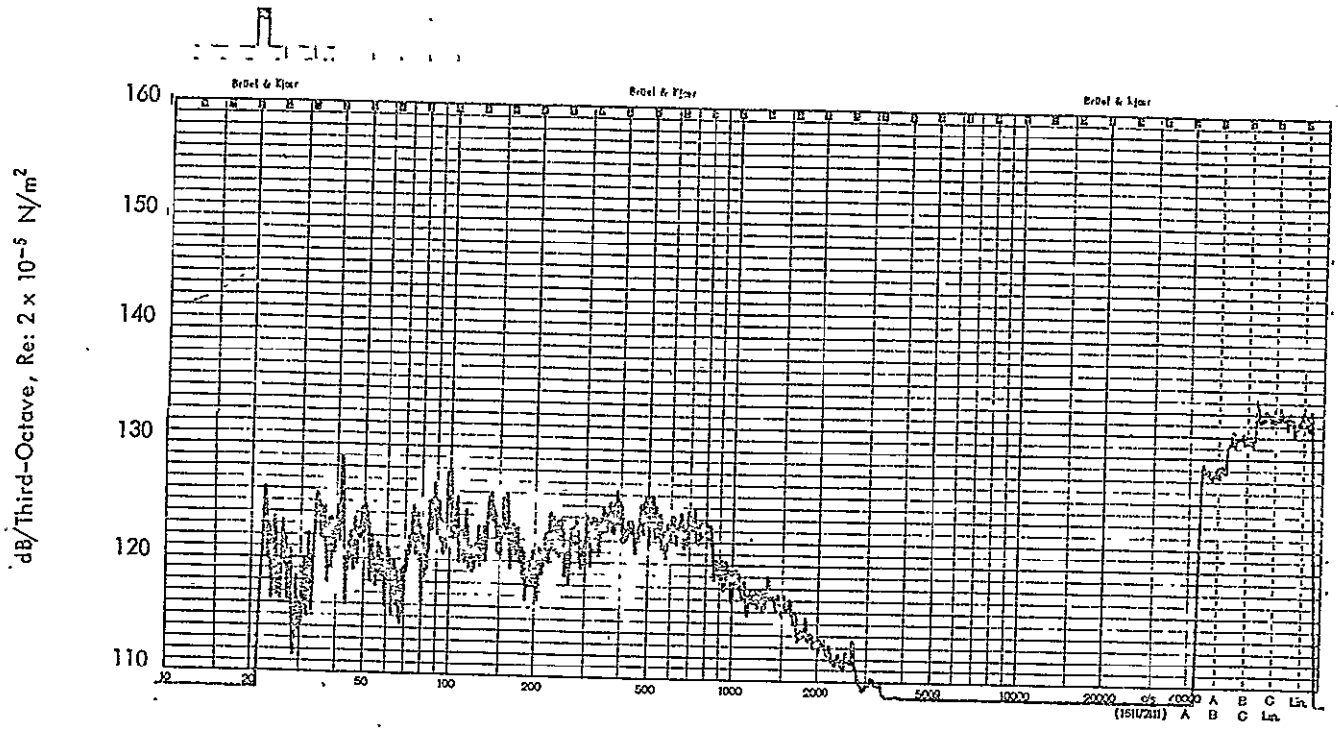

Figure B-13: Measured One-Third Octave Sound Pressure Levels, Experiment No. 2; External Microphone M3

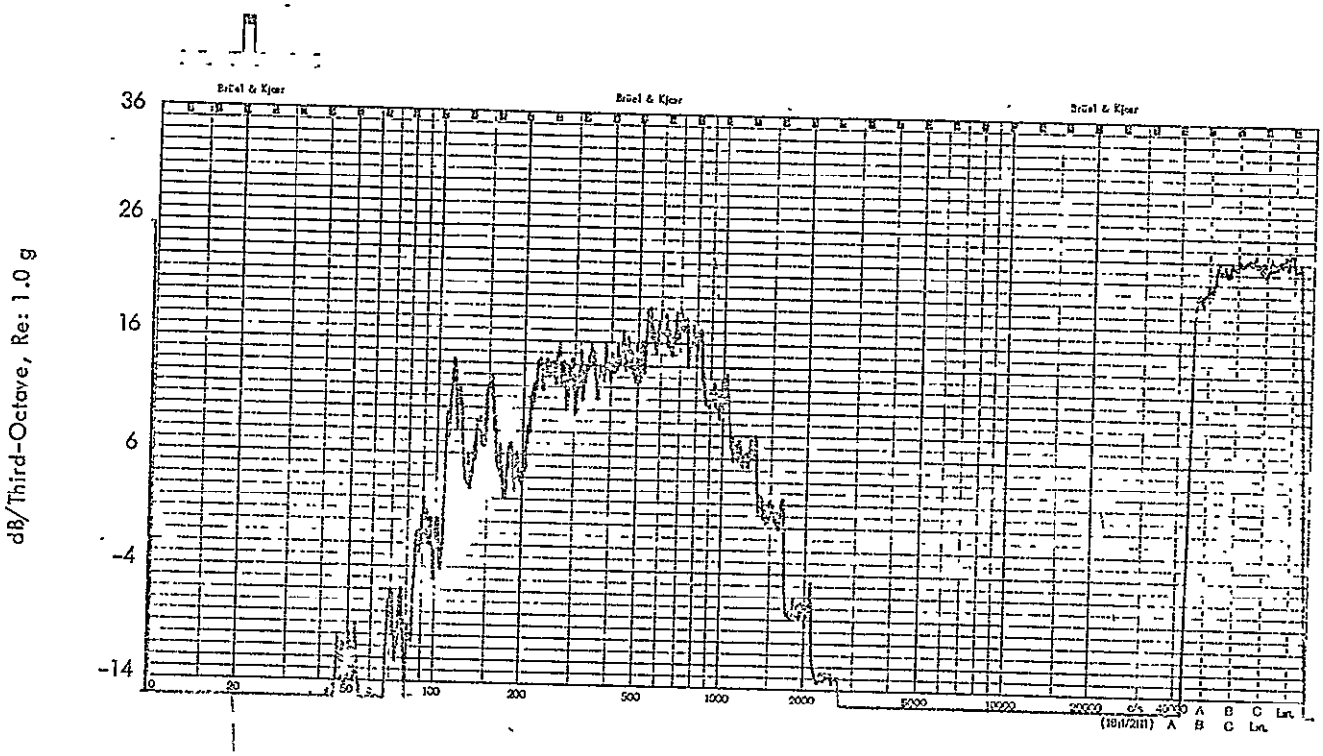

Figure B-14: Measured One-Third Octave Acceleration Response Levels, Experiment No. 2; Accelerometer A1

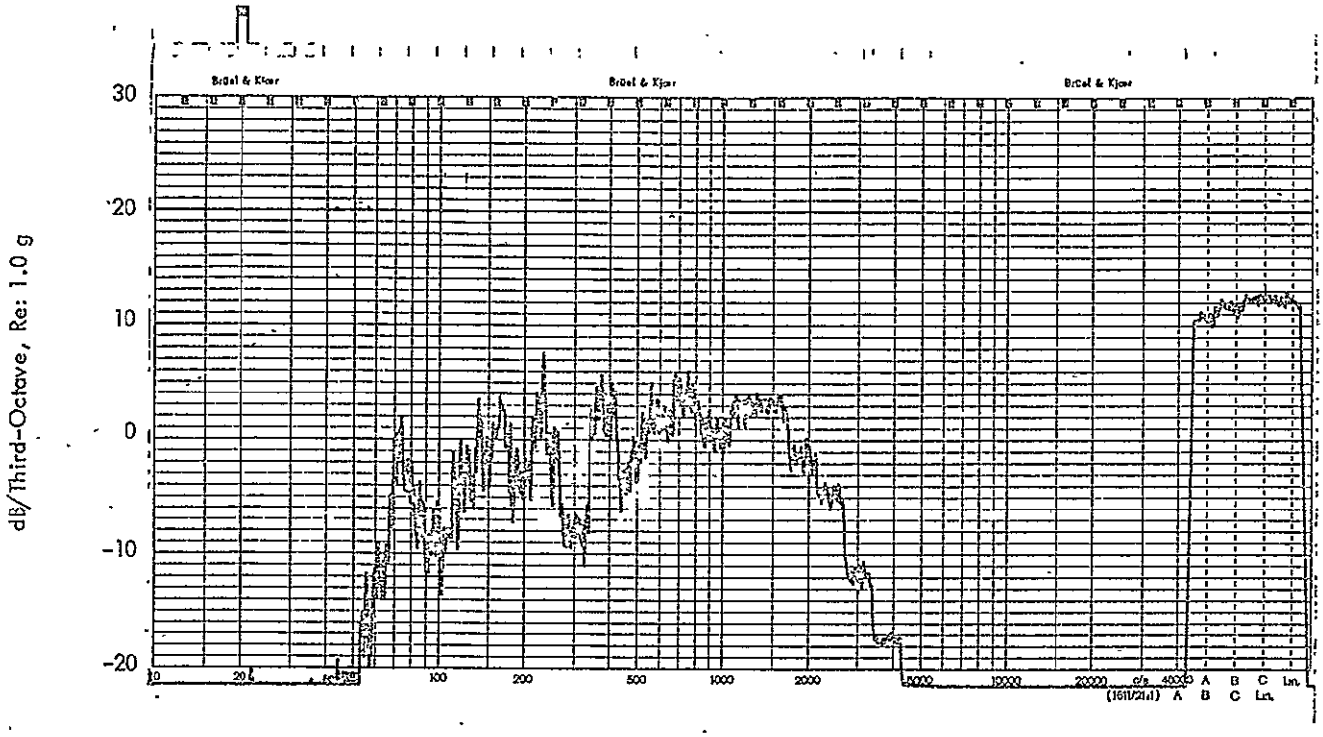

Figure B-15: Measured One-Third Octave Acceleration Response Levels, Experiment No. 2 ; Accelerometer A2

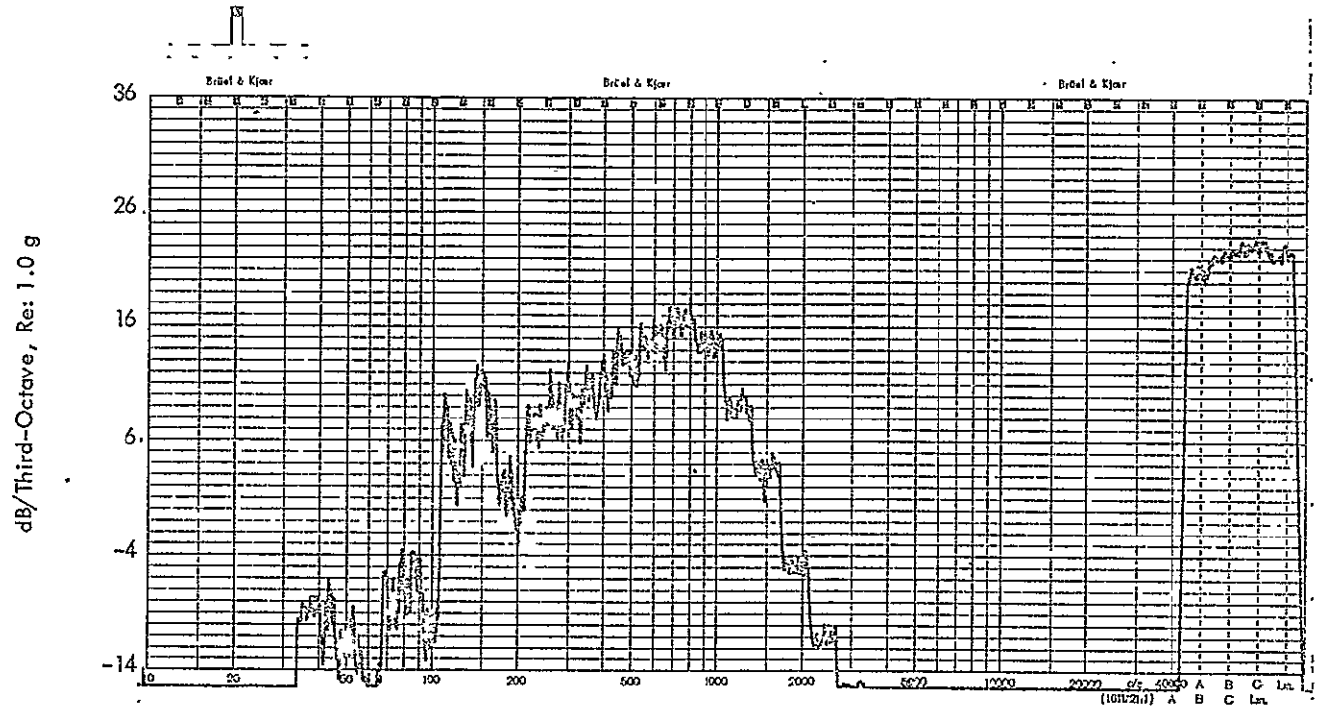

Figure B-16: Measured One-Third Octave Acceleration Response Levels, Experiment No. 2 ; Accelerometer A3

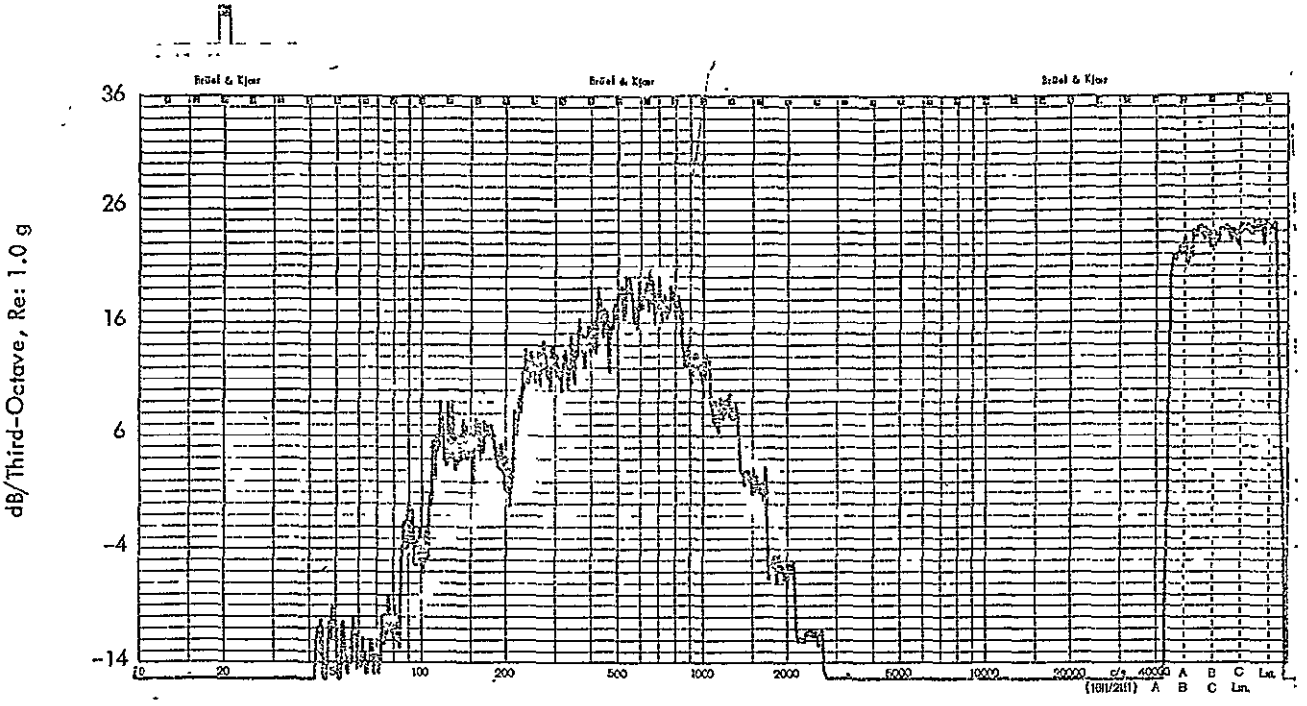

Figure B-17: Measured One-Third Octave Acceleration Response Levels, Experiment No. 2; Accelerometer A4

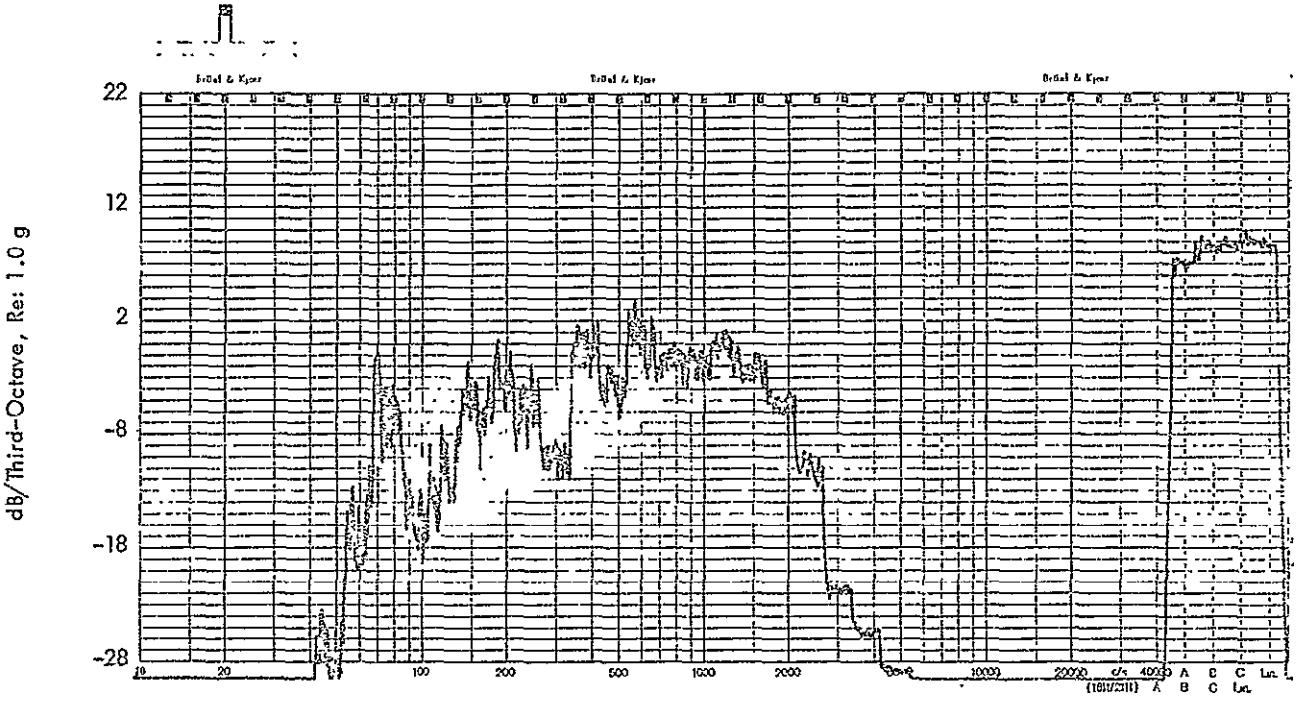

Figure B-18: Measured One-Third Octave Acceleration Response Levels, Experiment No. 2; Accelerometer A5

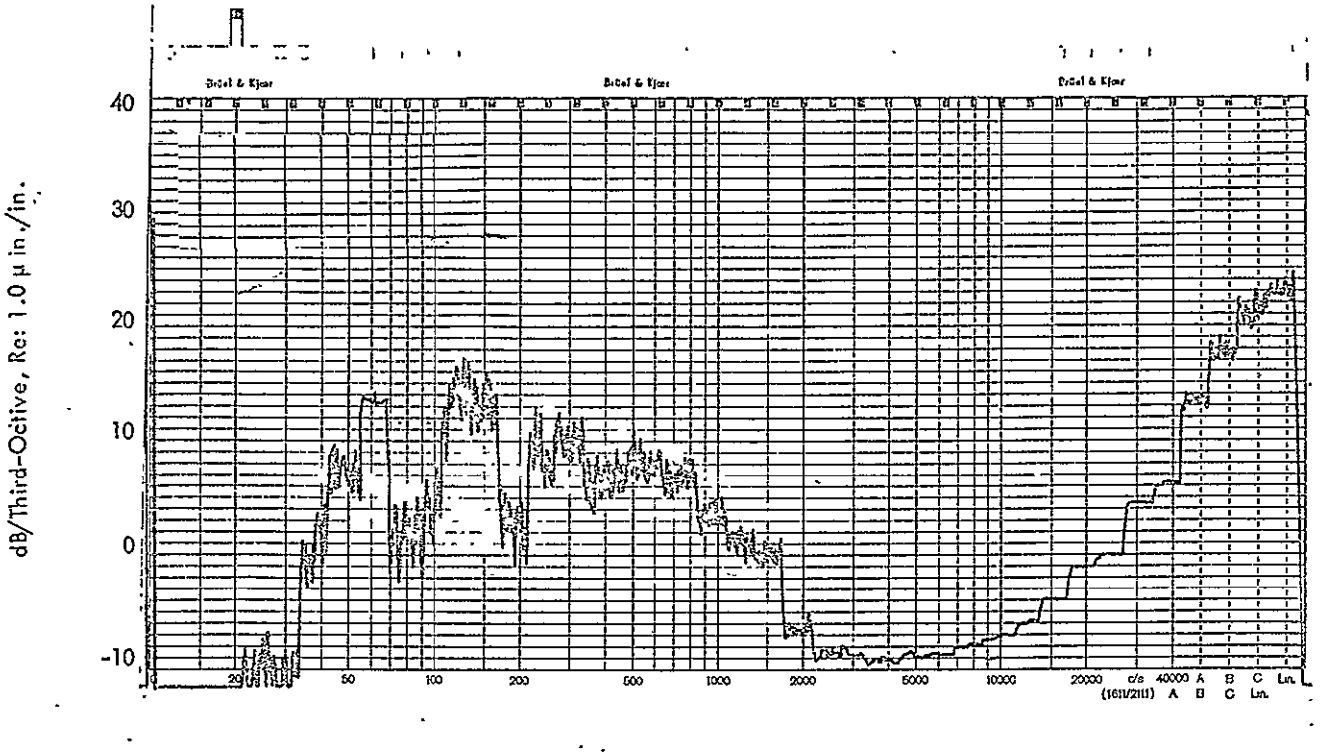

Figure B-19: Measured One-Third Octave Strain Levels, Experiment No. 2; Strain Gauge SG1

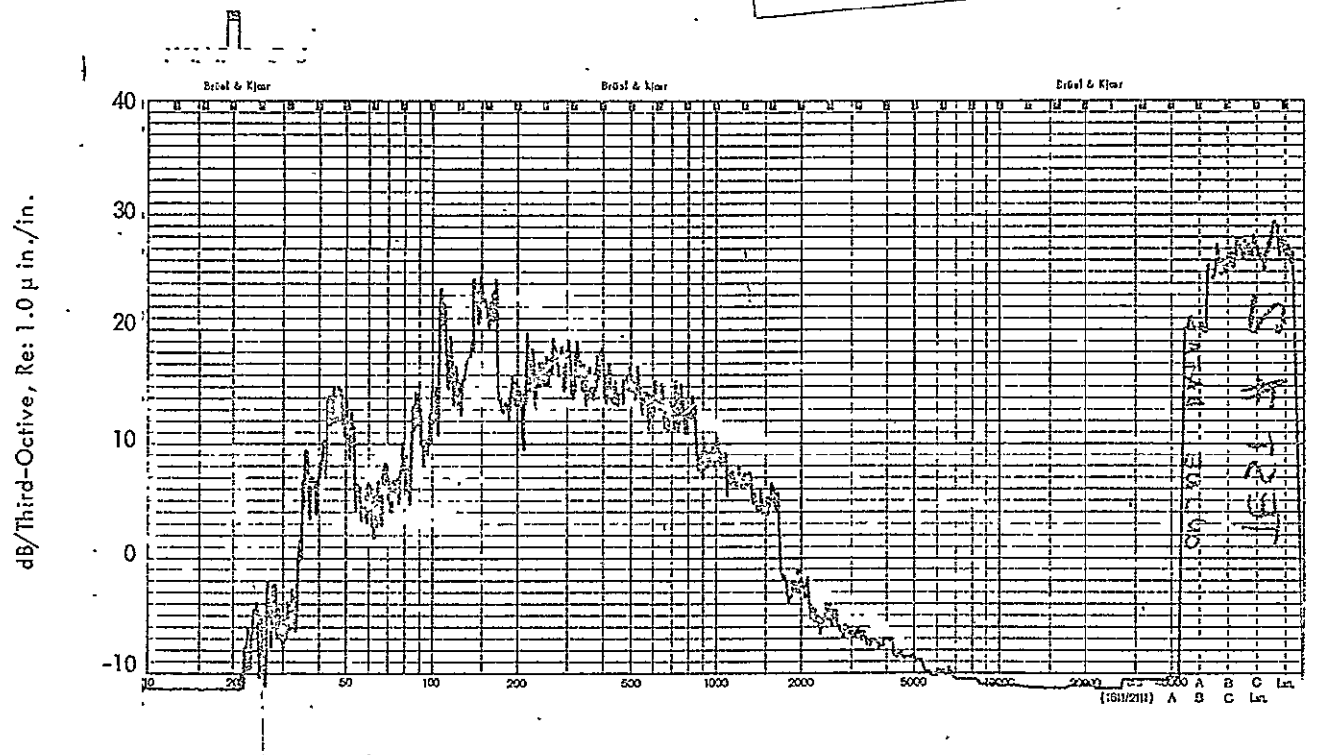

Figure B-20: Measured One-Third Octave Strain Levels, Experiment No. 2; Strain Gauge SG2

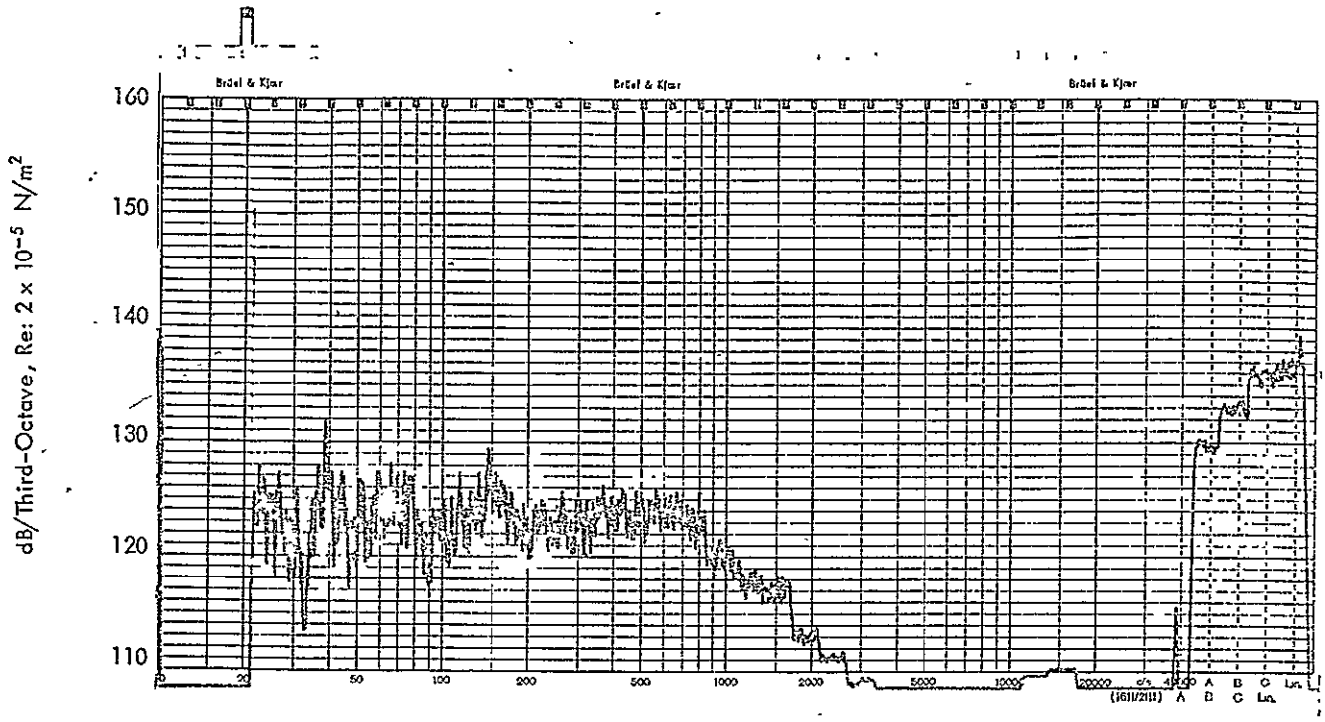

Figure B-21: Measured One-Third Octave Sound Pressure Levels, Experiment No. 3; External Microphone M1

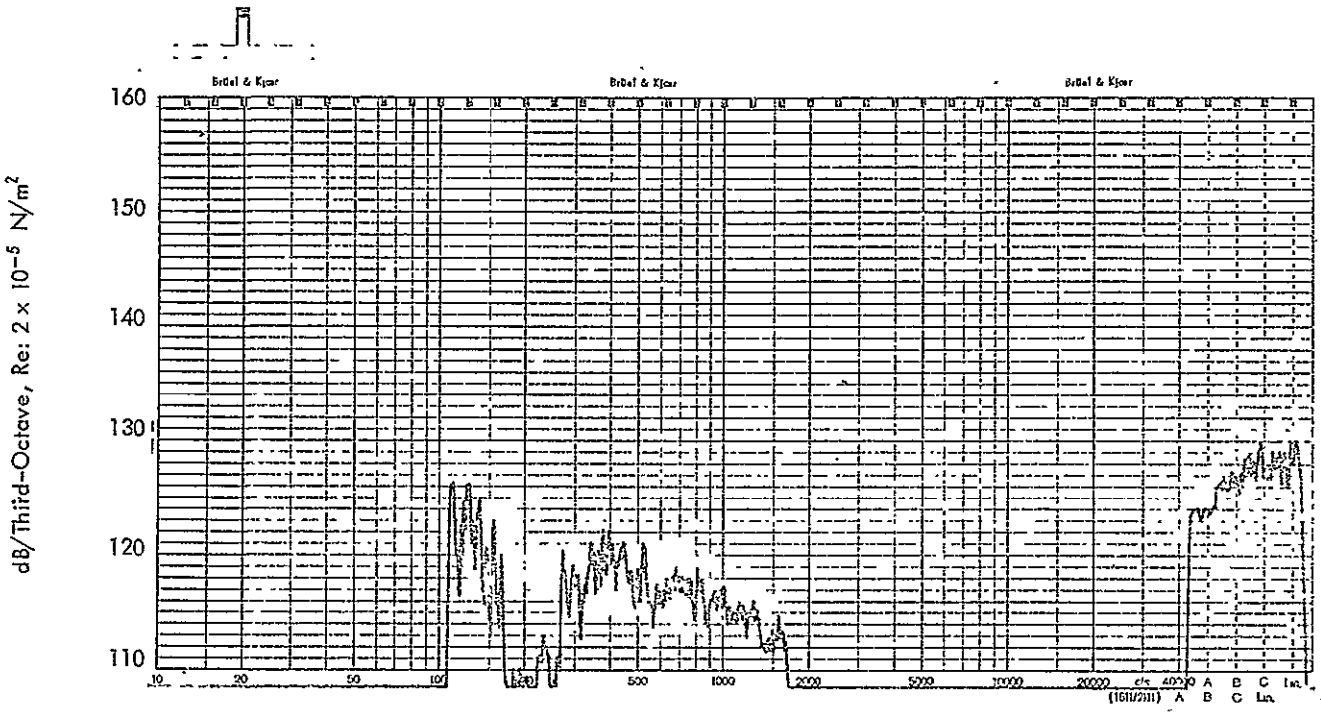

Figure B-22: Measured One-Third Octave Sound Pressure Levels, Experiment No. 3; Internal Microphone M2

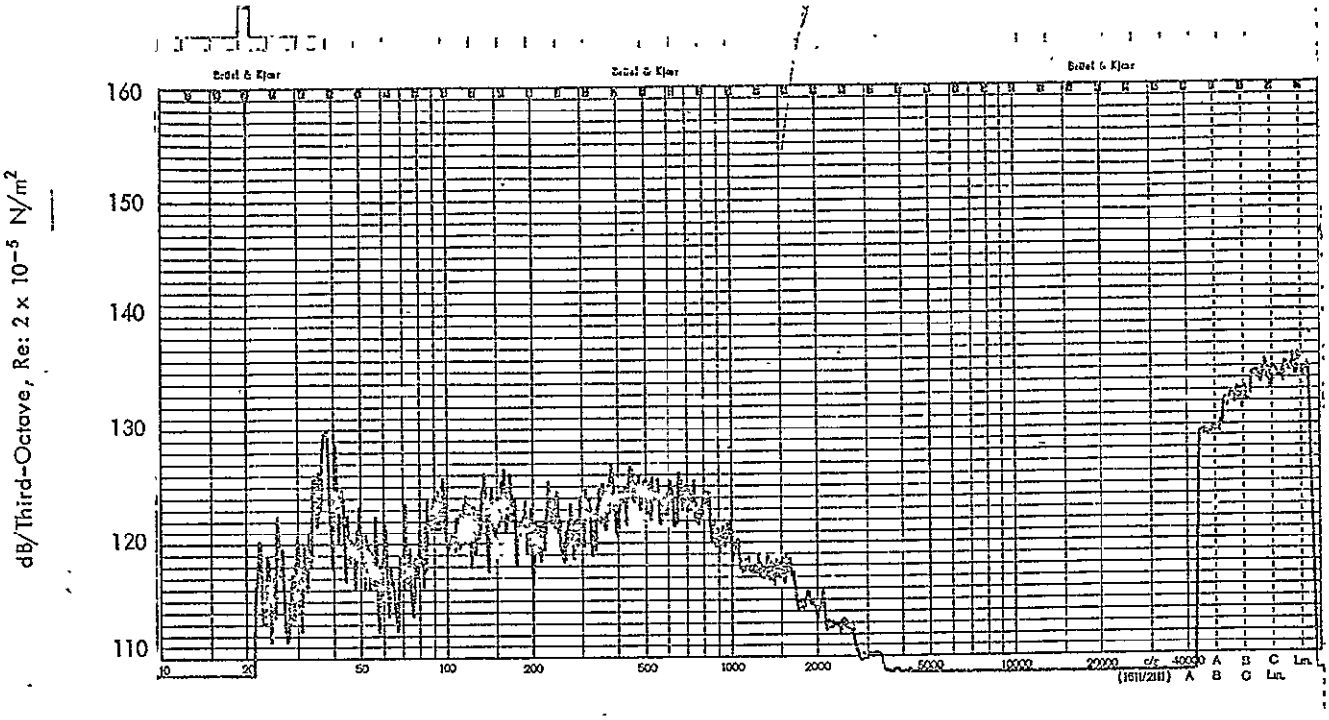

Figure B-23: Measured One-Third Octave Sound Pressure Levels, Experiment No. 3; External Microphone M3

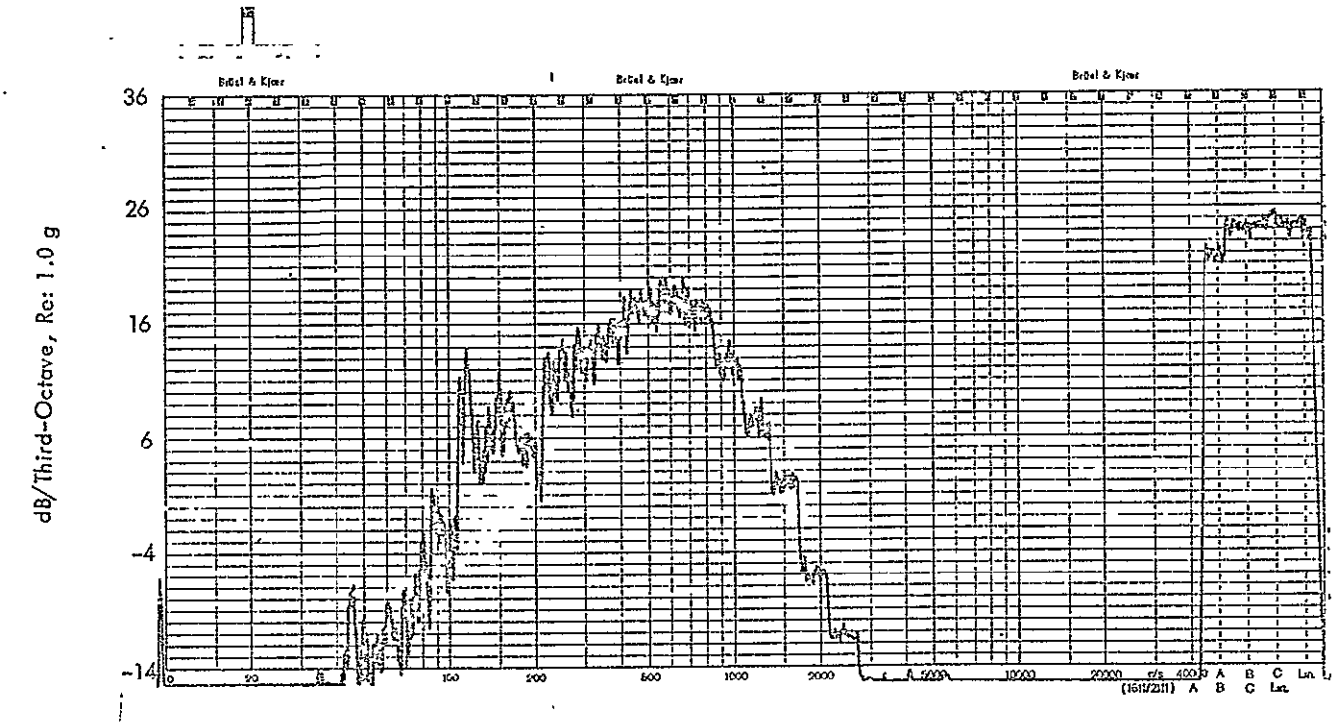

Figure B-24: Measured One-Third Octave Acceleration Response Levels, Experiment No. 3; Accelerometer A1

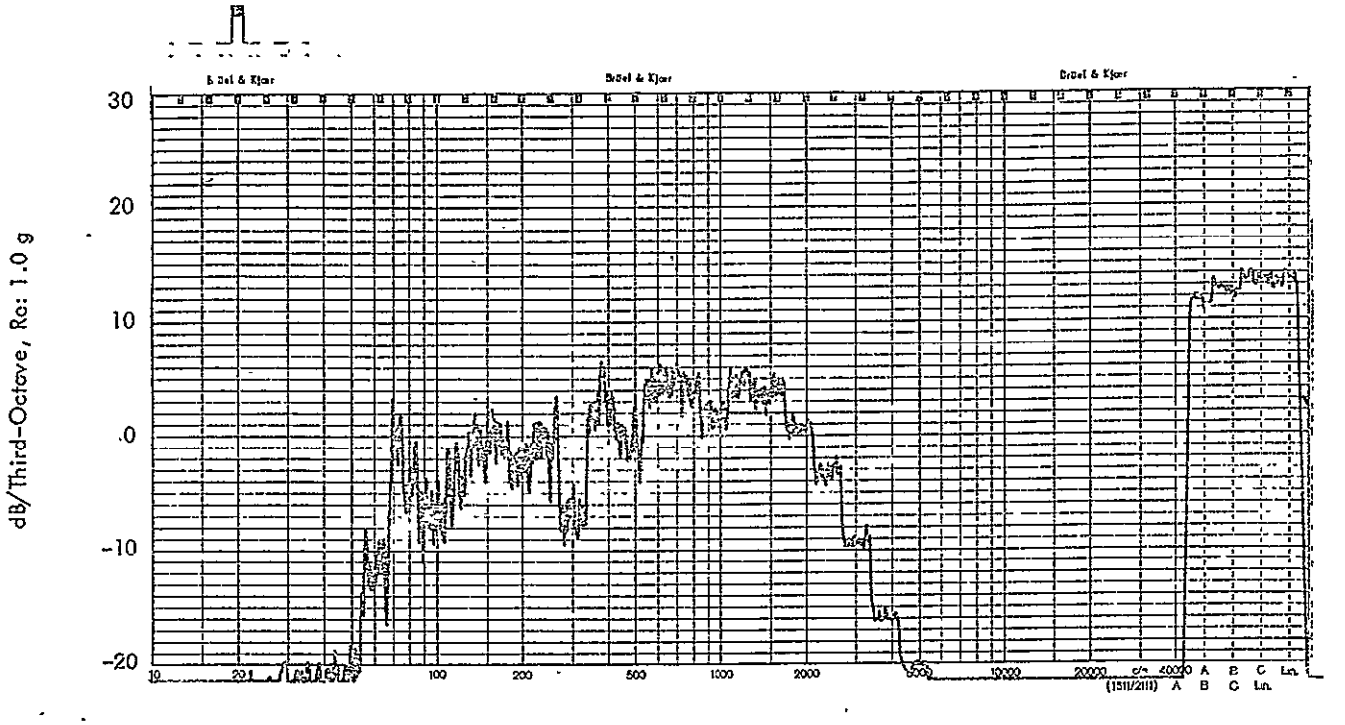

Figure B-25: Measured One-Third Octave Acceleration Response Levels, Experiment No. 3 ; Accelerometer A2

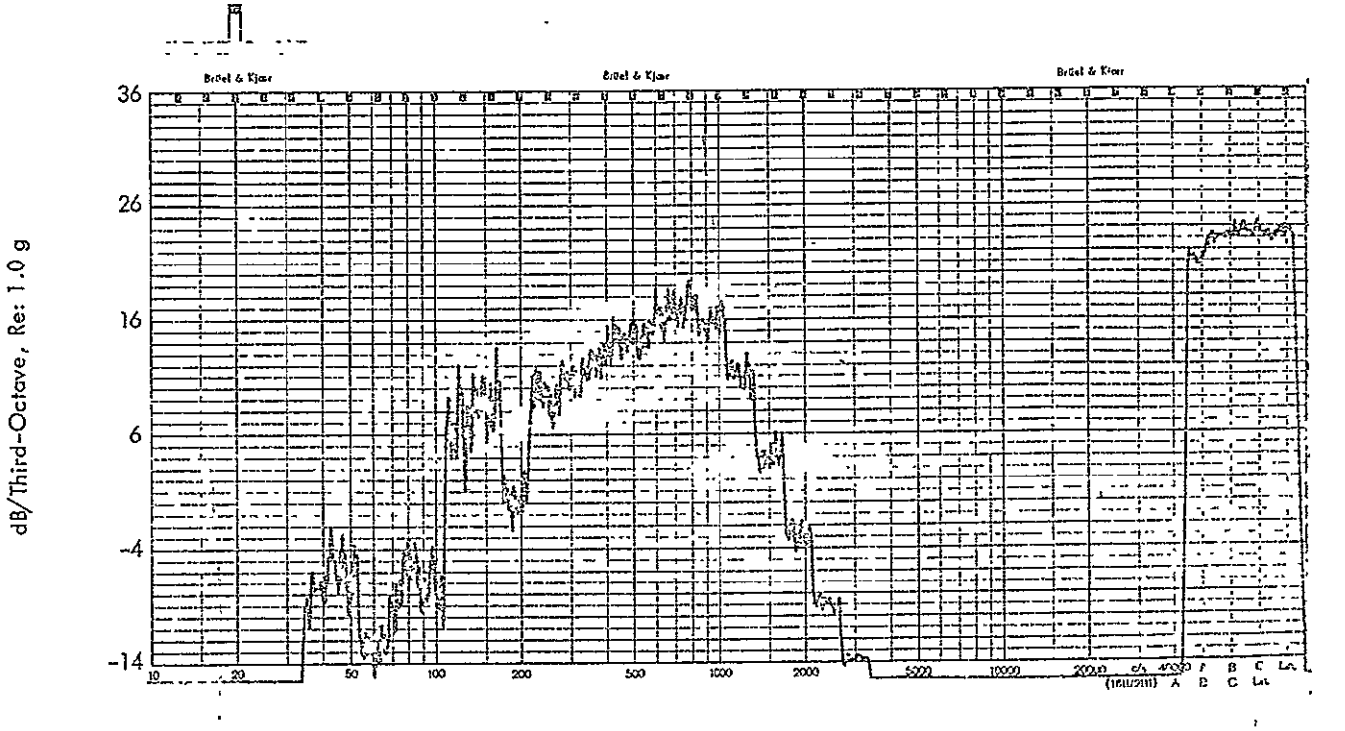

Figure B-26: Measured One-Third Octave Acceleration Response Levels, Experiment No. 3 ; Accelerometer A3

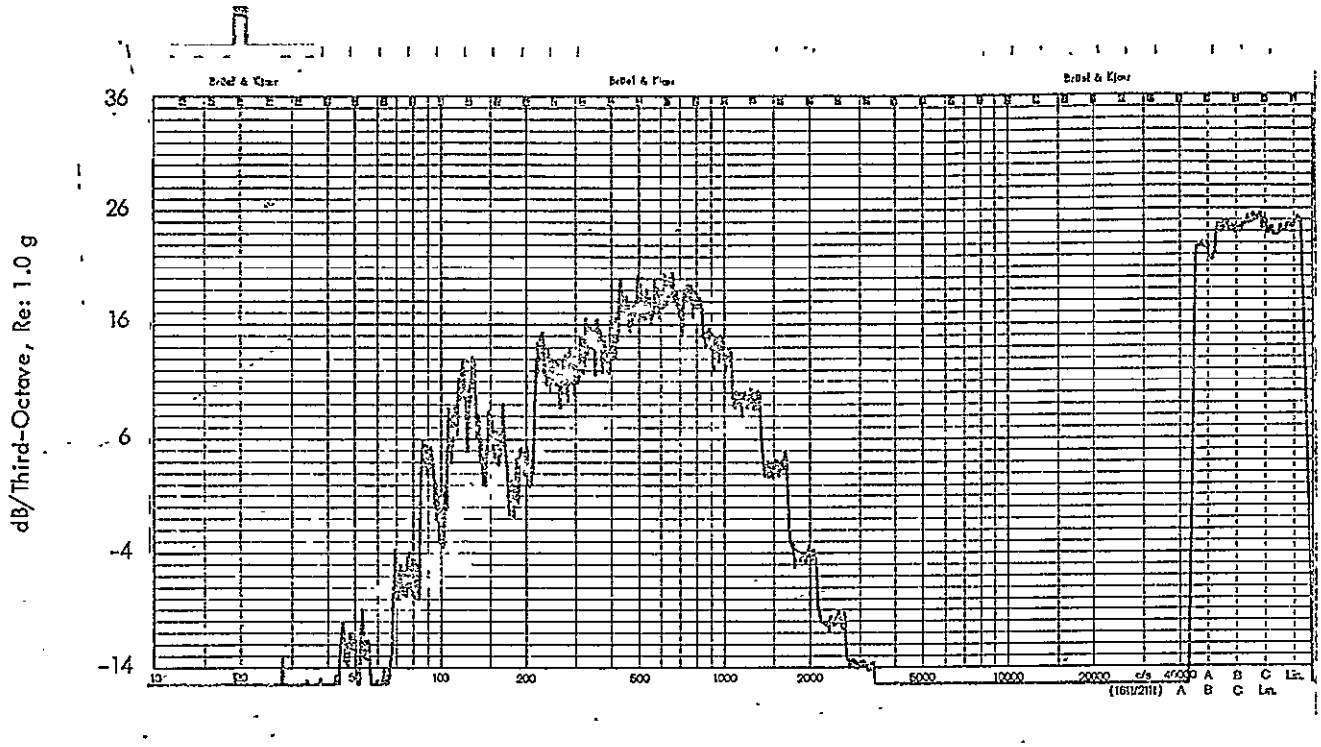

Figure B-27: Measured One-Third Octave Acceleration Response Levels, Experiment No. 3; Accelerometer A4

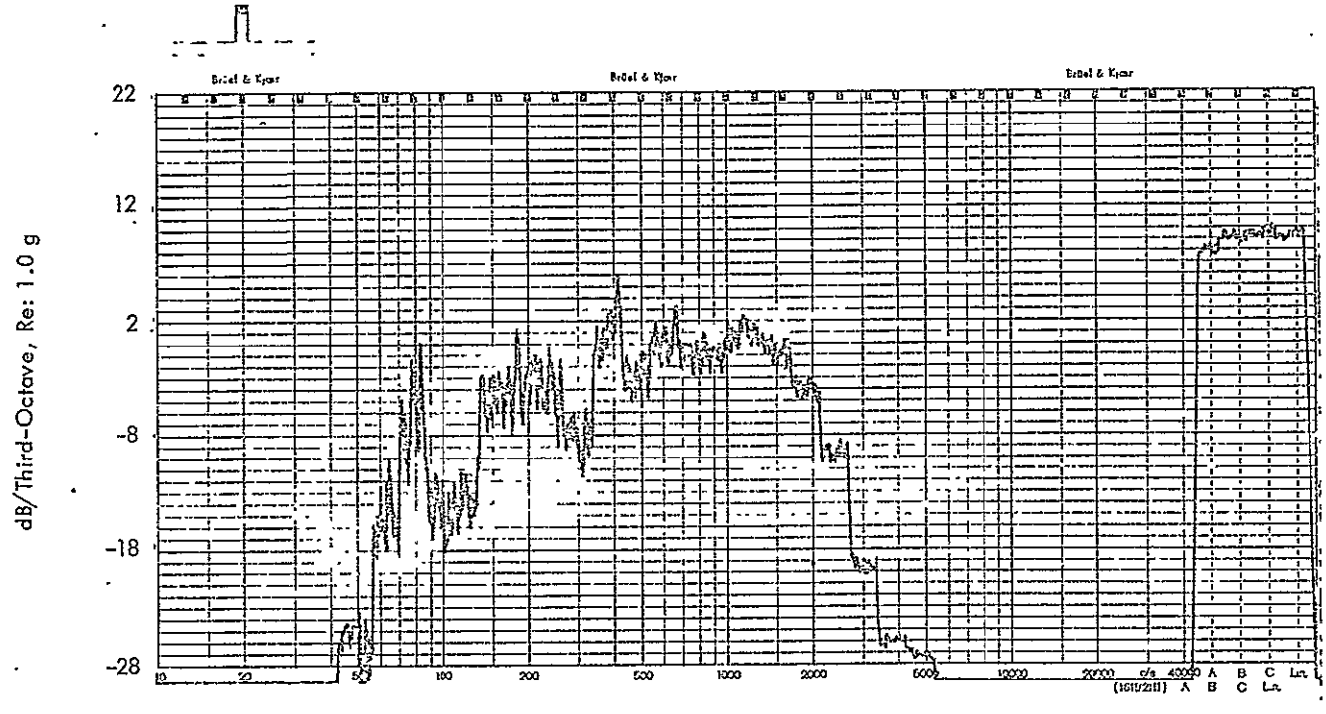

Figure B-28: Measured One-Third Octave Acceleration Response Levels, Experiment No. 3; Accelerometer A5

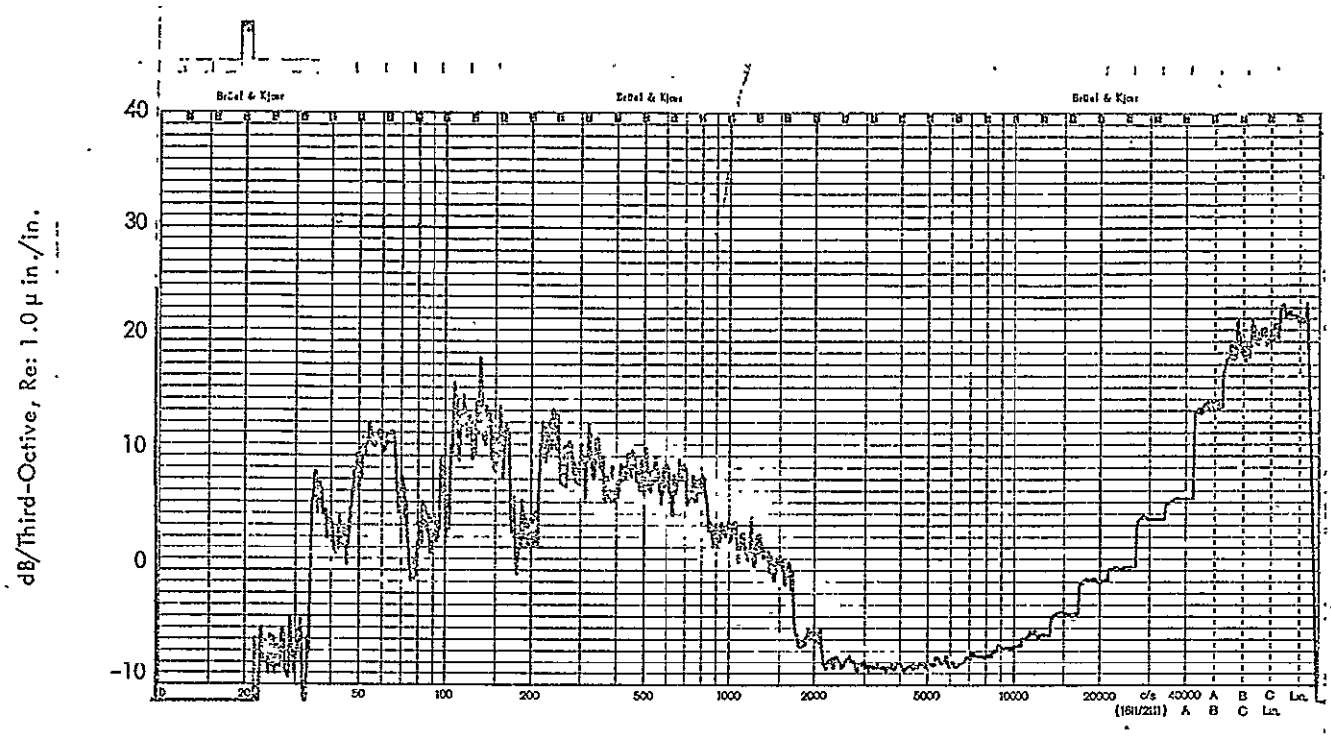

Figure B-29: Measured One-Third Octave Strain Levels, Experiment No. 3; Strain Gauge SG1

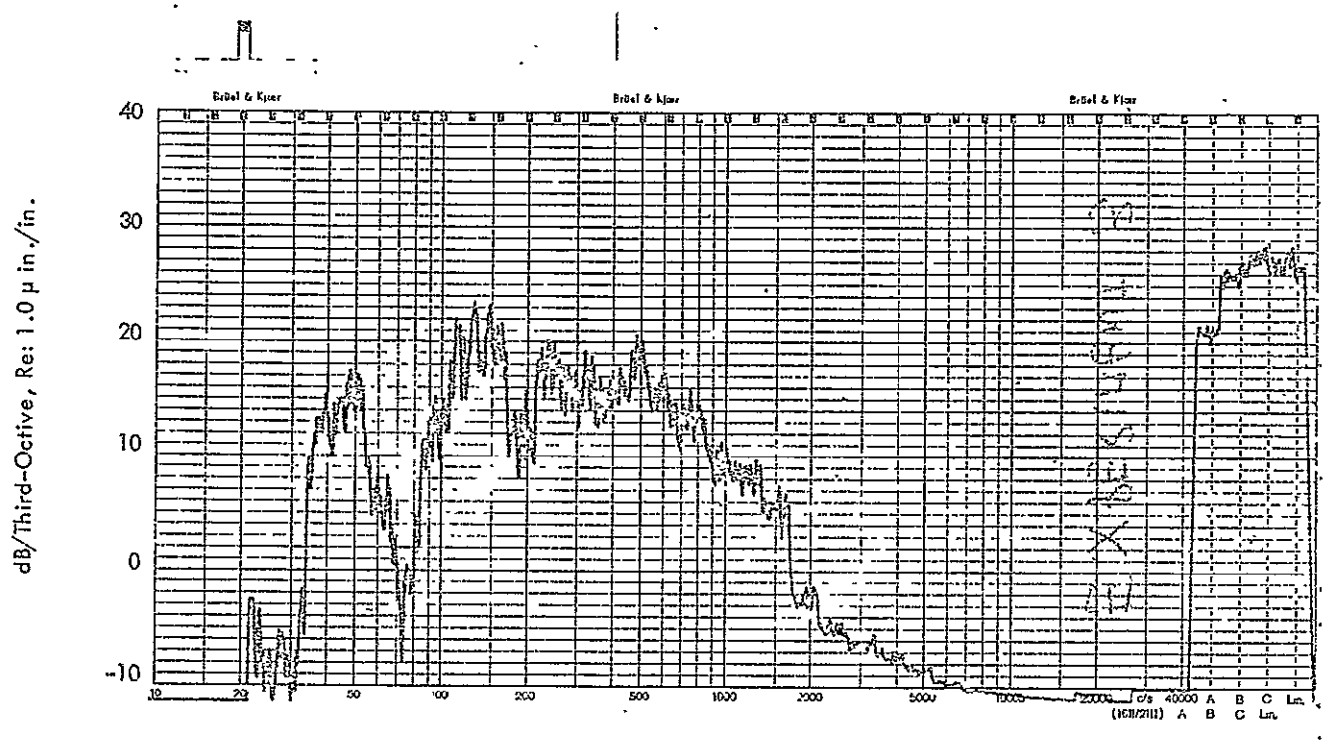

Figure B-30: Measured One-Third Octave Strain Levels, Experiment No. 3; Strain Gauge SG2

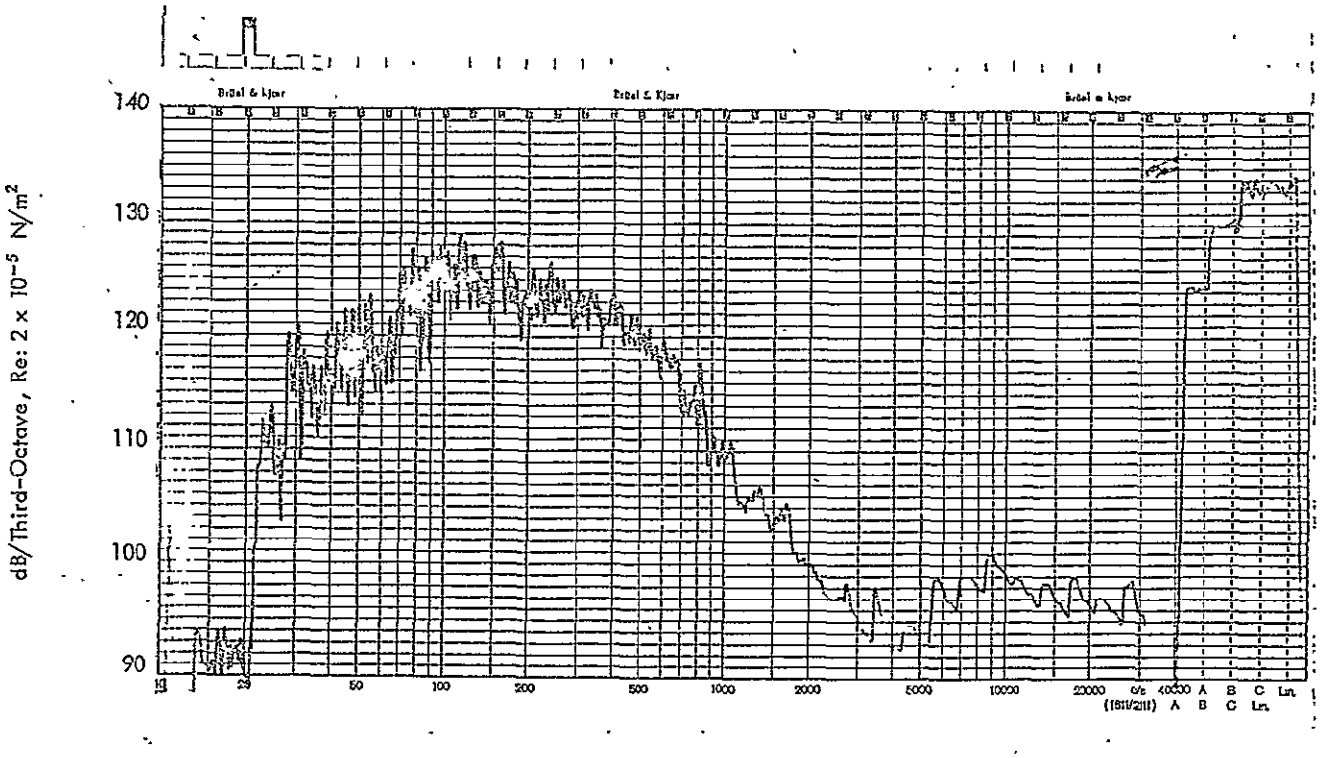

Figure B-31: Measured One-Third Octave Sound Pressure Levels, Experiment No. 4; External Microphone M1

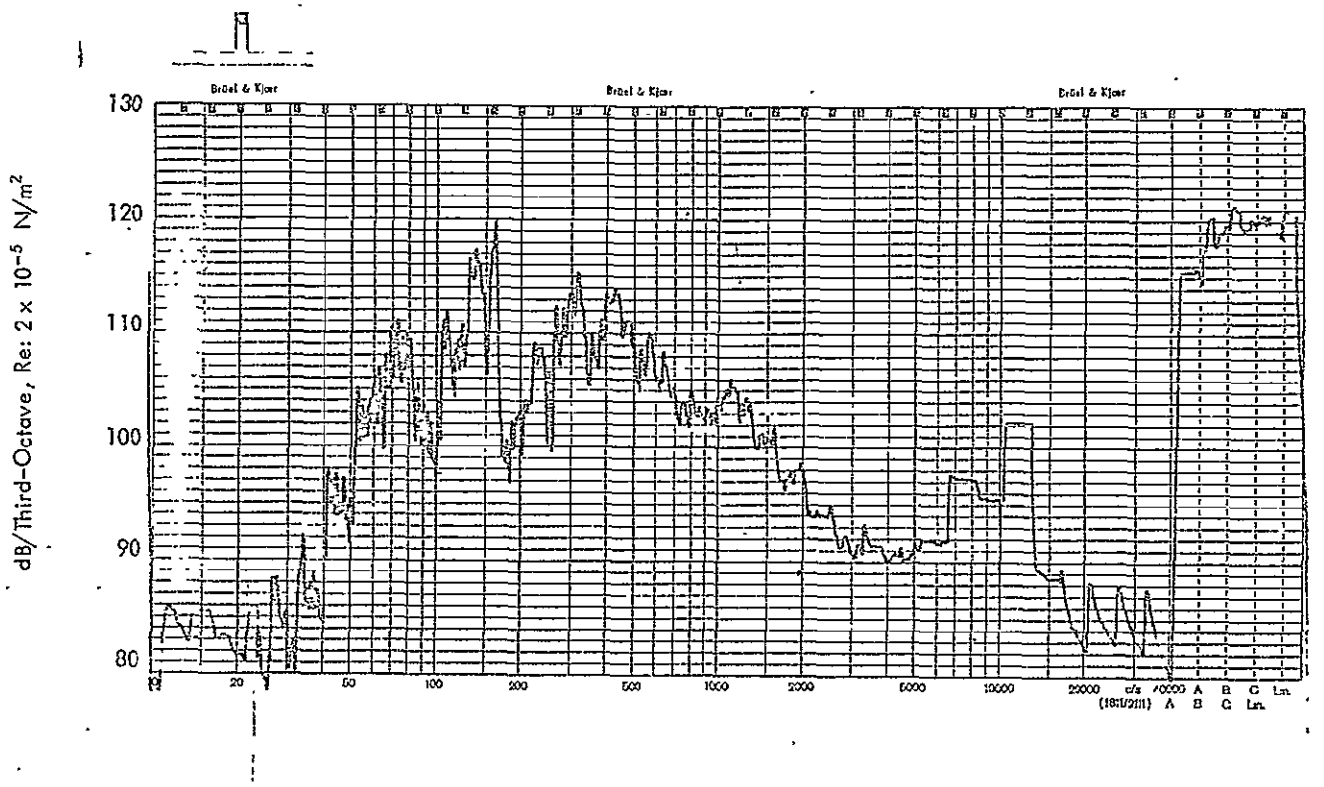

Figure B-32: Measured One-Third Octave Sound Pressure Levels, Experiment No. 4; Internal Microphone M2

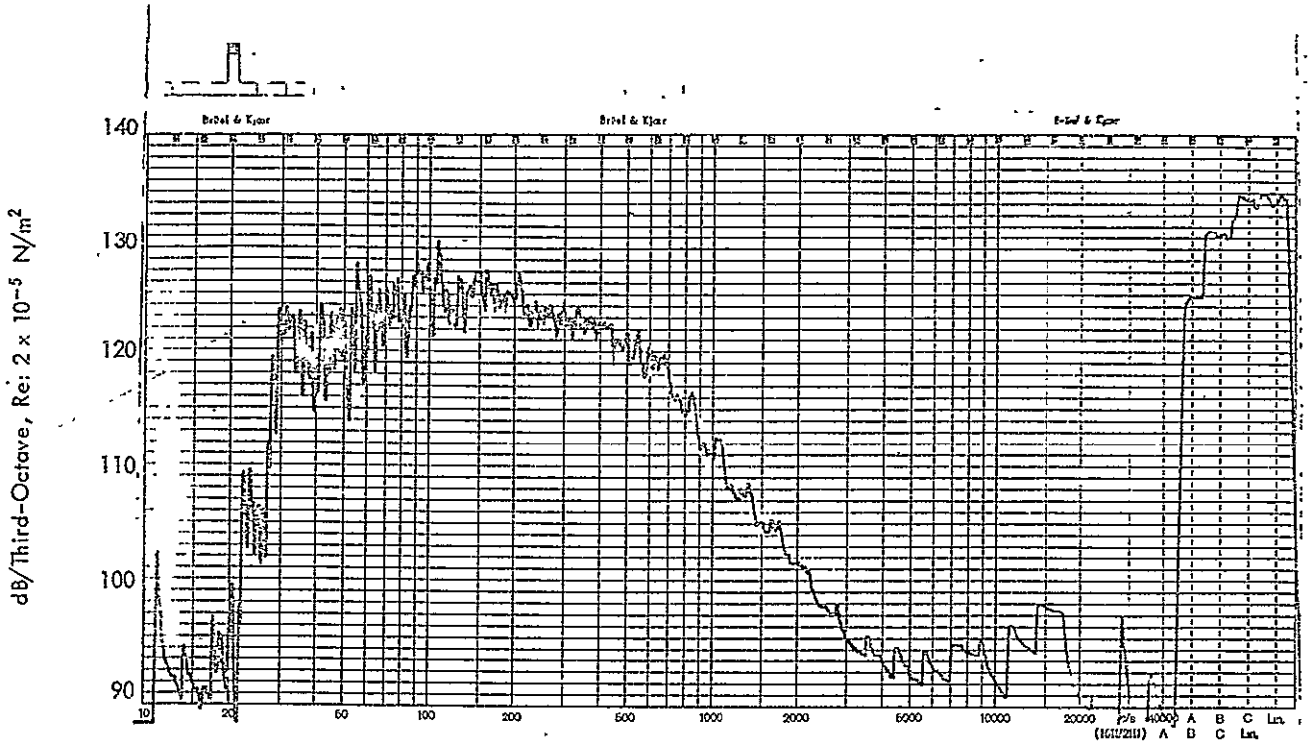

Figure B-33: Measured One-Third Octave Sound Pressure Levels, Experiment No. 4; External Microphone M3

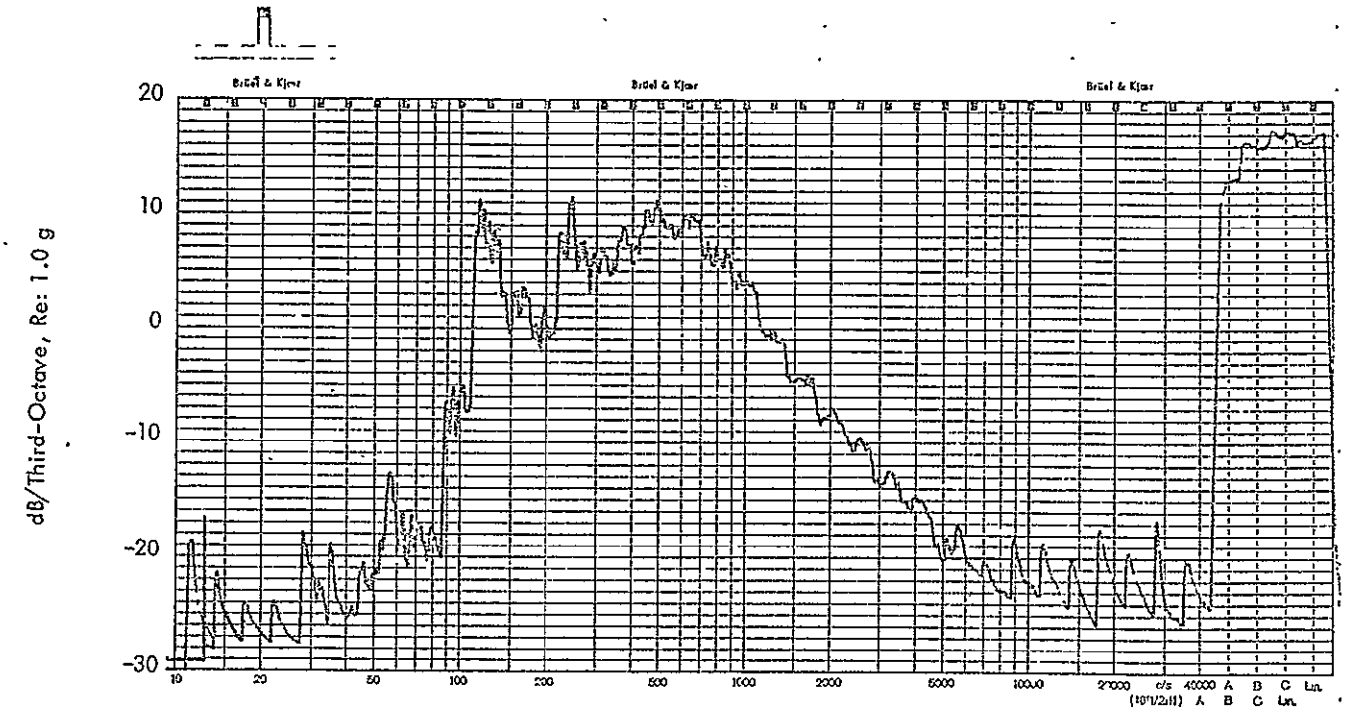

Figure B-34: Measured One-Third Octave Acceleration Response Levels, Experiment No. 4; Accelerometer A1

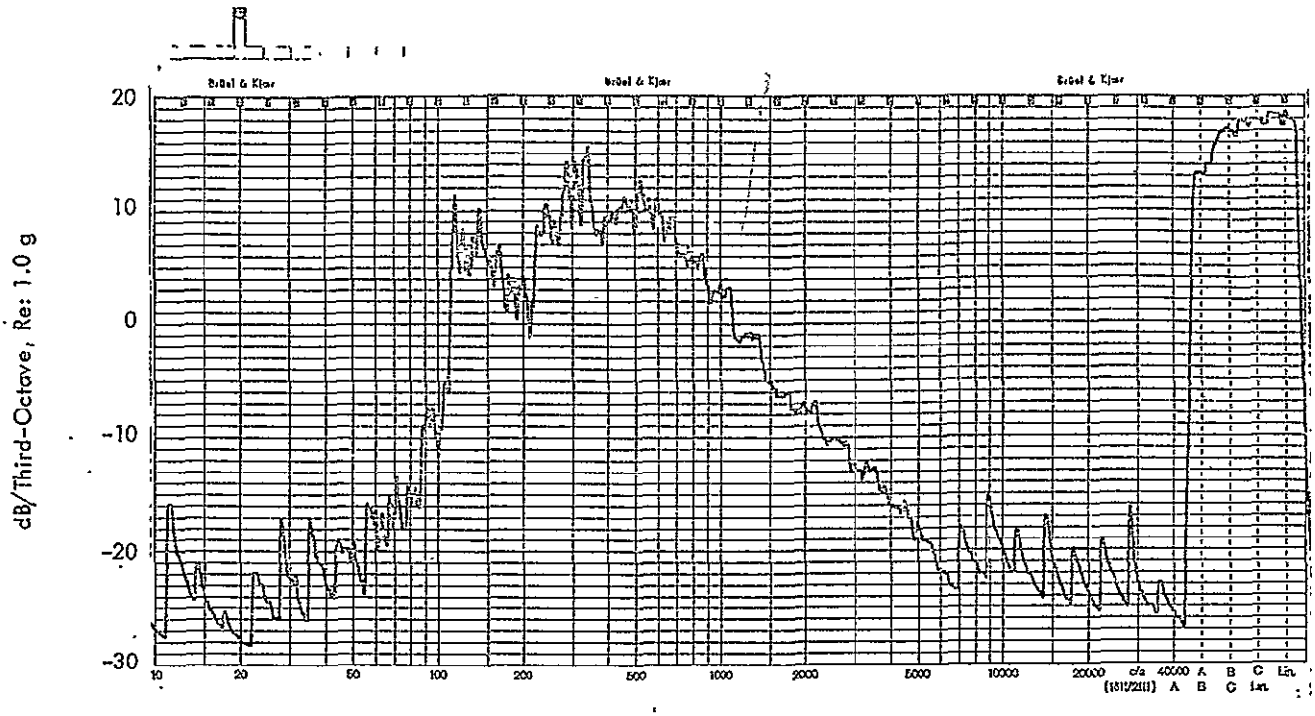

Figure B-35: Measured One-Third Octave Acceleration Response Levels, Experiment No. 4; Accelerometer A3

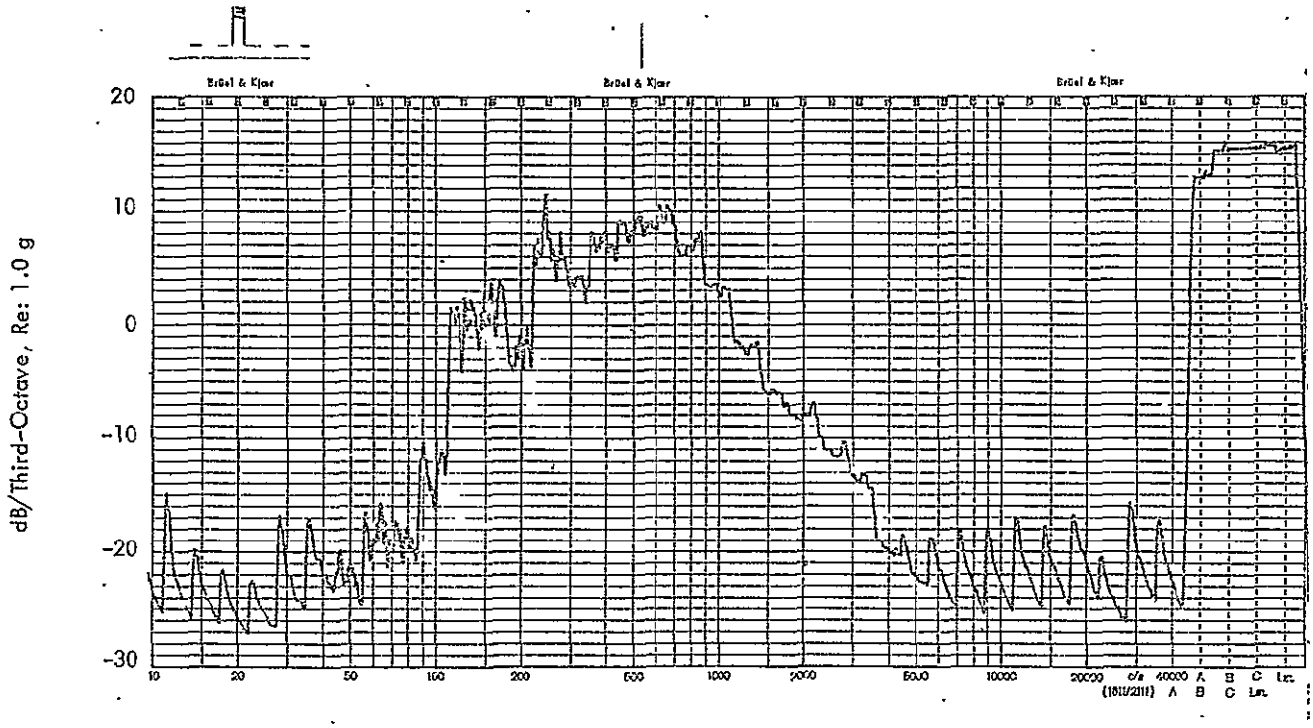

Figure B-36: Measured One-Third Octave Acceleration Response Levels, Experiment No. 4; Accelerometer A4

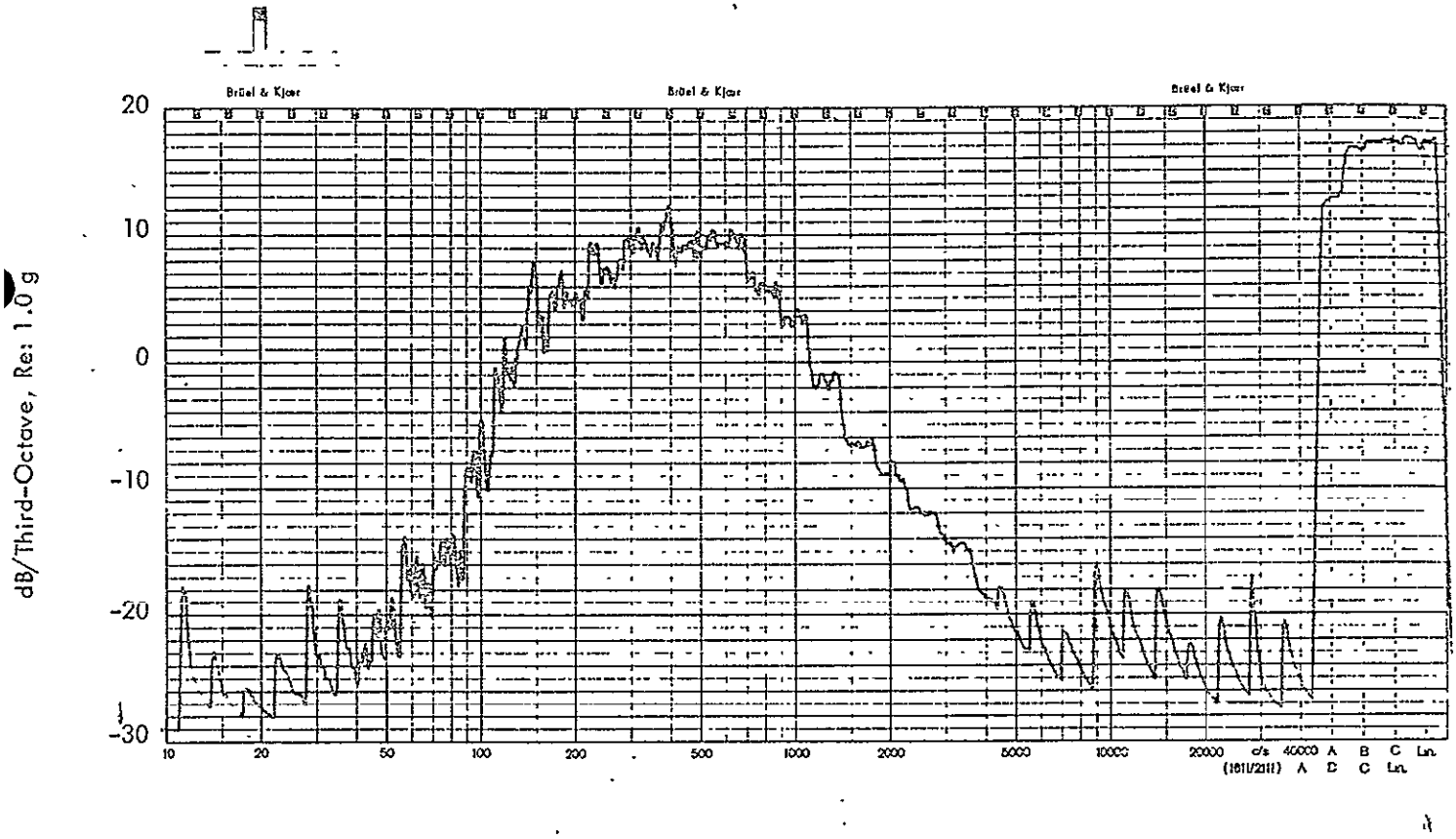

Figure B-37: Measured One-Third Octave Acceleration Response Levels, Experiment No. 4; Accelerometer A5

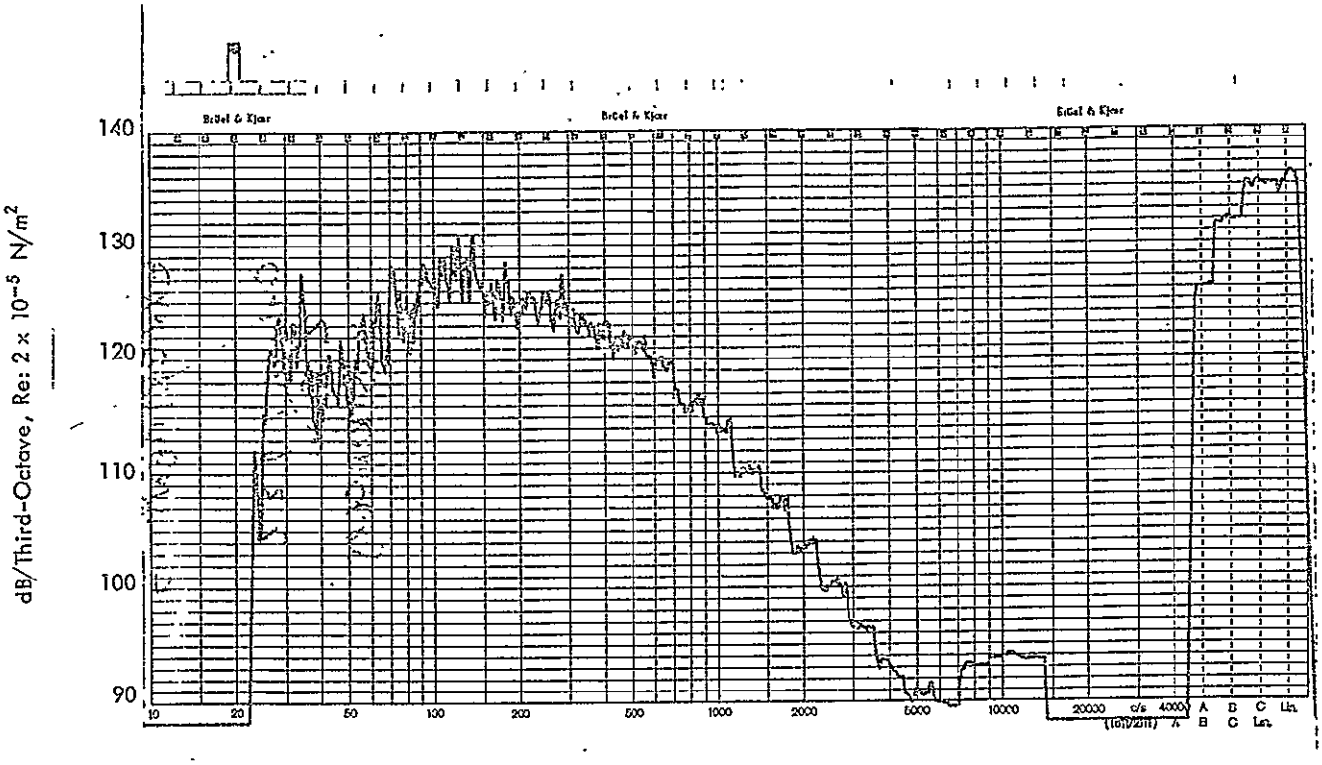

Figure B-38: Measured One-Third Octave Sound Pressure Levels, Experiment No. 5; External Microphone M1

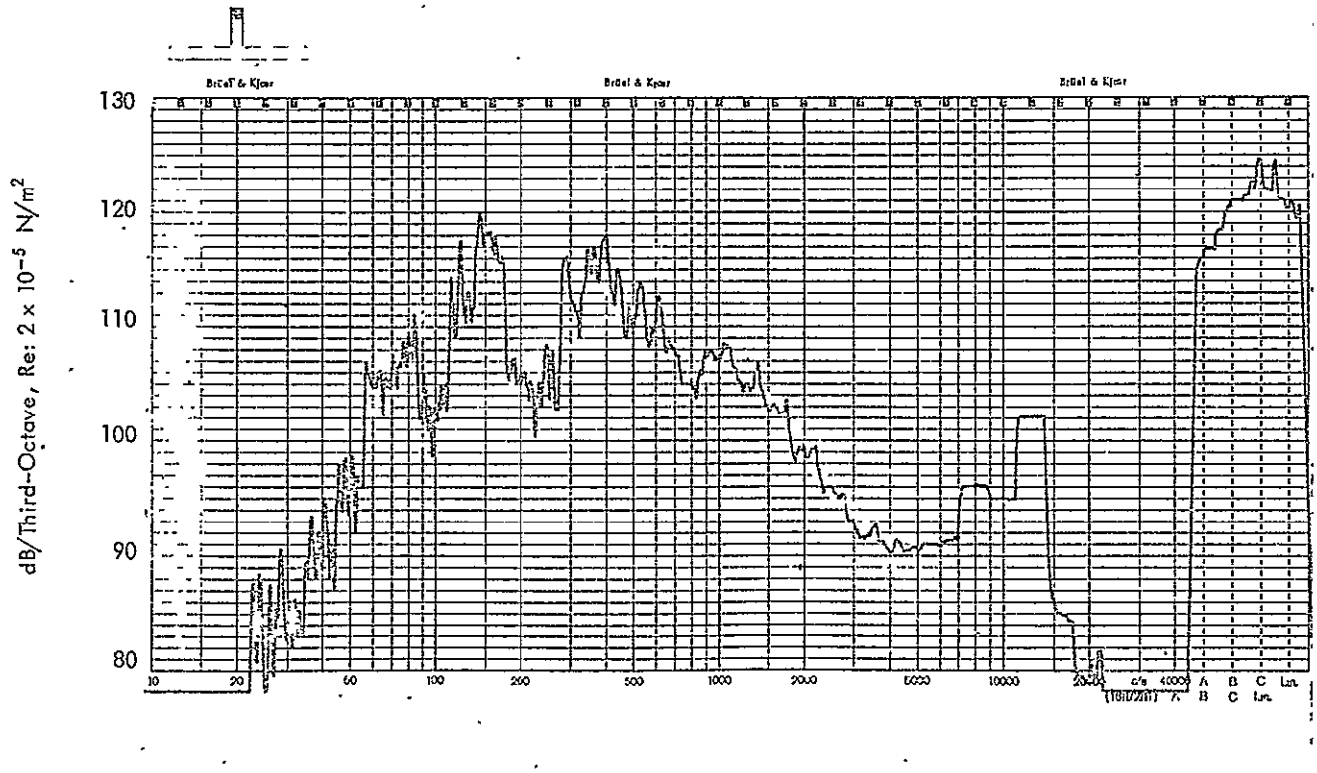

Figure B-39: Measured One-Third Octave Sound Pressure Levels, Experiment No. 5; Internal Microphone M2

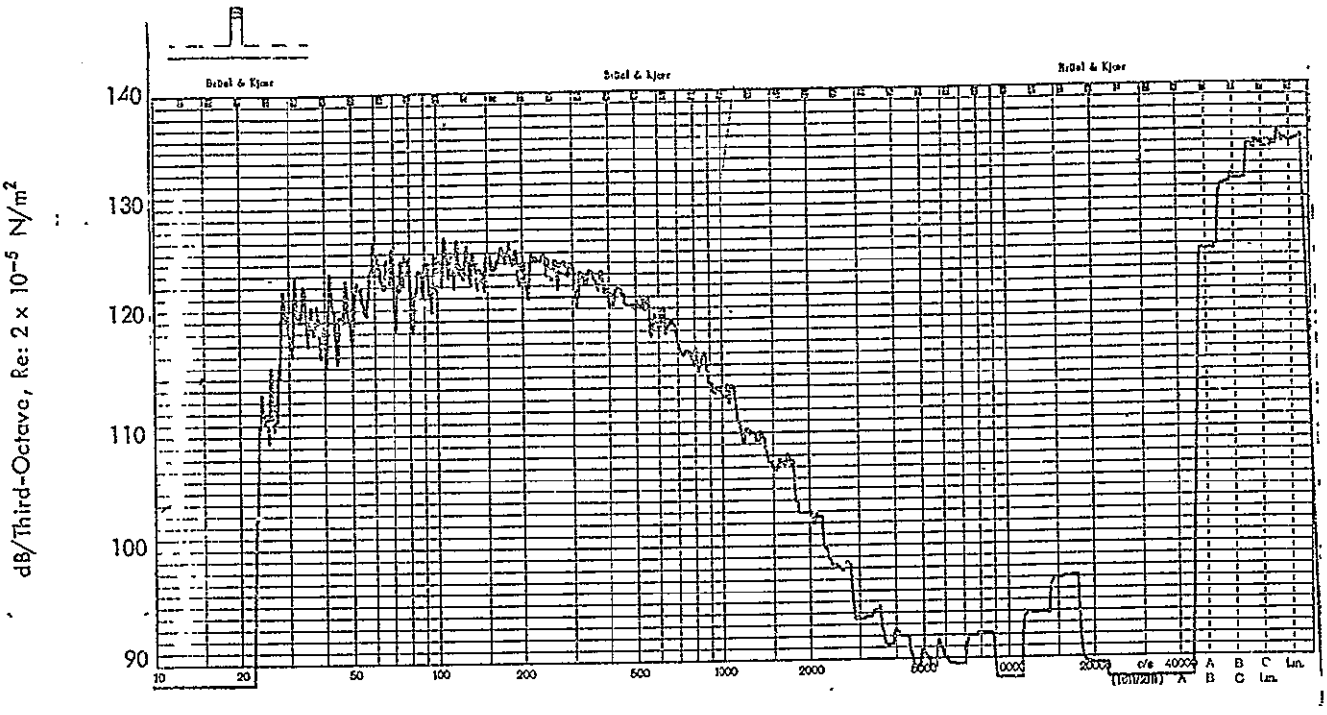

Figure B-40: Measured One-Third Octave Sound Pressure Levels, Experiment No. 5; External Microphone M3

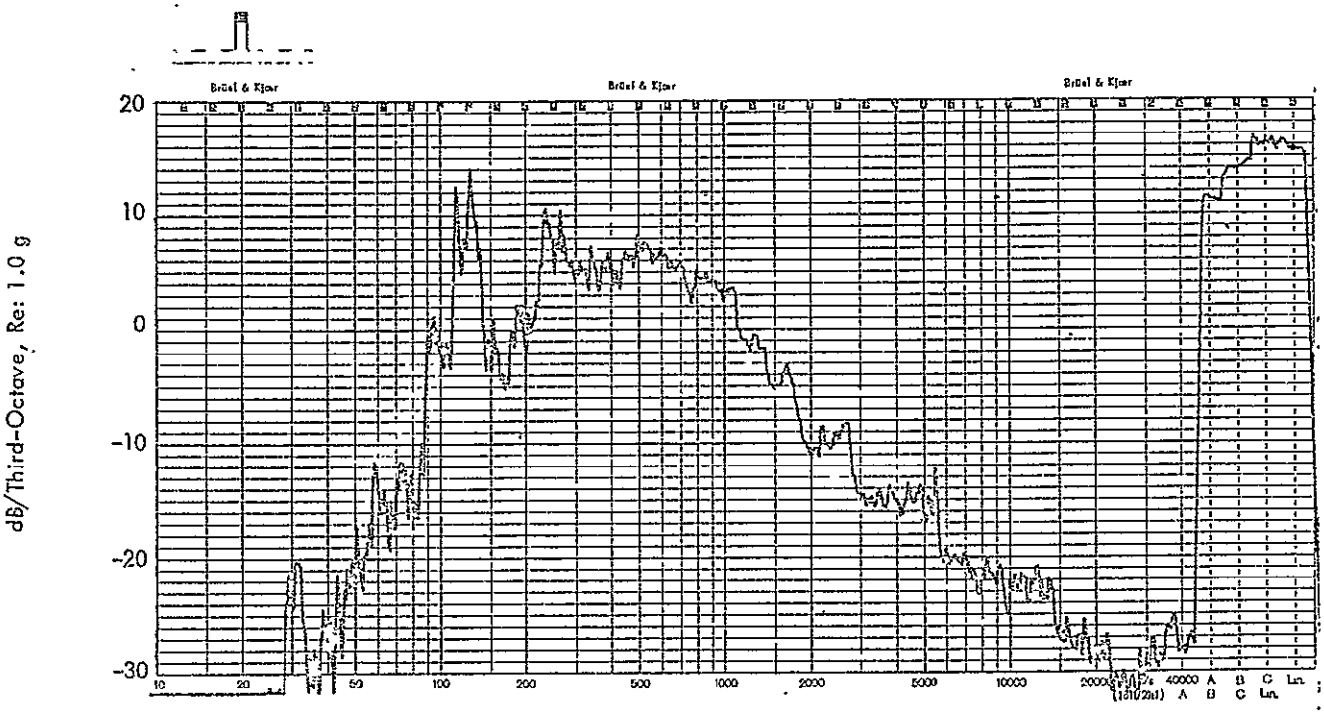

Figure B-41: Measured One-Third Octave Acceleration Response Levels, Experiment No. 5; Accelerometer A1

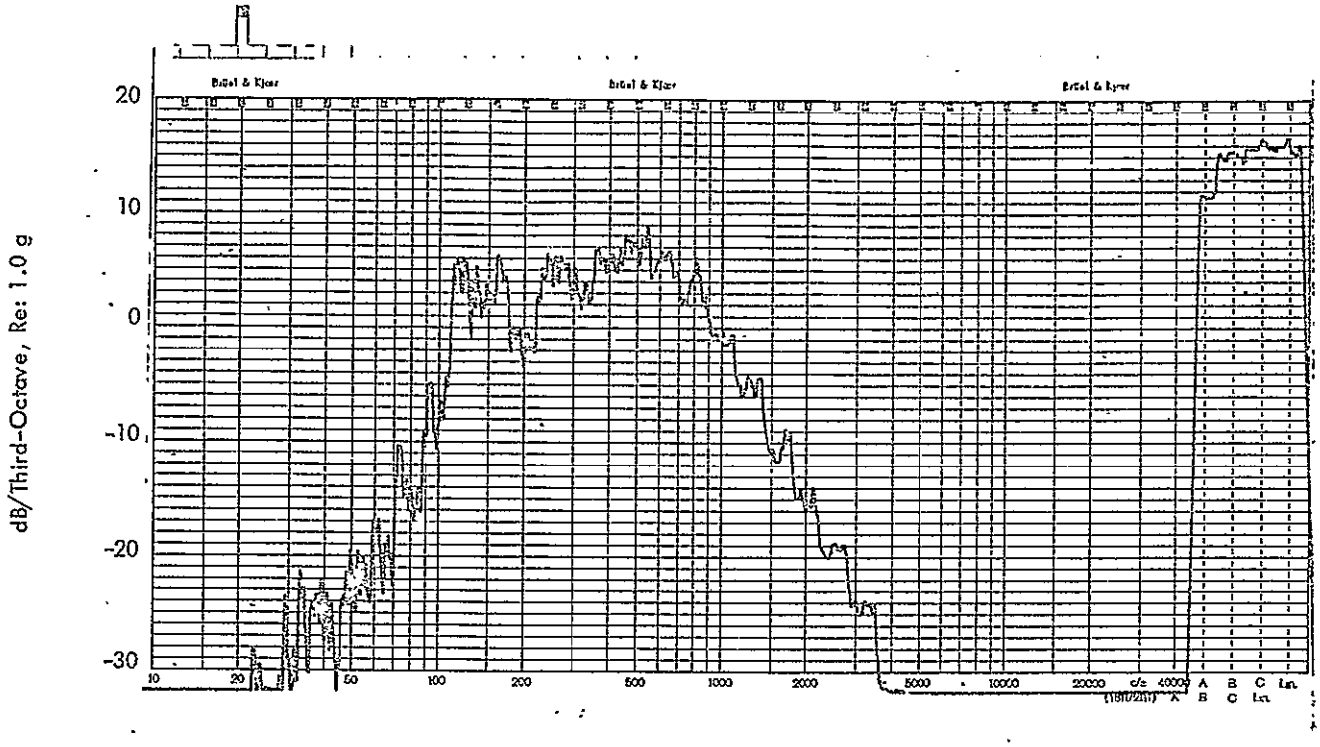

Figure B-42: Measured One-Third Octave Acceleration Response Levels, Experiment No. 5; Accelerometer A2

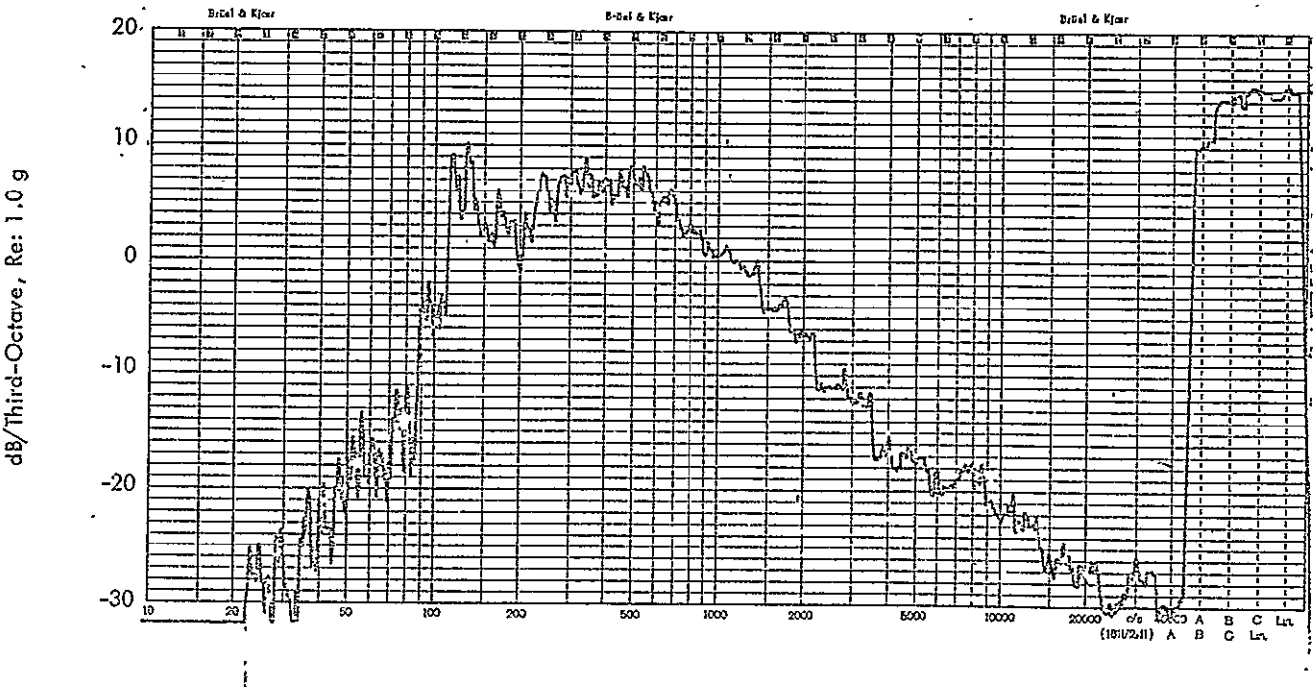

Figure B-43: Measured One-Third Octave Acceleration Response Levels, Experiment No. 5; Accelerometer A3

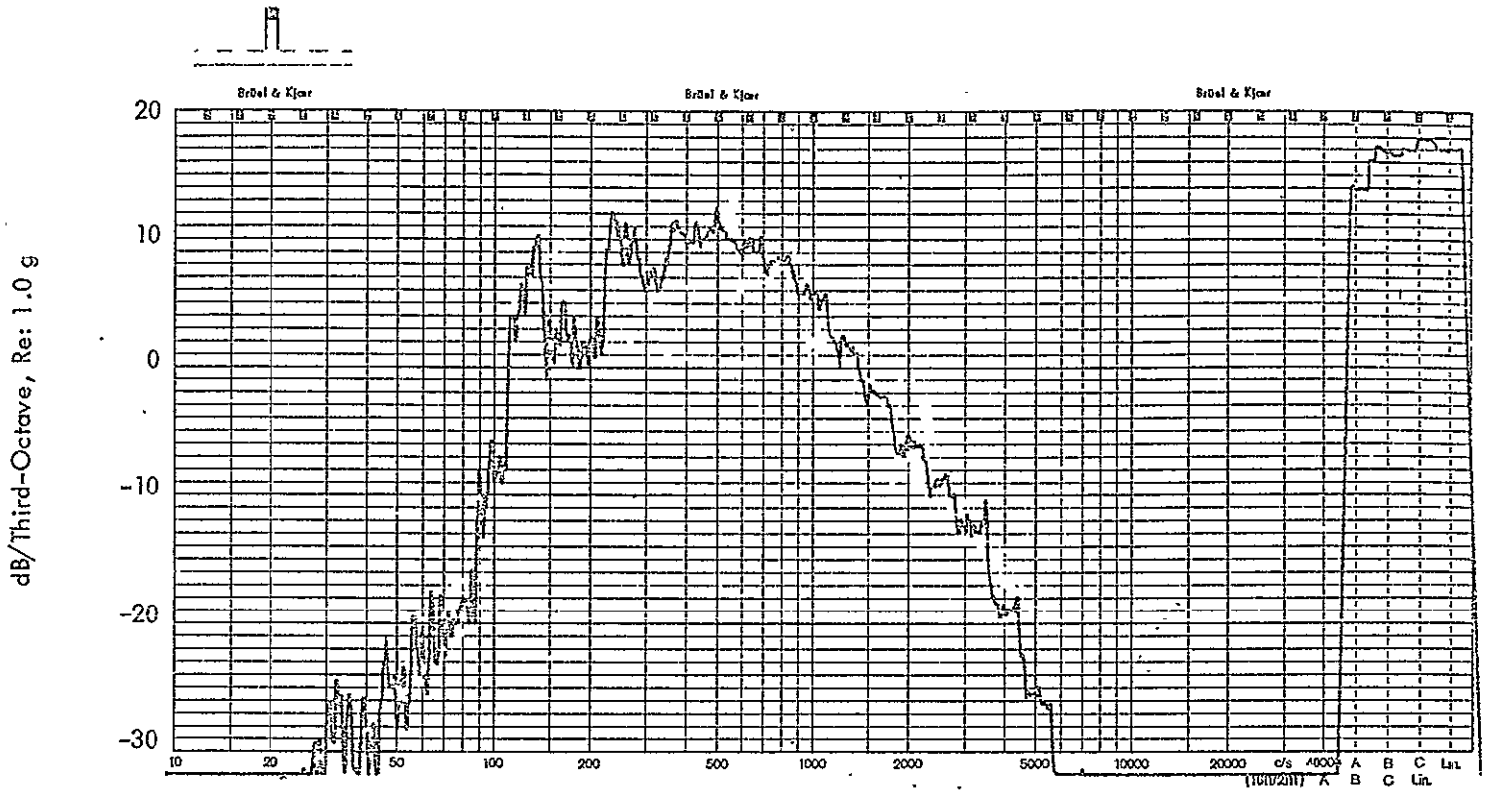

Figure B-44: Measured One-Third Octave Acceleration Response Levels, Experiment No. 5; Accelerometer A4

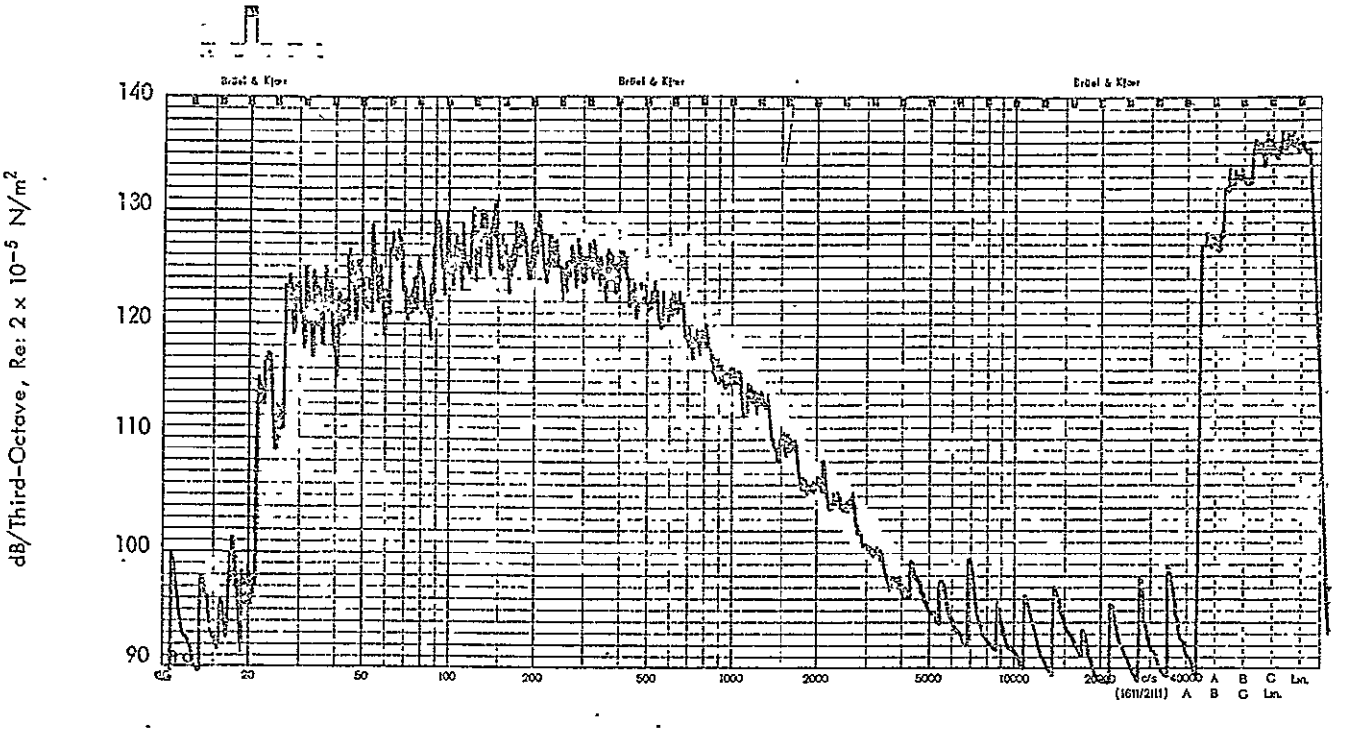

Figure B-45: Measured One-Third Octave Sound Pressure Levels, Experiment No. 6; External Microphone M1

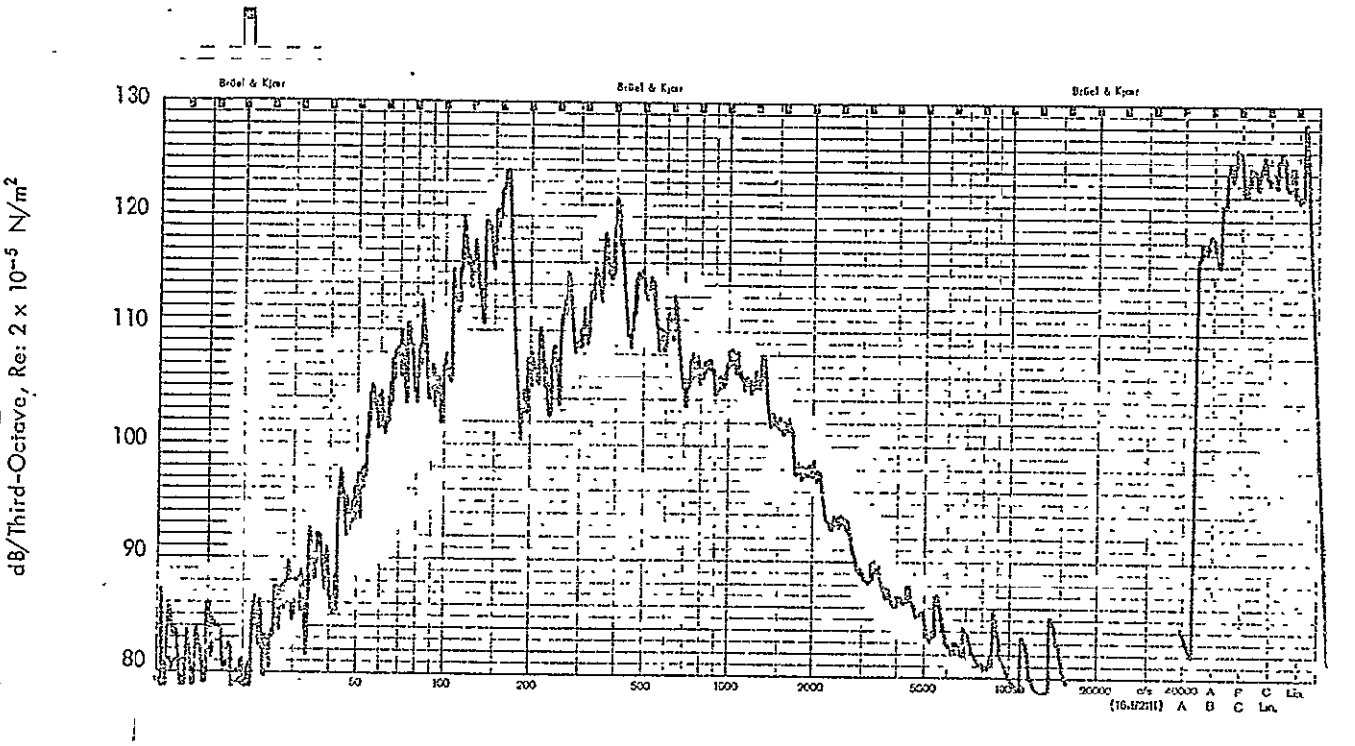

Figure B-46: Measured One-Third Octave Sound Pressure Levels, Experiment No. 6; Internal Microphone M2

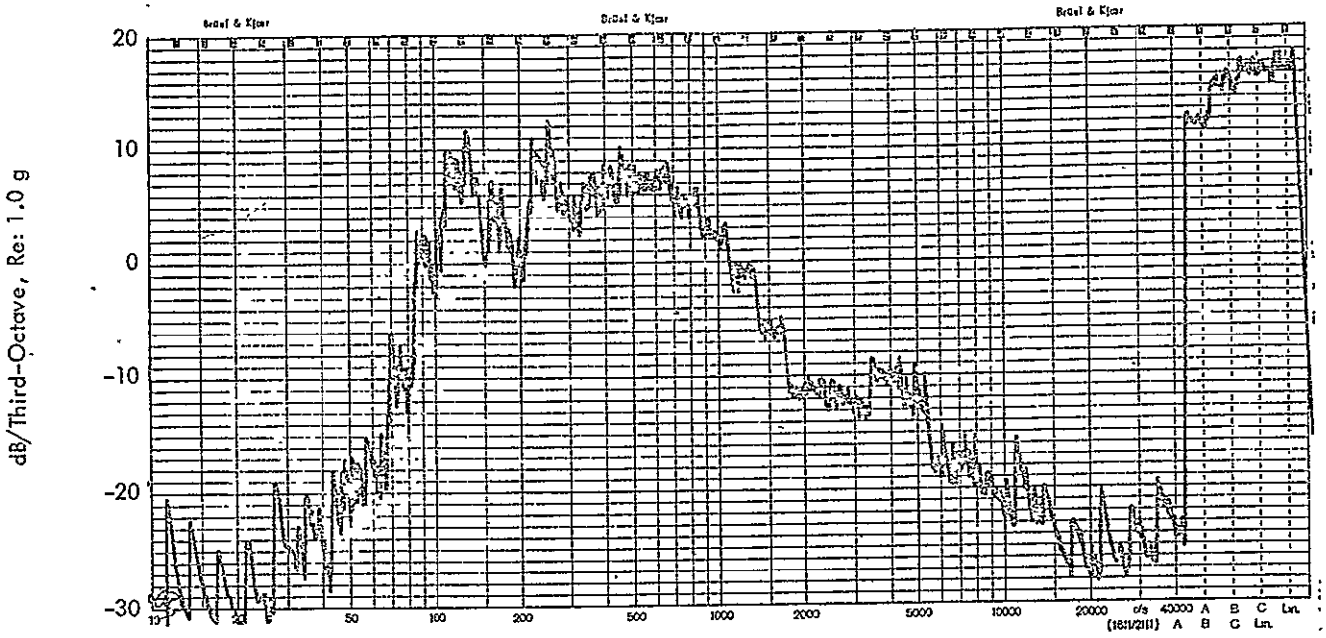

Figure B-47: Measured One-Third Octave Acceleration Response Levels, Experiment No. 6; Accelerometer A1

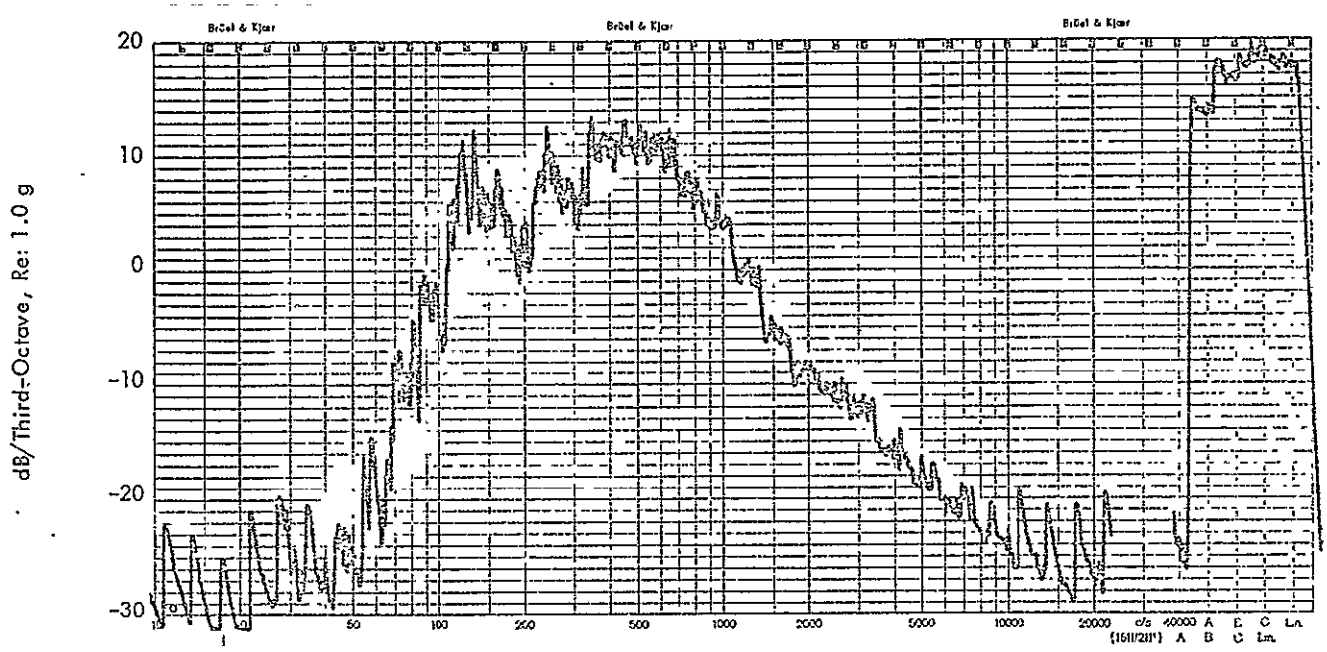

Figure B-48: Measured One-Third Octave Acceleration Response Levels, Experiment No. 6; Accelerometer A2

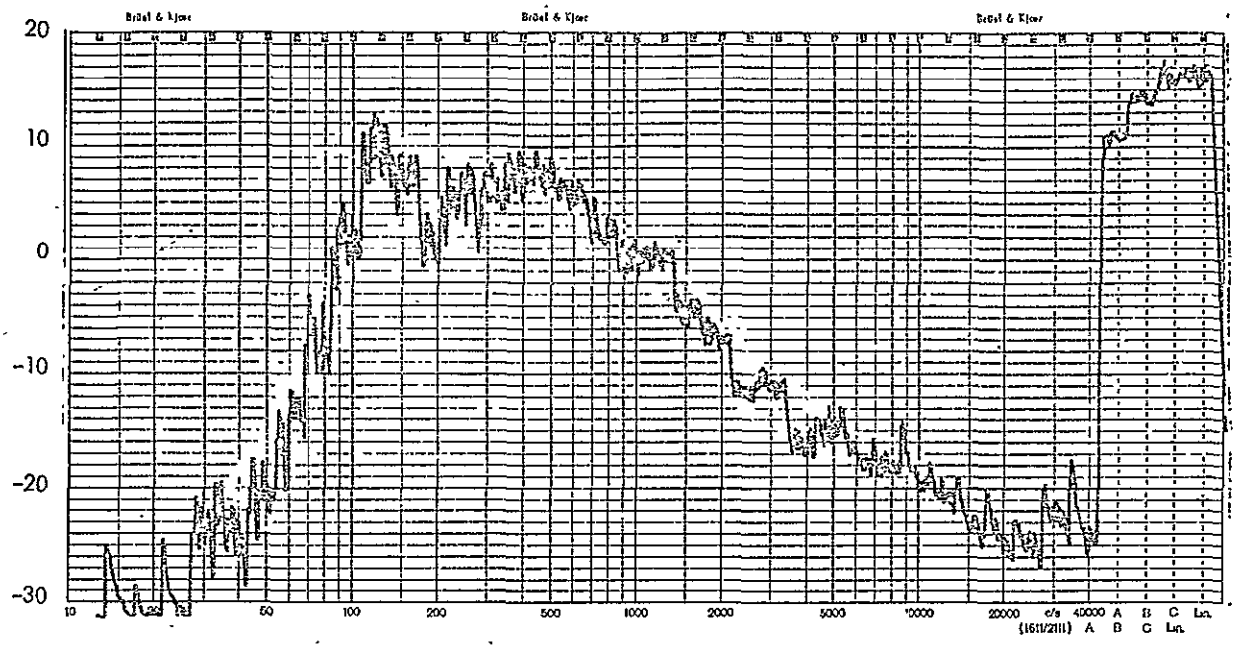

Figure B-49: Measured One-Third Octave Acceleration Response Levels, Experiment No. 6; Accelerometer A3

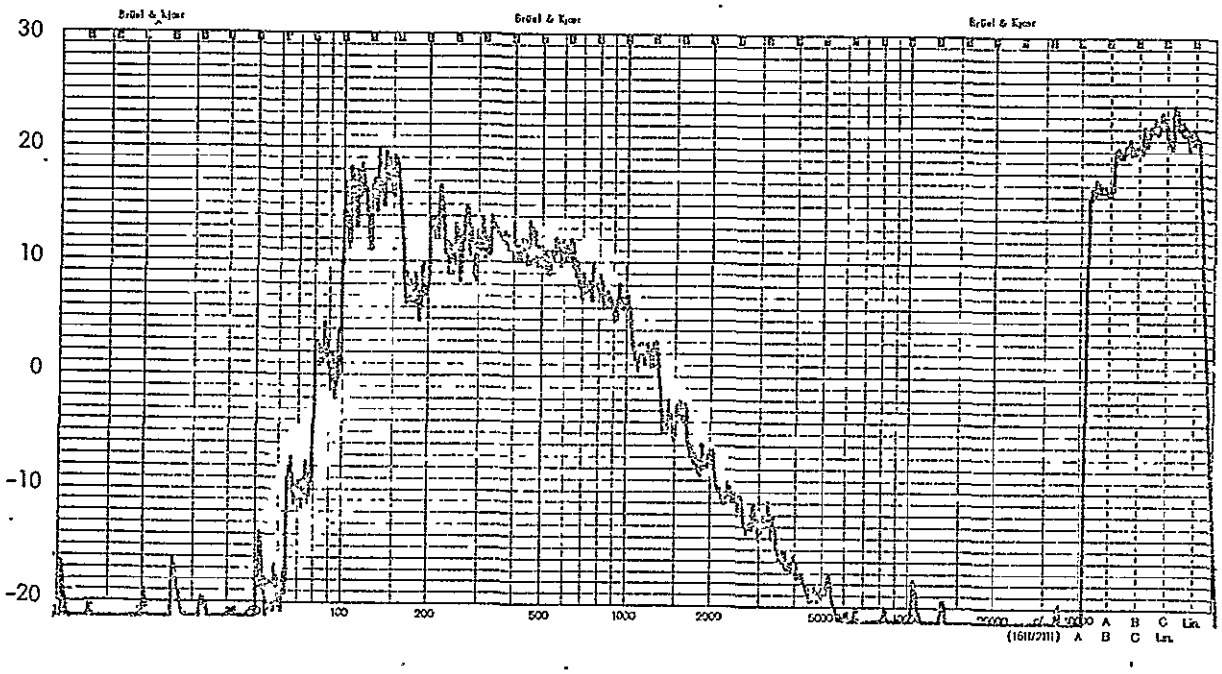

Figure B-50: Measured One-Third Octave Acceleration Response Levels, Experiment No. 6; Accelerometer A4

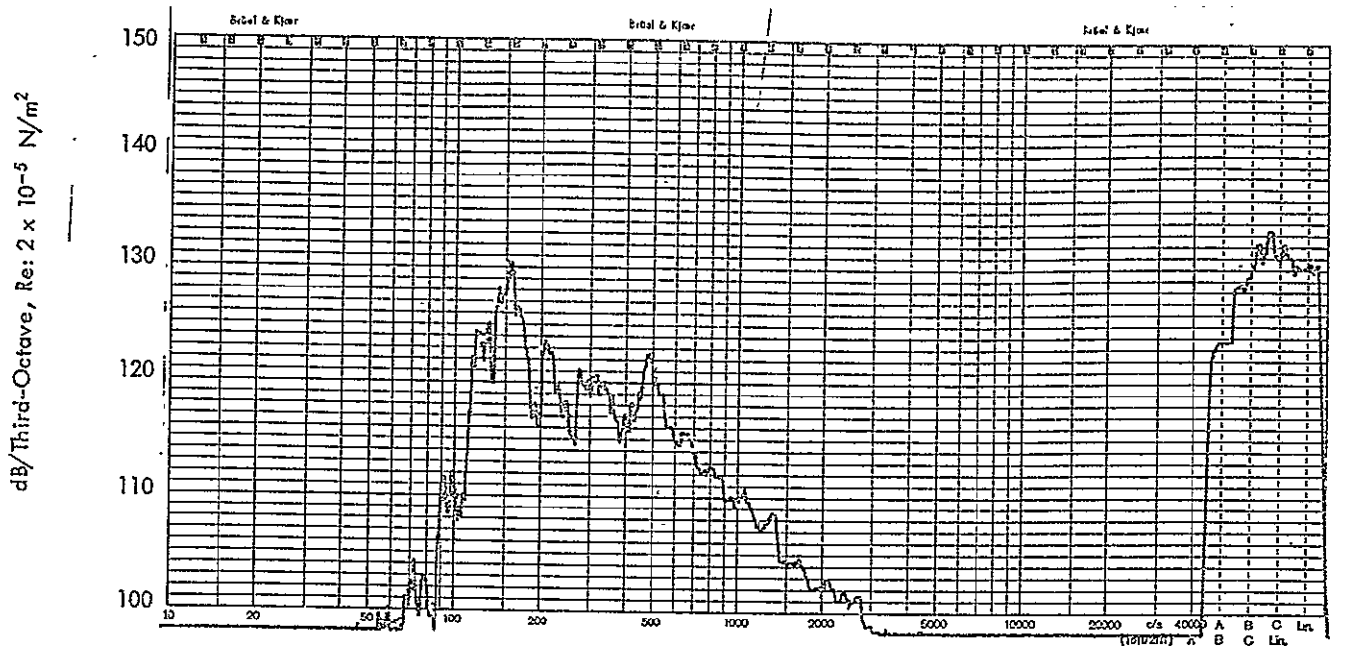

Figure B-53: Measured One-Third Octave Sound Pressure Levels, Experiment No. 7; Internal Microphone M3

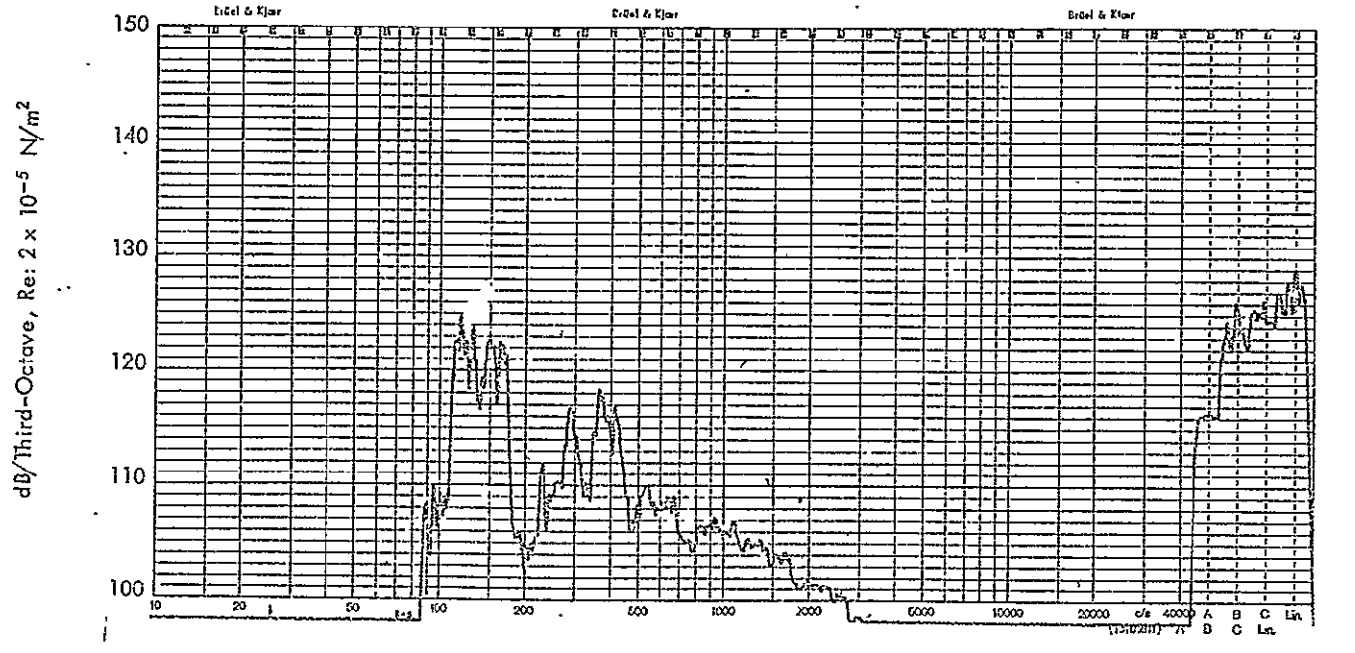

Figure B-54: Measured One-Third Octave Sound Pressure Levels, Experiment No. 7; Internal Microphone M4

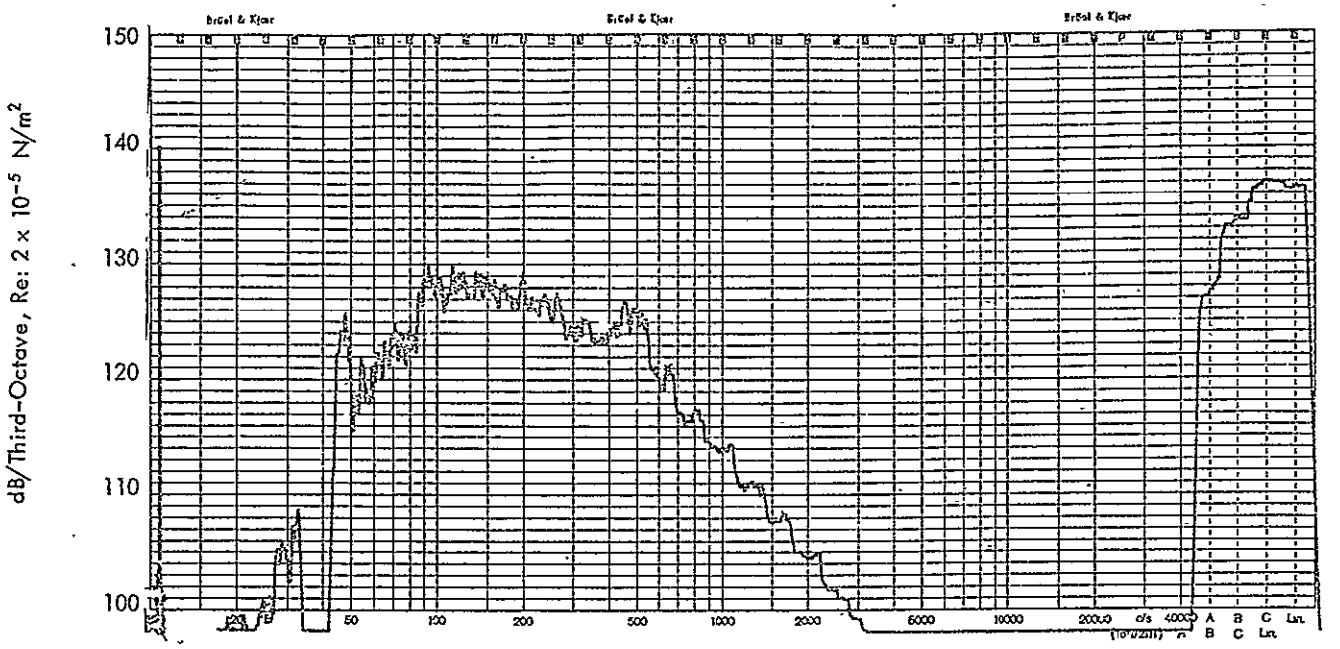

Figure B-51: Measured One-Third Octave Sound Pressure Levels, Experiment No.7; External Microphone M1

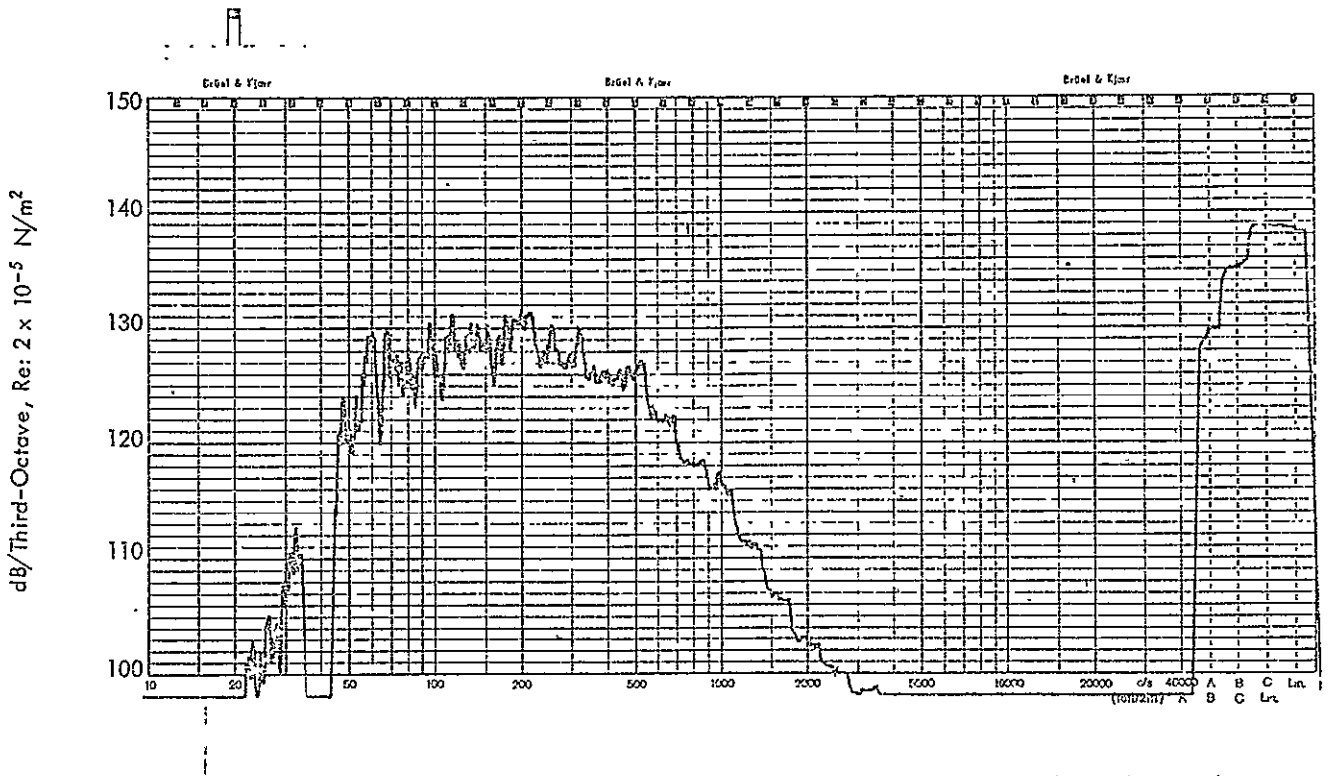

Figure B-52: Measured One-Third Octave Sound Pressure Levels, Experiment No.7; External Microphone M2

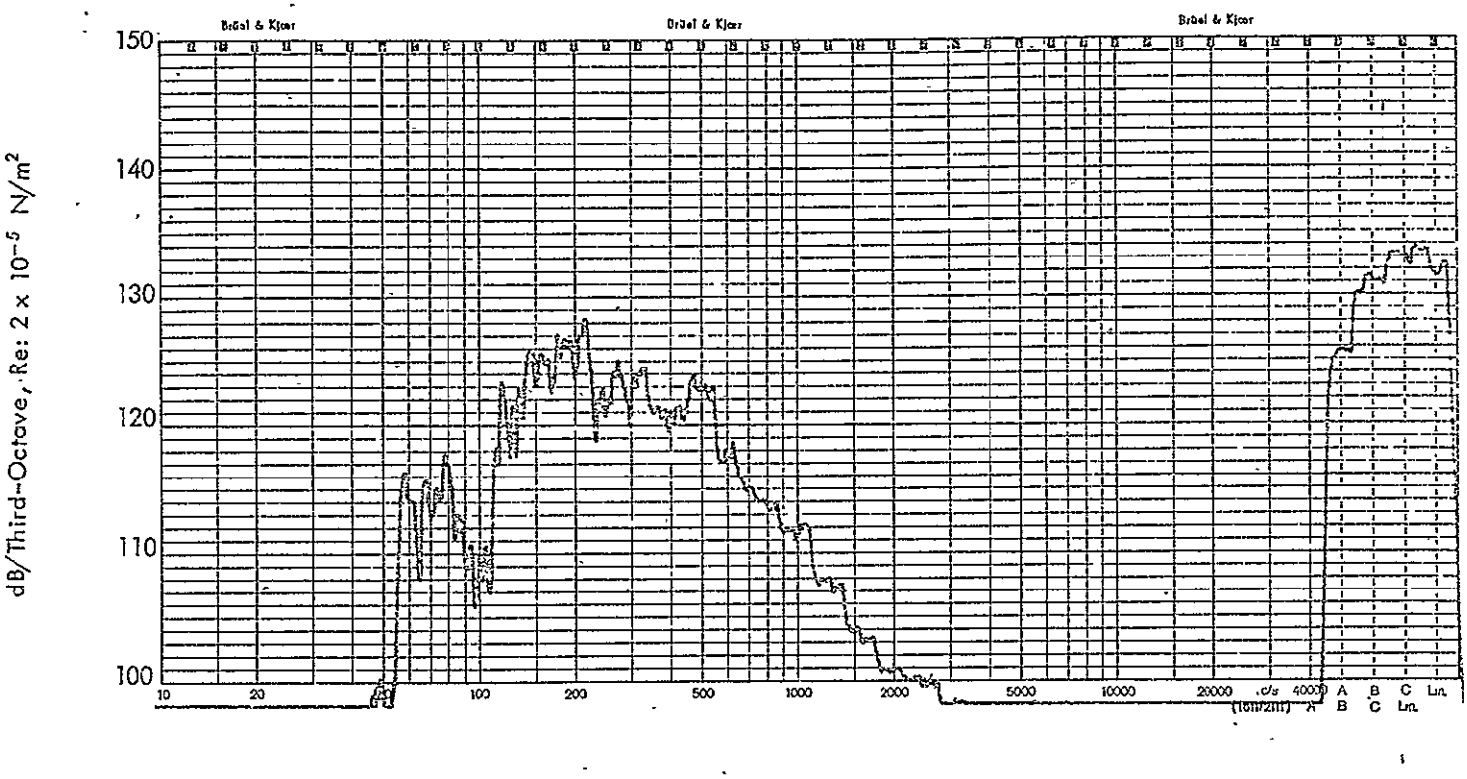

Figure B-55: Measured One-Third Octave Sound Pressure Levels, Experiment No. 7; Internal Microphone M5

Wyle WR 71-2

EXPERIMENTAL STUDY OF VIBRO-ACOUSTIC RESPONSE OF STIFFENED CYLINDRICAL SHELLS

V. M. Conticelli and R. W. White, January 1971

This report presents the results of an experimental vibro-acoustic research program in which an aluminum cylindrical shell was subjected to a reverberant acoustic field. The shell was tested with four different stiffener configurations. All stiffeners were uniformly spaced, and all configurations were tested with both ends of the shell closed by thick plywood bulkheads.

Measurements made included one-third octave band levels of the external acoustic field, internal acoustic field, axial and circumferential strains of the shell wall, and accelerations of the shell wall and stiffeners. These data are presented in tabulated form and are presented in graphs of normalized acceleration power spectral density. Theoretical response predictions are made for each configuration tested and for several assumed values of damping; and, these results are compared with measured response data. The comparison shows reasonably close agreement between theory and test when relatively low structural damping values are used in the computations.

I. CONTICELLI, V.M. WHITE, R.W.
II. WR 71-2
III. NAS9-10423
1. Cylindrical Shell
2. Vibration Response
3. Acoustics
4. Noise Reduction

Wyle WR 71-2

EXPERIMENTAL STUDY OF VIBRO-ACOUSTIC RESPONSE OF STIFFENED CYLINDRICAL SHELLS

V. M. Conticelli and R. W. White, January 1971

This report presents the results of an experimental vibro-acoustic research program in which an aluminum cylindrical shell was subjected to a reverberant acoustic field. The shell was tested with four different stiffener configurations. All stiffeners were uniformly spaced; and all configurations were tested with both ends of the shell closed by thick plywood bulkheads.

Measurements made included one-third octave band levels of the external acoustic field, internal acoustic field, axial and circumferential strains of the shell wall, and accelerations of the shell wall and stiffeners. These data are presented in tabulated form and are presented in graphs of normalized acceleration power spectral density. Theoretical response predictions are made for each configuration tested and for several assumed values of damping; and, these results are compared with measured response data. The comparison shows reasonably close agreement between theory and test when relatively low structural damping values are used in the computations.

I. CONTICELLI, V.M. WHITE, R.W.
II. WR 71-2
III. NAS9-10423
1. Cylindrical Shell
2. Vibration Response
3. Acoustics
4. Noise Reduction

Wyle WR 71-2

EXPERIMENTAL STUDY OF VIBRO-ACOUSTIC RESPONSE OF STIFFENED CYLINDRICAL SHELLS

V. M. Conticelli and R. W. White, January 1971

This report presents the results of an experimental vibro-acoustic research program in which an aluminum cylindrical shell was subjected to a reverberant acoustic field. The shell was tested with four different stiffener configurations. All stiffeners were uniformly spaced, and all configurations were tested with both ends of the shell closed by thick plywood bulkheads.

Measurements made included one-third octave band levels of the external acoustic field, internal acoustic field, axial and circumferential strains of the shell wall, and accelerations of the shell wall and stiffeners. These data are presented in tabulated form and are presented in graphs of normalized acceleration power spectral density. Theoretical response predictions are made for each configuration tested and for several assumed values of damping; and, these results are compared with measured response data. The comparison shows reasonably close agreement between theory and test when relatively low structural damping values are used in the computations.

I. CONTICELLI, V.M. WHITE, R.W.
II. WR 71-2
III. NAS9-10423
1. Cylindrical Shell
2. Vibration Response
3. Acoustics
4. Noise Reduction

Wyle WR 71-2

EXPERIMENTAL STUDY OF VIBRO-ACOUSTIC RESPONSE OF STIFFENED CYLINDRICAL SHELLS

V. M. Conticelli and R. W. White, January 1971

This report presents the results of an experimental vibro-acoustic research program in which an aluminum cylindrical shell was subjected to a reverberant acoustic field. The shell was tested with four different stiffener configurations. All stiffeners were uniformly spaced; and all configurations were tested with both ends of the shell closed by thick plywood bulkheads.

Measurements made included one-third octave band levels of the external acoustic field, internal acoustic field, axial and circumferential strains of the shell wall, and accelerations of the shell wall and stiffeners. These data are presented in tabulated form and are presented in graphs of normalized acceleration power spectral density. Theoretical response predictions are made for each configuration tested and for several assumed values of damping; and, these results are compared with measured response data. The comparison shows reasonably close agreement between theory and test when relatively low structural damping values are used in the computations.

I. CONTICELLI, V.M. WHITE, R.W.
II. WR 71-2
III. NAS9-10423
1. Cylindrical Shell
2. Vibration Response
3. Acoustics
4. Noise Reduction

Wyle WR 71-2

EXPERIMENTAL STUDY OF VIBRO-ACOUSTIC RESPONSE OF STIFFENED CYLINDRICAL SHELLS

V. M. Conticelli and R. W. White, January 1971

This report presents the results of an experimental vibro-acoustic research program in which an aluminum cylindrical shell was subjected to a reverberant acoustic field. The shell was tested with four different stiffener configurations. All stiffeners were uniformly spaced; and all configurations were tested with both ends of the shell closed by thick plywood bulkheads.

Measurements made included one-third octave band levels of the external acoustic field, internal acoustic field, axial and circumferential strains of the shell wall, and accelerations of the shell wall and stiffeners. These data are presented in tabulated form and are presented in graphs of normalized acceleration power spectral density. Theoretical response predictions are made for each configuration tested and for several assumed values of damping; and, these results are compared with measured response data. The comparison shows reasonably close agreement between theory and test when relatively low structural damping values are used in the computations.

I. CONTICELLI, V.M. WHITE, R.W.
II. WR 71-2
III. NAS9-10423
1. Cylindrical Shell
2. Vibration Response
3. Acoustics
4. Noise Reduction

Wyle WR 71-2

EXPERIMENTAL STUDY OF VIBRO-ACOUSTIC RESPONSE OF STIFFENED CYLINDRICAL SHELLS

V. M. Conticelli and R. W. White, January 1971

This report presents the results of an experimental vibro-acoustic research program in which an aluminum cylindrical shell was subjected to a reverberant acoustic field. The shell was tested with four different stiffener configurations. All stiffeners were uniformly spaced; and all configurations were tested with both ends of the shell closed by thick plywood bulkheads.

Measurements made included one-third octave band levels of the external acoustic field, internal acoustic field, axial and circumferential strains of the shell wall, and accelerations of the shell wall and stiffeners. These data are presented in tabulated form and are presented in graphs of normalized acceleration power spectral density. Theoretical response predictions are made for each configuration tested and for several assumed values of damping; and, these results are compared with measured response data. The comparison shows reasonably close agreement between theory and test when relatively low structural damping values are used in the computations.

I. CONTICELLI, V.M. WHITE, R.W.
II. WR 71-2
III. NAS9-10423
1. Cylindrical Shell
2. Vibration Response
3. Acoustics
4. Noise Reduction

Wyle WR 71-2

EXPERIMENTAL STUDY OF VIBRO-ACOUSTIC RESPONSE OF STIFFENED CYLINDRICAL SHELLS

V. M. Conticelli and R. W. White, January 1971

This report presents the results of an experimental vibro-acoustic research program in which an aluminum cylindrical shell was subjected to a reverberant acoustic field. The shell was tested with four different stiffener configurations. All stiffeners were uniformly spaced; and all configurations were tested with both ends of the shell closed by thick plywood bulkheads.

Measurements made included one-third octave band levels of the external acoustic field, internal acoustic field, axial and circumferential strains of the shell wall, and accelerations of the shell wall and stiffeners. These data are presented in tabulated form and are presented in graphs of normalized acceleration power spectral density. Theoretical response predictions are made for each configuration tested and for several assumed values of damping; and, these results are compared with measured response data. The comparison shows reasonably close agreement between theory and test when relatively low structural damping values are used in the computations.

I. CONTICELLI, V.M. WHITE, R.W.
II. WR 71-2
III. NAS9-10423
1. Cylindrical Shell
2. Vibration Response
3. Acoustics
4. Noise Reduction

Wyle WR 71-2

EXPERIMENTAL STUDY OF VIBRO-ACOUSTIC RESPONSE OF STIFFENED CYLINDRICAL SHELLS

V. M. Conticelli and R. W. White, January 1971

This report presents the results of an experimental vibro-acoustic research program in which an aluminum cylindrical shell was subjected to a reverberant acoustic field. The shell was tested with four different stiffener configurations. All stiffeners were uniformly spaced; and all configurations were tested with both ends of the shell closed by thick plywood bulkheads.

Measurements made included one-third octave band levels of the external acoustic field, internal acoustic field, axial and circumferential strains of the shell wall, and accelerations of the shell wall and stiffeners. These data are presented in tabulated form and are presented in graphs of normalized acceleration power spectral density. Theoretical response predictions are made for each configuration tested and for several assumed values of damping; and, these results are compared with measured response data. The comparison shows reasonably close agreement between theory and test when relatively low structural damping values are used in the computations.

I. CONTICELLI, V.M. WHITE, R.W.
II. WR 71-2
III. NAS9-10423
1. Cylindrical Shell
2. Vibration Response
3. Acoustics
4. Noise Reduction